The Evolution of a Transplantable Tumour

Ahmed Rokan

Thesis submitted for the degree of

Doctor of Philosophy

Division of Infection and Immunity

UCL

March 2025

“I, Ahmed Rokan confirm that the work presented in my thesis is my own. Where information has been derived from other sources, I confirm that this has been indicated in the thesis.”

Abstract

One of the hallmarks of cancer is the ability to evade the immune system. Remarkably, there are non-human cancers that can be transmitted across individuals irrespective of the histocompatibility barrier. A well-known example is the Canine Transmissible Venereal Tumour (CTVT), which is a contagious mammalian clonal allograft.

To understand how a mammalian cancer might evolve the ability to escape allogeneic recognition, we have passaged a genetically well-characterised mouse melanoma cell line from syngeneic mice (C57BL/6) into progressively more allogeneic mouse crosses and eventually into fully haplotype mismatched BALB/c mice. At each passage, we performed flow cytometry analysis on dissociated tumours to characterise the host intratumoural immune infiltrate and performed RNA-seq analysis on the isolated tumour cells to obtain a more comprehensive view of the evolution of these tumours.

Multiple passaging rounds resulted in a stepwise adaptation of the tumours to evade allogeneic recognition, eventually permitting their tolerance in fully mismatched mice. Flow cytometry showed greater immune infiltration in the earlier passages, including CD8+ and NK cells which, however, were unable to reject the tumour. In the later passages, CD8+ T cells were significantly reduced, while Dendritic Cells (DCs) increased. RNA-seq data on isolated tumour cells demonstrated changes in gene expression during passaging characterised by higher expression of inflammatory and antiviral markers and overexpression of intergenic Endogenous Retrotransposable Elements (RTE), MHC-I, PD-L1, and non-classical MHC

molecule Qa-1. MHC-I, PD-L1, and Qa-1 expression were all decreased in transplantable tumour cells when the RNA sensor RIG-I was knocked out. Following transplantation, antibody-mediated inhibition of both PD-L1 and Qa-1 caused tumour regression. These data demonstrate that our experimental model can successfully evolve tumours that bypass the histocompatibility barrier. Our model will provide new mechanistic insights into allograft tolerance that may be used to blunt organ transplant rejection.

Impact Statement

Organ transplantation is required to save the lives of many patients. A major challenge for organ transplantation is the scarcity of matched donors. This is because of the histocompatibility barrier which governs the process of accepting or rejecting a graft. Transmissible cancers which are allografts that transmit to mismatched hosts are a model for bypassing the histocompatibility barrier. In addition, cancer is the second leading cause of death globally. It accounts for approximately 10 million deaths annually. The immune system should detect and eliminate transforming cells but in many cases that does not happen due to cancer's immune escape.

In order to better understand how allografts might evade the histocompatibility barrier, I serially passaged a mouse melanoma into syngeneic animals first, then into increasingly mismatched mouse strains until a fully allo-transplantable tumour emerged. By Studying the adapted tumours our model may offer crucial insights into tumour immune evasion and tumour evolution. It also provides insight into how the immune system and cancer interact, as well as how cancer mutations allow it to escape the immune system. The model is also helpful for studying cancer immunology and how tumours alter the immune infiltration to promote growth or create an environment that suppresses the immune system. Additionally, the model is useful for researching allogeneic graft rejection and its prevention, which may be used for organ transplantation.

Thesis Contribution by Others

Tumour Transplantation Optimization:

Chapter 3: Early tumour transplantation to optimize the number of cells injected was made by Dr. Clare Bennett

Bioinformatics Analysis:

Chapter 5: Novogene mapped the RNA-seq readings. Additionally, Novogene carried out the Differential Expression study, which was examined by Jose des las Heras, a Fassati lab member. Jose des las Heras conducted the bioinformatics analysis displayed in panels a through d of Figure 5.5.

Chapter 5: Retrotransposable Elements Analysis in Figures 5.7, 5.8, and 5.9 were done by our collaborator George Kassiotis's group.

Acknowledgements

I would like to thank the members of the Fassati group for their support during my PhD journey. I would also like to thank my thesis committee members for their constructive feedback and everyone else in the extended Infection and Immunity family.

Special thanks to my PI Prof. Ariberto Fassati for all his hard work to guide and support me through my PhD journey.

I would like to dedicate this PhD and this work to my parents, my wife Somaya who shared this journey with me, and my family (Mohammed, Lutifah, Abdullah, Anas, Raed, Munirah) for all the love and support and the hard work they put in to get me to where I am.

Table of Contents

Table of Figures

Table of Tables

Abbreviations

AHL	age-related hearing loss
APM	antigen processing machinery
ARG-1	arginase-1
BRAF	B rapidly accelerated fibrosarcoma
Calr	Calreticulin
CARD	caspase activation and recruitment domain
Canx	calnexin
Cas9	clustered regularly interspaced short palindrome repeats associated protein 9
CCL5	chemokine (c-c motif) ligand 5
CD#	cluster of differentiation #
CDKN2A	Cyclin Dependent Kinase Inhibitor 2A
cGAMP	cyclic guanosine monophosphate-adenosine monophosphate
cGAS	cyclic guanosine monophosphate-adenosine monophosphate synthase
CMV	Cytomegalovirus
COX2	cyclooxygenase-2
CRISPR	clustered regularly interspaced short palindrome repeats
CTLA-4	cytotoxic T-lymphocyte associated protein 4
CTLs	cytotoxic T cells
CTVT	canine transmissible venereal tumour
CXCL10	c-x-c motif chemokine ligand 10
DC	dendritic cells
DDX58	DEAD box protein 58
DFTD	tasmanian devil facial tumour disease
DHX58	DExH-box helicase 58
DNMTis	DNA Methyltransferase Inhibitors

dsRNA	double-stranded RNA
EBV	epstein-barr virus
EDTA	ethylenediaminetetraacetic acid
EGFR	epidermal growth factor receptor
ELISA	enzyme-linked immunosorbent assay
ER	endoplasmic reticulum
ERE	endogenous retroelements
ERVs	endogenous retroviruses
EV	snp lentivector
F#	filial #
FC	flow cytometry
FPKM	fragments per kilobase million
GO	gene ontology
GSEA	gene set enrichment analysis
HBV	hepatitis b virus
HCV	hepatitis c virus
HLA	Human leukocyte antigen
hTG	human transgenes
ICB	immune checkpoint blockade
IF	immunofluorescence
IFNAR	interferon-α/β receptor
IFN	interferon
IPA	ingenuity pathway analysis
IP-10	interferon gamma-induced protein 10
IRDS	interferon-related DNA damage resistance signature
ISGF3	interferon-stimulated gene factor 3
ISG	interferon stimulated gene
KEGG	kyoto encyclopedia of genes and genomes
KO	knock out

LAG-3	Lymphocyte-activation gene 3
LGP2	laboratory of genetics and physiology 2
LOH	loss of heterozygosity
MAPK	mitogen-activated protein kinase
MAVS	mitochondrial antiviral signalling protein
MHC	major histocompatibility complex
MDA5	melanoma differentiation-associated protein 5
MDSC	myeloid derived suppressor cells
MFI	mean fluorescence intensity
MLV	murine leukaemia virus
MUGA	mini mouse universal genotyping array
N2	number of backcross generations 2
NHP	non-human primates
NIHL	noise-induced hearing loss
NK	natural killer
NOD	non-obese diabetic
PCA	principal component analysis
PD-1	programmed cell death protein 1
PD-L1	programmed death ligand 1
PI3K-AKT	Phosphoinositide 3-kinases- AKR mouse strain thymoma kinase
PRR	pattern recognition receptor
PTEN	phosphatase and tensin homolog
PTPRC	protein tyrosine phosphatase, receptor type, C also known as
RBC	red blood cells
RIG-I	retinoic acid-inducible gene I
RTEs	retrotransposable elements
SCID	severe combined immunodeficient mice
SNPs	single nucleotide polymorphisms
STING	stimulator of interferon genes

TAM	tumour associated macrophages
TCR	T cell receptor
TGFβ	transforming growth factor beta
TG	transgenic
Th	T helper
TIM3	T cell immunoglobulin and mucin domain-containing protein 3
TKO	triple knock out
TME	tumour microenvironment
TNF-α	tumour necrosis factor α
Treg	regulatory T cells
UNOS	united network for organ sharing
VEGF	vascular endothelial growth factor
YUMM1.7	yale university mouse melanoma

1

Introduction

Chapter 1: Introduction

1.1 Histocompatibility Barrier

The discovery of the Major Histocompatibility Complex (MHC) by George Snell marked a significant milestone in transplantation immunology, it provided insight into the genetic characteristics that prevented transplantation among different individuals. The implications of this discovery were profound and impacted the lives of numerous people since then, making it possible to identify which people are suitable for donating an organ to a recipient and shedding light on the immune functions that govern this process.

MHC is an important part of the immune system and it is critical for the identification of foreign substances by the immune system. It consists of the Major Histocompatibility Complex Class I (MHC-I) and MHC-II. MHC Class I exists in almost all nucleated cells and presents endogenous peptides to CD8+ cytotoxic T cells. MHC Class II is mainly found on professional antigen-presenting cells (APCs) such as dendritic cells, macrophages, and B cells. MHC-II presents exogenous peptides to CD4+ helper T cells. The MHC-Is extremely polymorphic, therefore there are many distinct alleles for each MHC gene. This polymorphism leads to a variety of immunological responses across individuals (Carreras et al., 2019). In humans, the MHC-I is known as the Human Leukocyte Antigen (HLA) system. As of December 2024, 41,003 HLA and associated alleles have been catalogued in the IPD-IMGT/HLA Database (Robinson et al., 2000). This extensive polymorphism underscores the complexity of the HLA system, which plays a crucial role in immune recognition and transplantation compatibility.

Because the immune system recognizes foreign antigens, histocompatibility barriers pose a major challenge in organ and tissue transplantation. The mismatch between the organ donor and the recipient histocompatibility leads to graft rejection in what is known as allogeneic rejection.

The study of allogeneic rejection dates back to the early 20th century, with pioneering experiments that shed light on the immune system's response to foreign tissues. In these experiments, Leo Loeb and Ernest Tyzzer observed that tissues transplanted between genetically distinct individuals were invariably rejected. These findings suggested that an immune-mediated process dictated graft survival (Little & Johnson, 1922). Loeb's mice experiments showed a correlation between genetic similarity and successful graft acceptance, while Tyzzer's tumour experiments revealed the role of genetic differences in transplant rejection (Little & Johnson, 1922). The inability of tumours to grow in mismatched hosts suggested a genetic barrier to acceptance, this understanding was the foundation for the histocompatibility barrier. Following these experiments in the 1940s Medwar showed that to treat a patient with severe skin burns, tissue from the same person (autograft) are accepted by the body, while skin tissue from a sibling donor (homograft) are first rejected slowly then upon a second transplantation attempt from the same donor the graft was rejected acutely (Gibson & Medawar, 1943). This work laid the ground for modern organ transplantation and influenced the understanding of the immune response towards transplanted organs.

1.1.1 Allogeneic Rejection in Mice

Ernest Tyzzer's experiments in 1916 with Japanese Waltzing Mice and non-Japanese Waltzing Mice and their crosses highlighted the role of genetic differences in allogeneic rejection. They experimented with subcutaneous injections of transplantable carcinoma (J.W.A.). This carcinoma was created especially for research to investigate the growth dynamics and tumour susceptibility of Japanese Waltzing Mice. Transplantable carcinoma J.W.A. was able to grow in 100% of susceptible Japanese Waltzing Mice and 0% in non- Waltzing Mice (resistant). Upon crossing waltzing and non-waltzing mice, the F1 hybrid offspring showed 100% tumour susceptibility, suggesting that susceptibility features are inherited dominantly. In F2 hybrids, the ratio of mice with tumour susceptibility to those with resistance was 9:7. Backcrosses between resistant non-waltzing mice and F1 hybrids demonstrated a significant reduction in susceptibility, indicating that the further the genetic composition of the host from the tumour the higher the rejection rate (Little & Tyzzer, 1916). Strong in 1926 experimented with a transplantable mammary adenocarcinoma (dBrB) that originated from the dilute brown (dBr) mouse strain and obtained the same results as Tyzzer in dilute brown (dBr) mouse strain tumour-susceptible, Bagg Albinos (Alb) tumour-resistant strain and F1 and F2 crosses (Strong, 1926a).

1.1.2 Development of Allo-transplantable Tumour

Following these experiments, the histocompatibility barrier was challenged by the reports from Strong of a tumour that could grow in all mouse strains irrespective of the genetic background. In 1926, Strong reported the emergence of an allo-transplantable tumour (dBrCX) that can grow in 100% of transplanted allogeneic hosts. No details were provided of the exact reasons for this emergence, but it happened after introducing the parental tumour into more allogeneic hosts which induced “mutations” that allowed it to grow in mismatched hosts. The mutation happened while maintaining tumours collected from old experiments in F1, F2, and backcross mice by injecting them into syngeneic hosts. The mutated tumour dBrCX showed an acceleration in growth dynamics where it reached 22 to 23 grams in 5 weeks vs 0.5 to 1 gram in 3 months for normal tumours in dBr mice. Subsequent experiments with tumour dBrCX showed that it can grow completely in dBr, F1 Hybrids (dBr × Alb), F2 generation, backcross generations, and Bagg Albinos (Alb) (Strong, 1926b). This experiment was the first to report the gain of mutations that allow tumours to grow in mismatched hosts.

1.1.3 Serial Passaging and Tumour Adaptation

Later in the 1950s, an experimental design of tumour gradual passaging in serially more allogeneic hosts showed the ability to produce tumours that can grow in mismatched hosts. Following earlier experiments which showed a 3-fold increase in the incidence of tumour take in relatively resistant backcross mice by first passaging parental tumours in F1 hybrid mice (BARRETT & DERINGER, 1950). Barrett and Deringer used a mammary adenocarcinoma (C3HBA) originating from the C3H

strain for tumour transplantation studies in C3H, Strain C (BALB/c), and their crosses. They created five groups of tumours which consisted of the original tumour (stock tumour) and other passaged tumours they termed sublines. First subline: Before being tested in backcross hosts, the tumour was grown in F1 hybrids. Second subline: Serial transplantation of tumours in backcross hosts. Third subline: Prior to testing in backcross mice, the tumour from the second subline returned to C3H hosts for several generations. Fourth subline: A tumour that was grown in F1 hybrids for one generation before returning to C3H hosts for several generations.

The comparison of tumour takes between the serially passaged and the non-passaged parental tumours showed an improved tumour takes in the serially passaged when transplanted into backcross mice. The tumour take rate for direct transplantation into backcross (F1 x BALB/c) mice was 8% (15/182 hosts). For the first subline: a 30% tumour take rate (26/86 hosts) was seen in backcross hosts after tumours were first grown in F1 hybrids**.** For the second subline: a 33% tumour take rate (142/427 hosts) was eventually achieved by serial implantation in backcross hosts. This demonstrated how the tumour adapted over many generations to the resistant backcross hosts. For the third subline: tumours that were returned to syngeneic C3H hosts for five generations maintained a high transplantability in backcross hosts with a tumour take rate of 34% (56/163 hosts). This shows that adaptation to backcross hosts was permanent. For the fourth subline: tumours grown in F1 hybrids for one generation and subsequently reintroduced into C3H hosts for five generations showed a tumour take rate of 22% in backcross strain (48/219 hosts) (Figure 1.1). Although less noticeable, the adaptability was nevertheless greater than that of the original tumour (Barrett & Deringer, 1952). This experiment highlights how

tumours have the ability to adapt to mismatched hosts when introduced gradually or by repeated passaging in the same hosts.

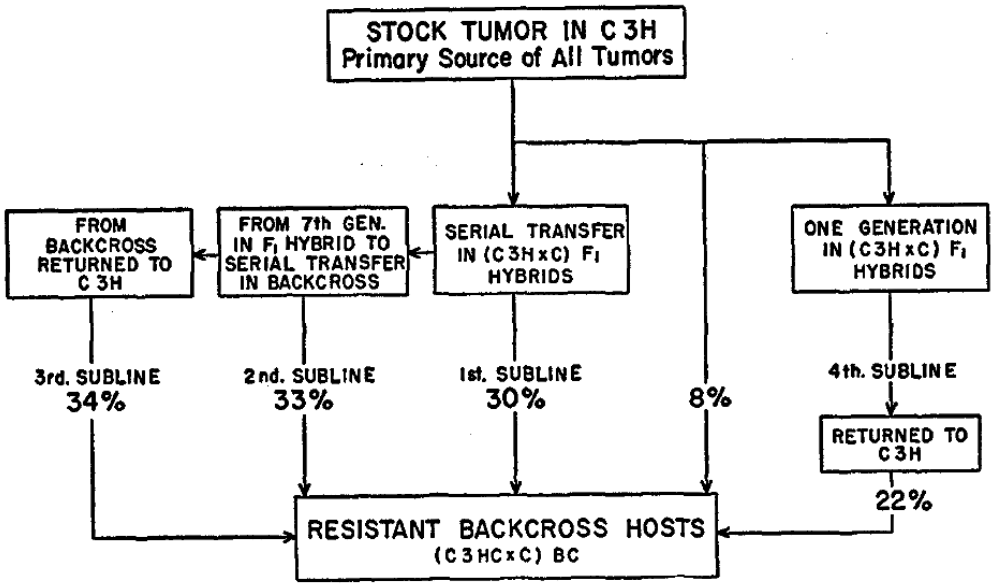

Figure1.1 A diagram illustrating the tumour sublines used and their take ratio in backcross mice.

Adapted from (Barrett and Deringer, 1952)

1.2 The Canine Transmissible Venereal Tumour

Cancer is a disease of genetic mutations more prevalent with aging when multiple mutations accumulate leading to oncogenes activation and tumour suppressor genes deactivation (Uzman et al., 2000). There are 10 hallmarks of cancer that allow it to grow in a living host. One of these is the ability to evade the immune system (Hanahan & Weinberg, 2011). The immune system can differentiate between self and non-self. Yet, in many cancers, a neoantigen gets produced without the ability of the immune system to clear that cancer (Sharma & Allison, 2015). In fact, there are examples of cancers in hosts other than humans that gained the ability to be transmitted as a clonal allograft from an infected host to a healthy recipient with a functioning immune system. These cancers are known as transmissible tumours. Well-known examples of these are the Canine Transmissible Venereal Tumour (CTVT), the soft-shell clam tumours and the Tasmanian Devil Facial Tumour Disease (DFTD) (Siddle & Kaufman, 2015).

1.2.1 CTVT Genetics

CTVT is a unique tumour that is of a clonal origin where the tumour cell itself transmits from the infected dog to a recipient dog. It arose from a single dog (founder dog) about 11,000 years ago and can infect different dog breeds through coitus (Murchison et al., 2014). The clonal origin of CTVT was proven by different methods. First, all CTVT samples included a tumour-specific genetic markers, such as a LINE-1 insertion upstream of the *c-MYC* oncogene, whereas the host tissues did not. Second, the tumour's clonal character is supported by a unique and invariant MHC

haplotype in CTVT cells that differs from the host's MHC alleles. Third, phylogenetic analysis of the tumour MHC sequences, and mitochondrial DNA (mtDNA) confirmed their common ancestry. Fourth, CTVT has a surprisingly stable karyotype with consistent chromosomal markers across geographically and chronologically different samples, while being significantly aneuploid. These findings indicate that there is a single ancestral lineage shared by all tumours (Murgia et al., 2006). The dog genome is diploid with 2n= 78 chromosomes. The CTVT genome is aneuploid and has accumulated 1.9 million somatic mutations and 646 genes deletions (Murchison et al. 2014). CTVT mutations suggest that it was exposed to low doses of UV light during its evolution. These include C>T and CC>TT mutations, which are characteristic of UV-induced DNA damage. These mutations are observed in human cancers that are associated with UV exposure such as skin cancers (Murchison et al., 2014).

CTVT has mutations in tumour suppressor genes. These include a homozygous deletion of *CDKN2A*, which is involved in regulating the cell cycle and inhibiting tumour growth (Murchison et al., 2014). *CDKN2A* is essential for controlling the cell cycle and its loss or inactivation results in uncontrolled cell proliferation, which is a hallmark of cancer development (Ganguly et al., 2016). Also, CTVT shows downregulation or deletion of *RASSF1* (Fêo et al., 2022). The tumour suppressor gene *RASSF1* is well-known for facilitating DNA damage repair. In CTVT, 65% of tumour biopsies show *RASSF1* downregulation with another 35% showing complete absence of expression. This downregulation is linked to tumour progression, indicating that lower RASSF1 expression plays a role in promoting CTVT progression (Fêo et al., 2022).

In addition, CTVT has mutations in oncogenes. The most characteristic mutation is the rearrangement of *MYC*. In this tumour, the *c-MYC* oncogene was rearranged by inserting to the 5' the first exon of a transposable genetic element sequence (LINE, long interspersed element) (Amariglio et al., 1991). Samples of CTVT from around the world showed the existence of the LINE/*c-MYC* insertion suggesting that all the tumours might have arisen from the same dog (Figure 1.2) (Amariglio et al., 1991) (Murgia et al., 2006).

Dogs have diverse genetic backgrounds and Dog leukocyte antigens (DLAs) are very polymorphic (Miyamae et al., 2023). Dogs express DLA class-I DLA-88, along with DLA-12 and DLA-64 and class II DLA genes DLA-DRB1, DLA-DQA1, and DLA-DQB1. CTVT has haplotype DLA-88, DRB1, DQA1, DQB1, which is conserved in all tumours worldwide and is different from the hosts' DLA haplotype (Murgia et al., 2006).

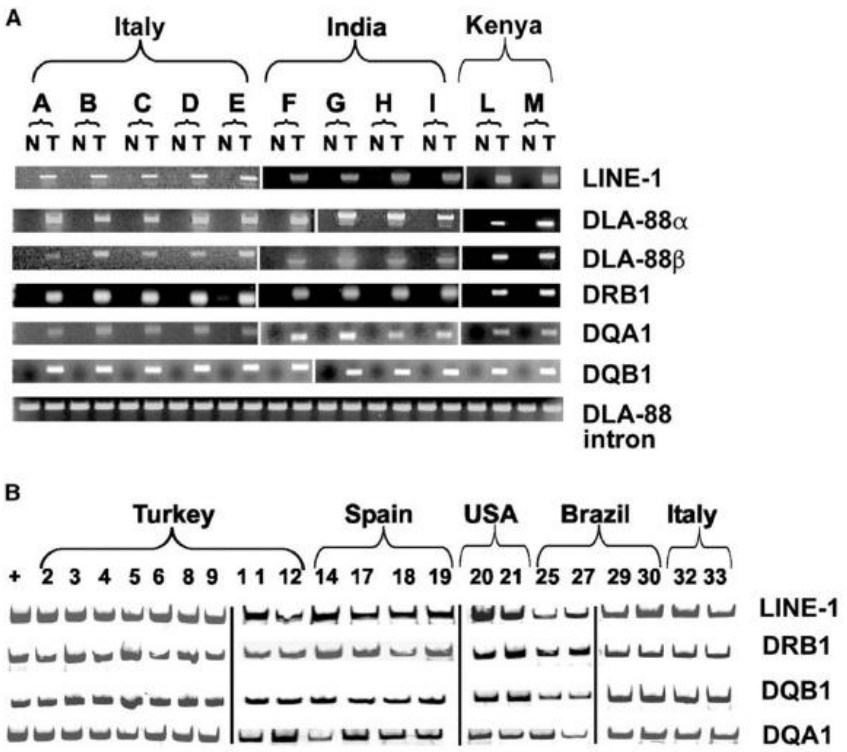

Figure1.2 LINE-*c-MYC* and specific DLA detection in CTVT sample compared to hosts from around the world. Analysis of CTVT and normal tissue from CTVT infected dogs collected from different countries showing the presence of the MYC-LINE-1 insertion and CTVT DLA haplotypes in tumour but not in normal tissue samples.

Adapted from (Murgia et al. 2006)

1.2.2 CTVT Transmission and World Distribution

The primary mode of CTVT transmission is by direct contact during mating, where living cancer cells are transferred between dogs during coitus as an allograft despite DLA polymorphisms, completely bypassing the histocompatibility barrier (Fassati, 2018). Other close contact methods can potentially spread CTVT such as licking or

biting the affected area (Ganguly et al., 2016). At least 90 nations have endemic cases of the disease, and areas with significant stray dog populations—such as sections of South and Central America, Africa, and Asia—have higher prevalence rates (Strakova & Murchison, 2014). While in developed countries, such as the UK, as a result of efficient dog control measures, the prevalence has decreased (Hayes et al., 2023).

1.2.3 CTVT Pathogenesis

In most cases, CTVT is not deadly, and metastasis only happens in 5% of cases. In some of the naturally infected dogs, regression happens spontaneously (Ganguly et al., 2016). After transmission, CTVT progression can be divided into 3 phases. The Progressive Phase (P-Phase), the Static Phase, Regression Phase (R-Phase). During the progressive phase, CTVT exhibits rapid growth and evasion of the host's immune system. In this phase MHC molecules are expressed by only a small percentage (2–5%) of tumour cells. Low MHC-I and MHC-II expression during this period helps the tumour evade immune recognition. In the static phase tumour growth stabilizes. The static phase is considered a transitional phase during CTVT transmission. Despite being less clearly characterised in the literature, this phase is thought to be a precursor to the regression phase. The tumour starts to shrink during the regression phase, due to the immune responses to the tumour. The infiltration of the tumour by Tumour-Infiltrating Lymphocytes (TILs) and their production of inflammatory cytokines such as Interferon gamma (IFN-γ) lead to the upregulation of MHC-I making the tumour more visible (Y.-W. Hsiao et al., 2002; Pai et al., 2011) (Y. W. Hsiao et al., 2008). In this stage, around 40% of tumour cells express MHC

molecules (Pai et al., 2011). Reduced proliferation, increased apoptosis, and increased immune infiltration, especially T lymphocytes, are characteristics of the regression phase. This stage is observed in the tumour's spontaneous remission, which is seen in immunocompetent dogs (Gonzalez et al., 2000).

1.2.4 CTVT Lab Diagnosis

The lab diagnosis of CTVT is based on cytological, immunohistochemical, cytogenetics, and molecular techniques. Histological diagnosis is less used due to the difficulty of differentiating CTVT from other round tumour cells. Cytologically, CTVT has a distinctive morphology with cell shapes ranging from spherical to oval, and they frequently have mitotic figures. CTVT cells have one or two noticeable nucleoli and chromatin clumping. The appearance of numerous transparent cytoplasmic vacuoles is the most distinctive cytological observation (Ganguly et al., 2016). Immunohistochemically, CTVT is stained with a panel of antibodies that target different components of the tumour cells, such as vimentin, lysozyme, *α*-1-antitrypsin and glial fibrillary acidic protein. CTVT is negative for keratins, S100 and muscle markers (Ganguly et al., 2016). Cytogenetics is a powerful tool to diagnose CTVT that provides a definitive diagnosis. CTVT has a distinctive karyotypic appearance, very different from normal cells. The normal chromosome number in dogs is 78 and all chromosomes except two are acrocentric (the centromere is located near one end of the chromosome resulting in one short and one long arms). In CTVT, usually there are 59 chromosomes, and the number could range from 57 to 64. Chromosome morphology also differs from normal cells with 40 or 42 chromosomes having an acrocentric shape, and 15 or 17 having metacentric shapes (the centromere is

located in the middle resulting in roughly similar lengths of the 2 arms) (Figure 1.3) (Ganguly et al., 2016). Molecular Biology also provides diagnostics results of CTVT. Polymerase Chain Reaction (PCR) can be used to detect the LINE-*c-MYC* insertion that is present in CTVT samples from dogs around the world.

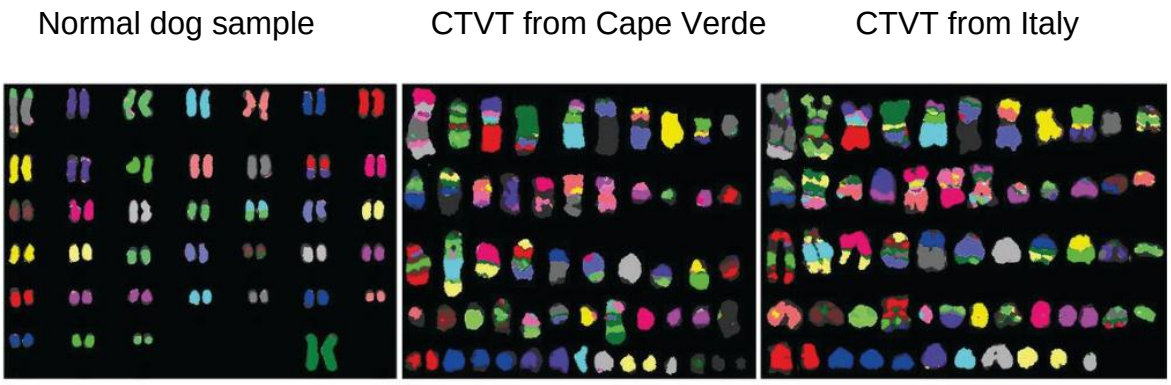

Figure1.3 Fluorescent in Situ Hybridization (FISH) of normal dog and CTVT. FISH of a normal dog sample (left panel), CTVT from Cape Verde (middle), and Italy (right). In normal dog sample 78 chromosomes in diploid arrangements are seen. CTVT samples from Cape Verde and Italy are showing 58 aneuploid chromosomes with different chromosomal additions, deletions, and translocations as indicated by the banding pattern.

Adapted from (Murchison et al. 2014).

1.2.5 CTVT Treatment

The chemotherapeutic agent vincristine sulphate is the most effective treatment for CTVT and is considered the gold standard. Vincristine works mainly by disrupting microtubule formation but also can interact with DNA causing disruption of normal

cell processes. Vincristine mainly inhibits microtubule assembly by binding to tubulin, a protein that builds microtubules, which blocks cell division and results in cell death (Garg et al., 2024). In CTVT-affected dogs, vincristine is typically administered intravenously once a week until tumour regression. Vincristine frequently results in complete remission, though the length of treatment can vary depending on the tumour's size and the surrounding conditions (Ganguly et al., 2016). The Fassati group showed that the immune system plays a major role in regression triggered by vincristine treatment. Tumour regression happens in a stepwise manner where first, the innate immune system gets activated early after treatment. This strong inflammatory response is defined by chemokines such as CCL5 being upregulated. Second, immune cells such as B cells, CD8+ and CD4+ T cells, and Natural Killer (NK) cells get recruited and infiltrate the tumour, which is accompanied by cell cycle arrest and tissue remodelling, leading to tumour clearance (Figure 1.4)(Frampton et al., 2018).

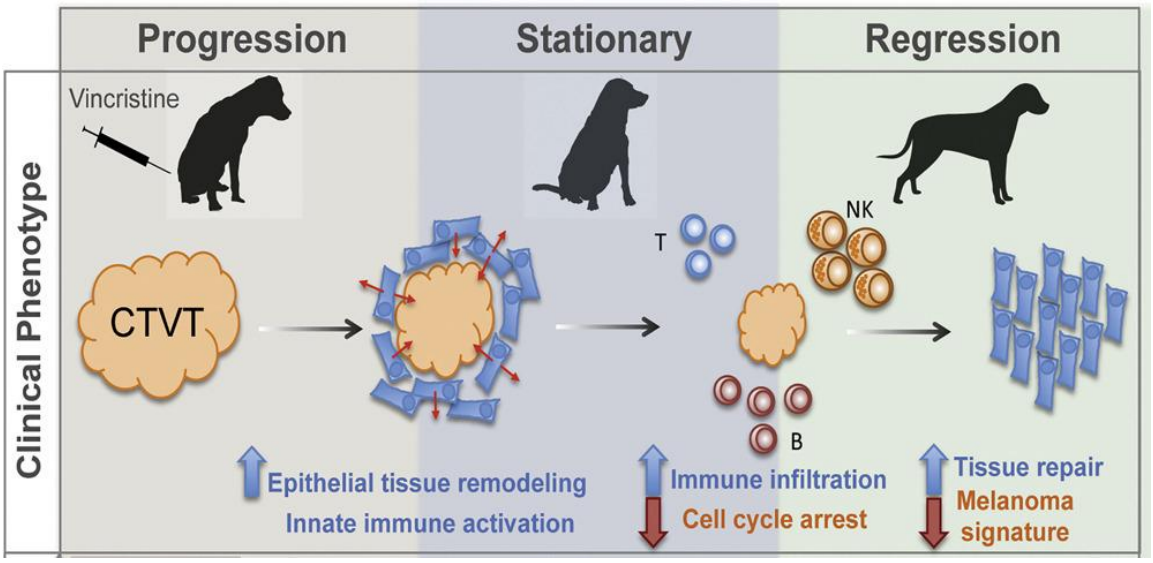

Figure1.4 Immune activation after CTVT treatment with vincristine. Vincristine treatment induced activation of the innate immune system in both tumour and normal epithelial cells surrounding the tumour, tumour growth arrest and tumour infiltration leading to regression.

Adapted from (Frampton et al., 2018,)

1.2.6 CTVT Immune Evasion.

The exact mechanism that led to transmissibility of CTVT is not known but several immune evasion strategies have been reported. These include the downregulation of the MHC-I molecule, the presence of immunosuppressive cytokines such as TGF-β in the Tumour Micro Environment (TME), impaired Dendritic Cells (DCs) function and upregulation of Vascular Endothelial Growth Factor (VEGF) which promotes angiogenesis and inhibit the infiltration of immune cells.

In contrast to many cancers that irreversibly lose MHC expression as a result of structural abnormalities such as deletions of the MHC heavy chain genes, CTVT downregulates MHC molecules through reversible regulatory pathways. This downregulation or loss of expression protects the tumour from immune surveillance and destruction. The reversibility of MHC expression is demonstrated by restoration of MHC expression during the R-phase and *in vitro* by co-culturing CTVT cells with TILs from the R-phase (Y.-W. Hsiao et al., 2002). *In vivo* studies of CTVT showed that the treatment with Interleukin-6 (IL-6) and IFN-γ induced the expression of the MHC molecules (Y. W. Hsiao et al., 2008). This MHC-I downregulation is due to the lack of β2-microglobulin (β2M) expression which is part of the MHC-I complex that is presented on the cell surface (Cohen et al., 1984). Unfortunately, little is known in CTVT on the other Antigen Presenting Machinery (APM) genes which are responsible for assembling and transporting the MHC molecule on the cell surface (Siddle & Kaufman, 2013). TGF-β has a complex dual role in the TME of CTVT, acting as both a tumour suppressor and a tumour promoter depending on the TME's context. During the P-phase, TGF-β1 promotes tumour growth by suppressing Natural Killer (NK) cell function. Moreover, tumour-derived TGF-β1 exerts potent immunosuppressive effects by inhibiting the production of IFN-γ from TILs (Y. W. Hsiao et al., 2008). This suppression prevents the upregulation of MHC-I expression. This immune evasive strategy ensures the tumour's survival and continued growth. Notably, in tumours resistant to vincristine treatment, tumour-derived TGF-β1 exerts an additional deleterious influence by suppressing endogenous TGF-β expression. The suppression of natural TGF-β, which typically mediates tumour suppression through the inhibition of cell proliferation and induction of apoptosis, paradoxically

facilitates tumour proliferation and progression. This dysregulation highlights the important role of tumour-derived TGF-β1 in modulating the tumour microenvironment, effectively hijacking natural growth-inhibitory mechanisms to promote malignancy (Ballestero Fêo et al., 2018).

CTVT has a major effect on the survival and functions of DCs. During the P-phase, CTVT significantly reduces the differentiation, survival, and function of monocyte-derived DCs (Liu et al., 2008). Both immature (iDCs) and mature (mDCs) DCs exhibit downregulation of important markers, including CD1a, CD83, CD80, CD86, and the MHC-I molecule. As a result of MHC-I and MHC-II downregulation, CTVT inhibits DCs' ability to present and uptake antigens, as shown by decreased allogeneic Mixed Lymphocyte Reaction (MLR) responses and endocytic activity (Liu et al., 2008). Tumour-derived soluble factors from progression-phase CTVT induce apoptosis of monocytes and DCs, further depleting the immune system's capacity to respond to the tumour (Liu et al., 2008). In addition, the peripheral blood's monocyte count is reduced by 40% in CTVT-infected dogs. The tumour significantly reduces the efficiency with which mDCs are produced from iDCs and DCs are produced from monocytes (Liu et al., 2008).

VEGF plays a critical role in establishing angiogenesis within CTVT. Very elevated VEGF expression has been reported in CTVT, highlighting its fundamental role in facilitating the tumour’s extensive vascularization and rapid growth. Increased VEGF activity is critical for ensuring the tumour’s survival by providing a continuous supply of nutrients and oxygen required for sustained proliferation and metabolic demands. Unlike many human cancers where elevated VEGF levels are strongly associated with poor prognosis and aggressive metastasises, CTVT's high VEGF expression is

not associated with metastasis (Ballestero Fêo et al., 2018). In other tumours, it has been demonstrated that VEGF inhibits immune infiltration of T-lymphocytes and macrophages. This is achieved by the reduction of NF-κB-induced endothelial activation, which lowers the expression of chemokines CXCL10 and CXCL11 that are important for T-cell recruitment (H. Huang et al., 2015; Turkowski et al., 2018).

1.3 The Tasmanian Devils Facial Tumour Disease

Devils Facial Tumour Disease (DFTD) is a type of transmissible cancer in Tasmanian Devils (*Sarcophilus harrisii*). Its spread among devils led to major declines in their populations, with an estimated 85% reduction in the devil's population since the 1990s. This caused the devils to be classified as an endangered species by the International Union for the Conservation of Nature (IUCN) (Murchison, 2008). The disease takes advantage of the devil's limited genetic diversity which allows the quick spread of the tumour among its population (Murchison et al., 2012). The disease spreads mainly through biting during mating or social interactions, where cancerous cells implant in the wound of the bitten animal. There are two types of DFTD that grow in Tasmanian devils: DFT1 and DFT2. DFT1 emerged in 1986 and DFT2 in 2011 (Stammnitz et al., 2023). DFT2 has emerged independently of DFT1 highlighting the vulnerability of the devils to this disease (Stammnitz et al., 2018).

1.3.1 DFTD Genetics

Although there are genetic differences between DFT1 and DFT2, both tumours have emerged from undifferentiated Schwann cells which are of neural crest lineage (Murchison et al., 2012; Stammnitz et al., 2018). DFT1 affects both male and female devil hosts equally and was initially generated from the cells of a female "founder devil". Conversely, DFT2 originated from a male devil and preferentially infects male hosts, possibly because of the immunogenicity of chromosome Y-derived antigens in female hosts (Stammnitz et al., 2023). The clonal origin of DFT1 was confirmed on the basis of genomic, karyotypic, and mitochondrial DNA evidence. First, the

DFT1 genome has more than 17,000 unique chromosomal structural rearrangements, copy number changes, and somatic base substitutions, many of which are acquired somatically and exist in all DFT1 samples. Second, cytogenetics reveals that DFT1 tumours consistently have a pseudodiploid karyotype with particular chromosomal rearrangements such as deletions on chromosomes 1, 2, and 3 and trisomy of chromosome 5p. These abnormalities exist in all DFT1 samples, independent of location or time period. Third, the mitochondrial genome analysis of DFT1 indicated that all tumours have the same or a very related mitochondrial haplotype. This suggests that the tumours originated from a single female Tasmanian devil, who established the lineage (Murchison et al., 2012).

DFT1 has mutations and deletions of important tumour suppressor genes such as *FANCD2, PTEN, MGA* and *MAST3*. Mutations in the *FANCD2* gene, which is involved in DNA repair, cause genomic instability in DFT1, contributing to cancer progression (Murchison et al., 2012). In DFT1, the *MGA* gene, which inhibits MYC activity, exhibits recurrent truncating mutations. Its function as a crucial tumour suppressor in DFT1 is demonstrated by these loss-of-function changes, which lead to uncontrolled cell growth (Stammnitz et al., 2023). DFT1 shows a mutation in *MAST3,* which regulates the tumour suppressor gene *PTEN*. By attaching to the PDZ domain, *MAST3* interacts with the tumour suppressor *PTEN*, stabilizing it and directing phosphorylation (Valiente et al., 2005).

DFT2 clonal and independent origin is supported by the following evidence: first, DFT2 has a distinct and consistent aneuploid karyotype that distinguishes it from both DFT1 and the host Tasmanian devil. This includes structural abnormalities such as extra material on chromosomes 1, 2, and 4, deletions on chromosome 5, and

monosomy on chromosome 6. Additionally, the presence of both X and Y chromosomes separates DFT2 from DFT1. Second, microsatellite analysis demonstrated that DFT2 tumours have identical genotypes at polymorphic loci, which are distinct from those of their host devils and DFT1. Third, DFT2 has a distinct MHC class I genotype from both DFT1 and the hosts. Taken together, this indicates that DFT2 tumours are not generated from the hosts but rather form a distinct clonal lineage. Finally, the analysis of somatic structural variations reveals no overlap between DFT2 and DFT1. This genetic divergence validates DFT2 as an independently arising transmissible cancer (Pye et al., 2016).

DFT2 shows homozygous deletions of *PTEN* which promotes tumour development and improves survival by inhibiting the PI3K/AKT pathway (Stammnitz et al., 2023). DFT2 demonstrates deletions in *TP73*, a p53 family member that is structurally and functionally similar to the well-known tumour suppressor *TP53*. It contributes to apoptotic cell death and can activate genes that respond to p53 (Stammnitz et al., 2023; Stiewe & Pu, 2002). DFT1 oncogene mutations include *RET*, which is recognized for its function in stimulating cell division (Murchison et al., 2012). DFT1 and DFT2 show amplification of the Platelet-Derived Growth Factor Receptor genes *PDGFRA* and *PDGFRB*, which increases cell proliferation and survival via receptor tyrosine kinase signalling. DFT2 has a higher rate of mutation than DFT1 due to chromosomal rearrangements and enhanced LINE-1 retrotransposon activity (Stammnitz et al., 2023).

Unlike CTVT, DFT1 and DFT2 have some genetic diversity, and subclonal populations play a role in the development and progression of tumours. Genetically different populations of cancer cells can coexist within a single tumour due to intra-

tumour heterogeneity (Stammnitz et al., 2023). Moreover, unlike CTVT, there is no evidence of UV-induced mutagenesis. Specific mutational signatures such as Single Base Substitution Signatures (SBS) SBS1 and SBS5, which are age-related, exist in both DFT1 and DFT2, demonstrating that endogenous age-related mutations are behind tumour evolution rather than externally induced mutagenesis (Stammnitz et al., 2018).

1.3.2 DFTD Transmission and Distribution

The main mode of transmission in devils is biting which is a common practice in mating devils. The disease affects the fitter devils as they are more reproductively active (Woods et al., 2020). Since going extinct on the Australian mainland 3000 years ago, the Tasmanian devil has only been found in the island state of Tasmania (Woods et al., 2018). Since its first discovery in 1996 in northeastern Tasmania, DFT1 has expanded to cover over 80% of the mainland of Tasmania. DFT2 first appeared in southeastern Tasmania in 2014 and is still limited to a smaller geographic area where it started (Woods et al., 2018).

1.3.3 DFTD Pathogenesis

After transmission through biting, DFTD grows rapidly and can reach large sizes. In untreated devils, tumours frequently spread to internal organs, exacerbating the disease severity. Tumours are distinguished by the fast growth of Schwann-like cancer cells, which avoid immune responses due to immune suppressive mechanisms. Tasmanian devils limited genetic variety lowers the chance of immune-

mediated rejection of DFTD cells, which are transmitted as an allograft. DFTD cells avoid immune detection by lack of MHC class I expression, as in DFT1, or by the expression of similar MHC-I alleles to host devils in DFT2. Immunohistochemistry (IHC) showed almost no immune cell infiltration within the tumour. MHC-II+ and CD3+ cells are uncommon, and when present, they were found in the periphery of the tumours or near blood vessels. As the disease progresses, devils exhibit substantial facial abnormalities, difficulty feeding, and ultimately systemic symptoms due to tumour burden and metastasis. Most untreated devils die from malnutrition, subsequent infections, or organ failure caused by metastatic tumours within a year of tumour transmission (Tovar et al., 2017).

1.3.4 DFTD Lab Diagnosis

DFTD can be diagnosed in the lab by histology, immunohistochemistry, cytogenetics, and molecular biology. It has been established that Schwann cells, a type of glial cells that is a component of the peripheral nervous system, are the source of DFTD tumours (Tovar et al., 2011). Therefore, numerous Schwann cell markers are expressed in DFTD tumours which are used in diagnosing DFTD histologically and immunohistochemically. Histologically, large nodular aggregates of tumour cells are frequently produced within a thin, fibrous pseudo-capsule, with minimal fibrovascular stroma supporting the majority of the neoplastic cells. Additionally, cells can be grouped into cords, bundles, or streams and divided by tiny collagen fibres. The cells have a high nucleus-to-cytoplasm ratio and are spherical to polygonal. It is typical to see up to seven mitotic figures in a field (Tovar et al., 2011). Immunohistochemically, different markers are used to identify DFTD with one

marker as the most specific and sensitive to DFTD which is Periaxin. Periaxin is normally expressed in myelinating Schwann cells. Periaxin expression was confirmed in a number of settings, such as primary DFTD tumours, metastases, cultured devil Schwann cells, and murine DFTD cell xenografts. Other markers of Schwann cells such as S100 protein, PMP22, and NGFR are among the other markers expressed in DFTD, but their expression was inconsistent compared to periaxin's consistency and specificity (Tovar et al., 2011). Cytogenetically, there is a diploid number of chromosomes in normal Tasmanian devil cells, which is 2n= 14. In healthy individuals, there are no notable chromosome abnormalities or rearrangements. DFT1 cells exhibit a high level of aneuploidy, exhibiting differences in the number and structure of chromosomes. Chromosomal abnormalities are detected, such as structural alterations in chromosomes 2, 4, and 6. There are new marker chromosomes, known as M1, M2, and M3, which are regularly seen in DFTD samples (Figure 1.5) (Pyecroft et al., 2007). DFT2 cells have a specific aneuploid karyotype that sets them apart from DFT1 and the typical devil karyotype. Additional genetic material on chromosomes 1, 2, and 4 are among the main abnormalities, as well as a deletion in chromosome 5 and chromosome 6 monosomy. Due to its male origin, DFT2 maintains both the X and Y sex chromosomes, in contrast to DFT1. The four unique marker chromosomes (M1–M4) seen in DFT1 are absent from DFT2, confirming its independent origin (Figure 1.6) (Pye et al., 2016).

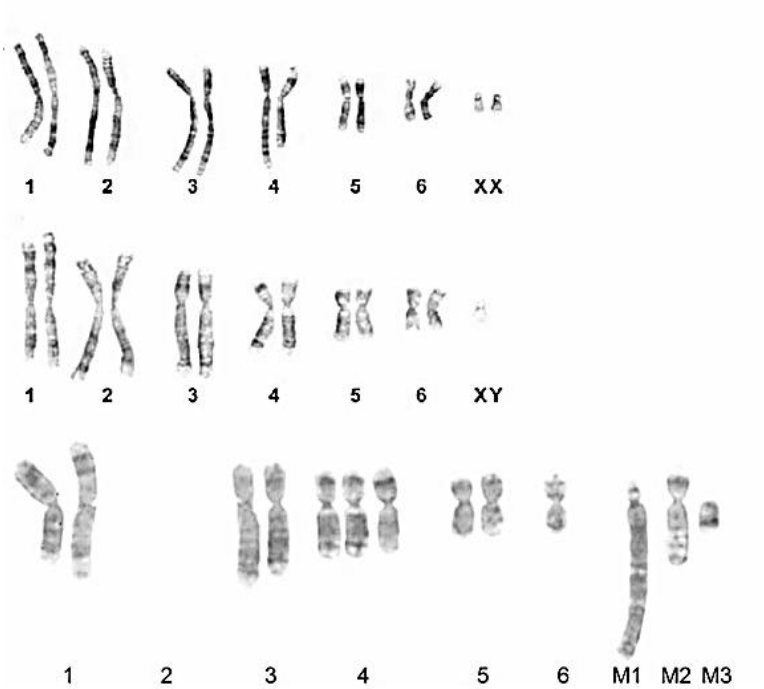

Figure 1.5 Chromosomal differences between DFT1 and Normal Tasmanian devil's cell. Karyotype results of normal Tasmanian devils with 7 diploid chromosomes (upper panel) for female (middle panel) male (lower panel) and DFT1 with deleted chromosome 2, trisomy chromosome 4, monosomy chromosome 6, and the formation of new M1, M2, and M3 markers.

Adapted from (Stephen B. Pyecroft et al. 2007)

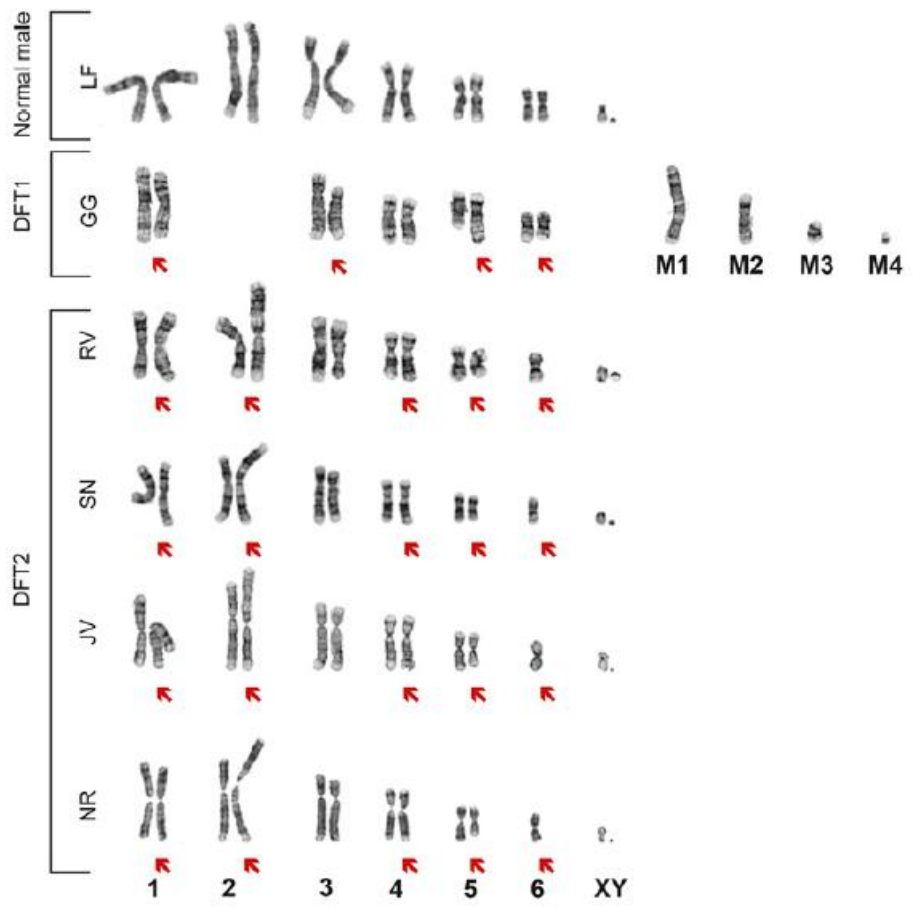

Figure 1.6 Chromosomal differences between DFT1, DFT2 and Normal Tasmanian devil's cells. Karyotype results of normal male Tasmanian devils (upper panel) DFT1 (middle panel) and DFT2 from 4 different samples sharing the same aneuploid karyotype confirming DFT2 is distinct from DFT1 (bottom panel). Red arrows indicate chromosomes with structural abnormalities (additional material to the chromosome, deletions, rearrangements). LF, GG, RV, SN, JV, and NR indicated the name of the sample.

Adapted from (Pye et al. 2015)

DFT1 and DFT2 can be diagnosed by using a PCR technique named “Tasman-PCR”. Tasman-PCR detects tumour-specific interchromosomal translocations unique to DFT1 and DFT2 and not normal cells, ensuring high specificity and sensitivity for detecting these transmissible cancers. Tasman-PCR has shown remarkable sensitivity and specificity, with 93.3% of confirmed DFTD tumours amplifying markers specific to DFT1 or DFT2 (Kwon et al., 2018).

1.3.5 DFTD Therapies

Both DFT1 and DFT2 are fatal diseases that led to a major and quick decline in the Tasmanian devil’s population (Stammnitz et al., 2023). Several therapeutic approaches are being investigated, including immunotherapy and immunisation, and small molecule therapies. *In vitro* treatment with IFN-γ of DFT1 cells leads to MHC-I expression and this strategy is utilized to vaccinate Tasmanian devils with DFT1 cells that are immunogenic (Tovar et al., 2017). Immunisation of healthy Tasmanian devils with DFT1 cells expressing surface MHC-I and adjuvant has showed promise in inducing antitumour responses. In a study, out of 5 immunized Tasmanian devils with immunogenic DFT1 cells and adjuvant, one Tasmanian devil showed no engraftment of the tumour and 3 showed tumour regression, which was associated with immune cell infiltration, predominantly CD3+ T cells and MHC-II+ antigen-presenting cells, and antibody responses against DFTD cells (Tovar et al., 2017). Small molecule treatment with Imiquimod showed promise in different *in vitro* studies. Imiquimod, an immunomodulatory molecule, has been studied for its ability to trigger apoptosis in DFTD cell lines. It promotes antitumour immunity via TLR7 signalling and induce apoptosis through ER stress pathways. Imiquimod therapy

downregulates anti-apoptotic gene expression and upregulates pro-apoptotic gene expression, making DFTD cells more susceptible to immunological responses (Patchett et al., 2016, 2018).

1.3.6 DFTD Immune Evasion

The main mechanism of immune evasion in DFT1 is through the lack of MHC-I expression on the cell surface. This lack of expression in DFT1 is reversible and is caused by transcriptional and epigenetic mechanisms. DFT1 downregulates essential genes in the antigen presentation pathway such as β2m and TAP1 and TAP2. DFT1 cells exhibit >450-fold lower expression of β2m compared to normal fibroblasts. TAP1 and TAP2, antigen-processing transporters, are undetectable or minimally expressed in DFT1 cells (Siddle et al., 2013). The downregulation of β2m and MHC-I genes is mediated by the ERBB-STAT3 axis. The ERBB-STAT3 signalling pathway is hyperactivated in DFT1 cells. This pathway disrupts the transcription of MHC class I-related genes by inhibiting the STAT1 pathway, which is normally involved in promoting MHC expression. Phosphorylated STAT3 sequesters STAT1 in heterodimers, decreasing its ability to regulate target genes such as β2m and MHC-I genes (Kosack et al., 2019). IFN-γ therapy effectively restores MHC class I expression in DFT1 cells. This involves upregulating β2m, TAP1, and TAP2 transcripts and reversing epigenetic repression. *In vivo*, lymphocyte-infiltrated tumours display enhanced MHC class I expression, indicating that the immune interaction with DFT1 cells can cause partial restoration of MHC-I expression (Siddle et al., 2013). Epigenetic modifications that lead to silencing of MHC-I expression include DNA methylation and histone modifications of promoters

of MHC class I-related genes. Similar to the transcription regulation reversal, epigenetic modification can be reversed by IFN-γ therapy or histone deacetylase inhibitors (e.g., trichostatin A) (Kosack et al., 2019; Siddle et al., 2013).

The lack of MHC-I expression should lead to the attack of tumour cells by NK cells. DFT1 is believed to inhibit NK cells' effector function by expression of non-classical MHC molecules. Five nonclassical MHC class I genes, including Saha-UD, Saha-UK, Saha-UM, Saha-MR1, and Saha-CD1, were detected in DFT1. However, there functions in DFTD is still hypothetical and needs more research (Cheng & Belov, 2014; Hussey et al., 2022). Unlike DFT1, DFT2 shows a detectable MHC-I expression in most of the tested tumour samples, suggesting that the development of a contagious cancer such as DFT2 does not absolutely require the absence of MHC-I. However, the MHC class I alleles that are most abundantly expressed in DFT2 cells are either non-polymorphic or common among host devils, which lowers the tumour's immunogenicity (Caldwell et al., 2018). Although DFT2 demonstrates MHC-I expression, there is a trend for MHC-I downregulation with time, possibly as the disease extends to new geographical areas with different MHC alleles (Caldwell et al., 2018).

Another mechanism for immune evasion by DFT1 and DFT2 is the upregulation of PD-L1. In normal conditions, DFT1 and DFT2 cells do not express PD-L1. However, IFN-γ, a cytokine normally generated during immunological activation, causes PD-L1 expression to be strongly upregulated leading to the inhibition of T cell functions (Flies et al., 2016). DFT1 also utilizes phenotypic plasticity and dedifferentiation as a mechanism of immune evasion. DFT1 cells respond to immunological pressure from immunized devils by de-differentiating toward a mesenchymal phenotype.

Reduced expression of Schwann cell markers and increased expression of mesenchymal genes are characteristics of this phenotype. Dedifferentiation promotes resistance to immune-mediated death by increasing tumour cell invasiveness and immunological suppression. During dedifferentiation, the ERBB signalling pathway, which controls Schwann cell myelination, is inhibited. The mesenchymal transition and resulting immunological tolerance are driven by the upregulation of PDGFRA signalling (Patchett et al., 2021).

1.4 Choriocarcinoma

Choriocarcinoma is an uncommon and aggressive malignant tumour that arises from trophoblastic cells, which are components of the placenta during pregnancy. It is divided into gestational and non-gestational forms, with differences in origins, clinical manifestations, and therapeutic approaches. Gestational choriocarcinoma (GC) develops from pregnancy-related tissues and is frequently linked to a Complete Hydatidiform Mole (CHM) or other gestational events. Most occurrences of androgenetic/homozygous XX choriocarcinoma are associated with a genetically related concurrent or preceding CHM (Savage et al., 2017) which is a form of trophoblastic disease during pregnancy that is defined by aberrant placental development in the absence of foetal tissue (Jacobs et al., 1980). Due to the fact that GC carries genetic material from both the mother and a genetically different source (father), GC is considered a hemi-allograft (Redman, 1990). Non-gestational choriocarcinoma (NGC) may develop from germ cells or be linked to somatic high-grade cancers (Mangla et al., 2024). The majority of choriocarcinomas arise from aberrant trophoblastic cells linked with pregnancy, non-gestational choriocarcinomas are rare and occur irrespective of pregnancy (Savage et al., 2017). NGC will not be discussed in this introduction as it is not considered mismatched to the host. Accurate staging and treatment of choriocarcinoma require distinguishing between gestational and non-gestational cases.

1.4.1 Choriocarcinoma Genetics

There are different genetic mutations that drive gestational choriocarcinoma oncogenesis, including mutations in *ARID1A*, *SMARCD1*, and *EP300*, which are involved in chromatin remodelling and were identified as significant driver mutations. *ARID1A* is a tumour suppressor gene, which is frequently mutated in many cancers. In multiple GC samples *ARID1A* displayed inactivating mutations and copy loss, indicating an involvement in tumorigenesis. *SMARCD1* interacts with p53 to regulate apoptosis and cell cycle arrest. Inactivating mutations in *SMARCD1* were discovered in GC, suggesting that its loss contributes to unchecked tumour growth. *EP300* which is a chromatin regulator involved in gene transcription, is mutated in GC, likely disrupting normal cellular control of proliferation (Jung et al., 2020). In addition, choriocarcinoma cell lines show overexpression of the oncogene *MDM2*. *MDM2* (Murine Double Minute 2) is an oncogene that is recognized for its ability to regulate the tumour suppressor p53. MDM2 is an E3 ubiquitin ligase that targets p53 for degradation. This interaction inhibits the p53-mediated tumour suppressive functions, including DNA repair, cell cycle arrest, and apoptosis (Landers et al., 1997).

Frequent chromosomal gains are found in 1q21.1-q44, 12p13.33-p11.1, 3p26.1-p22.2, and 14q, which contain oncogenes that contribute to tumour growth. Chromosomal losses are less prevalent and they include areas such as 8p21-p12. Copy-Neutral Loss of Heterozygosity (CN-LOH) was found in almost all GC cases and identified as a crucial early event in tumour development (Jung et al., 2020). CN-LOH is commonly detected in many cancers. CN-LOH happens when one allele is replaced by a duplicate of the other allele, resulting in a homozygous condition

without modifying the overall allele count. This can happen through processes like mitotic homologous recombination (H. Kim & Suyama, 2023).

1.4.2 Choriocarcinoma Prevalence and Risk Factors

Choriocarcinoma is rare, however it can occur after any type of pregnancy. Its prevalence varies greatly among populations and geographical areas. The incidence is roughly one per 24,096 pregnancies or one per 19,920 live births in the United States, with greater rates among non-white populations (Brinton et al., 1986). In North America and Europe, approximately 1 in 40,000 pregnant women get choriocarcinoma (Wahaibi et al., 2020). The prevalence is higher in Japan and Southeast Asia, at 9.2 per 40,000 pregnant women (Wahaibi et al., 2020). In Saudi Arabia, choriocarcinoma is very rare, with the majority of data obtained from case reports (Nasr et al., 2022). Risk factors for developing choriocarcinoma include age, race, pregnancy factors and some medications. Women under the age of 20 and those over the age of 40 have a higher incidence (Baltazar, 1976). Incidence rates are higher among non-white populations, such as African American, Asian, and American Indian women (Smith et al., 2003). There is increased risk in women with a history of foetal waste and with women with a history of prior molar pregnancies (Baltazar, 1976). Long-term use of oral contraceptives is linked to a higher risk of developing choriocarcinoma too (Wahaibi et al., 2020).

1.4.3 Choriocarcinoma Pathogenesis

GC is the result of residual abnormal trophoblastic cells, which are a component of the placenta, such as placental giant cells or intravascularly growing trophoblasts near the placenta. It is frequently the result of previous gestational events, including the most prevalent precursor, the hydatidiform mole. The disease may first appear immediately after pregnancy or years later, with cases being reported as far back as 25 years post-pregnancy (Mangla et al., 2017). The tumour is the result of genetic and cellular abnormalities in trophoblasts. GC starts at the uterine lining where the trophoblasts reside. Adjacent tissues, such as the uterine wall and pelvic structures, may be invaded by GC. Due to angiogenesis and vascular invasion and the immune evasion ability of GC, it can spread systemically. GC spreads predominantly via the bloodstream to the vagina, liver, brain, lungs, and kidneys. Symptoms caused by GC metastasis include abnormal uterine bleeding (vagina metastasis), haemoptysis (if lungs are involved), neurological symptoms (with brain metastases), and abdominal pain or jaundice (in liver involvement). However, even in metastatic stages, GC is highly treatable with appropriate chemotherapy (Brewer et al., 1978).

1.4.4 Choriocarcinoma Lab Diagnosis

Choriocarcinoma can be detected by checking serum levels for elevated pregnancy hormones, immunohistochemistry, chromosomal analysis, and molecular biology techniques. Beta human Chorionic Gonadotropin (beta-hCG) is a hormone produced normally in pregnancy, but GC beta-hCG levels can be three to 280 times higher than the highest values observed during a normal pregnancy. The beta-hCG to hCG ratio is much higher in choriocarcinoma compared to normal pregnancy (Ozturk et

al., 1988). Immunohistochemistry staining to detect elevated levels of beta-hCG is also used for the diagnosis of GC (Al-Attar et al., 2021). FISH technique is used to identify the presence of X and Y chromosome centromeres, which helps confirm the gestational origin of choriocarcinomas (Whaley et al., 2020). PCR-based microsatellite DNA assays are used to identify non-maternal (androgenic) genetic material, which verifies the tumour's gestational origin (Cankovic et al., 2006).

1.4.5 Choriocarcinoma Treatment

Chemotherapy is the standard of care for treating gestational choriocarcinoma. The treatment regimen is tailored according to the International Federation of Gynaecology and Obstetrics (FIGO) risk score. The FIGO scoring method divides patients into low-risk (score 0–6) and high-risk (score ≥7) groups. Low-risk GC can be effectively treated with single-agent chemotherapy, primarily Methotrexate (MTX) or actinomycin D. MTX works by firmly attaching itself to Dihydrofolate Reductase (DHFR) and inhibiting its activity (Bogani et al., 2023). Because of this inhibition, dihydrofolate cannot be converted to tetrahydrofolate, which is a prerequisite for the synthesis of purines and thymidylate, both of which are critical for DNA replication and cell division (Huennekens, 1994). Actinomycin D causes cancer cells to undergo apoptosis and cell cycle arrest. It causes cell death by activating the p53-dependent pathway, especially in cells with wild-type p53. Low dosages of actinomycin D are used in cyclotherapy to target cancer cells while protecting healthy cells (Guijarro et al., 2021). MTX regimens, particularly the 8-day treatment with leucovorin rescue, are widely utilized. With these regimens, up to 95% of low-risk cases go into remission (Bogani et al., 2023).

High-Risk GC requires multi-agent chemotherapy. The EMA-CO regimen (Etoposide, Methotrexate, Actinomycin D, Cyclophosphamide, and vincristine) is the standard protocol, achieving cure rates of 91–93% (Bogani et al., 2023). Etoposide stabilizes the DNA-topoisomerase II complex, inhibiting the re-ligation of cleaved DNA strands. This stabilization leads to an accumulation of DNA Double-Strand Breaks (DSBs), which are cytotoxic and may end in cell death if not adequately repaired (Montecucco et al., 2015). Cyclophosphamide acts mainly as an alkylating agent, creating cross-links in DNA that result in cellular apoptosis. This process is facilitated by its active metabolite, phosphoramide mustard, which triggers apoptosis in cancer cells by causing irreversible DNA damage (Voelcker, 2020).

Immune checkpoint inhibitors, such as PD-L1 inhibitors (e.g., pembrolizumab, avelumab), have demonstrated potential in chemotherapy-resistant GC and clinical trials have shown significant remission rates (Bogani et al., 2023).

1.4.6 Choriocarcinoma Immune Evasion

PD-L1 is highly expressed in trophoblasts in normal placentas, which provides immune tolerance at the foeto-maternal interface. PD-L1 is very intensely expressed in trophoblast cells of choriocarcinoma which enables immune evasion by suppressing T-cell activity. In GC tumours, PD-1-positive immune cells, including T cells, were identified, particularly in areas with a high prevalence of lymphocytes. This suggests that PD-L1-expressing tumour cells are actively suppressing the immune system (Veras et al., 2017). The Human Leukocyte Antigen Class I (HLA-A, HLA-B, HLA-C) expression varies in GC cell lines. In comparison to normal cells,

choriocarcinoma cells, including JEG-3 and BeWo, demonstrate a substantial decrease in HLA-A gene transcription. The HLA-A downregulation is attributed to genetic mutations in the enhancer elements of the proximal promoter region which is a major regulatory site of HLA-A expression. Unlike other reversible MHC tumour expression, the HLA-A expression in these choriocarcinoma cells is not inducible by IFN-γ, a cytokine that typically upregulates MHC class I expression. This absence of response highlights the tumour cells' ability to employ a robust immune evasion strategy (Lefebvre et al., 1999). The non-classical MHC molecules HLA-G and HLA-E are naturally expressed on the surface of trophoblasts where they play an important role in immune tolerance for the foetus (Apps et al., 2009). HLA-G and HLA-E expression are detected in the choriocarcinoma cell lines JEG-3 and JAR cells respectively (Gobin et al., 1997a). JEG-3 and JAR demonstrate resistance to NK cell lysis, and this resistance is primarily independent of HLA class I expression. The susceptibility to NK lysis was not increased by attempts to reduce HLA class I levels through acid treatment or masking with monoclonal antibodies (mAbs), highlighting the inhibitory function of non-classical HLA molecules (Avril et al., 1999). HLA-E works by binding the immune checkpoint receptor NKG2A on NK cells leading to inhibition of their activation and proliferation. Additionally, high expression of HLA-E in the tumour microenvironment results in the preferential expansion of the dysfunctional NKG2A+ NK cells (Kaulfuss et al., 2023). HLA-G promotes immune tolerance by interacting with the inhibitory receptor ILT2. This interaction leads to strong inhibitory signals that suppress the cytotoxic capacity of NK (Favier et al., 2010).

1.5 Bivalve Transmissible Neoplasia

Disseminated neoplasia (DN) is a leukaemia-like cancer in bivalves (e.g., clams, mussels, and oysters) characterised by the proliferation of abnormal, anaplastic cells in the haemolymph (circulatory system) (Martín-Gómez et al., 2013). There are many types of DN in bivalves but in the 2010s a transmissible type of DN called Bivalve Transmissible Neoplasia (BTN) was identified. BTN can spread between individual bivalves, such as clams and mussels, through the transmission of cancerous cells. Different independent types of BTN were identified that arose from different lineages and can infect different species (Hammel et al., 2022; Skazina et al., 2021a; Skazina, Ponomartsev, et al., 2023a). Each species typically hosts a distinct BTN lineage, and these lineages arose independently. However, rare cases of cross-species transmission have been documented, demonstrating BTN's ability to adapt and spread in certain marine environments. Over 10 BTN types were identified that affect over 20 species of bivalves (Bruzos et al., 2023; Metzger et al., 2015a, 2016; Weinandt et al., 2024). BTN was discovered in different geographical locations and is causing significant challenges to the marine ecosystem.

1.5.1 BTN Genetics

The clonal origin of BTN was confirmed by: first, nearly identical genotypes were found in cancer cells from several hosts in various places in New York, Maine, and Prince Edward Island. Differences between these genotypes and the genetic profiles of the host animals indicated that the cancer cells were spread from another source rather than starting in the specific host. Second, all cancerous haemocytes had the

Steamer retrotransposon, which is linked to tumour growth, at particular integration sites. A single clonal origin is strongly suggested by the fact that these integration sites were the same in samples from various geographic locations. Third, cancerous cells had unique mtDNA single nucleotide polymorphisms (SNPs) that distinguished them from host tissues. These mtDNA changes were shared by all cancerous cells, which further supports clonal transmission. Fourth, all leukemic samples displayed the same patterns for microsatellite loci in cancer cells. The microsatellite profiles of the host tissues varied, highlighting the fact that the cancer cells were a clonally transmitted lineage rather than being generated from the hosts' genomes. Fifth, tetraploid and aneuploid DNA content, a sign of clonal growth, was seen in cancer cells. All leukemic clams had the same abnormal ploidy level, which suggests a common ancestor. Sixth, leukaemia was effectively produced by transplanting malignant haemocytes into healthy clams. This direct experimental evidence showed that cancer cells spread the disease horizontally by acting as infectious agents (Metzger et al., 2015b).

Bivalve cancers exhibit many similarities to the genetic profiles of oncogenes and tumour suppressor genes shown in humans. The *Mytilus trossulus* Bivalve Transmissible Neoplasia 2 (MtrBTN2) lineage, which infects Blue Mussel, for example, shows activation in six of the ten key oncogenic signalling pathways often dysregulated in human cancers. (e.g., Hippo, Notch, Wnt, Myc, PI3K, and Cell Cycle pathways) (Burioli et al., 2023). For example, PI3K/AKT signalling was highly activated, with lower expression of its negative regulators. (*PTEN* and *PIK3R1*), which are known tumour suppressor genes. This activation promotes cell growth, metabolism, and survival. The *Cyclin D1* gene (*CCND1*), a major driver of cell cycle

progression, was significantly upregulated, facilitating unchecked proliferation in MtrBTN2 cells (Burioli et al., 2023). Other genes related to the cell cycle, such as members of the anaphase-promoting complex (*ANAPC1, ANAPC4, ANAPC5*), were also overexpressed, promoting tumour progression (Burioli et al., 2023).

MYC, an important oncogene that promotes cell proliferation and metabolic reprogramming has missense substitutions in its transcriptional activation region, indicating a strong oncogenic involvement in MtrBTN2 cells (Burioli et al., 2023).

Wnt pathway activators, such as *CTNNB1* and *APC*, were overexpressed, while negative regulators like *SFRP1* were suppressed, indicating pathway activation (Burioli et al., 2023).

The *p53* gene, known for its role in DNA damage repair and apoptosis, exhibited mutations unique to MtrBTN2, including synonymous and missense substitutions. *p53* ability to inhibit tumours may be compromised by these alterations. *MDM2*, a regulator of *p53*, showed several distinct mutations that could impair its ability to regulate apoptosis, promoting tumour growth (Burioli et al., 2023).

1.5.2 BTN Transmission and World Distribution

The transmissible cancer in Mya arenaria (soft-shell clam) is traced back to a single founder clam, with all current cancer cases descending from this origin. The cancer lineage is estimated to be between 344 to 877 years old, indicating it has been spreading undetected for centuries (Hart et al., 2022). It is transmitted by cellular transmission of neoplastic cells in an infected host to another clam (Metzger et al., 2015b). Different BTN cancers have been detected around the world. This includes

the North Pacific and Barents Sea, the Subarctic Sea of Okhotsk, the Southern Baltic Sea, Puget Sound and Washington Coastline, the French Atlantic Coast, and South America and Europe (Hammel et al., 2024; Michnowska et al., 2022; Skazina et al., 2021b; Skazina, Odintsova, et al., 2023; Skazina, Ponomartsev, et al., 2023b).

1.5.3 BTN Lab Diagnosis

Different techniques used to diagnose BTN in the lab including histology, flow cytometry, and molecular techniques. Tissue histology remains the gold standard for diagnosing BTN, providing details of the cellular morphology and structure of neoplastic tissues. Tissue histology for BTN involves calculating the Nuclear-to-Cell Ratio (NCR) by measuring the cell and nucleus area of both healthy haemocytes and neoplastic cells, which can reveal information about the abnormal characteristics of neoplastic cells. (Skazina, Odintsova, et al., 2023). Flow cytometry identification of DN in general including BTN is based on the detection of aneuploid cells (higher DNA content). Additional cell populations of aneuploid cells are indicative of neoplasia. DN is suggested if mussels' haemocytes contain at least 5% aneuploid cells among normal haemocytes. (Skazina, Odintsova, et al., 2023). Specific cancer lineages and their genotypes are identified using molecular approaches, such as mtDNA sequencing and the screening for the presence of specific loci known to be diagnostic for BTN including the nuclear elongation factor 1α (*EF1α*). This method helps in distinguishing between different BTN lineages, such as MtrBTN1 and MtrBTN2, and in detecting genetic chimerism, a hallmark of transmissible cancer (Hammel et al., 2022; Skazina et al., 2021a; Skazina, Ponomartsev, et al., 2023a).

1.5.4 BTN Immune Evasion

The immune system of bivalves is not fully understood yet. However, recent advances in the field of bivalve immunity showed that mussels have cellular and humoral immunity (Bouallegui, 2019).

1.6 Human Cases of Cancer Transmission

Human-to-human cancer transmission is an extremely uncommon occurrence; however, it can happen under specific circumstances. These include accidental transmission either in organ transplantation from a tumour carrying donor or during surgery to remove tumours, transplacental transmission from the mother to the foetus, and the transmission from mother to infant during labour.

1.6.1 Accidental Transmission

A surgery was performed in 1996 on a 32-year-old patient who had malignant fibrous histiocytoma, a kind of sarcoma. During the surgery, a 53-year-old surgeon unintentionally cut their hand using a tumour-cell-contaminated scalpel. The wound site was immediately disinfected and dressed (Gärtner et al., 1996). At the site of the injury, the surgeon discovered a tumour five months later that was genetically and histologically identical to the patient's tumour. The surgeon's and patient's tumours were classified as malignant fibrous histiocytomas of the storiform–pleomorphic subtype (Gärtner et al., 1996). Histologically, the tumours had the same cellular morphology, which included fibroblast-like and histiocyte-like cells with multiple mitotic figures and necrotic regions. HLA typing of HLA-DRB1 and HLA-DQB1 alleles revealed total mismatches between the tumour and the surgeon's HLA, confirming that the tumour cells transferred from the patient and that the tumour is not from the surgeon's tissues (Gärtner et al., 1996).

1.6.2 Transplacental Transmission

Maternofoetal transmission of maternal cancer happens when cancer cells from the mother cross the placenta into the foetal circulation. There have been about eighteen cases of this reported, including uterine cancer, lung cancer, leukaemia, and melanoma. (Arakawa et al., 2024). In a case of maternal melanoma transmission, a 6-month-old boy had a tumour in his temporal bone and left middle ear. The mother passed away few weeks after giving birth due to metastatic melanoma. Histological analysis of the tumour showed small to medium-sized cells with eosinophilic cytoplasm that was poorly defined and oval to round nuclei. (Raso et al., 2010). IHC revealed that the tumour was melanoma and was positive for the markers S100, HMB-45, and BAF47 and negative for epithelial membrane antigen, CD3, CD20, and other markers, ruling out other types of paediatric tumours. (Raso et al., 2010). The maternal origin was confirmed by tumour biopsies that showed a XX chromosomal profile in more than 60% of the tumour cells. The results were verified using FISH, which revealed similar maternal-derived XX cells in the tumour. (Raso et al., 2010). These results highlight how maternal melanoma cells can penetrate the placenta and develop into a tumour in the developing foetus.

1.6.3 Vaginal Transmission During Labour

In Japan two cases of paediatric lung cancer in a 23-month-old and 6-year-old boys were reported. Both cases involved vaginal deliveries of infants born to mothers with undetected cervical cancer. Tumour cells from the mothers' cervical carcinomas were likely transmitted to the infants through aspiration of vaginal fluids contaminated with tumour cells during delivery (Arakawa et al., 2021).

This process is distinct from the more frequently documented transplacental transmission, in which cancer cells from the mother enter the foetus's bloodstream through the placenta (Arakawa et al., 2021). Clinically, Patient 1: the 23-month-old boy was found to have neuroendocrine lung cancer, which was genetically and histologically identical to his mother's cervical tumour. Patient 2: The 6-year-old boy had lung mucinous adenocarcinoma, which was genetically identical to the cervical cancer of his mother (Arakawa et al., 2021). Shared mutations between the tumours in the mother and the baby were discovered by next-generation sequencing. Patient 1 had KRAS (c.G38A:p.G13D) and TP53 (c.G853A:p.E285K) mutations. While Patient 2 had KRAS (c.G35A:p.G12D) and STK11 (c.464+1G→A) mutations (Arakawa et al., 2021). The clonal transmission was confirmed by the presence of exonic SNPs from the mothers' tumours in both children, which were not present in the children's germline DNA (Arakawa et al., 2021).

1.7 Antitumour/ Allograft Immune Responses

The immune system plays an important role in detecting and clearing transformed cells as well as recognizing allogeneic grafts and destroying them. Both responses involve cells such as T cells, NK cells, DC among others (Böttcher et al., 2018) (Benichou & Thomson, 2009). Because transmissible cancers involve the transmission of an allogeneic tumour, its rejection may depend on immunological mechanisms involved in both allograft and tumour recognition.

1.7.1 Antitumour Immune Response

Different events take place in a successful anti-tumour immune response. NK cells recognize stress molecules and unusual features such as the absence of MHC-I expression or stress signals on transformed cells and directly lyse them (Bald et al., 2020). NK cells also help in recruiting DCs to the tumour (Böttcher et al., 2018) that detect neoantigens and immunogenic antigens produced by dead cancer cells (Bald et al., 2020). These antigens are then presented to the T Cell Receptor (TCR) loaded on MHC-I and MHC-II molecules, alongside a co-stimulatory signal such as CD28/(CD80, CD86), leading to the activation, proliferation and differentiation of effector Cytotoxic T Cells (CTLs) (Nunès & Olive, 2021). The co-stimulatory signals are essential for an effective immune response against tumours since T cell activation without co-stimulation can result in immunological tolerance, apoptosis, or T cell anergy (Appleman & Boussiotis, 2003). Activated T cells then migrate to the tumour site and infiltrate the tumour. These T cells recognize tumour antigens presented on MHC-I and kill these cells by granzymes, perforins, and Fas dependent

killing (Andersen et al., 2006), (Tay et al., 2021) (Dolina et al., 2021; Klement et al., 2018; Topham & Reilly, 2018) (Ben-Shmuel et al., 2020).

1.7.2 Allograft Immune Response

There are 2 types of allorecognition of an allograft by T cells, direct and indirect. Direct allorecognition happens when recipient T cells encounter allogeneic MHC molecules presented by the donor's "passenger" DC. This interaction can involve CD4+ or CD8+ T cells and lead to robust polyclonal T cell response involving 10% of the peripheral T cell repertoire (Benichou et al., 2011). As a result of this response, CD8+ T cells kill the donor cells leading to acute transplant rejection. Depletion of donor's graft DCs leads to prolonged graft survival (Boardman et al., 2016). This reaction is short in duration as the donor's DCs are eliminated (Benichou & Thomson, 2009). Indirect allorecognition happens when the donor's allopeptides are presented on the MHC molecule of the recipient DCs into T cells. The resulting immune response is less robust compared to the direct allorecognition and directed to one or a small number of the donor MHC antigen's dominant determinants (Benichou et al., 2011) (Benichou & Thomson, 2009). However, this response persists leading to chronic rejection of the allograft (Benichou & Thomson, 2009).

Tregs serve an important function in suppressing the immunological response to the donor alloantigens, which prevent graft rejection. Tregs are particularly effective in suppressing the indirect allorecognition pathway, which leads to "linked suppression", which make effector T cells recognizing other antigens on the same APC tolerant to these antigens (Walsh et al., 2004). Tregs function by

downregulating the expression of costimulatory molecules (e.g., CD80, CD86) and MHC class II on the APCs, limiting their ability to activate effector T cells. These APCs become tolerogenic, where they present antigens in a manner that induce suppression instead of activation (Walsh et al., 2004).

There are different mechanisms for allograft rejection depending on the tissue being transplanted. Skin allografts, for example, are characterised by acute rejection, where the graft is rejected 10-14 days after transplantation (J. Zhou et al., 2013a). Following vascularization of the skin graft, the donor's DCs migrate from the graft to the draining lymph node and prime the recipient's T cell either directly or indirectly by presenting the donor antigens to the recipient T cells or APCs respectively. Upon activation, CD8+ and CD4+ T cells recognize the allograft antigens and lyse them by granzymes, perforins, and Fas dependent killing (J. Zhou et al., 2013a). CD4+ T cells also can perform effector functions through the secretion of IFN-γ and Tumour Necrosis Factor α (TNF-α) (Tay et al., 2021). In the case of an allograft encounter, they detect the mismatched MHC molecule and then attack that graft (Dolina et al., 2021; Klement et al., 2018; Topham & Reilly, 2018).

NK cells can play a dual role, where they can either support rejection or delay it. NK cells are recruited to the graft due to the transient inflammation associated with transplantation. After their recruitment, NK cells exercise their cytotoxic activity on the graft contributing to rejection. Conversely, NK cells can attack the donor's DCs preventing them from presenting the donor's antigens to T cells leading to the delay of rejection (Wang et al., 2017a) (Reeves & James, 2017a).

1.8 Hypothesis and Aims

The mechanisms of how CTVT and DFTD became transmissible are unknown. Due to the lack of archival samples for both CTVT and DFTD, studying their evolution to be transmissible is not possible.

Therefore, in this project, we sought to evolve a transplantable tumour similar to CTVT in mouse models which will have many benefits. First, this will represent a good model to learn about evading the histocompatibility barrier. Second, it will be a model to learn about cancer tolerance. Finally, by understanding why these allografted tumours are not rejected and the immune tolerance/evasion mechanisms deployed by these tumours. These immune tolerance/evasion mechanisms could be applied to address medical challenges such as allogeneic rejection. The understanding of these mechanisms could also improve immunotherapies by targeting the molecules responsible for tolerance especially since different cancers employ similar strategies to evade the immune system (Lawson et al., 2020; Vinay et al., 2015).

1.8.1 Hypothesis

Serial passaging of melanoma cells YUMM1.7 into progressively more allogeneic mice will lead to tumour escape of allogeneic rejection.

1.8.2 AIMS

1- Generate the transplantable tumour

2- Evaluate the tumour microenvironment

3- Study the evolution of the tumour across the passages

4- Identify the mechanisms of immune evasion

2

Materials and Methods

Chapter 2: Materials and Methods

2.1 Materials

2.1.1 Buffers and Solutions

FACS buffer 1% FBS, 0.05% sodium azide, 5mM EDTA in PBS (1L):

10ml FBS

500µl NaN_3

10ml 0.5M EDTA

1L PBS

Tissue Lysis Buffer (20 ml):

Tris-Cl (1 M, pH 8.0-8.5): 2.0 ml

NaCl (5 M): 0.8 ml

SDS (10% in sterile H2O): 0.4 ml

EDTA (0.5 M): 0.2 ml

Sterile dH2O: 16.6 ml

2.1.2 Commercial Reagents, Enzymes and Antibodies for *In Vivo* Studies

Reagent	Catalogue	Source
RNeasy Mini Kit	74104	Qiagen
Phenol:Chloroform + Tris Buffer	11886714	Thermo Scientific

PROTEINASE K - SOLUTION	A4392.0005	VWR
Polybrene	SC-134220	INSIGHT BIOTECHNOLOGY LTD
Collagenase, Type IV, powder	10780004	Gibco
RBC Lysis Buffer (10X)	420301	Biolegend
FuGENE 6 Transfection Reagent	E2691	Promega
Cyto-Fast™ Fix/Perm Buffer Set	426803	Biolegend
*InVivo*Pure pH 7.0 Dilution Buffer	IP0070	BioXCell
*InVivo*MAb anti-mouse PD-1 (CD279)	BE0146	BioXCell
*InVivo*MAb anti-mouse Nonclassical MHC Class I molecule Qa-1b	BE0165	BioXCell
*InVivo*MAb mouse IgG1 isotype control, unknown specificity	BE0083	BioXCell
RU.521	HY-114180	MCE MedChemExpress
Mouse CXCL10/IP-10/CRG-2	DY466-05	R&Dsystems
Mouse CCL5/RANTES	DY478-05	R&Dsystems
DuoSet Ancillary Reagent Kit 3	DY009	R&Dsystems
QIAGEN Plasmid Midi Kit	12143	Qiagen

One Shot™ Stbl3™ Chemically Competent *E. coli*	C737303	Invitrogen

2.1.3 Table of Antibodies for Flow Cytometry

Marker	Fluorochrome	Catalogue	Source
MHC-II (I-A/I-E)	Alexa Flour 700	56-5321-82	Invitrogen
CD3	APC	17-0032-82	Invitrogen
CD11c	PE/Cy7	117318	Biolegend
CD335 (NKp46)	PE	12-3351-82	Invitrogen
CD4	FITC	116003	Biolegend
CD11b	BV711	101241	Biolegend
Gr-1	BV510	108437	Biolegend
CD8α	BUV805	612898	BD Bioscience
CD45	BV421	563890	BD Bioscience
F4/80	APC-eFlour780	47-4801-82	Invitrogen
H-2Db	PerCP/Cy5.5	111518	Biolegend
H-2Kb	Pacific Blue	116514	Biolegend

CD45	Alexa Flour 700	103128	Biolegend
CD44	APC	103012	Biolegend
H2-Kb	FITC	116505	Biolegend
H-2Db	FITC	111505	Biolegend
PD-1	BV711	135231	Biolegend
CD69	APC-eFlour780	104526	Biolegend
CD4	PerCP/Cy5.5	100434	Biolegend
CD3	BUV395	563565	BD Bioscience
Qa-1(b)	BV510	744386	BD Bioscience
PD-L1	PE	124308	Biolegend

2.2 Methods

2.2.1 Mice

6-8 weeks old inbred C57BL/6 (B6), BALB/c, CBA/Ca and FVB/N mice were acquired from Charles River and Envigo. For breeding, 2 males and 2 females breeders were set to get litters for the required mouse strains. Male and female mice were used for tumour implantation studies in equal ratios. C57BL/6, F1 (B6 x BALB/c), F2 (F1 x F1), N2 (F2 x BALB/c) crosses, BALB/c, were used in this project. All experiments were performed in accordance with UK Home Office regulations, project license number PP2330953 and number PC79FA7AB under study approval and supervision from the BSU at UCL in accordance with the 3R (Replacement, Reduction, Refinement) Principles. Genotyping was done using the Mini Mouse Universal Genotyping Array (MUGA) platform by Transnetyx on tumour or spleen cells.

2.2.2 Tissue Culture

YUMM1.7 were obtained from the American Tissue Culture Collection (CRL-3362). YUMM1.7 and dissociated tumour cells were grown in DMEM/F-12 media (Gibco) supplemented with 10% FBS (Labtech), 1% non-essential amino acids (Gibco), and 1% penicillin/streptomycin (Gibco). In t25 or t75 flasks and incubated at 37°C at 5% CO2 levels. Cells were passaged every 2-3 days at 70-80% confluency.

2.2.3 Tumour Transplantation

Tumour cells were grown *in vitro* for 2 to a maximum of 4 passages. Cells were suspended in sterile PBS at 10 million cells/ml and prepared for injection. Mice were anaesthetized, weighted, ear clipped, shaved at the site of injection and injected in the left flank area with 1 million cells in 100 µl PBS. Mice were monitored daily for tumour growth and their general health was assessed using the BSU scoring system. Mice weights were monitored and recorded on a bi-daily basis. Tumours were measured by calibre at regular intervals and if tumours reached 15 mm in diameter, the mice were culled, and tumours and spleens were collected for analysis. Tumour volume was calculated using this formula: 0.5 x Length x Width^2 (0.5 x L x W^2)

2.2.4 Tumour and Spleen Dissociation

Tumours were dissociated using the following protocol (Quintana et al., 2008). Tumours were dipped in 70% ethanol very briefly and then rinsed in Hank's buffer (HSS) + pen/strep. In a bijou, tumours were minced on ice for 10 minutes with two pairs of small scissors into small pieces (1 mm or less) in 1ml Hank's buffer + 200U/ml Collagenase IV + pen/strep (filter sterilised). After DNAseI addition (1 mg/ml final), the samples were incubated for 25 min at 37°C with gentle shaking. Samples were washed in 10 ml cold Hank's buffer, digested with 1 ml of 0.05% Trypsin-EDTA for 5 min at 37°C and filtered through a 70 µm nylon mesh adding HSS to prevent clogging. Samples were diluted in 30 ml HSS + pen/strep, centrifuged at 1,500 rpm in a benchtop centrifuge for 5 minutes and resuspended in the appropriate buffer. Mouse spleens were filtered through a 70 µm nylon mesh, and then RBCs were

lysed using RBC Lysis Buffer (Biolegend). Cells were washed and then resuspended in FACS buffer.

2.2.5 *In vitro* Cell Surface Staining

For *In vitro* staining: cells were grown in media until around 100% confluent. Then cells were washed with PBS, trypsinised (0.25%) and centrifugated for 5 minutes at 350X g. Cells were resuspended in FACS buffer (1% FBS, 0.05% sodium azide, 5mM EDTA in PBS) and aliquoted in 5ml polypropylene FACS tubes. For *ex vivo* staining: dissociated tumour cells were resuspended in FACS buffer and aliquoted in FACS tubes. For *in vitro* staining: cells were stained with the following antibodies: H2-Db (PerCP/Cy5.5, Biolegend), H2-Kb (Pacific Blue, Biolegend), PD-L1 (PE, Biolegend) and Qa-1(b) (BV510, BD Bioscience). For *ex vivo* staining dissociated cells were stained with the following antibodies: CD45 (BV421, BD Bioscience), CD3 (APC, Invitrogen), NKp46 (PE, Invitrogen), CD4 (FITC, Biolegend) CD8α (BUV805, BD Bioscience), Gr-1 (BV510, Biolegend), CD11b (BV711, Biolegend), F4/80 (APC-eFlour780, Invitrogen), MHC-II (I-A/I-E) (Alexa Flour 700, Invitrogen), CD11c (PE/Cy7, Biolegend), CD45 (Alexa Flour 700, Biolegend), CD3 (BUV395, BD Bioscience), CD4 (PerCP/Cy5.5, Biolegend), CD44 (APC, Biolegend), CD69 (APC-eFlour780, Biolegend), PD-1 (BV711, Biolegend), and Live/Dead (live dead blue, ThermoFisher). Antibodies were diluted 1:100 in FACS buffer containing the cells and incubated for 30 minutes at 4°C in the dark. Cells were washed with 2 ml PBS, resuspended in 200 μl FACS buffer + 200 μl 4% Paraformaldehyde (PFA) and analysed using BD Fortessa flow cytometers. The absolute count was calculated

using CountBright Absolute counting Beads (Invitrogen) following the manufacturer's instructions.

2.2.6 FMO

To assist with gating in the 16-colour panel, fluorescence minus one control was used, and then the gating strategy obtained from FMO was applied to *ex vivo* tumour samples. The gating method to identify populations of cells was created by comparing stains with and without a certain antibody.

2.2.7 *In vitro* Intracellular MHC-I Staining

Cells were grown in media until around 100% confluent. Then cells were washed in PBS, trypsinised and centrifugated. Cells were fixed in 500 μl fixation buffer for 20 minutes at room temperature in the dark. Cells were centrifugated at 350X g for 5 minutes and resuspended in 200 μl permeabilization/wash buffer, then centrifugated at 350X g for 5 minutes. The supernatant was decanted, cells were resuspended in 200 μl prem/wash buffer and centrifugated at 350X g for 5 minutes. After decanting the supernatant, the cells were stained with the antibodies at 1:100 dilution in the permeabilization/wash buffer and incubated for 20 minutes in the dark at 4°C. Cells were washed 2 times with perm/wash buffer and centrifugated at 350X g for 5 minutes. Cells were resuspended in 200 μl FACS buffer and analysed using BD Fortessa flow cytometers.

2.2.8 Fluorescent Immunocytochemistry (ICC) Staining

Cells were grown in media on top of a coverslip coated with 0.1% gelatin. Then cells were washed with PBS. Cells were stained with H2-Db antibody (1:100, Biolegend) and Concanavalin A (50 µg/ml, Invitrogen) for 30 minutes in the dark at room temperature. Cells were washed then fixed with 4% paraformaldehyde for 30 minutes at room temperature. Coverslips were transferred to slides on top of the nuclear stain with mounting media (DAPI, Invitrogen). Slides were imaged on a Nikon C2 confocal microscope.

2.2.9 Spleen Stimulation and Tumour and Spleen cGAS Inhibition

BALB/c mouse spleens were collected and filtered through 70µm strainers to get single-cell suspensions. RBCs were lysed with RBC lysis buffer, and then spleen cells were aliquoted at 1 million cells. Splenocytes were treated with the cGAS inhibitor RU.521 or DMSO for 3 hours and then transfected with 1 µg of DNA fragments generated by sonication using FuGENE transfection reagent at transfection reagent: DNA ratios of 3:1. After 24 hours incubation at 37°C in the tissue culture incubator splenocytes were stained with the multiparameter antibody panel and analysed by flow cytometer. For tumour cGAS inhibition: 1 million Balb/c-2 tumour cells were treated with the cGAS inhibitor RU.521 or DMSO and incubated at 37°C for 24 hours then stained and analysed by flow cytometer.

2.2.10 Bacterial Culture Transformation

One ShotTM Stbl3TM Chemically Competent E. coli cells (Invitrogen) were used for transforming the plasmids *Ddx58* gRNA1, *Ddx58* gRNA2, Empty Vector, pCMV-VSV-G envelope, and pCMV-Gag/Pol in accordance with the manufacturer's instructions. After transformation, bacteria were cultivated on LB agar plates supplemented with the ampicillin antibiotic and incubated overnight at 37°C. Single bacterial colonies were selected the following day and added to 5 ml of LB broth that contained 100 µg/ml ampicillin. These cultures were incubated in a shaking incubator (Kuhner ISF-1-W Incubator Shaker Pred ISF1-X/Z) set at 200 rpm for the entire night at either 37°C. The starter cultures were then expanded into 100 ml of antibiotic-containing LB broth in an Erlenmeyer flask and incubated for the entire night at 37°C while being shaken constantly.

2.2.11 Plasmid DNA Extraction and Glycerol Stock Preparation

QIAGEN Plasmid DNA Midiprep Kit was used for the extraction of plasmid DNA from bacterial cultures in accordance with the manufacturer's guidelines. A Nanodrop spectrophotometer was used for DNA concentration measurement. Glycerol stocks were made by combining equal parts of bacterial culture and 80% glycerol, and they were then stored at -80°C for long-term storage.

2.2.12 LB Agar Preparation

LB agar was prepared by dissolving 20 g of (Sigma) Luria-Bertani (LB) agar granules in 1 L of deionized water (dH2O), sterilizing the medium in an autoclave at 121°C for 15 minutes, and then cooling it before use.

2.2.13 LB Broth Preparation

To prepare (LB) broth, 20 g of Sigma's broth powder was dissolved in 1 L of deionized water (dH2O) and autoclaved for 15 minutes at 121°C. The broth was cooled at room temperature before use.

2.2.14 RIG-I KO by CRISPR/Cas9

To produce RIG-I KO Balb/c-2 cells, lentiviral particles containing the relevant KO constructs were prepared by transfecting 293T cells with FuGENE transfection reagent with 3 plasmids: eSpCas9-LentiCRISPR v2 with gRNAs targeting the *Ddx58* gene exons 4 (gRNA1) and exon 3 (gRNA2) (gRNA1: ATGTCTTATCAGATCCGACA, gRNA2: ATCCGAATGTTTGATTAATC) or Empty vector (GenScript); pCMV-VSV-G envelope and pCMV-Gag/Pol packaging vectors as previously described (Zhyvoloup et al., 2017). After 24 hours, the media was changed. The virus-containing supernatants were collected 48 and 72 hours after transfection. Balb/c-2 cells were infected with the lentivirus in the presence of 8 µg/ml Polybrene. Forty-eight hours after infection, fresh media containing puromycin (2 µg/ml) was added and clones were selected by limiting dilution.

2.2.15 DNA Extraction

DNA was extracted from different clones and control samples using phenol/chloroform. Cells were digested overnight in Tissue Lysis buffer + Proteinase K (200µg/ml) at 55 °C. Phenol chloroform isoamyl alcohol (25:24:1) was added to the lysed cells, tubes were inverted few times and centrifugated at 14000 RPM in a benchtop centrifuge for 15 mins at 4°C. The aqueous phase was collected and added to a new tube. 2 volumes of chilled 100% ETOH was added. Tubes were centrifugated at 14000 RPM for 15 mins at 4°C. The supernatant was discarded and 150 µl of chilled 70% ETOH was added. Tubes were centrifugated at 14000 RPM for 5 mins at 4°C. Supernatant was discarded and the remaining 70% ETOH was removed by pipette without disturbing the pellet. Molecular Grade H2O was added to the pellet and DNA concentration was measured by nanodrop.

2.2.16 PCR

PCR amplification was performed with the following primers: gRNA1 *Ddx58* (F: ATA CCG CTT CCA CAA AAG CT, R: CCA TGT AGT TCC CTT CCT CC) gRNA 2 *Ddx58* (F: AAG CCA TCG AAA GTT GGG AC, R: AAG GGG GCA ACT TTA ACT GC) Beta Actin (F: TGA GCT GCG TTT TAC ACC CT, R: AAG TCA GTG TAC AGG CCA GC). Thermocycling conditions were as follows: initial DNA denaturation step at 94°C for 10 minutes. Followed by denaturation for 30 seconds, annealing at 52°C for 30 seconds, extension at 72°C for 30 seconds for 30 cycles. Final extension at 72°C for 10 minutes. PCR products were resolved in a 2% gel.

2.2.17 ELISA

Tumour cells were grown *in vitro* in t25 flask in DMEM/F12 media with 10% FBS, 1% 1% non-essential amino acids, and 1% penicillin/streptomycin until almost 100% confluent. The supernatant was collected, then centrifugated briefly to remove debris and CXCL10 and CCL5 were measured using the R&Dsystems sandwich ELISA kit (DY466, DY478) in a 96 well plates using 100 µl undiluted supernatant. Optical density was determined by using a microplate reader at 450nm (Thermo Scientific). Standard curve was calculate using four parameter logistic curve.

2.2.18 *In Vivo* Neutralizing Antibodies Treatment

Mice were injected with 1 million cells in 100 µl sterile PBS of Balb/c-2 tumour cells. After the tumours were palpable, mice weights were measured, and mice were injected intraperitoneally with 4 doses of 5mg/Kg of the designated antibody on days 4, 7, 10, and 13 post-tumour injections. Mice were monitored daily, and tumour volumes were recorded. Mice were injected with the following neutralizing antibodies: Anti-mouse PD-1 (RMP1-14, BioXcell), anti-mouse Nonclassical MHC Class I molecule Qa-1b (4C2.4A7.5H11, BioXcell), and mouse IgG1 isotype control (MOPC-21, BioXcell). The antibodies were prepared in pH 7.0 dilution buffer (BioXcell).

2.2.19 RNA Extraction

Total RNA was extracted using the RNAeasy kit (Qiagen) following the manufacturer's instructions. Briefly, cells were trypsinised and washed with PBS.

Biopsies and cells were lysed with RLT buffer until totally homogenized. 1 volume of 70% ethanol was added, and the lysate was mixed and moved to the Rneasy spin column and centrifugated. The Flowthrough was discarded. The column was washed with RW buffer, and then RPE buffer twice. RNA was eluted with nuclease-free water and stored at -80 °C. RNA concentration was checked with a Nanodrop and RNA quality was checked with a tapestation analysis.

2.2.20 Library Preparation for Transcriptome Sequencing

Messenger RNA was purified from total RNA using poly-T oligo-attached magnetic beads. After fragmentation, the first strand cDNA was synthesized using random hexamer primers, followed by the second strand cDNA synthesis using either dUTP for directional library or dTTP for non-directional library. For the non-directional library, it was ready after end repair, A-tailing, adapter ligation, size selection, amplification, and purification for the directional library, it was ready after end repair, A-tailing, adapter ligation, size selection, USER enzyme digestion, amplification, and purification. The library was checked with Qubit and real-time PCR for quantification and bioanalyzer for size distribution detection. Quantified libraries will be pooled and sequenced by Novogene on Illumina platforms.

2.2.21 Clustering and Sequencing

The clustering of the index-coded samples was performed according to the manufacturer's instructions. After cluster generation, the library preparations were sequenced on an Illumina platform and 150 bp paired-end reads were generated.

2.2.22 RNA-seq Quality Control

Raw data (raw reads) of fastq format were firstly processed through in-house perl scripts. In this step, clean data (clean reads) were obtained by removing reads containing adapter, reads containing ploy-N and low-quality reads from raw data. At the same time, Q20, Q30 and GC content the clean data were calculated. All the downstream analyses were based on the clean data with high quality.

2.2.23 Reads Mapping to the Reference Genome

Reference genome and gene model annotation files were downloaded from genome website2 directly. Index of the reference genome was built using Hisat2 v2.0.5 and paired-end clean reads were aligned to the reference genome using Hisat2 v2.0.5. We selected Hisat2 as the mapping tool for that Hisat2 can generate a database of splice junctions based on the gene model annotation file and thus a better mapping result than other non-splice mapping tools.

2.2.24 Quantification of Gene Expression Level

FeatureCounts v1.5.0-p3 was used to count the reads numbers mapped to each gene. And then FPKM of each gene was calculated based on the length of the gene and reads count mapped to this gene. FPKM, expected number of Fragments Per Kilobase of transcript sequence per Millions base pairs sequenced, considers the effect of sequencing depth and gene length for the reads count at the same time,

and is currently the most commonly used method for estimating gene expression levels.

2.2.25 Differential Expression Analysis

Differential expression analysis of two conditions/groups (three or more biological replicates per condition) was performed using the DESeq2 R package (1.20.0). The resulting P-values were adjusted using the Benjamini and Hochberg's approach for controlling the false discovery rate. Genes with an adjusted P-value <=0.05 found by DESeq2 were assigned as differentially expressed.

2.2.26 GSEA Enriched Pathway Analysis

DE genes from each comparison (each passage against reference YUMM17) were combined, resulting in 7282 genes. The log2FC values were subjected to k-means hierarchical clustering with k=6, and the result was displayed as a heatmap using the R package 'pheatmap' v1.0.12 (https://CRAN.R-project.org/package=pheatmap). Each row represents one gene. Functional analysis for any group of genes of interest (clusters 1+4, Balb/c-2 vs F0) was performed using Gene Set Enrichment Analysis (GSEA) (Subramanian et al., 2005) implemented as a Java tool GSEA v4.1.0 (https://www.gsea-msigdb.org/gsea/index.jsp) using normalised counts and the following parameters: 'meandiv' normalisation, geneset permutation, n=1000 permutations per test, metric Signal2Noise, and weighted enrichment statistic. We queried functional genesets at the MSigDB database

(https://www.gsea-msigdb.org/gsea/msigdb/index.jsp) based on Gene Ontology terms, Reactome, Kegg, and others, and identified those with an FDR < 5%.

2.2.27 Ingenuity Pathway Analysis

Significantly differentially expressed genes were used in QIAGEN IPA core analyses. The following details were loaded into the input table describing the outcome of a differential gene expression analysis: Genome ID, the significance of the impact size is described by the mean expression across all samples, the log2 fold change ratio of the gene expression between the two groups, and the P-value/FDR of the differential-expression test between the two groups.

2.2.28 Analysis of Repeats

Repetitive regions were annotated as previously described (Attig et al., 2017). In brief, the mouse genome (GRCm38.78) was masked using RepeatMasker (RepeatMasker v.4.09, www.repeatmasker.org) configured with nhmmer (Love et al., 2014a) in sensitive mode using the Dfam 2.0 library (v150923). RepeatMasker annotates long terminal repeat and internal regions separately, complicating the summation of reads that span these divides. Tabular outputs were therefore parsed to merge adjacent annotations for the same element and to produce a gene transfer format (GTF) file compatible with popular read-counting programs. Read pairs were aligned with HISAT2 (D. Kim et al., 2015) and primary, stranded mappings were counted with featureCounts (Subread (D. Kim et al., 2015) using standard GTF files for annotated genes and the curated RepeatMasker GTF files for repeat regions. For

accuracy and to prevent ambiguity, only reads that could be uniquely assigned to a single feature were counted. Those reads remaining were normalized to account for variable sequencing depth between samples, using DESeq2 (Love et al., 2014b). All downstream differential expression analyses and visualization were carried out using Qlucore Omics Explorer 3.3 (Qlucore). Analysis of repeat expression was performed using the Qlucore Omics Analysis platform (qlucore.com). Scores below 0.1 were discarded and the data was logged to base 2. Repeats were filtered using a t-test for all samples before N2.1, and all samples after N2.1 inclusive. Filters were set at SD > 0.34, q <0.05, and fold-change >2. This was used to produce a heatmap, and 3D PCA plot. Repeats passing this threshold were exported from qlucore. R was used to examine the enrichment of repeat families. Fisher's exact tests were used to test for enrichment of repeat families in the up- and down-regulated repeat lists, compared to all repeats in the mouse genome. Benjamini Hochberg correction was applied to the resulting p-values to account for multiple testing. The same list of repeats was also tested for enrichment of inter or intragenic status of the repeats.

2.2.29 Annotation of Intergenic and Intragenic Repeats

Lists of inter and intragenic repeats were created by analysing the intersection of bed files of gene and repeat loactions. A bed file of gene locations from GRCm38.78 was prepared from the GTF using GFFUtils gtf2bed (github.com/fls-bioinformatics-core/GFFUtils). A second bed file was generated from the GTF of repeats using the same method. The intersection of these bed files was found using BEDtools Intersect (Quinlan & Hall, 2010). Qlucore annotation text files of lists of gene intersecting and non-gene-intersecting repeats were then made and used to annotate heatmaps. The

lists were also used for enrichment analysis in R. Both the chi-squared and Fisher's exact test results are reported.

2.2.30 Schematic Illustrations

Schematic Illustrations were performed using biorender.

2.2.31 Statistical Analysis

Statistical Analysis for samples of more than 3 groups was performed using Prism software and 1-way Anova or 2-way Anova with Tukey correction for multiple comparisons, P values of 0.05 or less were considered significant. Statistical analysis for samples less than 3 groups was carried out using unpaired t-test with Welch's correction, P values of 0.05 or less were considered significant.

3

Results

Chapter 3: Establishment of the Transplantable Tumour Model

3.1 Introduction

Organ transplantation is a vital aspect of contemporary medicine, providing patients with end-stage organ failure with potentially life-saving options. Despite major breakthroughs in transplantation medicine, various obstacles exist, including organ shortage, chronic rejection, and problems related to long-term immunosuppression. Organ shortage is the major challenge for organ transplantation. This is because of the histocompatibility barrier which necessitates that the transplanted organ be a close match to the recipient (Kupiec-Weglinski, 2022). As a result of this hurdle waiting lists for patients needing an organ are long. For example, the United Network for Organ Sharing (UNOS) reports that over 100,000 people are waiting for an organ transplant in the United States alone at any given moment (UNOS, 2025). The pitfalls of the current organ transplantation strategies raised the need for the adoption of new strategies to get around these problems. One of the new strategies that might be implemented is adopting the mechanisms employed by transmissible cancers such as CTVT to escape immune killing. Understanding the mechanisms of CTVT tolerance and applying them to the transplanted organs leading to a local tolerance of the organ could potentially solve problems such as shortage of organs and the use of systemic immunosuppression drugs that have many side effects such as infections by Herpes group viruses (CMV, EBV), Hepatitis viruses (HBV, HCV), bacterial infections (Pseudomonas species (spp), Mycobacterium tuberculosis), and fungal infections (Candida spp, Aspergillus spp) (Fishman, 2017) and malignancies such as Kaposi sarcoma, skin cancer, non-Hodgkin lymphoma, and liver cancer (Shekhar Gogna; Karan Ramakrishna; Savio John, 2024). Unfortunately, the

mechanisms of immune tolerance caused by CTVT are not entirely known. Nor is how this tumour evolved to be transmissible. This is because CTVT is estimated to have originated 8500-11000 years ago and we do not have ancient samples (Murchison et al., 2014) (Baez-Ortega et al., 2019). Therefore, one approach to understanding how a tumour became transmissible is by trying to create a transplantable tumour by selection through serial passaging in different mouse strains, which have well-characterised MHC-I and MHC-II haplotypes and immune system function, and are amenable to experimentation (affymetrix, 2024)

To evolve the transplantable tumour by adaptation, we decided to reproduce mouse tumour transplantation studies in the 1920s and 1950s reporting the occasional generation of tumours that were transplantable across different inbred strains (Barrett & Deringer, 1952; Strong, 1926b). This was achieved by serial passaging of a mouse mammary adenocarcinoma (C3HBA) initially in syngeneic mice (C3H), then into F1 mice (C3H x BALB/c), followed by N2 mice (F1 x BALB/c), then pure BALB/c mice (Barrett & Deringer, 1952). The Fassati group showed previously through RNA sequencing that CTVT transcriptional profile is most similar to skin cancer, cutaneous melanoma, and melanoma (Frampton et al., 2018). We therefore replicated the experimental design of the 1950s transplantation studies using the YUMM1.7 melanoma cells. YUMM (Yale University Mouse Melanoma) are genetically well-characterised cells generated by the dissociation of tumours that developed in a male $BRAF^{(V600E)}$ $Pten^{-/-}$ $Cdkn2a^{-/-}$ C57BL/6 mice (Meeth et al., 2016). These cells express detectable levels of MHC-I (Erkes et al., 2020), form tumours when injected into syngeneic C57BL/6 mice and the tumours do not respond to anti-CTLA4 and anti-PD-1 antibodies, suggesting low antigenicity (Wang et al., 2017a).

In addition to the melanoma origin, YUMM1.7 cells share with CTVT genetic features such as loss of *Cdkn2a* (Meeth et al., 2016), making them a suitable model to evolve a transplantable tumour.

The mutations in YUMM1.7 cells have major implications for melanoma pathogenesis. The $BRAF^{(V600E)}$ mutation results in the activation of the MAPK pathway promoting cell growth and proliferation; while CDKN2A loss affects cell cycle regulation and PTEN loss limits the control of the PI3K-AKT signalling pathway, resulting in reduced apoptosis and increased cell proliferation. Together, these mutations allow YUMM1.7 cells rapidly to proliferate in hosts which is a feature of melanoma tumours (Meeth et al., 2016). Another advantage of using the YUMM1.7 cell line is the close genetic resemblance to a significant subset of human melanomas. This also makes the YUMM1.7 cells a good model for studying the effects of the *Braf* mutation, which exists in around 50% of human melanomas, and 70-88% of these are $BRAF^{(V600E)}$ (Castellani et al., 2023) (Meeth et al., 2016). Additionally, tumours from injected YUMM1.7 get infiltrated by different immune cells which provides a better model of the TME and how these tumour cells interact with the immune system (Wang et al., 2017b). YUMM1.7 cells were therefore considered a good model to select a transplantable tumour.

Immunocompromised mice have been extensively used in tumour transplantation studies mainly to understand the roles of certain immune cells in tumour immunology, these include Nude mice which lack T cells, Severe Combined Immunodeficient mice (SCID) which lack functional T and B cells, and Non-Obese Diabetic (NOD) SCID mice lacking complement, NK cells, macrophages and dendritic cells functions in addition to T and B cells (Okada et al., 2019). These mice

models are not considered a good model for our study as the lack of immune cells will not lead to the selection of tumours that are completely immune evasive similar to transmissible cancers. Other than the studies from the 1920s and 1950s mentioned above, there have been limited studies to replicate or generate allo-transplantable tumours which could grow in non-immunocompromised mouse models. One study from 1996 reported the development of a spontaneous malignant fibrous histiocytoma (now termed undifferentiated pleomorphic sarcoma) in the ddY mouse strain that was able to grow in several allogeneic mouse strains. However, no explanation of what enabled this tumour to grow in mismatched hosts was provided (Yamamoto & Yamamoto, 1996). Another allo-transplantable tumour that has been reported is Sarcoma 180. It is a pleomorphic sarcoma that originated from a Swiss mouse tumour that developed spontaneously. This tumour grows rapidly, usually leading to the death of the grafted mouse within 3 to 4 weeks and it can be grafted into up to 20 mouse strains including C57BL/6 and BALB/c. This cell line has an impaired MHC-I expression due to a lack of β2m (Alfaro et al., 1992; Cui et al., 2003).

However, to our knowledge, there are no studies that have selected an allo-transplantable tumour and investigated the mechanisms leading to this phenotype. (Meeth et al., 2016) (N. Liu et al., 2023; Wang et al., 2017b)

3.2 Results

3.2.1 Passaging Strategy Rationale and Mouse Strains

In this study, we utilized the passaging strategy employed by Barret and Deringer (Barrett & Deringer, 1952) with minor changes (explained later). This strategy is better suited to gradual tumour adaptation that could lead to tumour growth in mismatched hosts. This is supported by experiments that showed tumours that were passaged in F1 hybrid mouse could grow in N2 hybrid mouse while the parental tumours not passaged in F1 could not (BARRETT & DERINGER, 1950). This method also has the advantage of inducing natural selection of immune evasive tumours without any requirement for host immune suppression or other tumour genetic alterations.

Choice of mouse strains and hybrids for transplantation experiments

C57BL/6 Mouse

Inbred C57BL/6 mouse strain is one of the most utilized mouse models in biomedical research due to their many advantages. They are known for having good health and longevity. As a result of the C57BL/6 genome sequencing, their genetic composition is well characterised. C57BL/6 phenotype is reproducible, and their immune system is well-defined (“Initial Sequencing and Comparative Analysis of the Mouse Genome,” 2002). The characterisation of the TME in C57BL/6 mice has been crucial in elucidating the ways in which immune cells and other components can either stimulate or suppress the formation of tumours (Perez-Lanzon et al., 2024). Regarding the MHC haplotype, C57BL/6 are H-2Kb H-2Db H-2Lnull I-Ab I-Enull MHC (affymetrix, 2024). YUMM1.7 the cell line is syngeneic to this mouse strain

therefore tumour implantation experiment should result in a successful tumour growth without rejection as has been shown by previous experiments (Moreno et al., 2016)

BALB/c Mouse

BALB/c mice, characterised by their albinism, are a stable of biomedical research. They are used in immunological, infectious diseases, and cancer studies due to their competent immune system, well-characterised genetics, and the propensity to produce antibodies in abundance (Köhler & Milstein, 1975). They express MHC haplotypes H-2Kd H-2Dd H-2Ld I-Ad I-Ed (affymetrix, 2024; Roitt et al., 2006). Understanding the mechanisms behind allograft rejection and tolerance has been greatly aided by the BALB/c mouse strain, which has a strong immune response and is susceptible to a variety of immunological treatments (Valujskikh et al., 2002). These reasons make BALB/c mice a good model for investigating the effector mechanisms of rejection, including the roles of cytokines, T cells, and B cells in mediating graft damage in these hosts (Tian et al., 2022). Since this mouse is fully mismatched to the C57BL/ strain, YUMM1.7 cells are expected to be rejected in BALB/c mice.

F1 Hybrid Mice

F1 hybrid mice were produced by crossing C57BL/6 with BALB/c mice. This causes the progeny to have a genetic background that combines the two inbred strains (Silver, 1995). Combining the unique H-2 haplotypes of their parental strains produces MHC heterozygosity in F1 hybrid mice, which leads to a varied array of MHC molecules on the cell surface. This genetic diversity helps T cells be exposed

to a greater variety of peptides, which may improve the immune system's capacity to identify and react to infections and malignancies (Roitt et al., 2006). F1 hybrid mice express MHC-I and MHC-II molecules from both parent strains (Celada & Welshons, 1962). Therefore, it is expected that YUMM1.7 cells would be accepted in this mouse strain.

F2 Hybrid Mouse

F2 hybrid mice are produced by crossing two F1 mice. When F1 mice mate, a unique random mixing of alleles from both parental strains produces F2 offspring (de Angelis et al., 2004). This genetic diversity makes F2 hybrid a good model for studying diseases related to genetics such as metabolic, cardiovascular diseases, and cancer. As a result of alleles from their F1 parents segregating and recombining, F2 hybrid mice have a broad variety of MHC genotypes which makes them a good model for transplantation studies (Barnes & Krohn, 1957). Skin graft transplantation experiments of parental mice skin grafts into F2 mice showed that, depending on the genotype of the parent, almost 100% of the transplanted grafts can survive for up to 2 weeks, although skin grafts are eventually rejected by a delayed response (Barnes & Krohn, 1957). Thus, this hybrid is expected to be suitable for short-term tumour selection.

N2 Hybrid Mouse

The F2 mice were backcrossed with BALB/c mice to generate the N2 hybrid. N2 mouse crosses have the advantage of some genetic heterogeneity while being closer to the genetic background of BALB/c mice (Falconer & Mackay, 1996) (Silver, 1995) (Falconer & Mackay, 1996) (Churchill & Doerge, 1994). Because N2 mice

express around 75% of the genome of one of the parental strains, it is possible to identify certain genome regions that are associated with disease development or progression through QTL mapping, including tumour adaptation *in vivo* and metastasis (Churchill & Doerge, 1994; Falconer & Mackay, 1996; Silver, 1995) (Klein-Rodewald et al., 2022). Tumour transplantation studies in the 1950s utilizing N2 mice (F1 X Backcrossed to the resistant parent strain) showed that 20 out of 58 tumours were able to grow if they were previously passaged in F1 hybrid mice. While 0 out of 30 grew when directly injected from parental strain to N2 hybrid mice (BARRETT & DERINGER, 1950). Therefore, YUMM1.7 cells are not expected to grow in the N2 mice.

CBA/Ca Mouse

CBA/Ca inbred mouse strain is used in the fields of audiology, immunology, cancer, and longevity (Henry & Chole, 1980) (Flurkey et al., 2007) (Henry & Chole, 1980) (Willott, 1986). They are susceptible to Noise-Induced Hearing Loss (NIHL) and Age-related Hearing Loss (AHL). Their resistance to spontaneous tumour development despite their long lifespan makes them a good model for immunological, cancer, and ageing studies (Flurkey et al., 2007) (Henry & Chole, 1980) (Willott, 1986). CBA/Ca mouse strains express the MHC haplotype H-2Kk H-2Dk H-2Lnull I-Ak I-E) (affymetrix, 2024) which is mismatched relative to both C57BL/6 and BALB/c mice.

FVB/N Mouse

FVB/N mice are characterised by their high fertility rate and physical robustness making them a good model for long-term studies. They are routinely used for the creation of Transgenic (TG) and Knockout (KO) mouse strains due to their large

pronuclei which makes it easier to introduce foreign DNA through injection (Taketo et al., 1991). TG and KO FVB mice are one of the most used models in biomedical research including cancer research to investigate gene functions in oncogenesis and tumour progression (Torrey et al., 2005; Yun et al., 2021). The FVB/N mouse strain has the MHC haplotype H-2Kq H-2Dq H-2Lq I-Aq I-Enull (affymetrix, 2024) and is therefore mismatched relative to CBA, C57BL/6 and BALB/c mice.

Table 3.1: MHC haplotypes for different mouse strains.

	MHC-I		MHC-II		
Mouse strain	**H-2K**	**H-2D**	**H-2L**	**I-A**	**I-E**
C57BL/6	b	b	null	b	null
BALB/c	d	d	d	d	d
CBA/Ca	k	k	null	k	k
FVB/N	q	q	q	q	null

3.2.2 Optimizing Tumour Cell Number for Injections

Initial experiments were carried out by Drs. Bennett and Fassati before I joined the Fassati lab to determine the optimal number of cells for injection and tumour growth; $1x10^5$ or $1x10^6$ YUMM1.7 cells were injected subcutaneously into the left flank of male and female C57BL/6 mice and tumour growth and mouse weight were monitored at regular intervals. No weight loss was observed at any of the tested cell

numbers. Injection of $1x10^6$ YUMM1.7 cells resulted in 100% (5/5) tumour growth within 1 week whereas injection of $1x10^5$ cells resulted in 80% (4/5) tumour growth with a slower kinetic (Figure 3.1). Therefore, all subsequent experiments were conducted with $1x10^6$ YUMM1.7 cells.

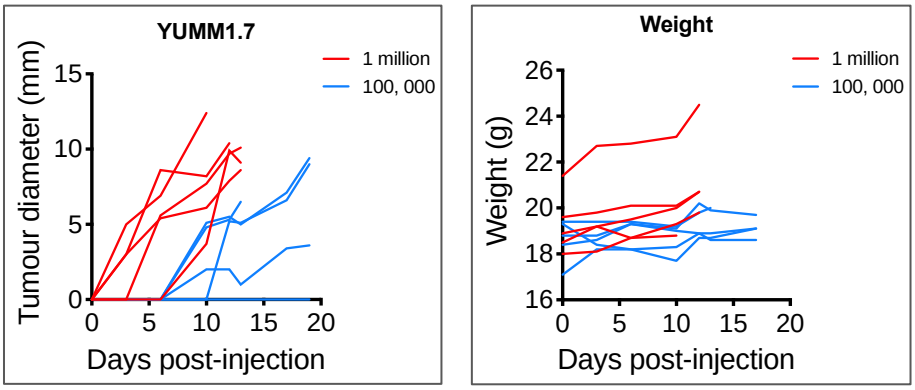

Figure 3.1. Adapted from Dr. Clare Bennett. Optimizing tumour cell injections**.** $1x10^5$ or $1x10^6$ YUMM1.7 cells were injected subcutaneously into the flank area of mice and tumour growth and mouse weight were monitored at regular intervals. Left panel, tumour diameter, right panel mouse weight.

3.2.3 Tumour Passaging Strategy

The experimental design involves injecting 1 million cells into the left flank of the mice under anaesthesia and monitoring tumour growth at daily intervals for 2 weeks, or until the tumour mass reaches the maximum allowed diameter of 15 mm. This time interval is based on skin allografts acute rejection, which happens within 10-14 days (J. Zhou et al., 2013b). At that point, mice were sacrificed by exposure to carbon dioxide and neck dislocation. Tumours were collected by surgical excision, avoiding

contamination with normal tissues such as skin and muscle. Excised tumours were immediately dissociated initially by mechanical mincing and then by digestion with collagenase and trypsin at a low concentration of 0.05%. Single cells were counted, expanded *in vitro* for 2-4 passages and 1 million cells were re-injected into the next mouse cross. The supernatant of confluent cultures was stored at -80C for ELISA testing. Aliquots of the cells were used to extract RNA and for multiparameter flow cytometry. Several aliquots were frozen in liquid Nitrogen.

I started by injecting 1 million YUMM1.7 cells into 17 syngeneic C57BL/6 mice. The tumours produced from this step (hereafter called F0) were passaged into the F1 mouse cross (C57BL/6 x BALB/c) to get the F1 tumours. Unlike the studies from the 1950s, we chose to add one more passaging step in the F2 mouse (F1 x F1) to better adapt the F1 tumours to the next passage in the N2 cross. Crossing the F1 mouse with a similar F1 mouse resulted in four different groups. The first group had black fur mimicking the C57BL/6 mouse. The second group had white fur mimicking the BALB/c mouse. The third group had a similar fur colour to the F1 mouse. Finally, the fourth group has a lighter shade of brown than the F1 mouse strain. All groups were used for the injection experiments, and tumours grew in each group, except the white fur. However, the fourth group was chosen for tumour collection and further passaging. This is because the fur colour indicates that they are genetically a step closer to BALB/c mice than the F1 hybrid mice.

To check the genetic composition of these F2 mice, some littermates were genotyped by Transnetyx using their validated platform of SNPs mini Mouse Universal Genotyping Array (MUGA) (Sigmon et al., 2020). Genotyping of spleen cells showed that the percentage of alleles that are coming from the BALB/c strain

ranged from 67-77% while the ones from the C57BL/6 strain ranged from 21-31% (Table 2). The F2 tumour cells were injected into N2 mice, tumours that grew were excised and dissociated and the cells were re-injected into the N2 mice, and this step was repeated two more times to improve adaptation. The resulting tumours were called N2.1, N2.2 and N2.3 respectively. Genotyping of a few N2 mice indicated that they are genetically more similar to BALB/c mice than the F2 mice, as alleles coming from BALB/c represented 80-87% while alleles from C57BL/6 were 12-19% (Table 2). After the successful growth of the passaged tumours in N2.3 mice, I inoculated dissociated N2.3 cells into completely allogeneic BALB/c mice. This passage gave the Balb/c-1 tumours, which were passaged into BALB/c mice again to obtain the Balb/c-2 tumours. Adapted tumours were injected in the parental syngeneic C57BL/6 mice to check if their transplantation potential had changed during selection. To confirm that the adapted tumour growth was due to general transplantability rather than a specific C57BL/6 to BALB/c adaptation, I passaged the Balb/c-2 tumours into CBA/Ca and FVB/N mice, both of which are mismatched to C57BL/6 and BALB/c and to each other (Figure 3.2). Dissociated tumour cells from all passages were genotyped using mini MUGA to check for strain genetic background and all tumour passages showed that they retained their C57BL/6 background (table 3).

At each passage, dissociated tumours were analysed by flow cytometry to study the intratumoural host immune cell infiltrate or after passaging *in vitro* to clear host immune cells, cells were analysed by flow cytometry to analyse tumour markers and nucleic acids were extracted for RNA-seq from the isolated tumour cells. Some tumour biopsies were frozen for further analysis (Figure 3.3).

Table 3.2: Genotyping using Mini MUGA platform of spleen cells from C57BL/6, F2, N2, and BALB/c mice.

Sample	Background	Zygosity	Informative Markers	Informative Markers %	Genome %
C57BL/6	C57BL/6J and C57BL/6JOlaHsd	N/A	8846	100.00%	100.00%
		Total	8846	100.00%	100.00%
F2_1	BALB/cAnNTac	Homozygous	1317	47.40%	55.40%
	C57BL/6J	Homozygous	310	11.20%	8.50%
	BALB/cAnNTac X C57BL/6J	Heterozygous	1119	40.30%	35.80%
	Unexplained	Homozygous	2	0.10%	0.00%
	Unexplained	Heterozygous	31	1.10%	0.30%
		Total	2779	100.10%	100.00%
F2_2	BALB/cAnNTac	Homozygous	1318	47.40%	55.40%
	C57BL/6J	Homozygous	310	11.10%	8.50%
	BALB/cAnNTac X C57BL/6J	Heterozygous	1120	40.30%	35.80%
	Unexplained	Homozygous	2	0.10%	0.00%
	Unexplained	Heterozygous	32	1.20%	0.30%
		Total	2782	100.10%	100.00%
F2_3	BALB/cAnNTac	Homozygous	1319	47.40%	55.40%
	C57BL/6J	Homozygous	310	11.10%	8.50%
	BALB/cAnNTac X C57BL/6J	Heterozygous	1120	40.30%	35.80%
	Unexplained	Homozygous	2	0.10%	0.00%
	Unexplained	Heterozygous	30	1.10%	0.30%
		Total	2781	100.10%	100.00%
F2_4	BALB/cAnNTac	Homozygous	1319	47.50%	55.40%
	C57BL/6J	Homozygous	311	11.20%	8.50%
	BALB/cAnNTac X C57BL/6J	Heterozygous	1117	40.20%	35.80%
	Unexplained	Homozygous	2	0.10%	0.00%
	Unexplained	Heterozygous	30	1.10%	0.30%
		Total	2779	100.10%	100.00%
F2_5	BALB/cJRj	Homozygous	1175	41.90%	47.30%
	C57BL/6J	Homozygous	119	4.20%	4.80%
	BALB/cJRj X C57BL/6J	Heterozygous	1468	52.30%	47.80%
	Unexplained	Homozygous	2	0.10%	0.00%
	Unexplained	Heterozygous	42	1.50%	0.20%
		Total	2806	100.00%	100.10%
F2_6	BALB/cJRj	Homozygous	1755	62.40%	62.00%
	C57BL/6J	Homozygous	174	6.20%	5.60%
	BALB/cJRj X C57BL/6J	Heterozygous	835	29.70%	32.20%
	Unexplained	Homozygous	5	0.20%	0.00%
	Unexplained	Heterozygous	43	1.50%	0.20%
		Total	2812	100.00%	100.00%
N2_1	BALB/cJRj	Homozygous	2109	75.10%	80.70%
	C57BL/6J	Homozygous	10	0.40%	0.00%
	BALB/cJRj X C57BL/6J	Heterozygous	649	23.10%	19.10%
	Unexplained	Heterozygous	41	1.50%	0.20%
		Total	2809	100.10%	100.00%
N2_2	BALB/cJRj	Homozygous	1700	60.70%	68.60%
	C57BL/6J	Homozygous	10	0.40%	0.00%
	BALB/cJRj X C57BL/6J	Heterozygous	1057	37.70%	31.20%
	Unexplained	Heterozygous	35	1.20%	0.20%
		Total	2802	100.00%	100.00%
Balb/c	BALB/cJRj	Homozygous	8826	99.90%	100%
	Unexplained	Homozygous	10	0.10%	0.00%
		Total	8836	100%	100%

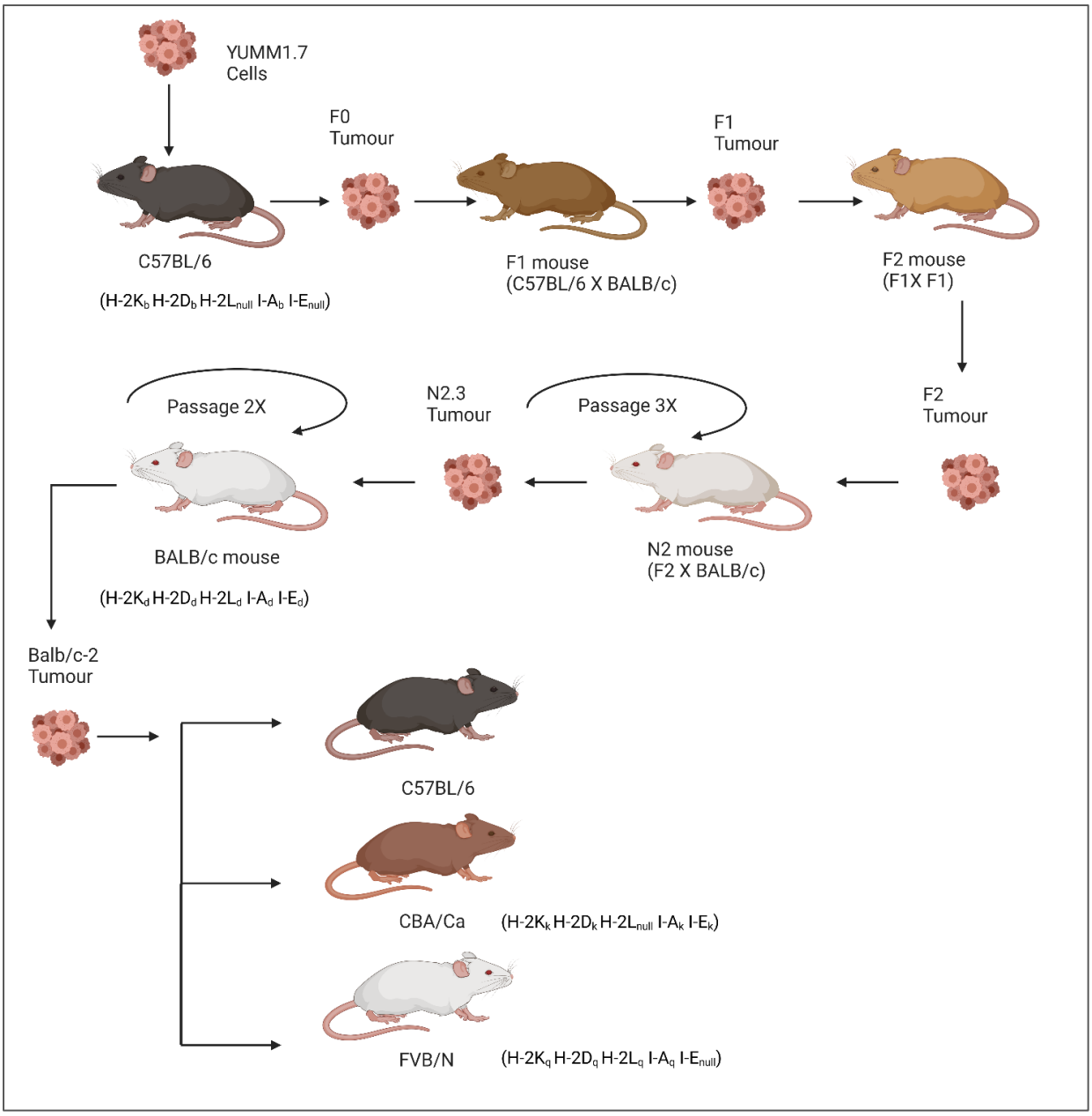

Figure 3.2: Summary of the experimental strategy to passage tumours. 1 million YUMM1.7 cells were injected into syngeneic C57BL/6 mouse. Tumours that grew in syngeneic mice (F0 tumours) were dissociated and tumour cells were expanded *in vitro* for 2 to 4 passages then 10^6 F0 tumour cells were injected into F1 mice. F1 tumours were passaged in F2 mice as before. The resulting F2 tumours were passaged in N2 mice serially three consecutive times, (N2.1, N2.2 and N2.3). The N2.3 tumours were injected into BALB/c mice two consecutive times (Balb/c-1 and

Balb/c-2). 10^6 Balb/c-2 cells were then inoculated into C57BL/6, CBA and FVB/N mice.

Table 3.3: Genotyping using Mini MUGA platform of tumour cells from F0, F1, F2, N2.1, N2.2, N2.3, Balb/c-1, Balb/c-2, CBA/Ca, and FVB/N passages.

Sample	Substrain	Homozygous Diagnostic Alleles	Heterozygous Diagnostic Alleles	Potential Diagnostic Alleles	% Observed
YUMM1.7	C57BL/6J	133	6	156	89.1
F0	C57BL/6J	133	6	156	89.1
F1	C57BL/6J	133	6	156	89.1
F2	C57BL/6J	133	6	156	89.1
N2.1	C57BL/6J	133	6	156	89.1
N2.2	C57BL/6J	133	6	156	89.1
N2.3	C57BL/6J	133	6	156	89.1
Balb/c-1	C57BL/6J	133	6	156	89.1
Balb/c-2	C57BL/6J	133	6	156	89.1
CBA	C57BL/6J	133	6	156	89.1
FVB	C57BL/6J	133	6	156	89.1

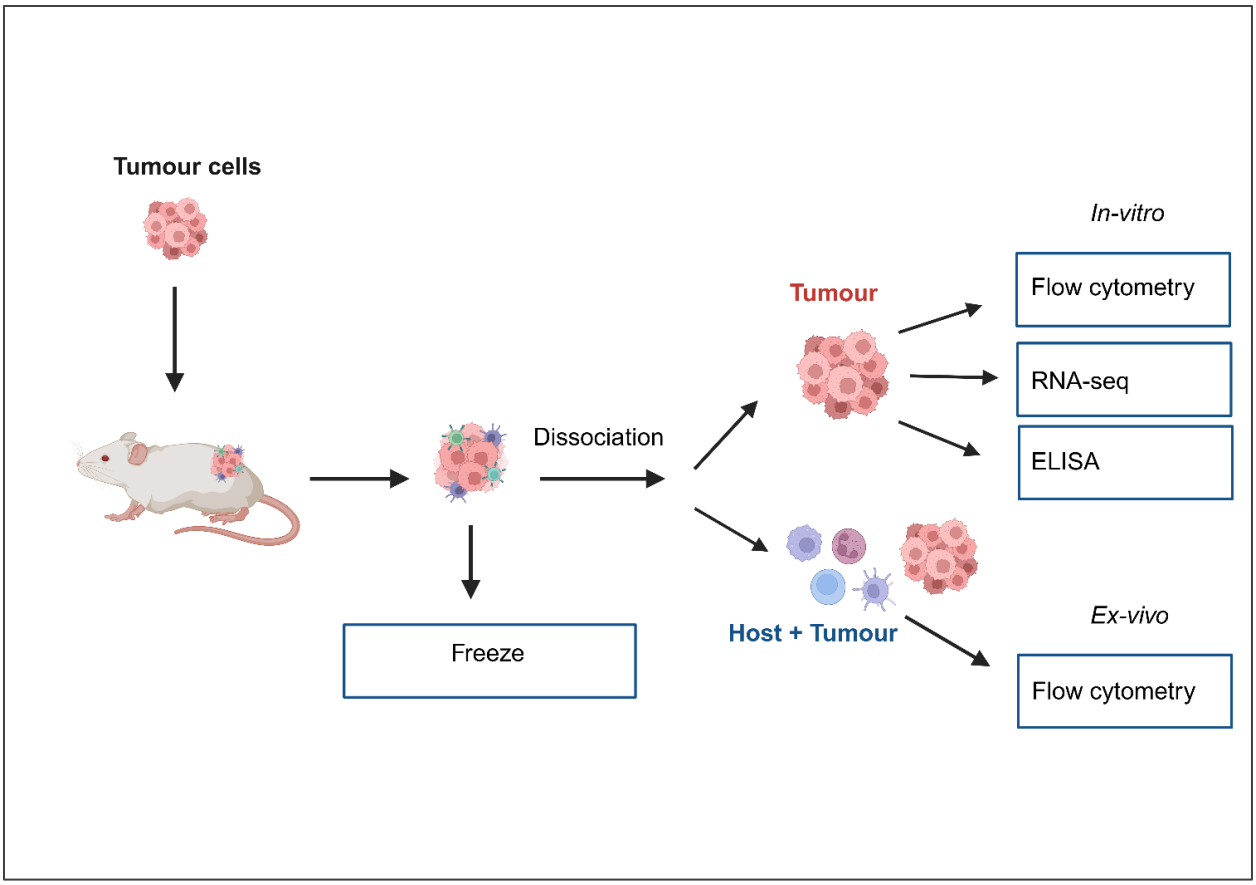

Figure 3.3: Methods to analyse the tumours. Tumour samples were collected; some tumours were frozen. Other tumours were dissociated to separate tumours from host immune cells. Tumour cells were grown *in vitro* for 2-4 passages to eliminate host immune cells then analysed *in vitro* by flow cytometry for tumour markers, or total RNA was extracted and analysed by RNA-seq. Tumour supernatant was collected for Enzyme-Linked Immunosorbent Assay (ELISA) analysis. The host immune infiltrate was analysed *ex vivo* by multiparameter flow cytometry.

3.2.4 Tumour Take Rates

During the experiments, mice were monitored for general signs of health, including activity, appearance, weight loss, clinical signs such as diarrhoea and dehydration, and whether there were changes to the mouse body condition i.e.: apparent skeletal structure or loss of muscles before and after tumour injections. According to the guidelines of the UCL BSU, the experiment had to stop if mice lost 20% of their weight or developed diarrhoea. None of the injected mice developed diarrhoea. The weights of the mice showed minor fluctuations after tumour injections but none of these mice lost more than 20% of their weight (Figure 3.4) or showed reduced activity or changes in appearance or body condition, indicating good health of the mice in general after tumour injections.

Table 3.4 shows the number of tumours “takes” at each mouse passage (a “take” is defined as a tumour that is measurable and is not rejected two weeks after cell injection). This is based on the fact that acute allograft rejection happens between 10 to 14 days (J. Zhou et al., 2013b). In the F0, F1, and F2 mouse crosses, no significant rejection was observed as 94.1%, 92.3, and 94.1% of tumours grew, respectively. However, the first N2 passage (N2.1) showed only a 40% take rate with 6/15 tumours growing without rejection. Another passaging round in the N2 mouse cross (N2.2) increased the tumour take to 46.7% (14/30), and a third round (N2.3) increased the tumour take to 100% (6/6). The N2.3 tumours grew successfully when injected into the completely allogeneic BALB/c mice with a take rate of 75%. A further round in the BALB/c mice (Balb/c-2) increased that to 93.8%. Balb/c-2 tumours passaged into CBA/Ca and FVB/N mouse strains grew successfully with a 100% take rate. Importantly, there were no takes when 1 million YUMM1.7 cells were

injected directly into N2 or BALB/c mice, demonstrating the strength of the allogeneic barrier in our model. Thus, serial passaging of YUMM1.7 cells into progressively immunological discordant mouse crosses resulted in tumour adaptation and greater allograft tolerance.

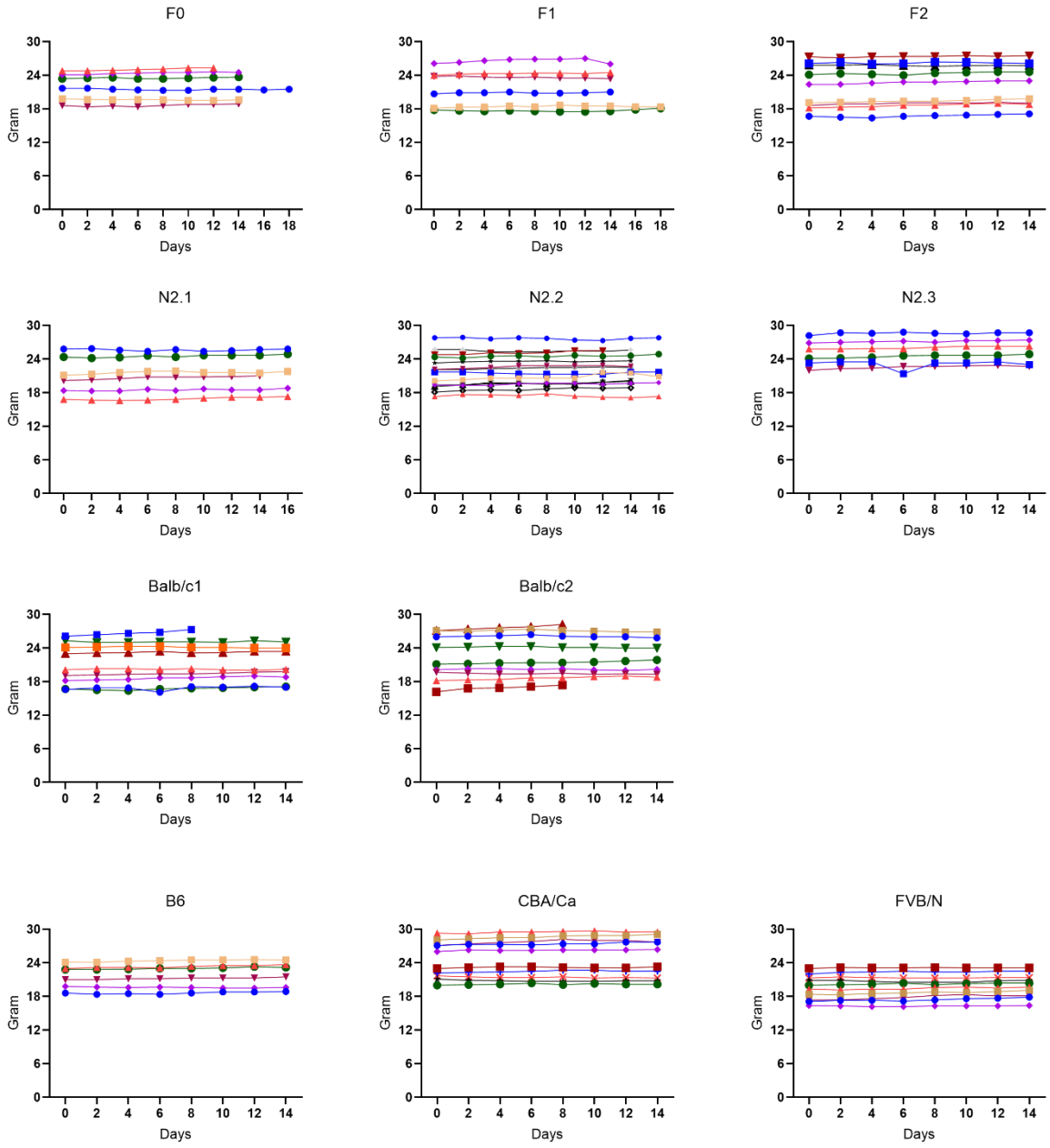

Figure 3.4: Mice Weights monitoring after tumour injection. Mice were injected with cells dissociated from different tumour passages. Mice weights were recorded on a bi-daily basis. Weight in grams for mice with successful tumour takes is shown.

Table 3.4: Tumour "takes" (tumours that grew in 2 weeks) and number of tumours dissociated at each passage. YUMM1.7 cells were also directly injected into N2 and BALB/c mice. Equal ratios of males and females were used for each passage.

Mouse strain	Tumour passage	No. of injected mice	No of takes	No of tumours dissociated
C57BL/6	F0	17	16	9
F1 (C57BL/6 x BALB/c)	F1	13	12	9
F2 (F1 x F1)	F2	17	16	5
N2 (F2 x BALB/c)	N2.1	15	6	6
N2	N2.2	30	14	3
N2	N2.3	6	6	3
BALB/c	Balb/c-1	12	9	5
BALB/c	Balb/c-2	16	15	5
C57BL/6	B6	6	6	4
CBA/Ca	CBA/Ca	10	10	4
FVB/N	FVB/N	10	10	4
N2	YUMM1.7	10	0	0
BALB/c	YUMM1.7	20	0	0

3.2.5 Phylogenetic Tree of Passaged Tumours

Due to the challenge of increasing mismatch between the hosts and these tumours, and to maximize the chance of tumour growth in the next passage, the two largest tumours were used at each passage for further propagation, except in N2.1 tumours where only 1 tumour was passaged due to the limited availability of N2 mice at this stage. The phylogenetic tree of the tumours is shown in Figure 3.5.

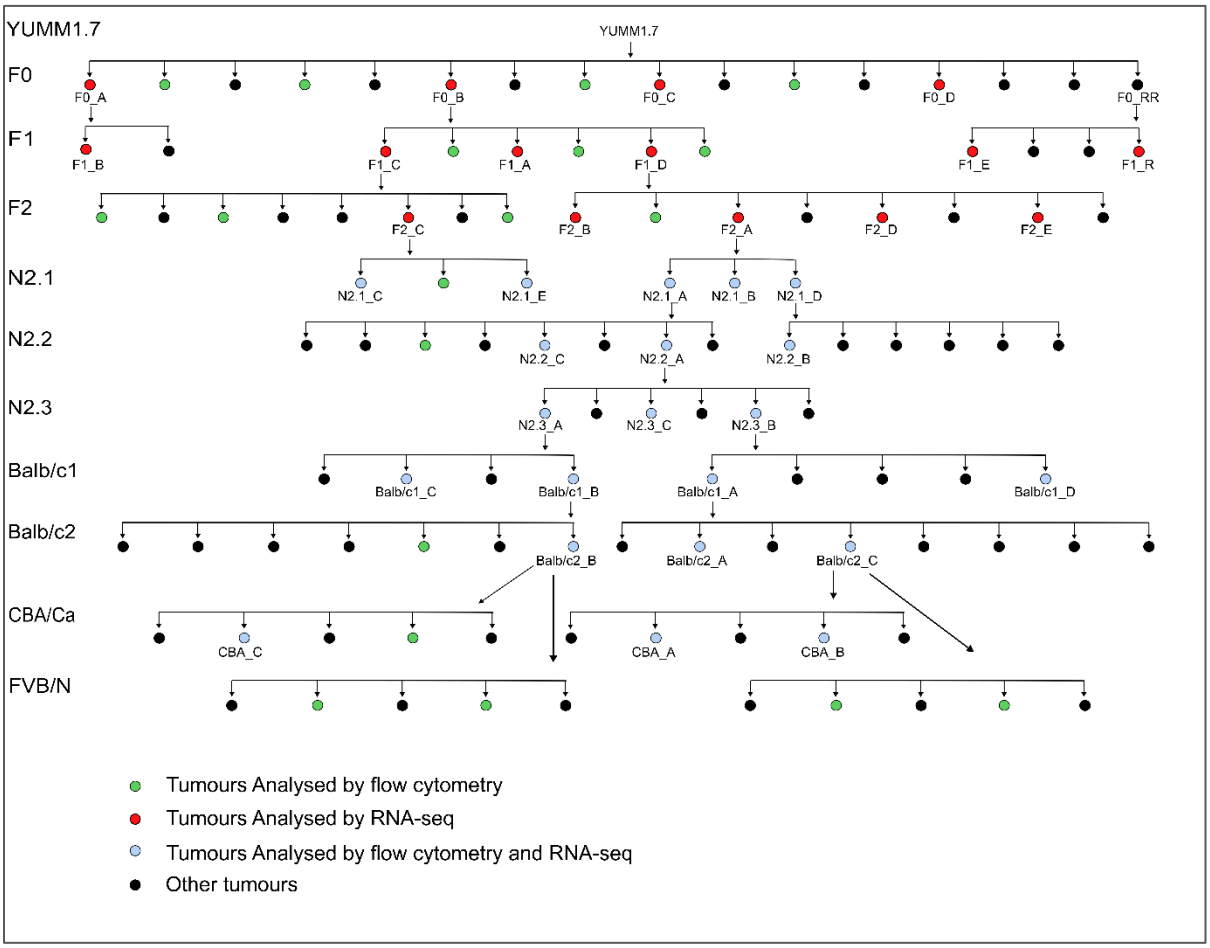

Figure 3.5. Phylogenetic tree of passaged tumours. YUMM1.7 cells were passaged using the strategy described in Figure 3.2. The 2-3 best-growing tumours were chosen for passaging into the next mouse generation except for the N2.2 passage.

3.2.6 Tumour Growth Kinetics

To better understand the adaptation process, I monitored tumour growth daily and then calculated tumour volume using the formula 0.5 x Length x Width^2 (0.5 x L x W^2) (Figure 3.6a). Tumour growth kinetics showed some differences across the passages. The F0 tumour started to appear 4 days after injection and grew at a rapid, constant rate. F1 tumours were slower as most tumours started to appear at day 6 post-injection. These tumours showed two patterns: tumours that grew exponentially or tumours that were stationary without being rejected. A similar behaviour was observed for N2.1 and N2.2 tumours. N2.3 tumours grew more rapidly than F1, N2.1 and N2.2 tumours, suggesting better adaptation to the N2 mouse cross after repeated passaging. However, when injected into BALB/c mice, N2.3 tumours grew more slowly with several tumours being stationary like in the F1 passage. Faster tumour growth was recorded in the second Balb/c (Balb/c-2) passage, with some tumours first appearing as soon as day 2 post-injection, suggesting better tumour adaptation to the BALB/c mice after repeated passaging. Balb/c-2 tumours injected in C57BL/6 mice showed an exponential growth pattern exceeding the one seen with the F0 tumours. The growth kinetics were different between CBA/Ca and FVB/N strains. In the CBA/Ca mice, the tumours started appearing on day 4 after injection and then grew exponentially until tumour collection. Whereas FVB/N tumours started to appear 2 days post-injection but showed slower tumour growth (Figure 3.6b).

Concerning tumours that grew and then regressed, these were all tumours that did not manage to grow large (<150 mm^3), and regression happened gradually, 8-12 days after tumour appearance (Figure 3.6b). A similar pattern was observed for YUMM1.7 cells injected directly, without prior adaptation, into the N2 or BALB/c mice.

Only 3/10 N2 mice injected with 1 million YUMM1.7 cells grew small tumours, which were all eventually rejected. Two of these tumours did not exceed 20 mm^3 and one 65 mm^3. Only 5/20 BALB/c mice injected with YUMM1.7 cells were able to grow detectable tumours. These tumours did not exceed 32 mm^3 and three of these were rejected rapidly whilst two were rejected more slowly (Figure 3.6c). Overall, these results indicate a stepwise adaptation of tumour cells to progressively immunologically discordant mouse crosses.

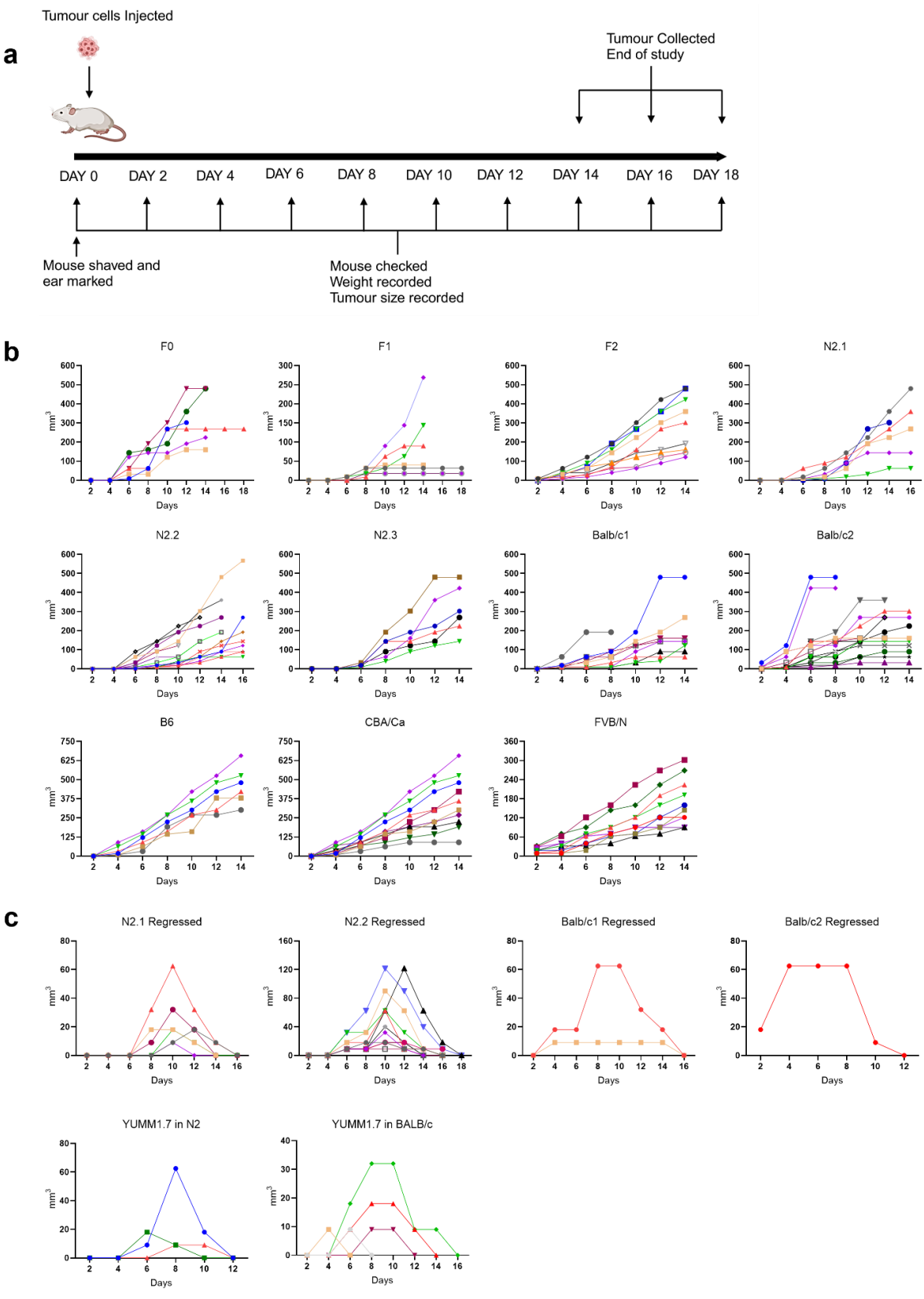
a
Tumour cells Injected
Tumour Collected
End of study
DAY 0
DAY 2
DAY 4
DAY 6
DAY 8
DAY 10
DAY 12
DAY 14
DAY 16
DAY 18
Mouse shaved and
ear marked
Mouse checked
Weight recorded
Tumour size recorded
b
F0
F1
F2
N2.1
N2.2
N2.3
Balb/c1
Balb/c2
B6
CBA/Ca
FVB/N
mm3
Days
c
N2.1 Regressed
N2.2 Regressed
Balb/c1 Regressed
Balb/c2 Regressed
YUMM1.7 in N2
YUMM1.7 in BALB/c

Figure 3.6: Tumour growth curves. a) Experiment timeline, mice were checked daily after injection for tumour growth. The results are presented as tumour volume using the formula ($0.5 \times L \times W^2$). b). Tumour volume in mm^3 for non-regressed tumours are shown. c) Tumour volume in mm^3 for regressed tumours.

3.3 Discussion

Here we showed that, in agreement with the results reported by Barrett and Deringer in the 1950s (Barrett & Deringer, 1952), serial tumour passaging into progressively more mismatched mouse crosses allowed the tumours to evade the histocompatibility barrier. We used melanoma YUMM1.7 cells for our transplantation studies because CTVT is likely derived from a melanoma and shares with YUMM1.7 cells some important genetic features (Broit et al., 2021; Cohen, 1985; Frampton et al., 2018). However, the early tumour transplantation studies reported a mouse mammary adenocarcinoma growth in mismatched mouse strains (Strong, 1926b) and later studies reported an adaptation for adenocarcinoma and sarcomas (Barrett & Deringer, 1952) (Dunham & Stewart, 1953). This suggests that cancer, at least in mice, has an intrinsic evolutionary potential to evade allogeneic rejection. The lack of allogeneic rejection makes it more likely that Balb/c-2 tumours might be transmitted across individuals, although we have not tested this possibility.

To create the allo-transplantable tumour we used fully immunocompetent mice, which has advantages compared to immunocompromised mice. Immunocompromised mice such as Nude, SCID, and NOD SCID lack important immune cells that are essential in the anti-tumour and transplantation immune responses. Therefore, tumour adaptation might not happen due to the lack of selective pressure exerted by the immune system on tumour cells (Dunn et al., 2004). This is clear in our study where only 40% of the N2.1 tumours were able to grow in N2 mice but two more rounds of passaging in the same host increased that to 100% while non-adapted parental YUMM1.7 did not grow at all in this host. Additionally, this model can be very useful in tumour evolution studies. There are

three stages regulating cancer-immune system interactions (Schreiber et al., 2011; Vesely et al., 2011). The first one is immune surveillance where normal cells undergoing malignant transformation are detected and killed by the immune system. This selective pressure forces the tumour to make changes to evade the immune surveillance in a process known as cancer immunoediting which is the second stage for cancer development. The third stage is immune evasion where cancer clones that successfully underwent immune editing can escape the immune system and proliferate causing clinically apparent cancer. Within this framework, our approach could be helpful in shedding light on tumour evolution strategies to escape immune surveillance.

Although we believe this model provides many benefits to study mechanisms of both allogeneic rejection and tumour immune escape, there are also limitations. These include the long time required to produce all the hybrid mouse strains. It is difficult to collect samples that regressed which limits the analysis to successful tumours only. Moreover, there are differences between tumours and normal organs that give tumours advantages in escaping the immune system. Firstly, tumours are conditioned to escape immune detection to be able to grow and metastasize by going through the aforementioned steps of selection. Secondly, tumour plasticity allows it to make phenotypic and functional changes *in vivo* that allow it to escape the immune system. Thirdly, this project focuses on acute rejection, therefore whether the adapted tumours can survive chronic rejection is not known. Finally, the self-renewal abilities of tumours are not possessed by normal organs which could still lead to chronic rejection if no complete graft tolerance is achieved.

4

Results

Chapter 4: Analysis of Tumour Immune Infiltrate

4.1 Introduction

Different immune cells play different roles which either support or inhibit tumour growth. Myeloid cells such as macrophages and immature cells expressing Gr-1 and CD11b have immune suppressive functions, leading to tumour progression. Tumour Associated Macrophages (TAM) are abundant in the TME. They are divided into two types M1 and M2. M1 macrophages play an inflammatory role. While M2 or alternative macrophages have immune suppressive functions. M2 macrophages reduce inflammation and suppress T cell functions by secreting factors such as IL-10 and TGF-β (M. Li et al., 2022a). CD11b+ Gr-1+ cells (markers of Myeloid Derived Suppressor Cells [MDSCs] or neutrophils) are a group of heterogeneous populations of myeloid cells. They play an immune suppressive function on T cells through the production of factors such as arginase (ARG-1), TGF-β, IL-10, and COX2 (Gabrilovich, 2017). They also produce factors such as VEGF leading to angiogenesis and tumour progression (Gabrilovich, 2017).

Although DCs have a very important anti-tumour role in presenting tumour antigens, there is increasing evidence of dysfunctional DCs leading to tumour tolerance. Tolerogenic DCs are quiescent immature cells that lead to the differentiation of T cells into more tolerant Th2 and regulatory T cells (Treg) instead of effector Th1 and Th17 T cells (Podestà et al., 2015a). These cells have been reported to prevent allotransplant rejection in murine models (Podestà et al., 2015a) and promoting tumour progression (Del Prete et al., 2023) (Bald et al., 2020).

Lymphoid cells such as CD4+, CD8+ T cells, and NK cells are important in fighting cancer cells. CD4+ T cells play an important role in coordinating the immune response against tumours. They exercise their antitumour role mainly by helping CD8+ CTLs. In order for naïve T cell to be activated two events need to take place. First, antigen on the surface of MHC-II of mature DC gets presented to TCR of T cells (signal one). Second, costimulatory signal such as CD28/(CD80, CD86) (signal two) interaction between mature DC and T cells.

In this chapter, I have therefore examined the TME to understand the different immune infiltrate at different tumour passages and correlate it with allogeneic tumour rejection, or lack of it.

4.2 Results

4.2.1 Immune Cell Markers and Spleen Staining

To understand the interactions between tumours and the host immune system, I assessed the intratumoural immune infiltrate by multiparameter flow cytometry. Different immune cells that are involved in the anti-tumour response and graft rejection were investigated, including total leukocytes (CD45+), lymphocytes (CD45+ CD3+), T cells (CD45+ CD3+ CD4+ or CD8+), NK cells (CD45+ CD3- NKp46+), dendritic cells (CD45+ CD3- MHC-II+ CD11c+), macrophages (CD45+ CD3- CD11b+ F4/80+) MDSCs or Neutrophils (CD45+ Gr-1+ CD11b+) (Bronte et al., 2016; Dean et al., 2024; Diao et al., 2018; Qiao et al., 2023). To test the validity of the antibodies and to set the gating strategy, spleen samples from C57BL/6 mice were collected, RBCs were lysed, then cells were stained with the multiparameter antibodies panel (Figure 4.1). The results showed that the chosen antibody panel identified the desired cell types, which were detected at frequencies that matched known reference values (Table 1) (Bio-Rad, 2017; Stemcell Technologies, 2013).

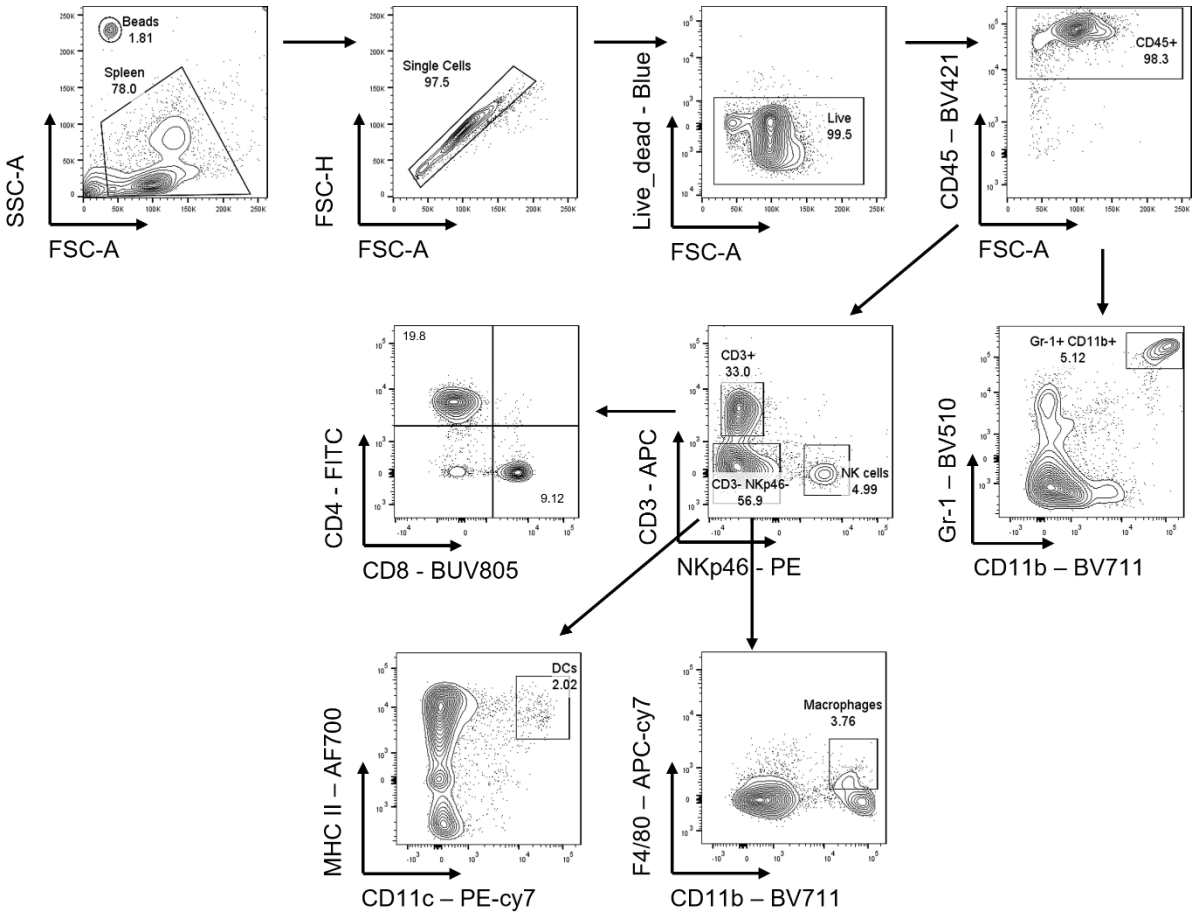

Figure 4.1: Spleen multiparameter staining. C57BL/6 mouse spleens were collected and filtered through 70µm strainers to get single-cell suspensions. RBCs were lysed, then spleen cells were aliquoted, stained with the multiparameter antibody panel and analysed by flow cytometry.

Table 4.1: Frequencies of the indicated cell populations found in the spleen. Comparing normal spleen frequency according to reference values and spleens used for the experiments described here.

Cell Type	Normal Spleen Frequency	Tested Spleens
T cells	21-35%	25-30%
CD4+ T cells	13-20%	15-19%
CD8+ T cells	7-15%	8-11%
NK cells	1-5%	2-5%
Monocyte/Macrophage	3.5-5%	2-4%
Dendritic cells	0.5-3%	0.5-1.8%

The dissociation protocol included an incubation step with 0.05% trypsin for 5 minutes. Some reports have shown that trypsin can digest some antigens from the cell surface of immune and tumour cells when used at a higher concentration (0.25%) and incubated for 30 minutes or more (Tsuji et al., 2017). Therefore, to assess if the low trypsin concentration used for tumour dissociation affected antigen surface levels, I carried out tumour dissociation in the presence or absence of 0.05% Trypsin-EDTA for 5 minutes and analysed the cells by flow cytometry using the same panel of antibodies described above. The results showed that a short incubation with trypsin at a low concentration increased the yield of dissociated cells and did not

appreciably reduce the intensity of the surface markers, except for an apparent small reduction in Gr-1 (Figure 4.2).

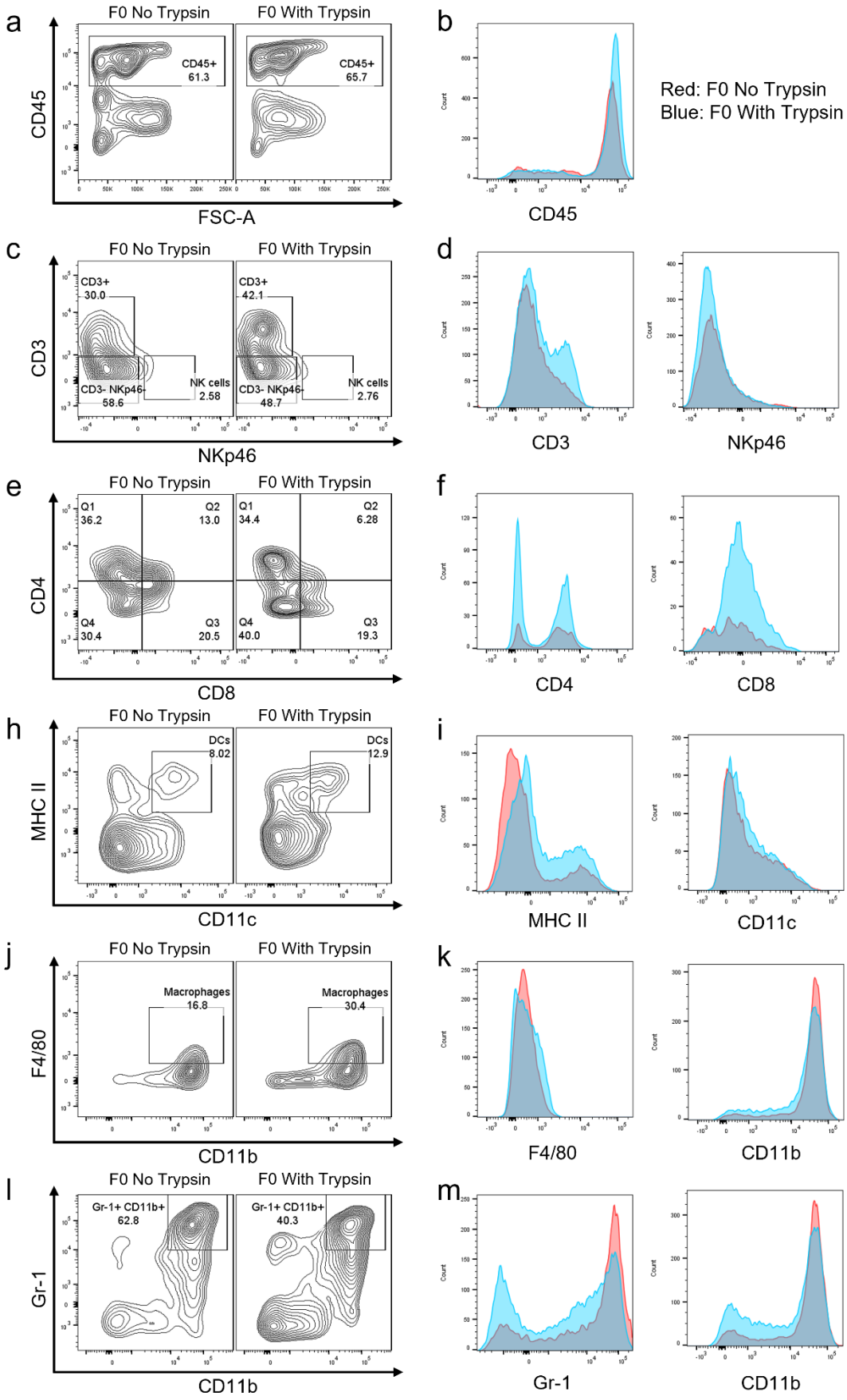
a
F0 No Trypsin
F0 With Trypsin
CD45+
61.3
CD45+
65.7
CD45
FSC-A
b
Red: F0 No Trypsin
Blue: F0 With Trypsin
CD45
c
F0 No Trypsin
F0 With Trypsin
CD3+
30.0
CD3+
42.1
CD3- NKp46-
58.6
NK cells
2.58
CD3- NKp46-
48.7
NK cells
2.76
CD3
NKp46
d
CD3
NKp46
e
F0 No Trypsin
F0 With Trypsin
Q1
36.2
Q2
13.0
Q4
30.4
Q3
20.5
Q1
34.4
Q2
6.28
Q4
40.0
Q3
19.3
CD4
CD8
f
CD4
CD8
h
F0 No Trypsin
F0 With Trypsin
DCs
8.02
DCs
12.9
MHC II
CD11c
i
MHC II
CD11c
j
F0 No Trypsin
F0 With Trypsin
Macrophages
16.8
Macrophages
30.4
F4/80
CD11b
k
F4/80
CD11b
l
F0 No Trypsin
F0 With Trypsin
Gr-1+ CD11b+
62.8
Gr-1+ CD11b+
40.3
Gr-1
CD11b
m
Gr-1
CD11b

Figure 4.2: Testing the effect of incubating cells with 0.05% trypsin-EDTA for 5 minutes during tumour dissociation. F0 tumours were dissociated following the protocol described in the methods section (Quintana et al., 2008) in the absence or presence of 0.05% trypsin-EDTA for 5 minutes. After dissociation, samples were stained using the same antibodies shown in Figure 4.1. Flow cytometry plots for CD45+ cells (a) CD3+ and NK cells (c) CD4+ and CD8+ T cells (e) DCs (h) macrophages (j) Gr-1+ CD11b (l). Histogram overlays of the two conditions tested (red: F0 no trypsin, blue: F0 with trypsin) for CD45 (b), CD3 (left panel) NKp46 (right panel) (d), CD4 (left panel) CD8 (right panel) (f), MHC-II (left panel) CD11c (right panel) (i), F4/80 (left panel) CD11b (right panel) (k), Gr-1 (left panel) CD11b (right panel) (m).

4.2.2 Evaluation of Intratumoral Immune Infiltrate

Using this tumour dissociation protocol, the tumour infiltrate was characterised at each passage. To comprehensively evaluate the tumour immune infiltrate, I used two parameters: 1- Absolute Counts and 2- Frequency of immune cell population within the CD45+ cell population. I analysed 5 key tumour passages that can shed light on the adaptation of tumours during passaging and their interaction with the immune system. F0 is the starting point of passaging in the syngeneic mouse strain (C57BL/6), N2.1 the first tumour passage that showed high regression/rejection rates, Balb/c-2 is the last step of passaging in a fully mismatched mouse strain (BALB/c), and CBA/Ca and FVB/N that represent two different strains mismatched to both C57BL/6 and BALB/c.

The number and frequency of leukocytes (CD45+ cells) showed an increase in the N2.1 passage compared to F0 and their number and frequency decreased in the subsequent passages Balb/c-2, CBA/Ca, and FVB/N (Figure 4.3a,b,c). This indicated that the high tumour regression rates in N2.1 most likely exerted a strong selective pressure on the subsequent tumours to be less immunogenic.

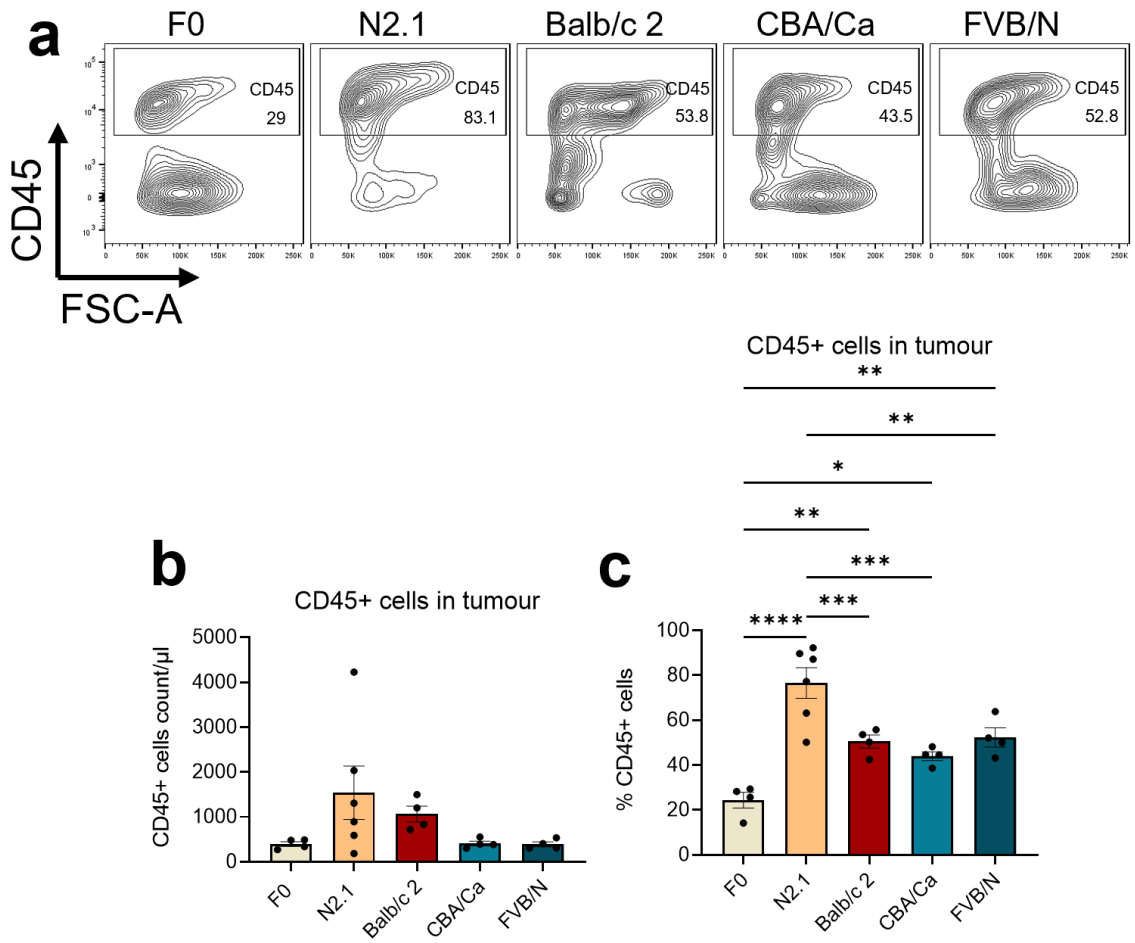

Figure 4.3: Analysis of the tumour CD45 immune infiltrate. F0, N2.1, Balb/c-2, CBA/Ca and FVB/N tumours were dissociated and freshly isolated cells were stained with the same antibodies described in Figure 4.1. Samples were analysed by flow cytometry according to the gating strategy shown in Figure 4.1. (a) Flow cytometry plots for CD45+ cells. (b) CD45+ cells count. (c) Frequency of CD45+ cells in tumours. F0 (n=4), N2.1 (n=6), Balb/c-2 (n=4), CBA/Ca (n=4), and FVB/N (n=4). Statistical analysis was carried out using two-way ANOVA with Tukey's multiple comparison correction. Each dot represents a different tumour. * Denotes (P= < 0.05). ** Denotes (P= <0.01). *** Denotes (P=0.001) **** Denotes (P<0.0001).

Lymphocytes (CD3+) numbers showed a trend similar to CD45+ cells (Figure 4.4b) but their frequency relative to CD45+ cells was different. F0 tumours showed the highest frequency of CD3+ T cells. A gradual decrease was noticed in N2.1 then Balb/c-2 which had the lowest frequency of CD3+ T cells. The frequency of CD3+ T cells gradually increased in CBA/Ca and FVB/N tumours respectively (Figure 4.4a,c). CD4+ T cell numbers mirrored the CD3+ T cells trend (Figure 4.4e) while their frequency showed an upward trend in tumour passages after F0 (Figure 4.4d,f). This suggests that they might be regulatory T cells (Tregs) which are inhibitory in nature, but Tregs were not specifically analysed. CD8+ T cell numbers showed a significant increase from F0 to N2.1. Remarkably, Balb/c-2, CBA/Ca, and FVB/N tumours had low levels of infiltrating CD8 T cells (Figure 4.4g) despite the fact that these tumours expressed high levels of MHC-I (explained later). This suggested impaired homing activity of CTLs. The CD8+ T cells frequency showed a gradual decrease from F0 to N2.1 to Balb/c-2 and CBA/Ca although FVB/N showed a slightly higher frequency of CD8+ T cells than CBA/Ca (Figure 4.4d,h). NK cell numbers showed a sharp increase from F0 to N2.1 and Balb/c-2 followed by a sharp decrease in CBA/Ca and FVB/N (Figure 4.4i). The relative percentage of NK cells in the CD45+ population showed a sharp increase from F0 to N2.1 which gradually decreased in the subsequent tumour passages but remained higher than the baseline levels (Figure 4.4a,j).

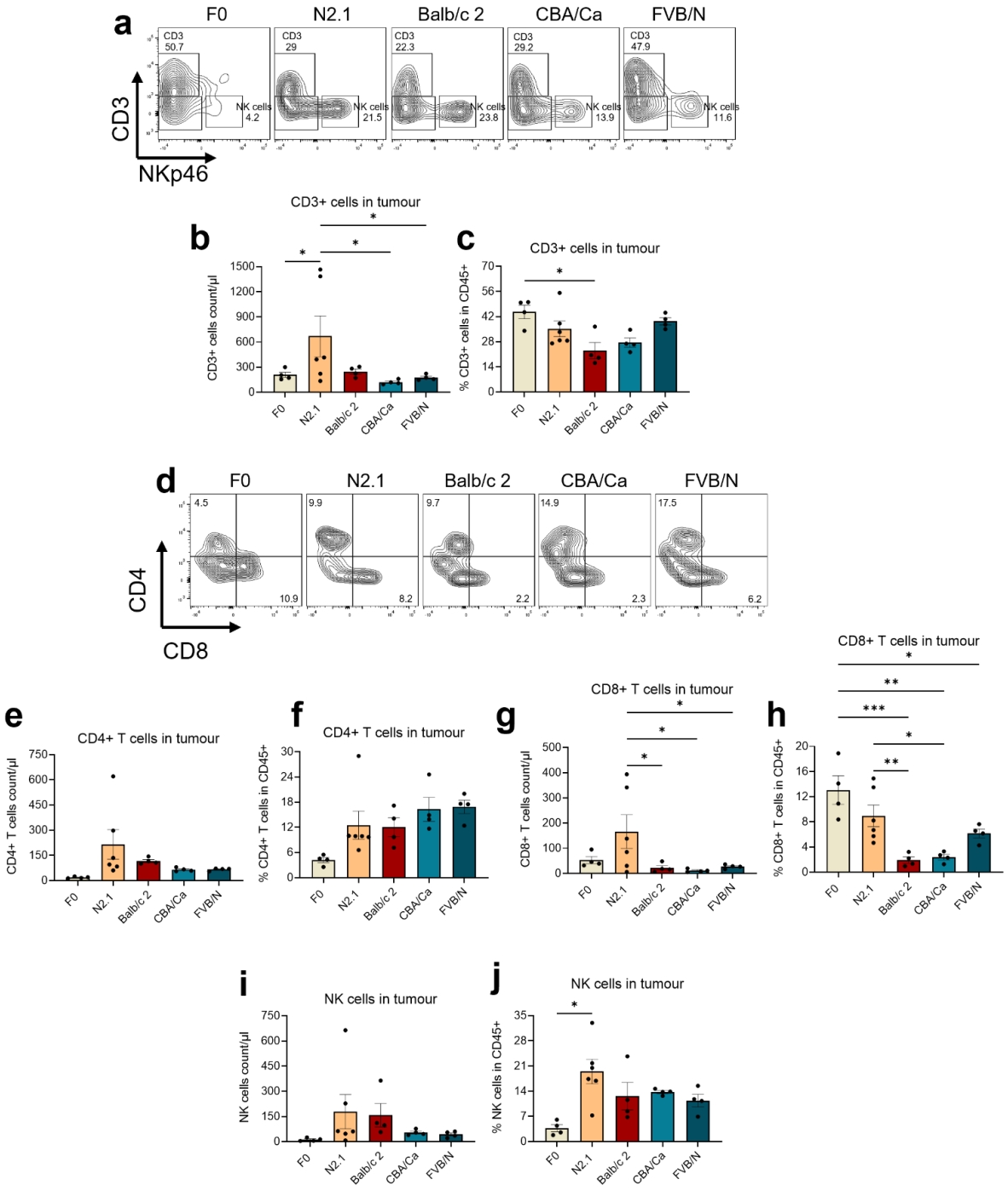
a
F0
N2.1
Balb/c 2
CBA/Ca
FVB/N
CD3
NKp46
CD3 50.7
NK cells 4.2
CD3 29
NK cells 21.5
CD3 22.3
NK cells 23.8
CD3 29.2
NK cells 13.9
CD3 47.9
NK cells 11.6
b
CD3+ cells in tumour
CD3+ cells count/µl
c
CD3+ cells in tumour
% CD3+ cells in CD45+
d
CD4
CD8
4.5
10.9
9.9
8.2
9.7
2.2
14.9
2.3
17.5
6.2
e
CD4+ T cells in tumour
CD4+ T cells count/µl
f
CD4+ T cells in tumour
% CD4+ T cells in CD45+
g
CD8+ T cells in tumour
CD8+ T cells count/µl
h
CD8+ T cells in tumour
% CD8+ T cells in CD45+
i
NK cells in tumour
NK cells count/µl
j
NK cells in tumour
% NK cells in CD45+

Figure 4.4: Analysis of the tumour lymphoid cells infiltrate. F0, N2.1, Balb/c-2, CBA/Ca and FVB/N tumours were dissociated and freshly isolated cells were stained with the same antibodies described in Figure 4.1. Samples were analysed by flow cytometry. (a) Flow cytometry plots for CD3+ and NK cells. (b) CD3+ cells count. (c) Frequency of CD3+ cells in CD45+ cells. (d) Flow cytometry plots for CD4+ and CD8+ T cells. (e) CD4+ T cells count. (f) Frequency of CD4+ T cells in CD45+ cells. (g) CD8+ T cells count. (h) Frequency of CD8+ T cells in CD45+ cells. (i) NK cells count. (j) Frequency of NK cells in CD45+ cells. F0 (n=4), N2.1 (n=6), Balb/c-2 (n=4), CBA/Ca (n=4), and FVB/N (n=4). Statistical analysis was carried out using two-way ANOVA with Tukey's multiple comparison correction. Each dot represents a different tumour. * Denotes (P= < 0.05). ** Denotes (P= <0.01). *** Denotes (P=0.001) **** Denotes (P<0.0001).

I also analysed the myeloid compartment; the number of dendritic cells (MHC-II+ CD11c+) showed a gradual increase from F0 to N2.1 to Balb/c-2 which was significant. CBA/Ca and FVB showed also higher levels than baseline F0 tumours (Figure 4.5b). The relative proportion of dendritic cells in the CD45+ population showed an upward trend and it was significantly higher in the Balb/c-2 and CBA/Ca tumours relative to the F0 and N2.1 passages (Figure 4.5a,c). Macrophages numbers were higher in N2.1 and Balb/c-2 tumours compared to other tumour passages which showed similar levels (Figure 4.5f). Balb/c-2 tumours also showed an increase in the percentage of macrophages within the CD45+ population, without reaching statistical significance, compared to other tumour passages (Figure 4.5e,j).

Finally, the numbers of CD11b+ Gr-1+ cells (markers of MDSCs or neutrophils) (Chiu et al., 2017; Dunay et al., 2008; M. Y. Park et al., 2020; Zalfa & Paust, 2021) were higher in N2.1 and Balb/c-2 tumours compared to other passages (Figure 4.5i). However, the population of CD11b+ Gr-1+ cells within the CD45+ did not show significant changes in the different tumour passages (Figure 4.5h,j).

Taken together, these results indicate that the intratumoural immune infiltrate changed during passaging with the highest numbers of CD8+ T cells infiltration observed in the N2.1 tumours, whereas Balb/c-2 tumours had an overall lower lymphoid infiltration relative to N2.1, and higher myeloid infiltration, especially for DCs and macrophages. Balb/c-2 tumours were not rejected, suggesting that the greater myeloid infiltration may have exerted an immune suppressive function, which has been well documented in the mouse and human tumour microenvironment (M. Li et al., 2022b; Ness et al., 2021a; Podestà et al., 2015b).

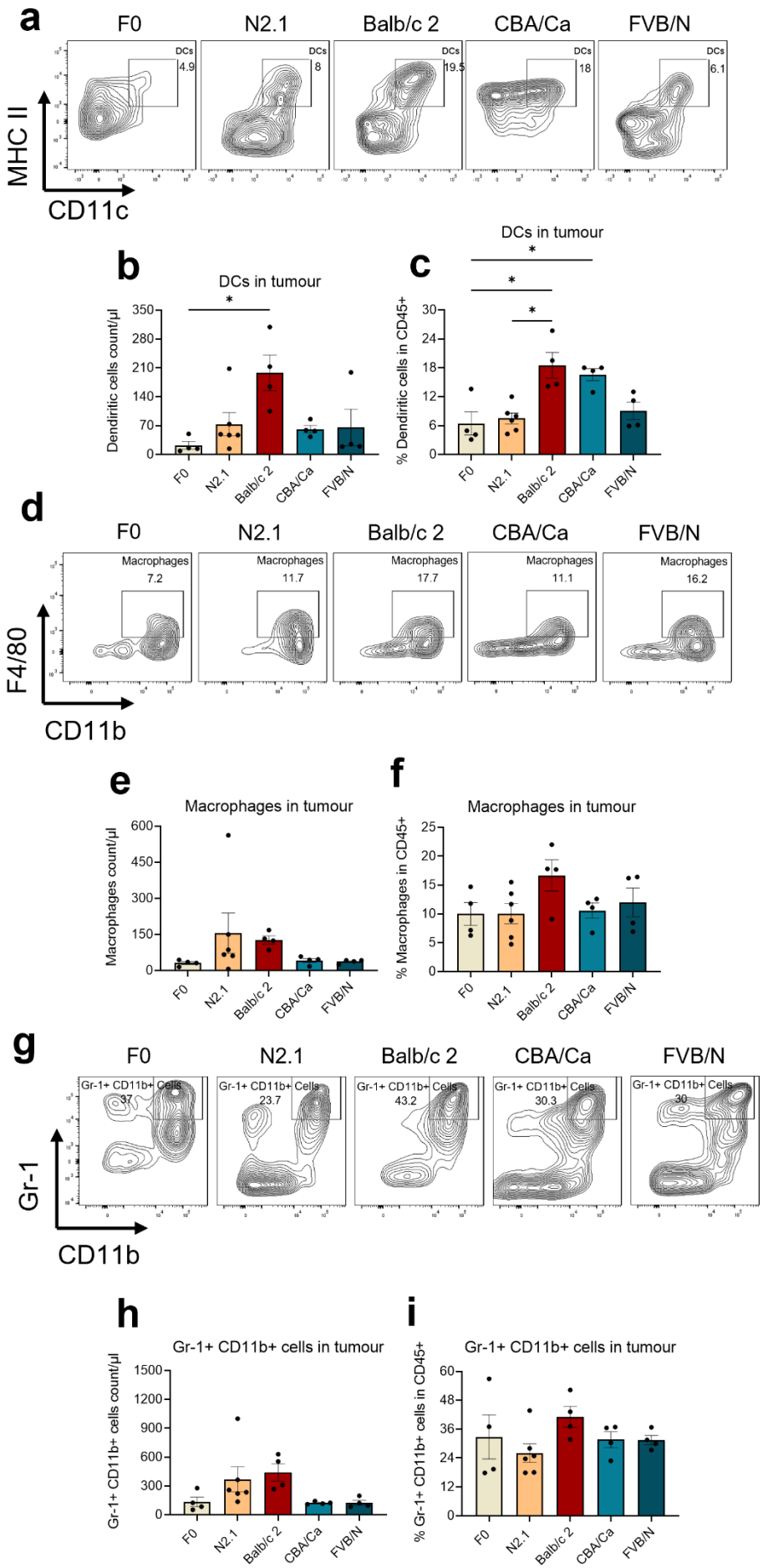
a
F0
N2.1
Balb/c 2
CBA/Ca
FVB/N
DCs
4.9
8
19.5
18
6.1
MHC II
CD11c
b
DCs in tumour
Dendiritic cells count/µl
c
DCs in tumour
% Dendiritic cells in CD45+
d
Macrophages
7.2
11.7
17.7
11.1
16.2
F4/80
CD11b
e
Macrophages in tumour
Macrophages count/µl
f
Macrophages in tumour
% Macrophages in CD45+
g
Gr-1+ CD11b+ Cells
37
23.7
43.2
30.3
30
Gr-1
CD11b
h
Gr-1+ CD11b+ cells in tumour
Gr-1+ CD11b+ cells count/µl
i
Gr-1+ CD11b+ cells in tumour
% Gr-1+ CD11b+ cells in CD45+

Figure 4.5: Analysis of the tumour myeloid cells infiltrate. F0, N2.1, Balb/c-2, CBA/Ca and FVB/N tumours were dissociated and freshly isolated cells were stained with the same antibodies described in Figure 4.1. Samples were analysed by flow cytometry. (a) Flow cytometry plots for DCs. (b) DCs count. (c) Frequency of DCs cells in CD45+ cells. (d) Flow cytometry plots for macrophages. (e) Macrophages count. (f) Frequency of macrophages in CD45+ cells. (g) Flow cytometry plots for Gr-1+ CD11b+ cells. (h) Gr-1+ CD11b+ cells count (i) Frequency of Gr-1+ CD11b+ cells in CD45+ cells. F0 (n=4), N2.1 (n=6), Balb/c-2 (n=4), CBA/Ca (n=4), and FVB/N (n=4). Statistical analysis was carried out using two-way ANOVA with Tukey's multiple comparison correction. Each dot represents a different tumour. * Denotes (P= < 0.05). ** Denotes (P= <0.01). *** Denotes (P=0.001) **** Denotes (P<0.0001).

4.2.3 Characterisation of T Cells Activation Status

T cells are key for a successful tumour or allograft immune response. Activated CD4+ T cells secreting Interleukin 2 (IL-2) can directly activate CD8+ T cells expressing the IL-2 receptor (CD25). Activated CD4+ T cells also directly and indirectly enhance CD8+ T cell functions by maintaining proinflammatory DCs which present antigens to CD8+ T cells leading to their activation (Tay et al., 2021).

I examined the expression of the following markers: CD69, CD44, and PD-1. CD69 is an early T cell activation and tissue residency marker and in combination with CD103 can identify tissue-resident memory T cells (Luangrath et al., 2021; S. L. Park et al., 2019; Topham & Reilly, 2018). CD44 is an adhesion molecule and a well-established activation marker that is expressed on effector and memory T cells but

not naïve T cells (Schumann et al., 2015). Programmed cell Death Protein-1 (PD-1) is expressed on the surface of T cells and other immune cells. It acts as an immune checkpoint to protect against autoimmunity. It interacts with its ligand PD-L1 to suppress T cell functions, a prevalent mechanism employed by cancers to suppress the anti-tumour immune response. PD-1 is considered one of the exhaustion markers when expressed on T cells in association with CTLA-4, TIM-3, LAG-3 (Tietscher et al., 2023) (Dolina et al., 2021; Thommen & Schumacher, 2018). Activated tumour infiltrating lymphocytes upregulate the expression of CD44, CD69, and PD-1 (Lin et al., 2023; Mita et al., 2018) (Tietscher et al., 2023).

The gating strategy of these markers on spleen cells is shown in (Figure 4.6). The frequency of CD44 expressing CD4+ T cells was highest in F0 tumours (Figure 4.7a). Other passages showed lower levels that were half the levels seen in the F0 tumours (Figure 4.7a). Similarly, the proportion of CD4+ T cells expressing the activation marker CD69 was the highest in F0 tumours, while the lowest levels were observed in N2.1 tumours (Figure 4.7b). The expression of the immune checkpoint PD-1 was significantly lower in F0 compared to all the other tumour passages (Figure 4.7c).

Taken together, F0 tumours showed more activated and less inhibited CD4+ T cells, while the subsequent tumour passages showed the opposite. These data suggest that the TME in later passages suppressed CD4+ T cell activation. Unfortunately, CD8+ T cell frequencies in the late tumours (Balb/c-2, CBA/Ca, and FVB/N) were very low which prevented a reliable assessment of these activation and inhibitory markers. Therefore, our analysis was limited to CD4+ T cells.

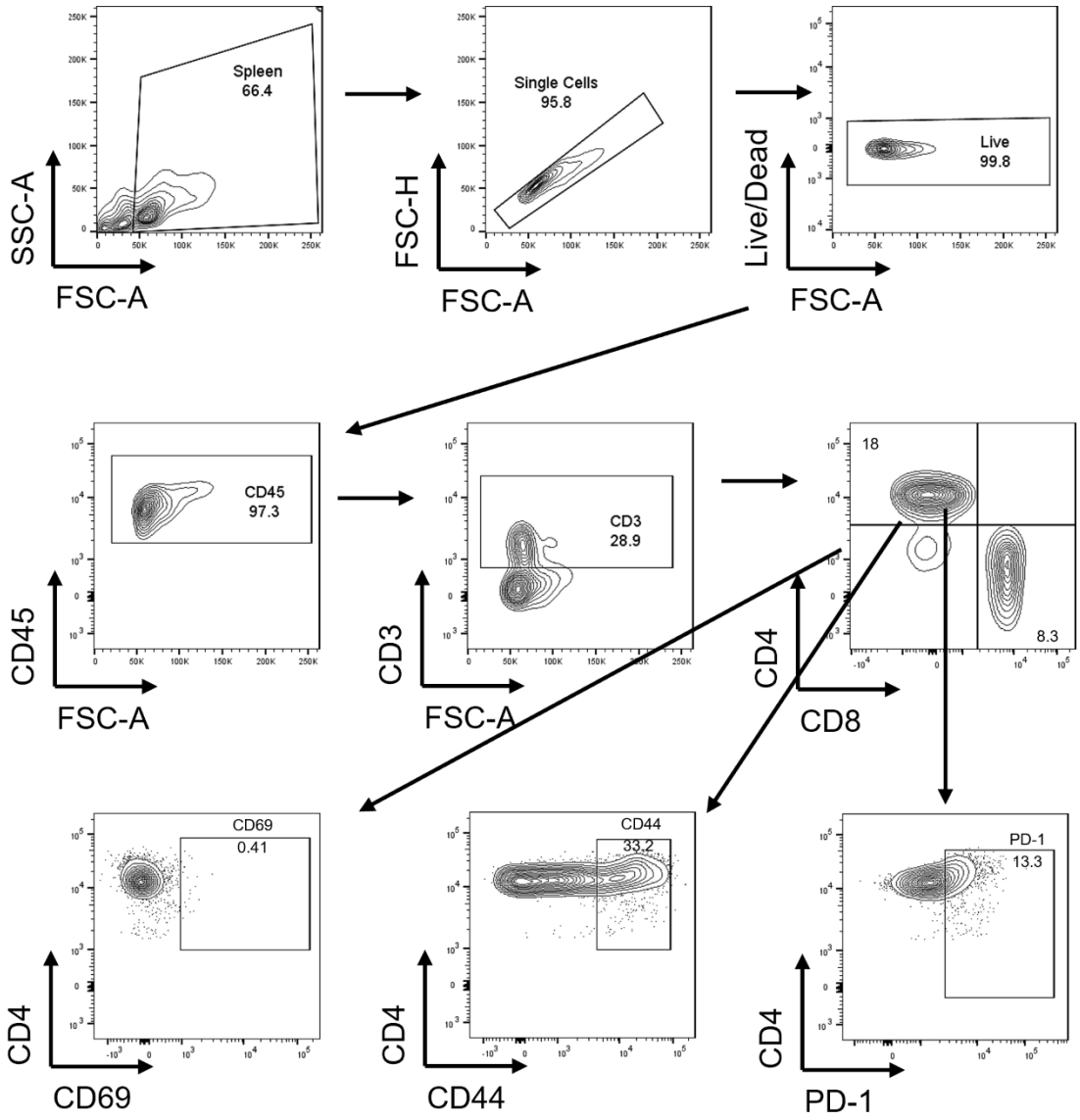

Figure 4.6: Spleen CD4+ T cells CD44, CD69, PD-1 staining. C57BL/6 mouse spleens were collected and filtered through 70µm strainers to get single-cell suspensions. RBCs were lysed, then spleen cells were aliquoted, stained with the multiparameter antibody panel and analysed by flow cytometer.

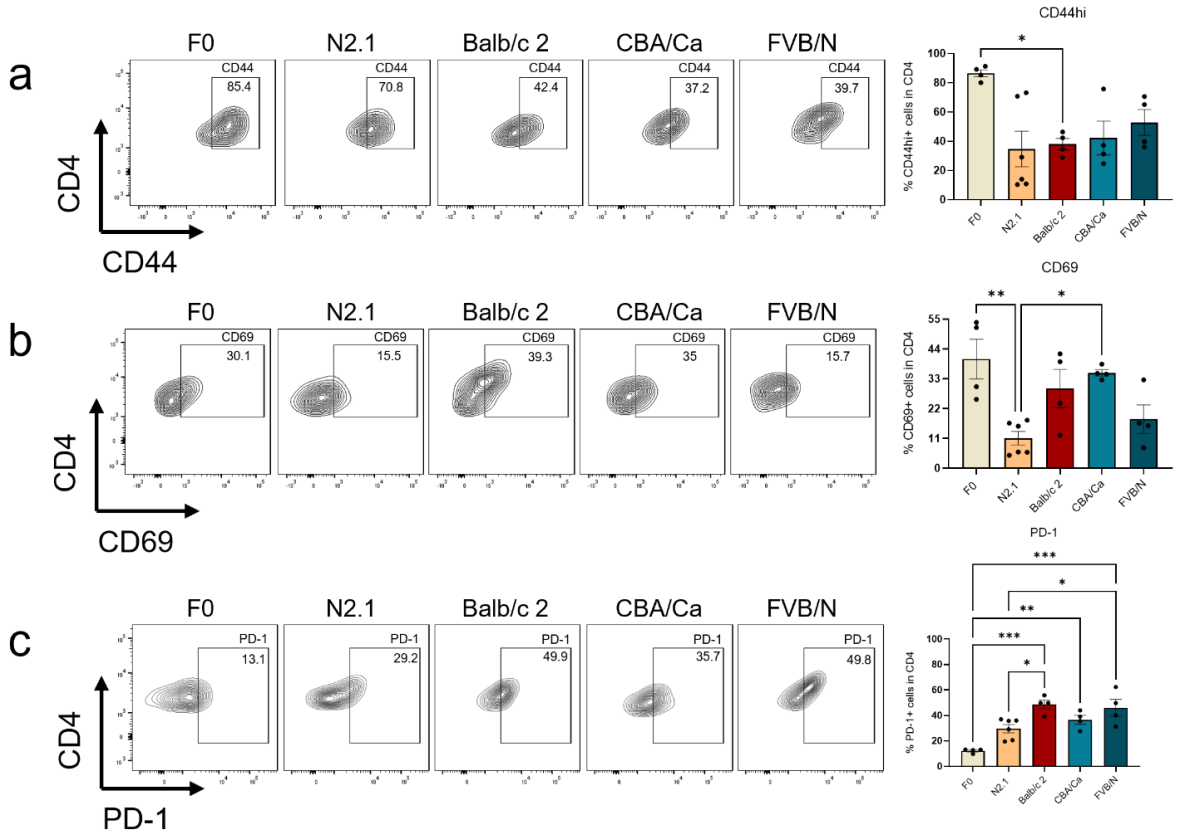

Figure 4.7: Analysis of the tumour CD4+ T cells CD44, CD69, PD-1 expression. Tumours were dissociated and freshly isolated cells were stained with the same antibodies described in Figure 7. Samples were analysed by flow cytometry. (a) Left panels, flow cytometry plots for CD44+; right panels, bar graphs showing the average percentage of CD44+ cells +/- SD. (b) Left panels, flow cytometry plots for CD69+ cells; right panels, bar graphs showing the average percentage of CD69+ cells +/- SD. (c) Left panels, flow cytometry plots for PD-1+ cells; right panels, bar graphs showing the average percentage of PD-1+ cells +/- SD. F0 (n=4), N2.1 (n=6), Balb/c-2 (n=4), CBA/Ca (n=4), and FVB/N (n=4). Statistical analysis was carried out using two-way ANOVA with Tukey's multiple comparison correction. Each dot represents

a different tumour. * Denotes (P= < 0.05). ** Denotes (P= <0.01). *** Denotes (P=0.001)**** Denotes (P<0.0001).

4.2.4 Systemic Versus Local Tolerance

In addition to the immune suppressive environment in the TME, there is evidence that the YUMM1.7 cell line can cause systemic immune suppression when injected into mice, characterised by fewer CD8+ T cells and increased M2-type macrophages in circulation (L. Huang et al., 2024). Therefore, we wanted to investigate whether tolerance to Balb/c-2.1 tumours was localized or due to systemic immune suppression caused by the tumours. To this end, we designed an experiment (Figure 4.8) where I injected 10 BALB/c mice with Balb/c-1 tumours in the left flank, then after 1 or 2 weeks I injected the right flank with the parental YUMM 1.7 cells (Balb/c-2.1 + YUMM1.7). If tolerance to Balb/c-2 tumours was dependent on systemic immune suppression caused by the tumours themselves, the expectation was that Balb/c-2.1 tumours would tolerize the mice to YUMM1.7 cells. Otherwise, the YUMM1.7 cells should be rejected as observed before (Table 3.4). The results showed that BALB/c mice sequentially injected with Balb/c-2.1 and YUMM1.7 cells, initially grew the Balb/c-2 tumours then after the injection of YUMM1.7 cells, these tumours regressed and no new tumour was detectable in either flank (Table 2). This indicated that tolerance to Balb/c-2 tumours is reversible and not systemic in nature.

Table 4.2: Tumour takes and the number of tumours dissociated at each passage in the double tumour injection experiment. YUMM1.7 cells were also directly injected into BALB/c mice. Equal ratios of males and females were used for each passage. (Balb/c-2 and YUMM1.7 data are taken from Table 3.4 and shown here for comparison).

Mouse strain	Tumour passage	No of injected mice	No of takes	No of tumours dissociated
BALB/c	Balb/c-2.1 + YUMM1.7	10	0	3
BALB/c	Balb/c-2	16	15	5
BALB/c	YUMM1.7	20	0	0

To understand what might have induced the regression of Balb/c-2 tumours in the Balb/c-2.1 + YUMM1.7 mice, we decided to analyse the tumour immune infiltrate. Regressing YUMM1.7 tumours were too small for dissociation, however, I managed to collect and dissociate three regressing Balb/c-2 tumours, which were dissociated and analysed by flow cytometry (Figure 4.8). Comparing the flow cytometry results previously collected for the Balb/c-2 tumours with the regressing Balb/c-2 + YUMM1.7 tumours (hereafter called B2.1) revealed a similar profile of intratumoral immune infiltrate in the two groups (Figure 4.9,b,d), except for a stark difference in the percentage of CD3+ NKp46+ cells, which were less than 2% in Balb/c-2 tumours and >45% in the B2.1 regressing tumours (Figure 4.9f). In addition, NK cells trended higher and CD4+ T cells lower in B2.1 relative to Balb/c-2 tumours (Figure 4.9e,I,h).

Unfortunately, the myeloid lineages could not be analysed due to insufficient cells obtained from B2.1 regressing tumours and insufficient counts by flow cytometry.

These data suggest that the introduction of the immunogenic YUMM1.7 cells into the Balb/c-2.1 + YUMM1.7 mice activated the CD3+ NKp46+ cell population, which infiltrated the Balb/c 2.1 tumours leading to their regression. A CD3+ NKp46+ cell population has been previously described in cattle, mice and humans that have features of both CTLs and NK cells and includes TCRα/β, TCRγ/δ and invariant TCR lineages (Connelley et al., 2014; Tomasello et al., 2012; Walzer et al., 2007). It is possible that the high levels of MHC-I expression found in Balb/c tumours (please see later) might have facilitated recognition and killing of tumour cells by the CD3+ NKp46+ cells.

Figure 4.8: Schematic depiction of experimental design of double injection experiment. Balb/c-1 tumours were injected into the left flank of BALB/c mice. After 1-2 weeks, when tumours were palpable, YUMM1.7 cells were injected into the right flank of the same mice. Tumour growth was monitored, and three regressing tumours were collected.

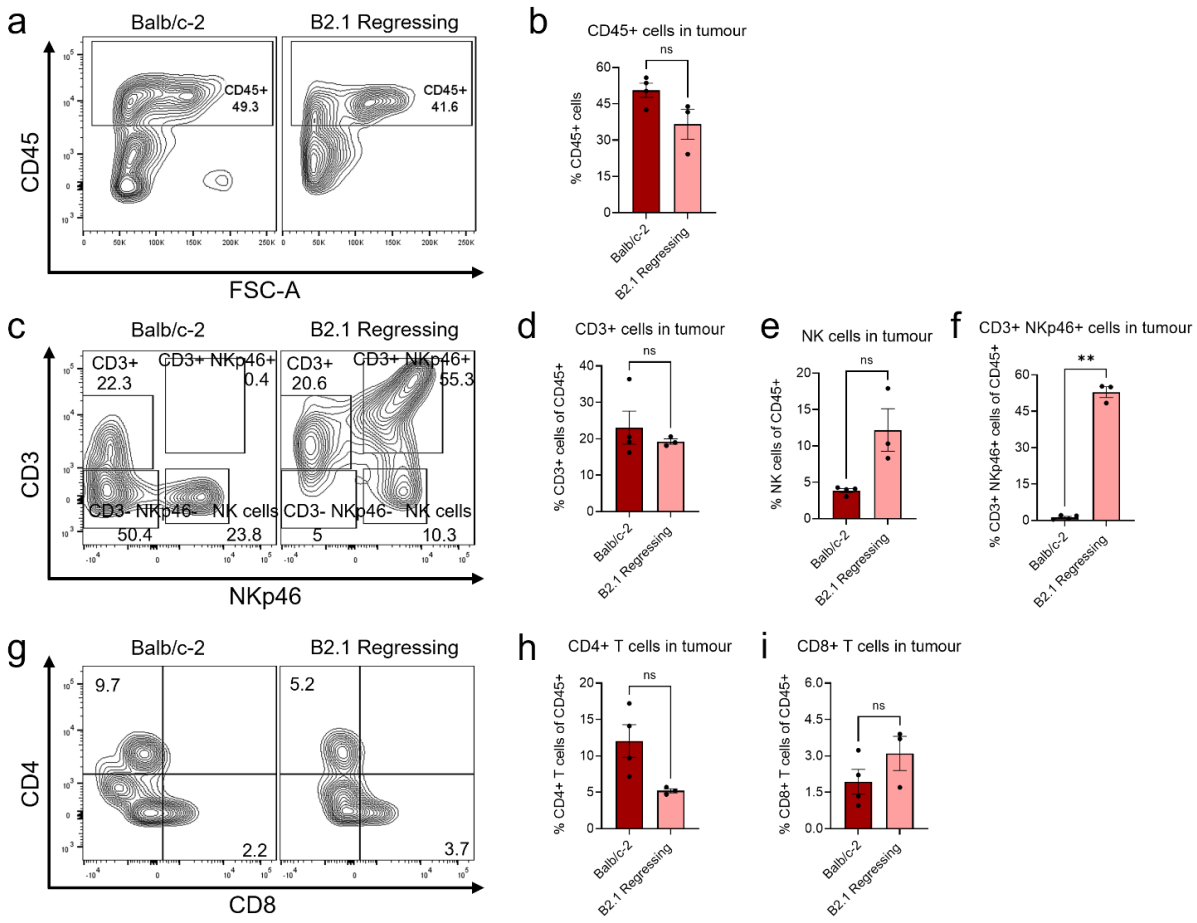

Figure 4.9: Analysis of the tumour immune infiltrate in regressing tumours (the Balb/c-2 data taken from Chapter 4 Figures 3-4 and shown here for comparison). Tumours were dissociated and freshly isolated cells were stained with the same antibodies described in Figure 4.1. Samples were analysed by flow cytometry. (a) Flow cytometry plots for and results for CD45+ cells. (b) Frequency of CD45+ cells in tumours. (c) Flow cytometry plots for CD3+ and NK cells. (d) Frequency of CD3+ cells in CD45+ cells. (e) Frequency of NK cells in CD45+ cells. (f) Frequency of CD3+ NKp46+ cells in CD45+ cells. (g) Flow cytometry plots for CD4+ and CD8+ T cells. (h) Frequency of CD4+ T cells in CD45+ cells. (i) Frequency of CD8+ T cells in CD45+ cells. Balb/c-2 (n=3) and B2.1 Regressing (n=3). Statistical analysis was

carried out using an unpaired t-test. Each dot represents a different tumour. * Denotes (P= < 0.05). ** Denotes (P= <0.01). *** Denotes (P=0.001) **** Denotes (P<0.0001).

4.3 Discussion

Our results indicate that tumour adaptation to grow in allo-mismatched mice was reflected in the host immune system tumour infiltrate. Tumours were moderately immunogenic in the F0 passage, became more immunogenic at the N2.1 passages, in which the rejection rate was highest, then reduced their immunogenicity in the Balb/c-2, CBA/Ca, FVB/N passages despite the fact that grafted tumour and host had a fully mismatched MHC-I haplotype. The higher immunogenicity of N2.1 tumours was accompanied by higher levels of T cell infiltration. The Balb/c-2, CBA/Ca, and FVB/N tumours were characterised by lower T and NK cells immune infiltration which suggests a less immunogenic tumour profile and a very suppressive TME.

Remarkably, serially passaged Balb/c-2 tumours showed more infiltration by DCs in both the relative percentage and the counts, and macrophages in relative percentage and to a lower extent, counts. The increase in the relative frequency of macrophages and DCs could be due to the reduced frequency of other cells notably CD3+ lymphocytes. Alternatively, the increased recruitment of TAMs and DCs may be due to the production of certain chemokines such as CCL2, CCL4, and CCL5 from the tumour that attract these cells (Kohli et al., 2022) (Xiang et al., 2021). TAMs are known to suppress effector immune cells by the production of soluble factors such as Arginase-1 (ARG1) and IL-10 leading to tumour survival and tolerance (Xiang et al., 2021). DCs are well known to contribute to anti-tumour immunity and allograft rejection, but there is evidence for an inhibitory or tolerogenic role of immature and some subsets of plasmacytoid DCs where they increase allograft survival (Ness et

al., 2021b; Podestà et al., 2015c). Therefore, better characterisation of macrophages and DCs in the TME is needed to draw any firm conclusion.

A more in-depth analysis of tumour infiltrating T cells at different passages using a panel of activation markers showed that a large proportion of CD4+ T cells were highly activated in the F0 tumour, while the later tumour passages showed a less activated and more inhibited state. CD4+ T cells in the TME of later passages were characterised by lower levels of activation markers and higher PD-1 expression relative to F0 tumours suggesting that TILs might be dysfunctional. Exhausted CD4+ T cells exhibit a dysfunctional state earlier than CD8+ T cells and demonstrate loss in effector functions such as the production of IFN-γ, TNF-α and IL-2 (Pauken & Wherry, 2015). Unfortunately, CD8+ T cells could not be analysed due to the very small number of cells in later tumour passages, but it is conceivable that CD8+ T cells exhibit similar status to CD4+ T cells due to the immune suppressive nature of the late tumours.

Overall, the data suggest that the immune suppressive status in the later tumour passages may be due to T and NK cell exhaustion, lower migration from the periphery, anergy and/or death. Macrophages and DCs (possibly tolerogenic), which would be attracted into the tumour by inflammatory mediators, likely contribute to this environment leading to allograft acceptance (Ness et al., 2021b; Podestà et al., 2015c; Xiang et al., 2021).

Notably, comparing Balb/c-2 experiments with experiments in mice that received YUMM1.7 cells after the injection of Balb/c tumour cells demonstrated that allograft tolerance was not due to systemic immunosuppression, rather it was achieved

locally. This finding has important implications for allotransplanted organ tolerance because it may point to approaches designed to affect the donor's organ rather than the recipient's immune system. The fact that both YUMM1.7 and Balb/c-2 cells were rejected in doubly injected mice demonstrates that tolerance is metastable and can be broken in the right conditions, which is similar to what is observed in CTVT (Frampton et al., 2018).

Our tumour transplantation model will be useful in understanding mechanisms for allogeneic tolerance, which may lead to improved allograft tolerance after organ transplantation. However, our results have several limitations. Firstly, we used a limited number of immunological markers to characterise the TME, several cell types such as NKT, B cells Tregs and other immune cells were not tested which could play an important role in establishing tolerance. Secondly, other than the reduced CD8+ T cells in the later tumour passages no other immune cells showed a stark difference that could explain the immune tolerance. Thirdly, CD8+ T cells could not be extensively analysed due to their low number in late tumour passages. Fourthly, we have no information on the clonal expansion or deletion of T cells infiltrating the tumour. Lastly, although DCs and macrophages could be potentially involved in the tumour tolerance of later passages, we do not have yet a mechanistic link between DCs and macrophages and escape from allogeneic rejection. These issues will need to be addressed in future work.

5

Results

Chapter 5: Tumour Immune Escape

5.1 Introduction

One of the hallmarks of cancer is the ability to evade the immune system (Hanahan & Weinberg, 2011). Cancers employ different strategies to evade the immune system. One of the main strategies is the downregulation of the MHC-I. MHC-I is located on the surface of all nucleated cells and its main function is to present endogenous peptides to CD8+ T cells that can detect non-self or mutated antigens and destroy them (Wu et al., 2023). Tumours downregulate MHC-I expression either by the reducing gene expression of the MHC-I gene complex, or the genes encoding for APM, which is responsible for proper folding and assembling the MHC-I on the cell surface (Shklovskaya & Rizos, 2021). The selective pressure from CD8+ T cells and the genomic instability of tumours can lead to somatic gene alterations leading to a deficient MHC-I in what is known as Loss of Heterozygosity (LOH) that can trigger NK cell detection (Garrido & Aptsiauri, 2019; Shklovskaya & Rizos, 2021).

For successful antigen presentation by MHC-I, different steps have to take place. First, endogenous proteins are fragmented by proteosomes into peptides. These peptides are then moved from the cytoplasm into the Endoplasmic Reticulum (ER) by transporters such as TAP1 and TAP2. In the ER these peptides are processed into smaller fragments 8-10 amino acids length. Also, in the ER the MHC complex is assembled by Calnexin and stabilized by chaperones such as ERp57 and Calreticulin. Then TAP1/2 and Tapasin deliver the processed peptides into the newly assembled MHC-I molecule. This MHC-I complex is transferred via the Golgi apparatus where it is glycosylated and then into the cell surface where the antigen

is presented to CD8+ T cells (Pishesha et al., 2022). Tumours can manipulate any of these steps to prevent or downregulate MHC-I expression on the cell surface (Dhatchinamoorthy et al., 2021).

Tumour cells express different ligands that interact with the different immune cells leading to their activation or inhibition. Key molecules include PDL-1 (CD274), which can inhibit the activation of NK and T cells by binding to the immune checkpoint molecule PD-1 and can be upregulated by different proinflammatory cytokines such as IL-6, IFN-γ, and TNF-α (Cha et al., 2019). Galectin -9, which interacts with different receptors on immune cells such as the inhibitory molecule TIM-3 expressed on T cells and NK cells leading to a reduction in T cell expansion and effector functions. Galectin-9 can also interact with CD40 leading to the inhibition of T cell proliferation and cell death (Vaitaitis & Wagner, 2012). CD155, which interacts with the coinhibitory receptors TIGIT and CD96, is expressed on T and NK cells to prevent their activation (J. Gao et al., 2017). CD155 interaction with TIGIT on NK cells suppresses their ability to produce IFN-γ. B7-H3 is an inhibitory ligand which suppresses T cell activation and proliferation by the early inhibition of IL-2 production which is required for T cell activation and proliferation (Leitner et al., 2009). In addition, non-classical MHC-I molecules play an important immune modulatory function. H2-M and H2-Q MHC molecules, which are the mouse homologues of the human HLA-G MHC molecules, are normally expressed on trophoblasts and suppress the immune response against the placenta leading to foetal-maternal immune tolerance. HLA-G molecules are upregulated in different tumours such as melanoma, renal, colorectal, and lung cancers and leukaemia. They bind to the inhibitory receptors LILRB1 and KIR leading to the inhibition of NK cells' cytotoxic

functions and CD8+ T cells apoptosis. Their expression on tumours also promotes the expansion of Gr-1+ CD11b+ cells and the shift of DCs to the tolerogenic DCs which suppress CD4+ and CD8+ T cells. Like H2-M, mouse H2-T (HLA-E in humans) non-classical MHC molecules are expressed on trophoblasts. H2-T molecules are frequently upregulated by tumours such as melanoma, gliomas, and lymphomas. HLA-E binds to the inhibitory receptor NKG2A expressed on T and NK cells leading to the suppression of their functions. Interestingly, HLA-G can induce the upregulation of HLA-E (Kochan et al., 2013).

To understand which of these mechanisms is important to confer escape from allogeneic rejection, I have analysed the expression of MHC-I, non-classical MHC-I and PD-L1 on tumour cells at each passage, and we have performed RNA-seq to investigate in an unbiased way additional mechanisms for immune evasion.

5.2 Results

5.2.1 MHC-I Expression in Tumour Cells

MHC-I is key in controlling allotransplant rejection by allogeneic antigen presentation by self MHC-I ("indirect" presentation) or allogeneic antigen presentation by non-self (donor) MHC-I ("direct" presentation) (Benichou et al., 2011). Furthermore, down-regulation or Loss of Heterozygosity (LOH) of MHC-I is a well-known mechanism of tumour immune evasion (Reeves & James, 2017b). I therefore analysed MHC-I expression on the surface of tumour cells by flow cytometry. The specificity of the antibodies was tested by staining both C57BL/6 and BALB/c mice spleens for MHC-I alleles H2-Db and H2-Kb, specifically expressed on C57BL/6 cells. C57BL/6 spleens showed high positivity for H2-Db and H2-Kb (Figure 5.1a). When BALB/c spleens were stained with the C57BL/6-specific H2-Db and H2-Kb antibodies, no positivity was detected (Figure 5.1a). Taken together, these results indicated that the chosen antibody panel could detect C57BL/6 cells specifically, with little or no cross-staining of BALB/c cells. Therefore, this antibody panel was suitable for monitoring MHC-I expression in the parental YUMM1.7 cells and subsequent tumour passages.

To evaluate MHC-I expression, dissociated cells from each tumour passage were expanded *in vitro* for 2 to 4 passages, which eliminated non-adherent cells, stained with the C57BL/6-specific MHC-I H2-Db and H2-Kb antibodies and analysed by flow cytometry using Fluorescence Minus One (FMO) controls to set the gate (Figure 5.1a). I found a high frequency of MHC-I expression on the parental YUMM1.7 cells (mean = 89.8%), however expression decreased gradually with passaging, reaching a nadir in N2.1 tumours (mean= 4.3%) and then gradually rising again in the N2.3 and subsequent tumour passages (Figure 5.1b). Mean fluorescence intensity (MFI)

of H2-Db and H2-Kb followed a similar pattern (Figure 5.1c,d). These results suggested that tumours were under selective pressure to downregulate surface expression of MHC-I up to the N2.1 passage but this pressure was lost or perhaps even reversed at later passages.

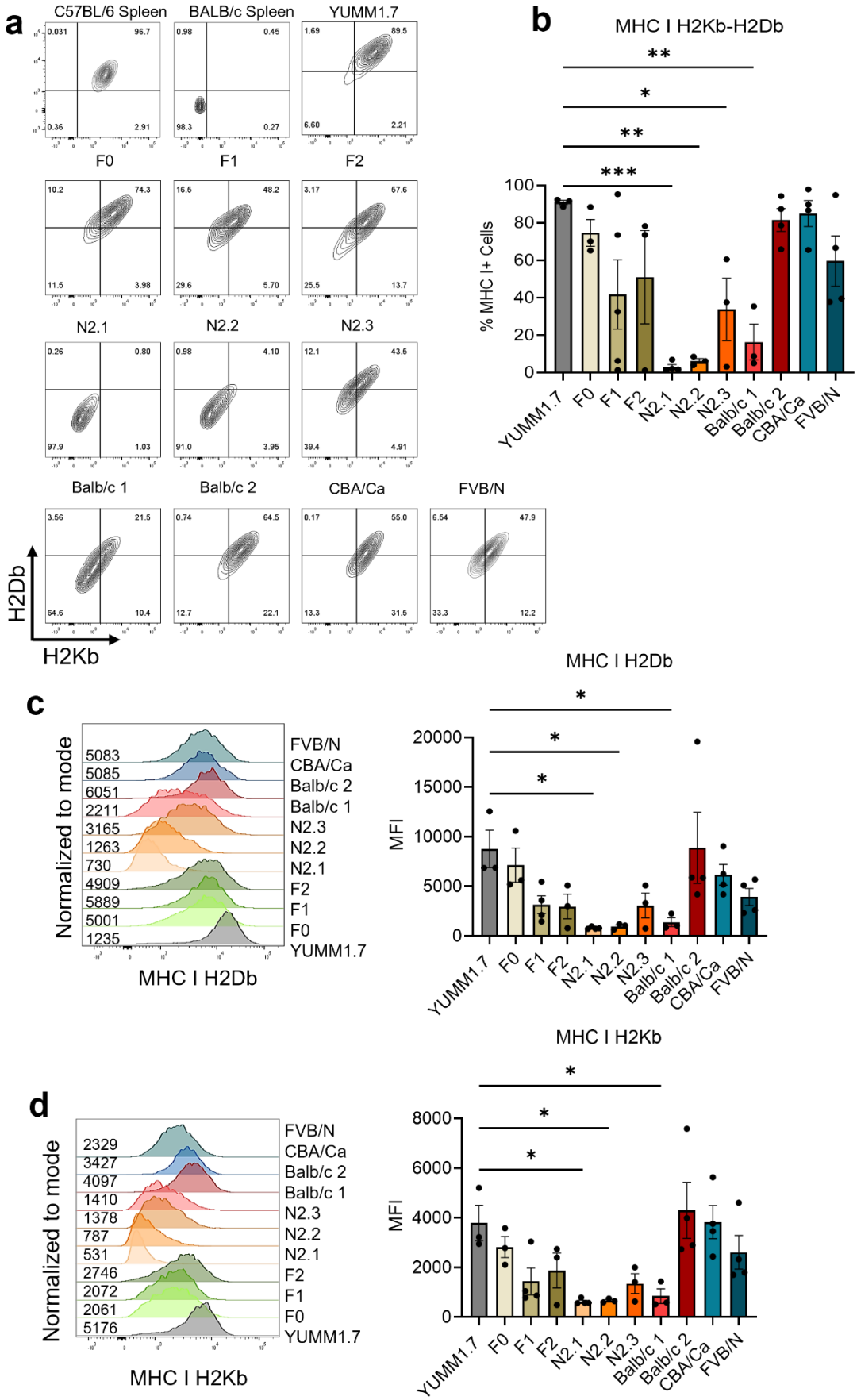
a
C57BL/6 Spleen
BALB/c Spleen
YUMM1.7
F0
F1
F2
N2.1
N2.2
N2.3
Balb/c 1
Balb/c 2
CBA/Ca
FVB/N
H2Db
H2Kb
b
MHC I H2Kb-H2Db
% MHC I+ Cells
c
Normalized to mode
MHC I H2Db
MFI
MHC I H2Kb
d
Normalized to mode
MHC I H2Kb
MFI

Figure 5.1. Surface expression of MHC-I on tumour cells after passaging. a) Spleen samples from C57BL/6 and BALB/c mice were collected; after RBCs lysis, the spleens were stained for C57BL/6-specific MHC-I alleles H2-Db and H2-Kb, representative flow cytometry plots are shown (upper left and middle panel). After dissociation, tumour cells were expanded *in vitro* for 2-4 passages to eliminate non-adherent cells and then analysed by flow cytometry for H2-Db and H2-Kb surface expression. Representative flow cytometry plots are shown in a. b) Percentage of H2-Db+ H2-Kb+ cells. c) Representative Mean Fluorescence Intensity (MFI) flow cytometry histograms for H2-Db at different tumour passages (left Panel). MFI values of H2-Db at different passages (Right panel). d) Representative MFI flow cytometry histograms for H2-Kb at different tumour passages (Left panel). MFI values of H2-Kb at different passages (Right panel). Each dot represents a different tumour sample. YUMM1.7 (n=3), F0 (n=3), F1 (n=5), F2 (n=3), N2.1 (n=4), N2.2 (n=3), N2.3 (n=3), Balb/c-1 (n=3), Balb/c-2 (n=4), CBA/Ca (n=4), FVB/N (n=4). Statistical analysis was carried out using one-way ANOVA. Each dot represents a different tumour. * Denotes (P= < 0.05). ** Denotes (P= <0.01). *** Denotes (P=0.001) **** Denotes (P<0.0001).

To better understand the mechanism of this reversible down-regulation of the MHC-I, I analysed RNA-seq data (described in greater detail later) obtained from the tumour cells, focussing on the MHC-I genes and other genes important for MHC-I processing, maturation and surface expression (components of the APM) [21]. We found progressively higher expression of *H2-K1*, *H2-D1* (MHC-I) and APM

components beta-2-microglobulin (*B2m*), *Tapbp*, *Tap-1* and *Tap-2* genes (Figure 5.2a,b). Whereas chaperones involved in the assembly of the newly found MHC-I complex and its proper folding Calnexin (*Canx*), Calreticulin (*Calr*), *Pdia3*, and *Hspa5* gene expression showed moderately lower gene expression levels in the N2.1 and N2.2 tumours relative to the other passages (Figure 5.2c).

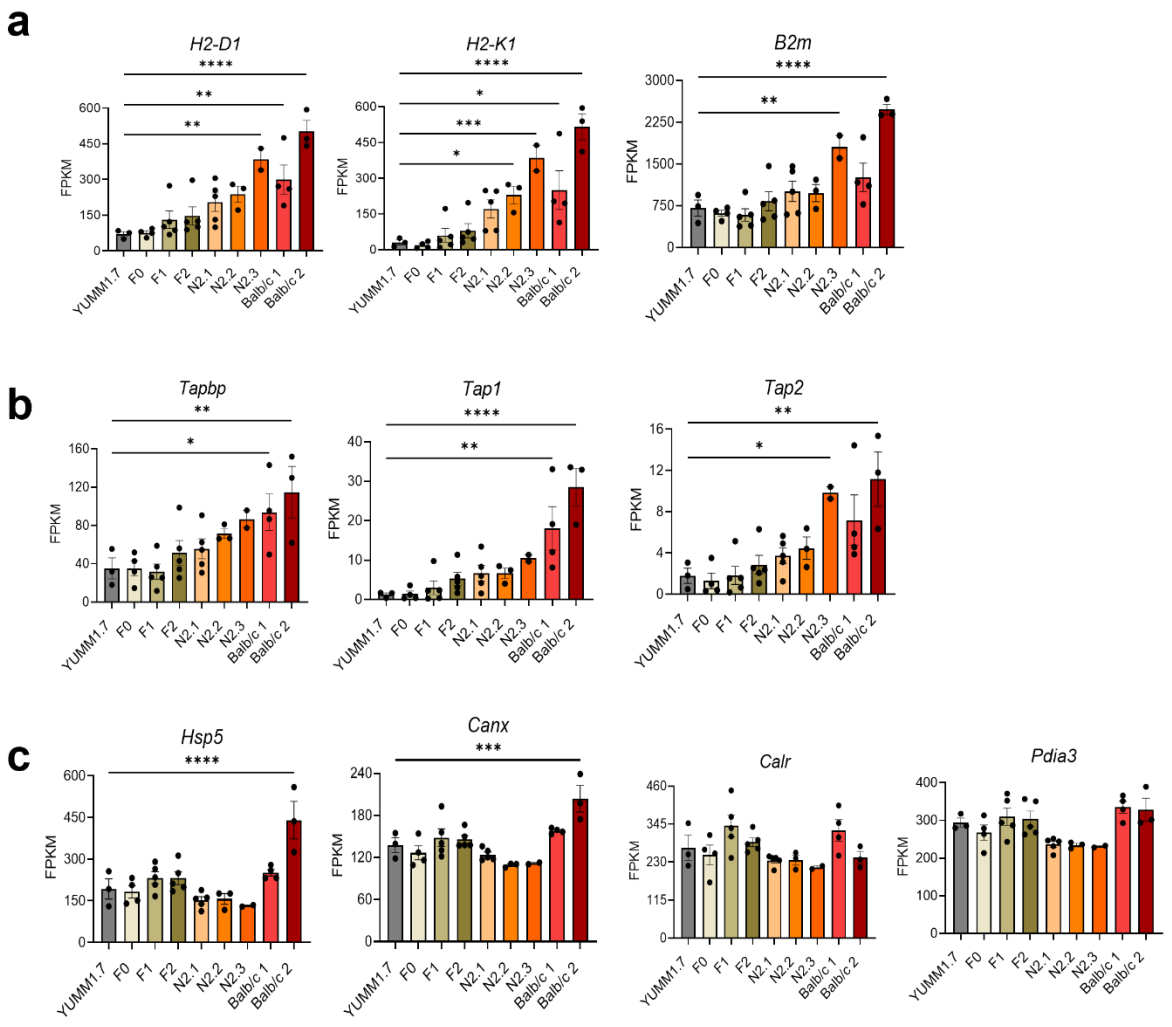

Figure 5.2. Gene expression of MHC-I and APM components in tumour cells after passaging. After dissociation, tumour cells were grown *in vitro* for 2-4 passages to eliminate host immune cells then total RNA extracted and RNA libraries sequenced. Gene expression values in FPKM for different MHC-I and APM genes.

a) Gene expression of MHC-I components. b) Gene expression of transporter components of APM. c) Gene expression of chaperone components of APM. YUMM1.7 (n=3), F0 (n=4), F1 (n=5), F2 (n=5), N2.1 (n=5), N2.2 (n=3), N2.3 (n=2), Balb/c-1 (n=4), Balb/c-2 (n=3). Each dot represents a different tumour sample. Statistical analysis was carried out using one-way ANOVA. Each dot represents a different tumour. * Denotes (P= < 0.05). ** Denotes (P= <0.01). *** Denotes (P=0.001) **** Denotes (P<0.0001).

These results demonstrated that the low MHC-I surface expression detected in the N2 tumours was not caused by transient gene silencing. The lower gene expression of APM components suggested possible assembly defects of the MHC-I complex, leading to defects of surface expression. I therefore measured the level of intracellular H2-Db and H2-Kb by flow cytometry to compare F0, N2.1 and Balb/c-2 cells. I found a similar intracellular H2-Db signal across the three passages, and a significantly higher H2-Kb signal in Balb/c-2 tumours relative to YUMM1.7 and N2.1 cells (Figure 5.3a-d). Thus, some defect prevented proper surface expression of H2-Db and H2-Kb in N2.1 cells even if these genes were transcribed at substantially higher levels in the N2.1 tumours compared to parental YUMM1.7 cells and at levels similar to Balb/c-2 cells. These results were confirmed by fluorescent immunolabelling of tumour cells on coverslips followed by confocal microscopy imaging, which showed more cytoplasmic localization of H2-Kb and to a lesser extent H2-Db in N2.1 tumours, and lower cell surface staining compared to YUMM1.7 and Balb/c-2 cells (Figure 5.3e,f).

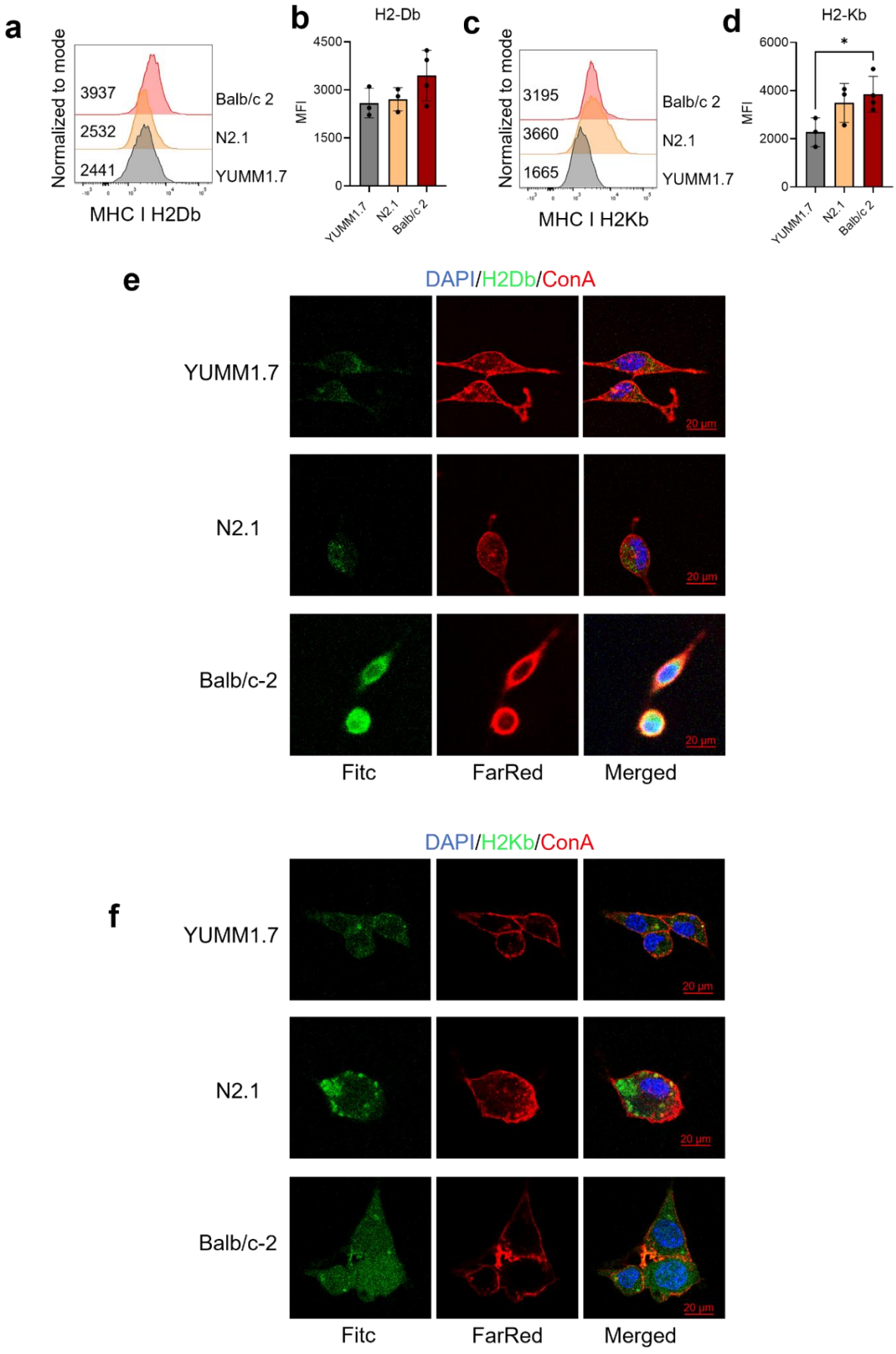
a
Normalized to mode
3937
2532
2441
Balb/c 2
N2.1
YUMM1.7
MHC I H2Db
b
H2-Db
MFI
4500
3000
1500
0
YUMM1.7
N2.1
Balb/c 2
c
Normalized to mode
3195
3660
1665
Balb/c 2
N2.1
YUMM1.7
MHC I H2Kb
d
H2-Kb
MFI
6000
4000
2000
0
*
YUMM1.7
N2.1
Balb/c 2
e
DAPI/H2Db/ConA
YUMM1.7
N2.1
Balb/c-2
20 µm
Fitc
FarRed
Merged
f
DAPI/H2Kb/ConA
YUMM1.7
N2.1
Balb/c-2
20 µm
Fitc
FarRed
Merged

Figure 5.3. Intracellular expression of MHC-I in tumour cells after passaging. a) After dissociation, tumour cells were expanded *in vitro* for 2-4 passages to eliminate non-adherent cells and then stained for intracellular H2-Db and H2-Kb and analysed by flow cytometry a) Representative flow cytometry histograms for H2-Db for YUMM1.7, N2.1, and Balb/c-2 tumour cells. b) MFI for H2-Db for YUMM1.7, N2.1, and Balb/c-2 tumours. YUMM1.7 and N2.1 (n=3), Balb/c-2 (n=4). c) Representative flow cytometry histograms for H2-Db for YUMM1.7, N2.1, and Balb/c-2 tumour cells. d) MFI for H2-Db for YUMM1.7, N2.1, and Balb/c-2 tumours. YUMM1.7 and N2.1 (n=3), Balb/c-2 (n=4). e) Immunofluorescence (IF) staining of H2-Db in YUMM1.7, N2.1, and Balb/c-2 tumour cells. f) IF staining of H2-Kb in YUMM1.7, N2.1, and Balb/c-2 tumour cells. Each dot represents a different tumour sample. Statistical analysis was carried out using one-way ANOVA. Each dot represents a different tumour. * Denotes (P= < 0.05). ** Denotes (P= <0.01). *** Denotes (P=0.001) **** Denotes (P<0.0001).

5.2.2 Changes in Gene Expression of the Tumour During Adaptation

To examine, in an unbiased way, changes in gene expression during tumour passaging, we performed RNA-seq on isolated tumour cells. For this analysis, we used all the passages up to the Balb/c-2, in which tumours became fully allo-transplantable. As described earlier, after dissociation, tumour cells were expanded *in vitro* for 2 to 4 passages in DMEM/F12 + 10% FBS. This eliminated non-adherent, and host immune cells. Total RNA was extracted and RNA-seq libraries were generated from poly-T oligo-enriched mRNAs using the NEBNext UltraTM RNA

Library Prep Kit. After sequencing, paired-end clean reads were aligned to the mouse reference genome using the Spliced Transcripts Alignment to a Reference (STAR) software. Differential expression analysis between groups was performed using the DESeq2 R package (2_1.6.3) and the resulting P-values were adjusted using Benjamini and Hochberg's approach for controlling the False Discovery Rate (FDR). The results showed excellent and uniform sequencing and mapping coverage across all the different tumour passages (Figure 5.4b). The absence of contaminating immune cells was confirmed by the absence of transcripts for CD45 (*Ptprc*) in each tumour passage (Figure 5.4a). In addition, transcripts for CD3 (*Cd3g*)*, Cd4, and* CD8 (*Cd8b1*) were not detectable (not shown).

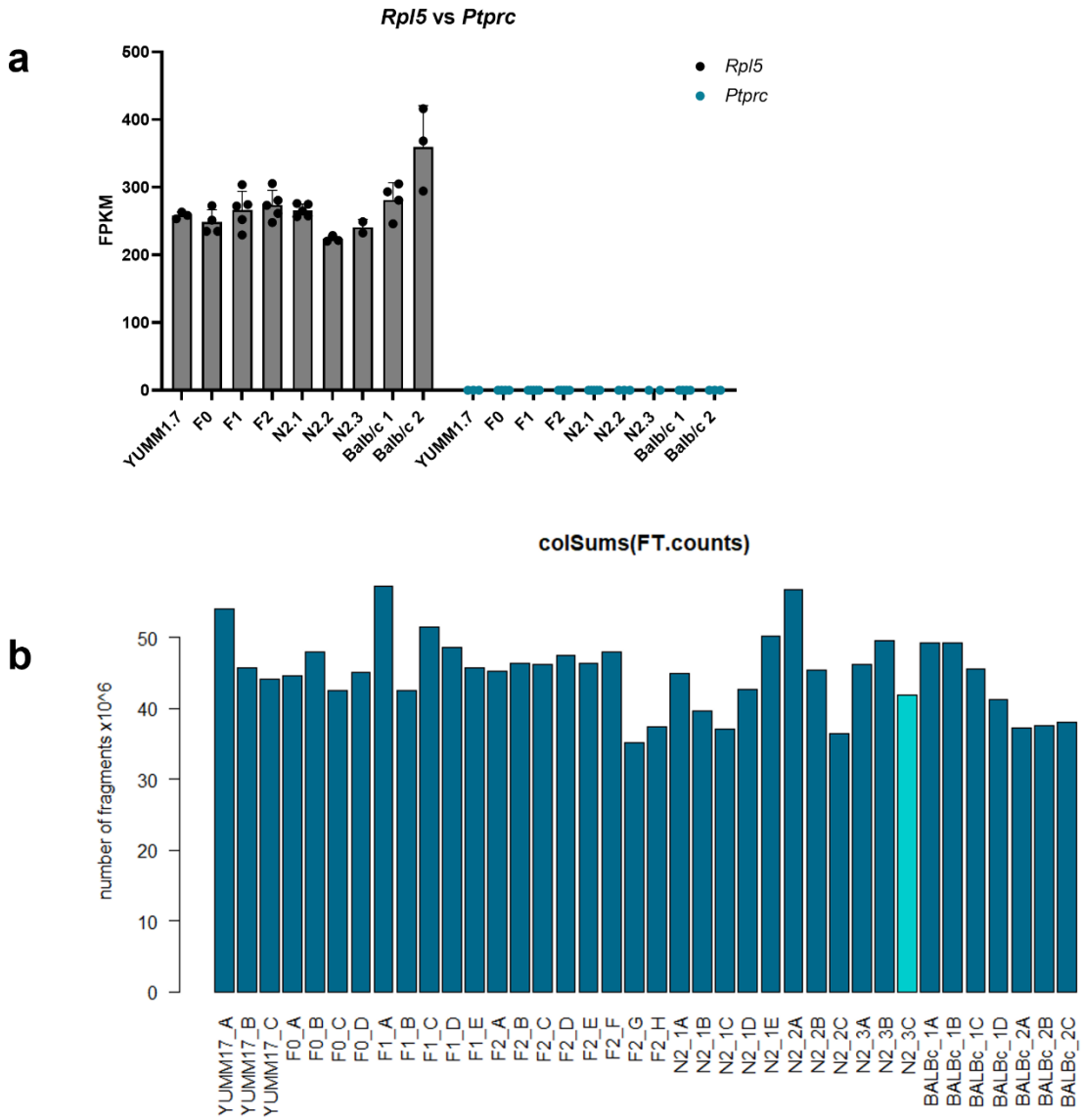

Figure 5.4. **RNA-seq of tumour cells.** Tumour cells were expanded in culture for 2-4 passages. RNA was extracted from tumour cells and RNA sequenced (a) FPKM values for housekeeping gene *Rpl5* vs *Ptprc* (CD45). (b) Number of fragments x 10^6 is shown. The light blue bar indicates one sample that was not taken forward because gene expression analysis showed it was muscle, most likely due to an error in collecting a small tumour, or to heavy contamination of the biopsy.

We used Principal Component Analysis (PCA) to determine the level of similarity across the different tumour passages. This analysis showed that YUMM1.7 and F0 tumours overlap and that F1 and F2 tumours form a cluster that partly overlaps with YUMM1.7 cells. However, PCA showed separate clusters for N2.1, N2.2 and N2.3 and for Balb/c tumours, indicating a stepwise adaptation of the tumours (Figure 5.5a). Sample N2.3C was an outlier and subsequent analysis using gProfiler revealed high expression of many muscle-related genes (not shown), indicating contamination of the tumour with skeletal muscle, presumably because muscle was inadvertently collected and dissociated in this case. Sample N2.3C was therefore removed from subsequent analyses.

Overall, progressively more genes were differentially expressed during passaging, with a step-change occurring at passage N2.1 (Figure 5.5b). To assess which genes were differentially regulated at each tumour passage, we applied thresholds of FDR 5% and log2FC >0.5 and compared each passage to the parental YUMM1.7 cells. This led to a set of 7282 Differentially Expressed Genes (DEGs), and unsupervised hierarchical clustering demonstrated a stepwise expression pattern as shown in the heatmap in Figure 5.5c. The results showed that the most dramatic gene expression changes occurred in the N2.1 tumours and that several gene clusters followed the same or a similar pattern of expression. Using k-means hierarchical clustering, it was possible to identify 6 distinct groups of generally co-expressed genes, 3 upregulated and 3 downregulated (Figure 5.5d). The largest upregulated gene cluster was 6, which contains 2561 genes that are weakly upregulated. These genes started to get slightly upregulated in the F0 tumours (log2FC <2) and kept relatively similar expression levels throughout consecutive passages. The second largest

upregulated gene cluster was 4, which contains 917 genes that are strongly upregulated (log2FC 2-3). In this cluster, genes started to upregulate in the F0 tumours but then sharply raised in N2.1 tumours and maintained high levels of expression in the subsequent passages. Cluster 1 follows a similar pattern as cluster 4 and contains 287 genes that are very strongly upregulated (log2FC >3) (Figure 5.5d). The biggest downregulated gene cluster was 5 containing 2857 genes (log2FC</-2), followed by cluster 3 with 488 genes (log2FC -2) then cluster 2 with 172 genes (log2FC >/-3) (Figure 5.5d). The downregulated genes mirrored the upregulated genes in their patterns of expression (Figure 5.5d).

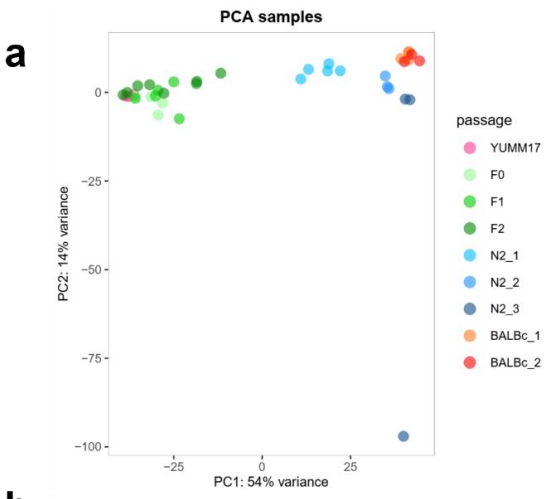
a
PCA samples
PC2: 14% variance
PC1: 54% variance
passage
YUMM17
F0
F1
F2
N2_1
N2_2
N2_3
BALBc_1
BALBc_2

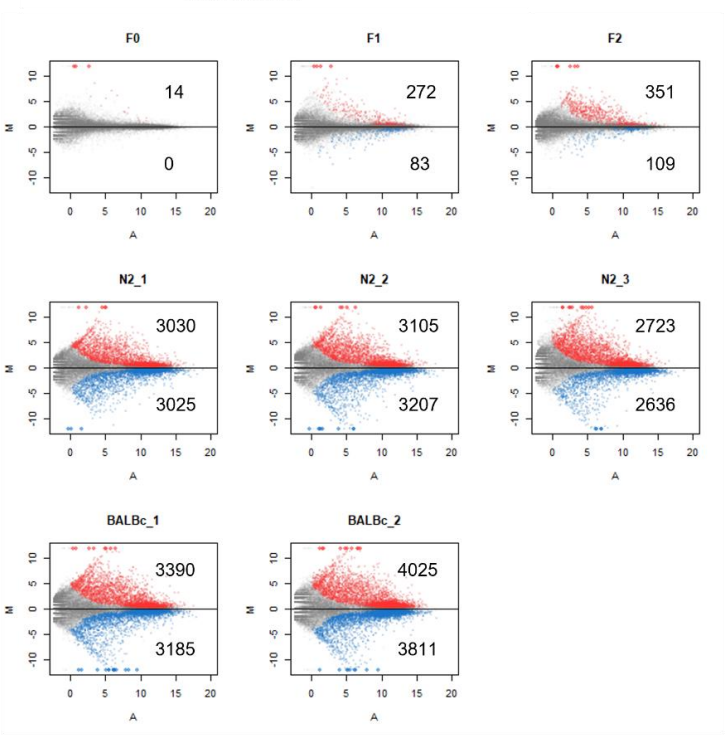
b
F0
14
0
F1
272
83
F2
351
109
N2_1
3030
3025
N2_2
3105
3207
N2_3
2723
2636
BALBc_1
3390
3185
BALBc_2
4025
3811
M
A

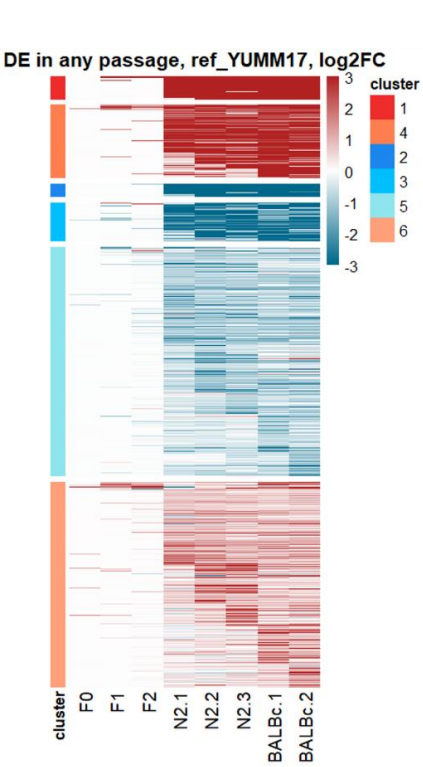
c
DE in any passage, ref_YUMM17, log2FC
cluster
1
4
2
3
5
6
cluster
F0
F1
F2
N2.1
N2.2
N2.3
BALBc.1
BALBc.2

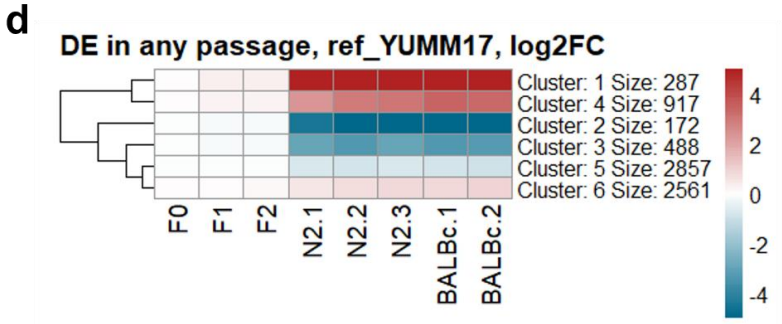
d
DE in any passage, ref_YUMM17, log2FC
Cluster: 1 Size: 287
Cluster: 4 Size: 917
Cluster: 2 Size: 172
Cluster: 3 Size: 488
Cluster: 5 Size: 2857
Cluster: 6 Size: 2561
F0
F1
F2
N2.1
N2.2
N2.3
BALBc.1
BALBc.2

Figure 5.5. **Tumour gene expression changes during passaging.** Analysis of tumour passages by RNA-seq. Tumour biopsies were collected at the indicated passage, dissociated and cells expanded *in vitro* for 2-4 passages before bulk RNA and DNA extraction. RNA-seq libraries were generated from poly-T oligo-enriched mRNAs using the NEBNext UltraTM RNA Library Prep Kit. After sequencing, paired-end clean reads were aligned to the mouse reference genome using the Spliced Transcripts Alignment to a Reference (STAR) software. Differential expression analysis between groups was performed using the DESeq2 R package (2_1.6.3). The resulting P-values were adjusted using the Benjamini and Hochberg's approach for controlling the False Discovery Rate (FDR). a) PCA of gene transcripts FPKM in tumour passages from YUMM1.7 to Balb/c-2 (note that sample N2.3C is an outlier). b) Scatterplot of gene expression changes of the tumours at each passage relative to YUMM1.7. Each dot represents a gene, red for up-regulated and blue for down-regulated. X-axis A value = average log2 counts; Y-axis M value = log2FC. c) Heatmap clustered on the tumour passages showing cumulative gene expression changes for genes with significant differential expression (DE < 5% FDR). FC= fold change. Values for each passage correspond to the log2FC relative to YUMM1.7 cells, where positive and negative values indicate upregulation and downregulation respectively. d) Genes differentially expressed between any consecutive passage were identified (5% FDR) and their expression pattern was followed along the passages. K-means unsupervised hierarchical clustering was used to identify 6 clusters of genes with similar expression patterns, displayed as a heatmap where each individual cluster of genes is represented by a row. The number of genes in each cluster is indicated on the right of each row. Values for each passage

correspond to the log2FC relative to YUMM1.7 cells. In every passage. The RNA-seq reads were mapped by Novogene. The DEG analysis was also performed by Novogene and reviewed by Jose des las Heras, a member of the Fassati lab. The Bioinformatics analyses shown in panels a to d were performed by Jose des las Heras.

5.2.3 Pathway Enrichment Analysis of Clusters 1 and 4

Next, I analysed the functional pathways enriched in the different clusters and we focused on the very strongly upregulated clusters 1 and 4. Ingenuity Pathway Analysis (IPA) of clusters 1 and 4 showed enrichment for inflammatory pathways such as interferon signalling. In addition, pattern recognition receptors, antigen presentation, and the Retinoic acid-Inducible Gene I (RIG-I) sensing pathway were enriched in Balb/c-2 tumours in the IPA analysis (Figure 5.6a). I also performed Gene Set Enrichment Analysis (GSEA) to compare F0 tumours to Balb/c-2 tumours using the Gene Ontology (GO) and KEGG databases. The GSEA results using KEGG and GO databases were in very good agreement with the IPA and confirmed the anti-viral and pro-inflammatory profile of Balb/c-2 tumours. Specifically, we observed increased IFN signalling, IFN-stimulated genes, antigen presentation signalling and pathogen sensing signalling. Among the genes most frequently found enriched in the gene sets were the OAS family members (*Oas1*, *Oas2*, *Oas3*, *Oasl*) (found in 31/32 most significant pathways), which are IFN-induced and activate latent RNase L resulting in viral RNA degradation (Leisching et al., 2019); MDA5 (found in 28/32 most significant pathways) and RIG-I (found in 23/32 most significant pathways),

both of which are innate immune receptors that sense RNAs and induce IFNs (Hartmann, 2017) (Figure 5.6b).

For the downregulated clusters 3 + 5, IPA and GSEA based on GO did not show any significant pathways (FDR <5%).

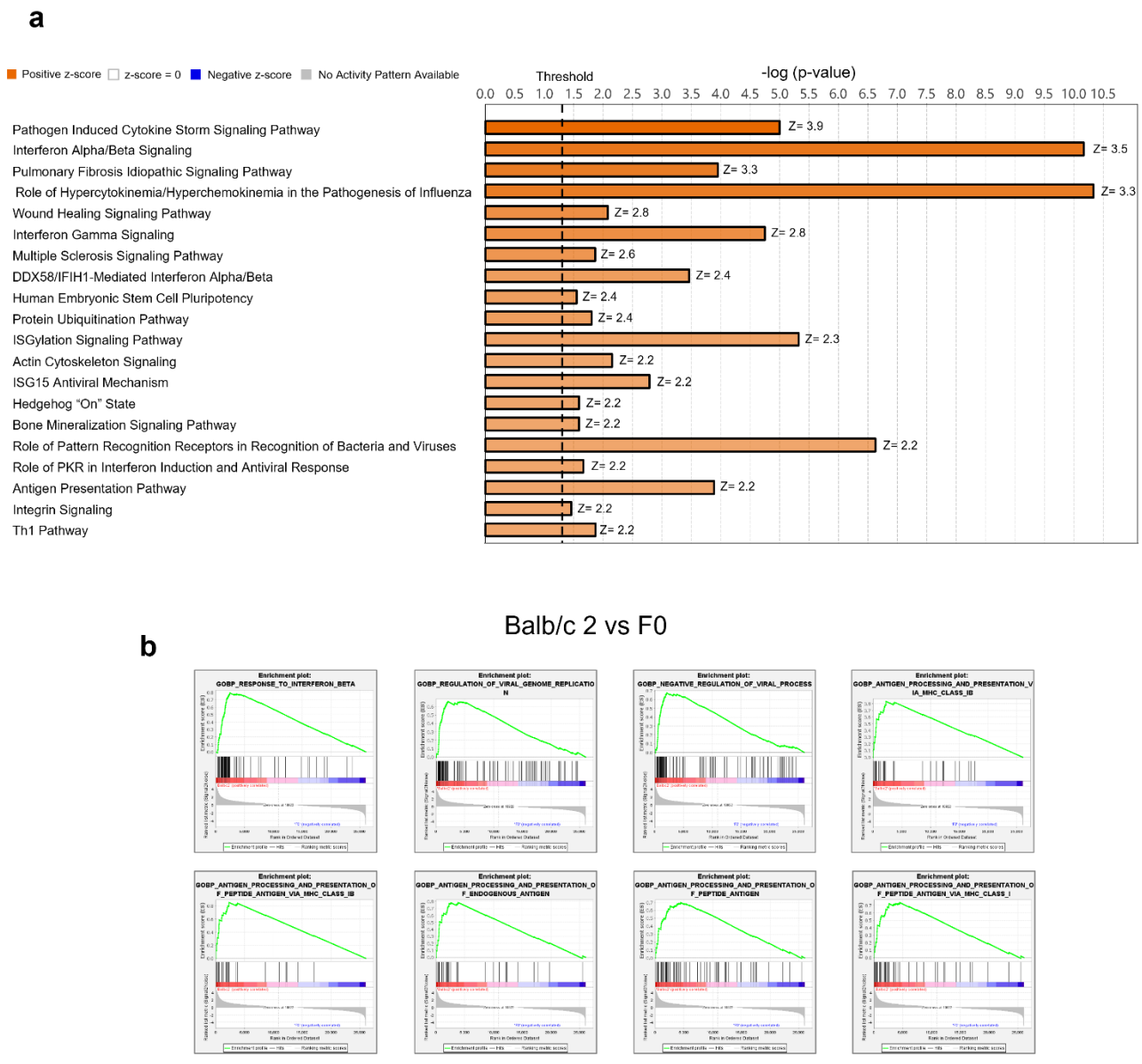

Figure 5.6. **Pathway Enrichment Analysis of gene clusters 1 and 4.** a) IPA core analysis was performed on clusters 1 and 4 and canonical pathways are shown, orange bars indicate activated pathway, b) Functional analysis comparing Balb/c-2

vs F0 cells was performed using GSEA. GSEA plots showing the top 8 enriched pathways using the GO database (FDR q<0.05).

5.2.4 Analysis of Retrotransposable Elements Genes Expression

The upregulation of nucleic acid sensing genes RIG-I (*Ddx58*) and MDA5 (*Ifih1*), and the upregulation of IFN-stimulated genes with anti-viral function suggested the activation of Retrotransposable Elements (RTE) and/or Endogenous Retroviruses (ERVs). ERVs are part of the eukaryotic cell genome as a result of ancient germline infections and are upregulated in different human and mice cancers (Kassiotis & Stoye, 2016). Their activation has been reported in transplantable mouse models and genetic mouse cancer models (Ottina et al., 2018). In normal conditions, ERVs are under epigenetic repression but conditions such as cancer can lead to their epigenetic derepression by mechanisms such as global hypomethylation or changes to histone modification (Kassiotis & Stoye, 2016). This results in the production of viral proteins such as envelope proteins and the accumulation of double-stranded RNA (dsRNA) that trigger innate immune sensors, such as RIG-I and MDA5, within tumour cells.

RTE are mobile genetic elements that have a role in the genetic and epigenetic regulation of gene expression. There are two families of RTE: Long Terminal Repeat (LTR) elements and Non-LTR Retrotransposons. LTR-RTEs contains the LTR/ERVK and LTR/ERV1 subfamilies, which are intergenic and have independent regulation of gene expression. Endogenous Retroelements (EREs) are part of the LTR elements family. Non-LTR Retrotransposons include the LINEs (Long

Interspersed Nuclear Elements) and SINEs (Short Interspersed Nuclear Elements) subfamilies which are mostly intragenic and are usually not fully independent in their gene expression regulation (Jang et al., 2019; Senft & Macfarlan, 2021). Both LTR and non-LTR RTEs have been shown to drive oncogenes expression and modulate the immune response to favour tumour growth (Jang et al., 2019; Senft & Macfarlan, 2021). For example, HLA-G expression is enhanced by the ERV1 element, which causes invasive trophoblast cells to develop immunological tolerance (Senft & Macfarlan, 2021). Transplantable mouse tumour cell lines can contain infectious retroviruses, made from recombination between defective ERVs which restore infectivity. The restoration of infectivity influences the immune response to the tumour (Ottina et al., 2018). In C57BL/6 mice, ERV infectivity is restored by recombination with Emv2, a single copy endogenous Murine Leukaemia Virus (MLV) on this genetic background, which delivers a functioning ecotropic MLV envelope glycoprotein. The inclusion of infectious MLVs in transplantable cancer cell lines leads to significantly enhanced expression of ecotropic MLV envelope, compared to the presence of merely the faulty *Emv2* copy.

To test the hypothesis that upregulation of RTEs might cause sensing and hence the anti-viral signature, we collaborated with George Kassiotis's group at the Crick Institute, London. They utilized an in-house analysis pipeline to determine the expression of all RTEs in the mouse genome as well as the expression of endogenous MLV (Attig et al., 2017). The analysis of RNA-seq data from the tumour passages for the expression of ecotropic MLV, as indicated by *Emv2*-related sequences, or other endogenous MLV provirus, did not show clear difference

between YUMM1.7 cell passages and other tumour passages, suggesting the lack of presence of *Emv2*-based infectious MLVs in these cells (Figure 5.7).

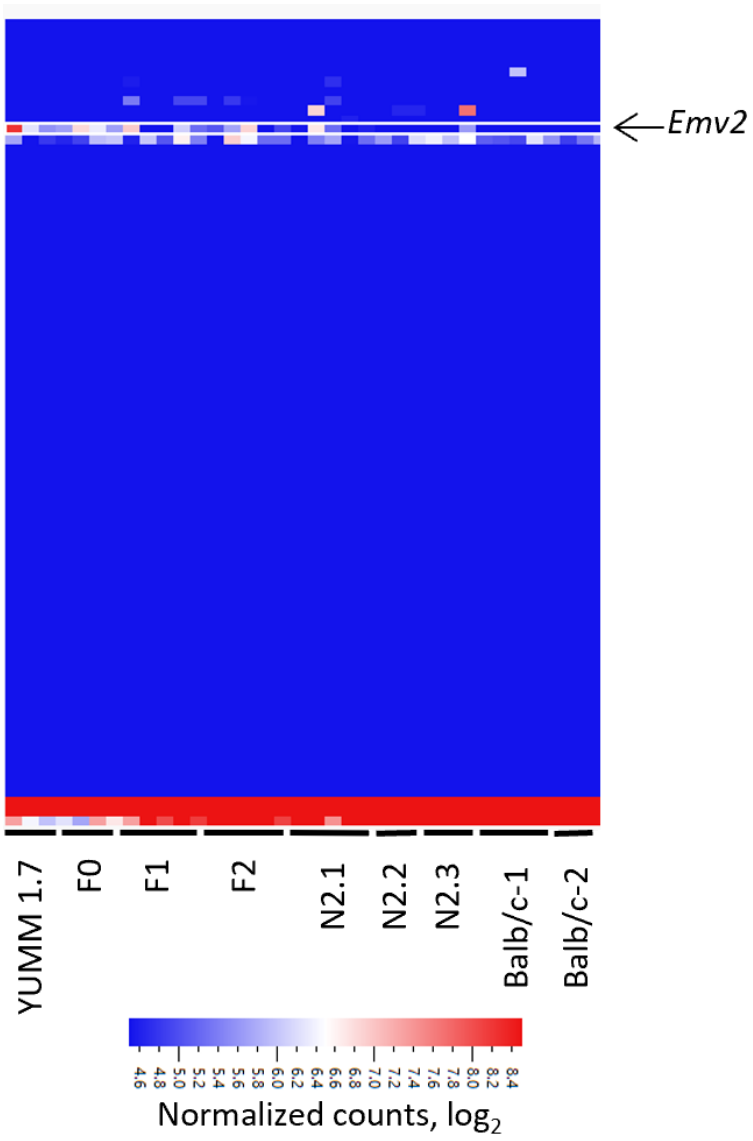

Figure 5.7. MLV Analysis in tumours. a) Expression (normalised counts) of endogenous MLVs in the different tumour passages. *Emv2* is indicated.

The RNA-seq data from the tumour passages revealed that numerous RTEs were significantly modulated between YUMM1.7 and Balb/c-2 cells, with a noticeable switch at the N2 passages (Figure 5.8). Significantly upregulated RTEs in late passages were comprised of many intergenic elements which are independently transcribed (Figure 5.9a). Significant enrichment was observed for LTR/ERVK and LTR/ERV1 subfamilies of LTR elements, and LINE/L1, SINE/B4, SINE/Alu and SINE/B2 subfamilies of non-LTR elements (Figure 5.9b). Conversely, downregulated RTEs in later tumour passages were intragenic, which are controlled by the activity of the genes in which they have integrated (Figure 5.9a). These findings supported the hypothesis that the tumour cells developed an inflammatory and antiviral signature as a consequence of RTEs upregulation.

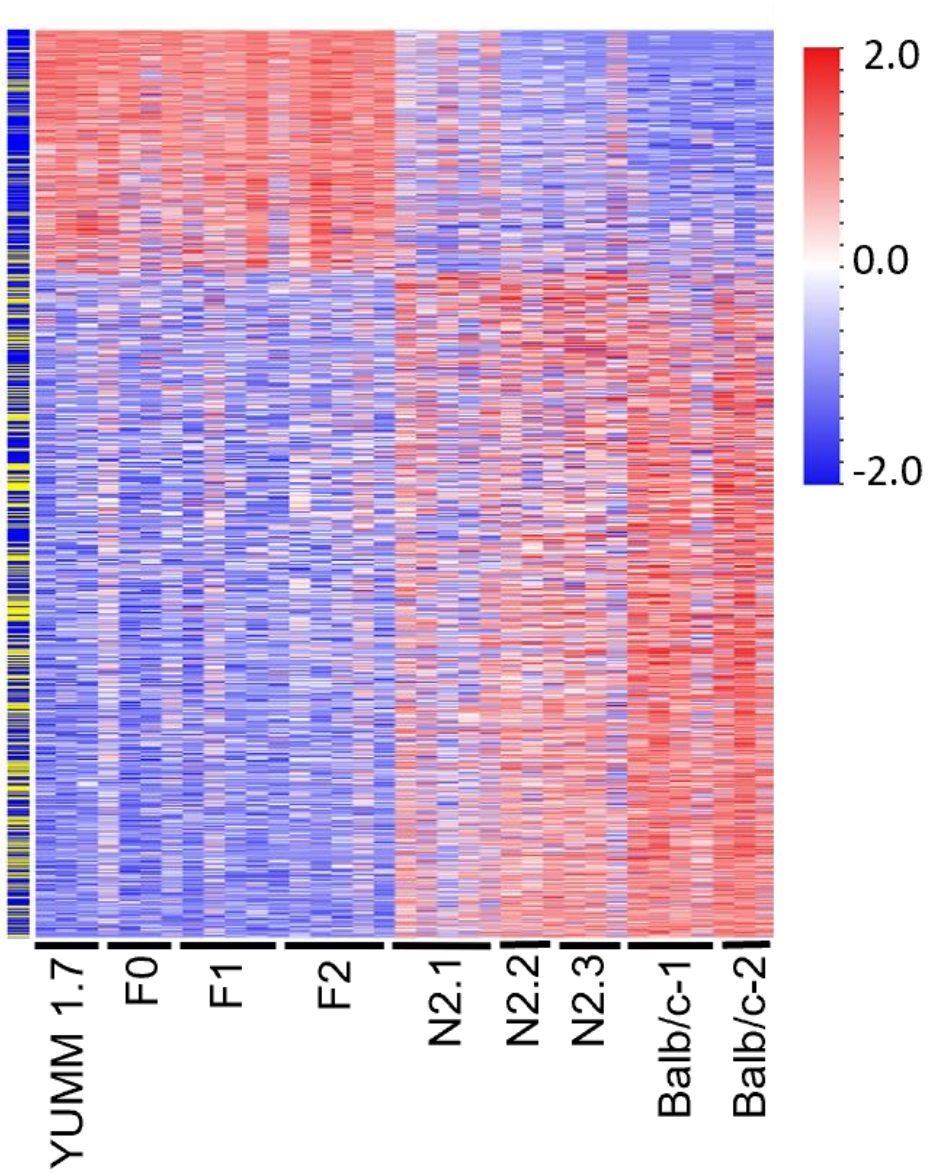

Figure 5.8. RTE Analysis in tumours. Heatmap of repeat expression per tumour passages measured. Repeats are filtered for a t-test between different passages before and after N2.1 with a q value <0.05, fold-change >2 and SD >0.39. Heatmap made with z-scores. Intergenic repeats are annotated in yellow, and intragenic repeats are annotated in blue.

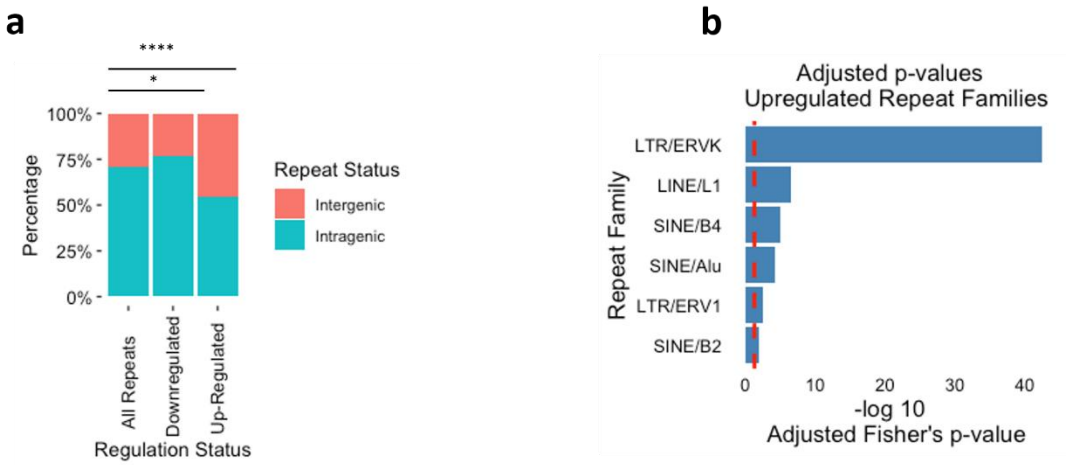

Figure 5.9. RTE families detected in late tumour passages. a) Scaled barplot of the ratios of intergenic and intragenic repeats across the whole genome, and those which are up- or down-regulated as in Figure 5.7. b) Barplots of the –log10 adjusted Fisher's test p-value for the enrichment of each repeat superfamily in up- or down-regulated genes as defined by the t-test in a. A red dotted line is used to show p=0.05. *Adjusted fisher's exact p=1.61e-02, adjusted chi-squared p=1.79e-02. **** adjusted fisher's exact p= 1.67e-39, adjusted chi-squared p= 1.05e-42.

The IPA and GSEA results showed an enrichment in anti-viral pathways characterised by chemokines production and IFN signalling pathway activation. Therefore, we investigated the gene expression levels of chemokines *Cxcl10* (IP-10) and *Ccl5* that can be produced by inducing sensors of viral RNA (Brownell et al., 2014; Zhao et al., 2024). Gene expression analysis of *Cxcl10* and *Ccl5* showed a significant upregulation in later tumour passages compared to YUMM1.7 cells (Figure 5.10a,c). The supernatant was collected from confluent tumour cells in

culture and analysed by ELISA specific for the two cytokines. The ELISA results revealed significantly higher levels of CXCL10 and CCL5 in Balb/c-2 relative to YUMM1.7 cells (Figure 5.10b,d), confirming the pro-inflammatory profile of Balb/c tumours detected by RNA-seq.

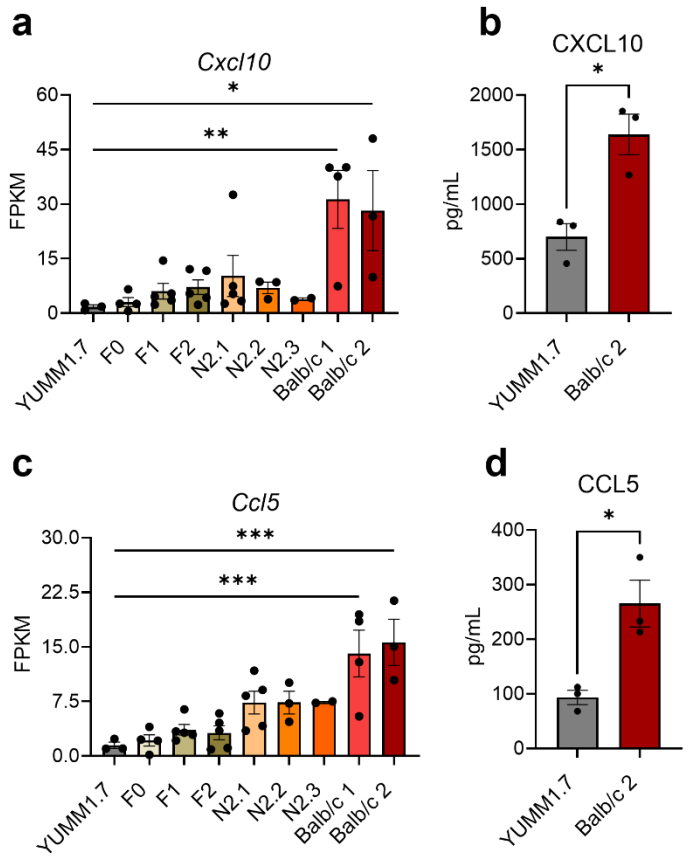

Figure 5.10. Antiviral chemokines production. a) Expression levels of *Cxcl10* (FPKM) in the different tumour passages. b) CXCL10 protein levels measured by ELISA in culture supernatants. c) Expression levels of *Ccl5* (FPKM) in the different tumour passages. d) CCL5 protein levels measured by ELISA in culture supernatants. For RNA-seq (a,c) YUMM1.7 (n=3), F0 (n=4), F1 (n=4), F2 (n=5), N2.1 (n=5), N2.2 (n=3), N2.3 (n=2), Balb/c-1 (n=4), Balb/c-2 (n=3). Statistical analysis was

carried out using one-way ANOVA. For ELISA (b,d) YUMM1.7 (n=3), Balb/c 2 (n=3). Statistical analysis was carried out using an unpaired t-test with Welch's correction. * Denotes (*P*= < 0.05). ** Denotes (*P*= <0.01). *** Denotes (*P*=0.001) **** Denotes (*P*<0.0001).

5.2.5 Targeted Analysis of Tumour Cells Gene Expression

I also took a targeted approach and used the RNA-seq dataset to analyse gene expression levels in tumour cells of known immunomodulatory molecules such as PD-L1, Galectin-9, B7-H3, CD155 and non-classical MHC molecules *H2-M*, *H2-Q* and *H2-T* (Figure 5.11a). I found that these molecules were expressed at low levels in the parental YUMM1.7 cells or in the F0, F1 and F2 tumour passages, however they were upregulated in the later passages, either gradually in the case of *Cd274* (PD-L1) *and Cd276* (B7-H3) or suddenly in the N2.1 passage *Lgals9* (Gal-9) or the Balb/c-2 passage *Pvr* (CD155) (Figure 5.11b). Non-classical MHC molecules *H2-Q4*, *H2-Q5*, and *H2-Q7* were also up-regulated starting from the N2.1 passage, whereas *H2-T10*, *H2-T22*, *H2-T24*, and *H2-M3* showed gradual upregulation (Figure 5.11b). To assess if higher gene expression levels translated into higher protein surface expression levels of PD-L1 and the non-classical protein Qa-1 encapsulating the *H2-Q, H2-T, and H2-M* gene families (Goodall et al., 2019), I analysed YUMM1.7 and Balb/c-2 tumours by flow cytometry, which confirmed an upregulation of PD-L1 and Qa-1 (Figure 5.11c).

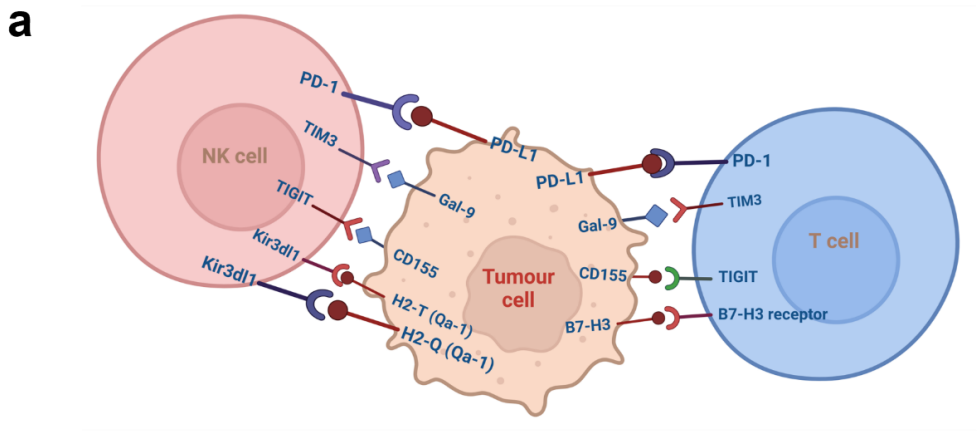
a
NK cell
PD-1
TIM3
TIGIT
Kir3dl1
Kir3dl1
PD-L1
Gal-9
CD155
H2-T (Qa-1)
H2-Q (Qa-1)
Tumour cell
PD-L1
Gal-9
CD155
B7-H3
PD-1
TIM3
TIGIT
B7-H3 receptor
T cell

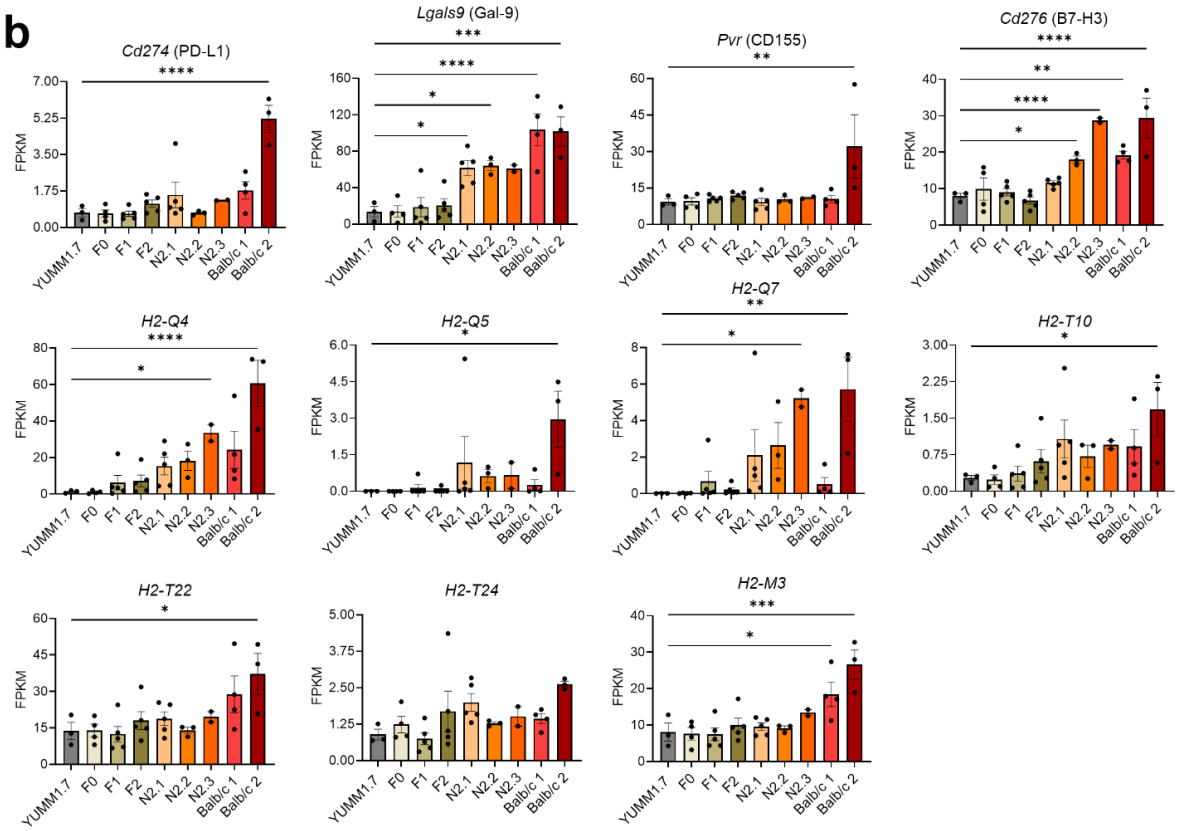
b
Cd274 (PD-L1)
Lgals9 (Gal-9)
Pvr (CD155)
Cd276 (B7-H3)
H2-Q4
H2-Q5
H2-Q7
H2-T10
H2-T22
H2-T24
H2-M3
FPKM
YUMM1.7
F0
F1
F2
N2.1
N2.2
N2.3
Balb/c 1
Balb/c 2

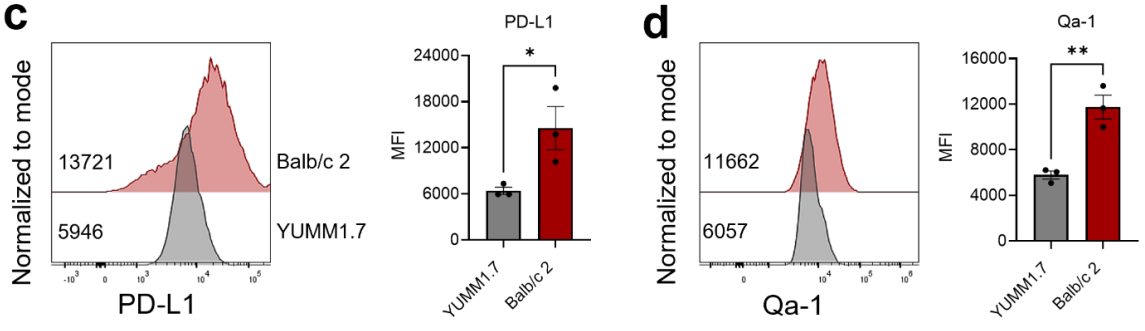
c
Normalized to mode
13721
Balb/c 2
5946
YUMM1.7
PD-L1
PD-L1
MFI
YUMM1.7
Balb/c 2
d
Normalized to mode
11662
6057
Qa-1
Qa-1
MFI
YUMM1.7
Balb/c 2

Figure 5.11. **Tumour expression of immune inhibitory molecules.** a) Diagram showing immune modulatory molecules expressed by tumour cells and their receptors on host immune cells. b) Gene expression FPKM values of the indicated molecules at each tumour passage. c) YUMM1.7 (n=3) and Balb/c-2 (n=3) tumour cells were stained *in vitro* with anti-PD-L1 antibodies and flow cytometry histograms (Left panel) and MFI values (Right Panel) are shown. d) YUMM1.7 (n=3) and Balb/c-2 (n=3) tumour cells were stained *in vitro* with anti-Qa-1 antibodies and flow cytometry histograms (left panel) and MFI values (right panel) are shown. Each dot represents a different tumour. Statistical analysis was carried out using a two-tailed unpaired t-test. * Denotes (P= < 0.05). ** Denotes (P= <0.01). *** Denotes (P=0.001) **** Denotes (P<0.0001)

Taken together, these results suggested that sensing RTEs activated during passaging might induce a chronic inflammatory state that contributes to tumour tolerance by selecting for tumours with upregulated markers that are immune inhibitory to protect against T and NK cell killing.

5.3 Discussion

Analysis of MHC-I expression in the different tumour passages revealed a surprising pattern where the tumours gradually downregulated the MHC-I reaching the lowest levels in the N2.1 passage which showed the highest tumour rejection rates. This MHC-I downregulation is an expected and common mechanism employed by tumours to evade immune rejection (Cornel et al., 2020; Dhatchinamoorthy et al., 2021; Wu et al., 2023). This pattern was reversed in the subsequent tumour passages including in allogeneic BALB/C, CBA/Ca, and FVB/N mice indicating the adoption of a different immune escape or immune suppressive strategy.

Notably, the later passage tumours developed an anti-viral and inflammatory signature that could lead to the exhaustion of effector cells and the recruitment of suppressor cells (Fang et al., 2022; Zhao et al., 2021). These tumours also expressed markers that can specifically inhibit T and NK cells (Cha et al., 2019; J. Gao et al., 2017; Kochan et al., 2013; Leitner et al., 2009; Vaitaitis & Wagner, 2012) as well as the upregulation of the MHC-I molecule, which protects from NK cell killing (Wu et al., 2023). The data suggest that the sensing of RTEs by RIG-I and MDA5 leads to the upregulation of the interferon-stimulated genes including MHC-I and immune modulatory PD-L1 and non-classical MHC molecules.

Our tumour gene expression analyses demonstrated a striking anti-viral inflammatory profile that was most evident in the later passages, pointing to its evolutionary relevance. According to our GSEA, the most significantly upregulated pathways were IFN signalling, anti-viral responses and cytosolic nucleic acids sensing. Among the most significantly upregulated genes were the OAS family, *Ifih1*

(MDA5) and *Ddx58* (RIG-I), which converge on the defence pathway against viral RNAs (Rehwinkel & Gack, 2020a). Recent evidence indicates that aberrant activation of endogenous retroelements in tumour cells is detected by cytosolic nucleic acids sensors that trigger an inflammatory and anti-viral response (Chiappinelli et al., 2015a; Griffin et al., 2021; Sheng et al., 2018). RTEs can be sensed by RIG-I as RNAs, or by cGAS after reverse transcription of their RNA into DNA, leading to the activation of inflammatory pathways including IFN signalling (Attig et al., 2017; Dhillon et al., 2023; D. Gao et al., 2013).

Interferon-Stimulated Genes (ISGs) can be upregulated indirectly as a result of IFN exposure in the canonical pathway or directly in the non-canonical pathway (Swaraj & Tripathi, 2024a). Although often this inflammatory response favours tumour immune rejection, it is also well known that a chronic inflammatory TME promotes cancer immune evasion (Wen et al., 2022). One hypothesis, therefore, is that epigenetic changes in N2 and Balb/c-2 tumours resulted in the aberrant expression of endogenous retroelement nucleic acids that are sensed and generate a highly inflammatory TME. This would then lead to the upregulation of ISGs including immunosuppressive molecules on the tumour cell surface that are either stimulated by interferon, directly or indirectly (Swaraj & Tripathi, 2024b) (Swaraj & Tripathi, 2024a).

Alternatively, sustained exposure to IFNs during the earlier stages of tumour adaptation in the different mouse hybrids might have epigenetically imprinted a chronic inflammatory state, and the greater infiltration of DCs in the Balb/c tumours might add to the IFN type-I signature because DCs, and in particular the plasmacytoid lineage, are known to secrete large amounts of IFN type I (Mitchell et

al., 2018). In support of this idea, it was recently shown that serial passaging in syngeneic mice of melanoma cells that invaded the lymph nodes resulted in upregulation of MHC-I, PD-L1 and the IFN signature. This was attributed to sustained exposure of the tumour cells to IFN in the lymph nodes (Reticker-Flynn et al., 2022a).

Overall, the data suggest that, paradoxically, allo-transplantable tumours might have evolved a chronic inflammatory state characterised by an IFN-related signature with consequent upregulation of immune-suppressive molecules, including PD-L1 and classical and non-classical MHC, to induce T and NK cell exhaustion, anergy and/or death.

6

Results

Chapter 6: Tumour Signature Inhibition and Immunotherapy.

6.1 Introduction

RIG-I is a cytosolic pattern recognition receptor (PRR) in addition to the other RNA sensing PRRs MDA5 and LGP2. RIG-I detects ssRNA and dsRNA in host cells leading to the initiation of an innate immune response. The triggering of RIG-I leads to the activation of a signalling cascade for the production of type I interferons (IFN-α and IFN-β) and other pro-inflammatory cytokines as an antiviral cell response (Thoresen et al., 2021). After RIG-I binding to RNA, the Caspase Activation and Recruitment Domain (CARD) domains of RIG-I interacts with the Mitochondrial Antiviral Signalling Protein (MAVS) on the outer membrane of the mitochondria. MAVS then recruits adaptor proteins such as TRAF3 and TRAF6, leading to the activation of the kinases TBK1 and IKKε (Rehwinkel & Gack, 2020b). TBK1 and IKKε phosphorylate transcription factors IRF3 and IRF7 leading to their translocation to the nucleus. The NF-κB pathway is activated through phosphorylation and degradation of IκB, allowing NF-κB to enter the nucleus, where alongside IRF3 and IRF7, it drives the expression of type I interferon and other pro-inflammatory cytokines (Kato et al., 2006; Thoresen et al., 2021; Yoneyama & Fujita, 2010). Secreted type I interferons then bind to the Interferon-α/β Receptor (IFNAR) on the surface of the same or neighbouring cells leading to the activation of the JAK-STAT pathway through phosphorylation of STAT1 and STAT2 (Yoneyama & Fujita, 2010). STAT1 and STAT2 form a complex with IRF9 forming a transcription activator known as IFN-Stimulated Gene Factor 3 (ISGF3) which translocate to the nucleus inducing the expression of hundreds of ISGs (Schoggins & Rice, 2011).

The production of type I IFN can lead to the upregulation of MHC-I (Gessani et al., 2014), PD-L1 (Jacquelot et al., 2019), and non-classical MHC (Mitsdoerffer et al., 2005). Type I interferon significantly upregulates MHC-I expression by increasing the transcription of MHC-I heavy chain genes and components of the antigen-processing machinery (Seliger et al., 2008) (Gessani et al., 2014). IFN upregulates PD-L1 via the JAK-STAT pathway leading to an immunosuppressive environment, a mechanism exploited by cancers to avoid excessive inflammation and tissue damage (Doi et al., 2017). The upregulation of non-classical MHC Qa-1 by IFN leads to the inhibition of NK cells function through the engagement of the CD94/NKG2A pathway (Vance et al., 1998).

The activation of the DNA cytosolic sensing receptor cGAS can also lead to the activation of IFN signalling and ISGs upregulation (Weichselbaum et al., 2008).

Cytosolic DNA is detected by cGAS, leading to its activation and the production cyclic GMP-AMP (cGAMP). cGAMP then triggers the synthesis of IFN-I by activating the Stimulator of Interferon Genes (STING) pathway (Weichselbaum et al., 2008).

Direct ISGs activation in the non-canonical pathways include different mechanisms. These mechanisms that operate independently of the canonical IFN-JAK-STAT signalling pathway. For instance, viral proteins can activate ISGs by binding to specific promoter elements, such as Interferon-Stimulated Response Elements (ISREs) which can trigger the expression of ISGs directly without interferon production. Additionally, unphosphorylated ISGF3, which consists of unphosphorylated STAT1, STAT2, and IRF9, can activate ISREs and induce ISGs without the need for IFN signalling (Swaraj & Tripathi, 2024b).

ISGs play complicated and context-dependent functions in tumour growth and immunological tolerance. Recent studies have shed light on the dual roles that ISGs play in preventing tumour growth and, paradoxically, promoting immunological evasion and therapy resistance. Overexpression of the ISGs STAT1 promotes tumour cell survival by activating anti-apoptotic pathways (Efimova et al., 2009). The Interferon-Related DNA Damage Resistance Signature (IRDS), a subset of ISGs including *STAT1*, *IRF7*, *ISG15*, and *IFITM1*, is associated with resistance to chemotherapy and radiotherapy in breast cancer and glioblastoma (Weichselbaum et al., 2008). IRDS can also be induced by the activation of RIG-I and MDA5 (Padariya et al., 2021).

The emergence of Immune Checkpoint Blockade (ICB) therapy has revolutionized cancer treatment. Therapies such as anti-PD-1 monoclonal antibodies restore T-cell function and mediate durable anti-tumour responses. It has shown good efficacy in cancers such as melanoma (van Breeschoten et al., 2021). A study of $BRAF^{(V600-E)}$ mutant advanced melanoma patients who received anti-PD-1 antibodies (pembrolizumab or nivolumab) or BRAF/MEK inhibitors (dabrafenib + trametinib or vemurafenib + cobimetinib) showed better 2-year overall survival for the anti-PD-1 relative to the BRAF/MEK inhibitors group (42.3 months vs. 19.8 months) and better response rate of 65.4% vs 41.7% (van Breeschoten et al., 2021).

Non-classical MHC such as HLA-G and HLA-E expression in tumours is associated with poor prognosis necessitating the development of therapeutic approaches (André et al., 2018; Swets et al., 2016). The interaction of HLA-E (Qa-1b in mice) with its receptor NKG2A leads to the inhibition of NK and CD8+ T cells effector functions (André et al., 2018). Monalizumab, a monoclonal antibody targeting

NKG2A, showed promising results in a phase II clinical trial in previously treated squamous cell carcinoma of the head and neck with a 31% objective response rate when combined with cetuximab (anti-Epidermal Growth Factor Receptor (EGFR) antibody) (André et al., 2018). Preclinical studies of A20 B cell lymphoma which express Qa-1 showed that the combination of anti-NKG2A and anti-PD-L1 controlled tumour growth and rescued 75% of mice from death vs 40% in anti-PD-L1 mAb alone (André et al., 2018).

The results shown in Chapter 5 indicated that nucleic acids sensing, PD-L1 and non-classical MHC upregulation were associated with tumour escape from allogeneic rejection. To further investigate this aspect, I have tested if inhibition of sensing affected the anti-viral tumour signature and if downregulation of PD-L1 and non-classical MHC-I induced cancer rejection in our mouse model.

6.2 Results

6.2.1 cGAS Inhibition in Tumours

Our results showed that the upregulation of RTEs in the late tumour passages correlates with an inflammatory signature and ISGs activation. Reverse-transcribed DNA from ERVs or RTEs is detected by cGAS, causing cGAMP to be produced, which in turn activates the STING pathway. As a result, type I interferons and other cytokines which are necessary for antiviral immunity are induced leading to activation of ISGs (Dhillon et al., 2023; D. Gao et al., 2013). Therefore, I investigated the expression of cGAS and whether its inhibition could reverse the upregulated ISGs, MHC-I, PD-L1, and non-classical MHC Qa-1. The RNA-seq results showed similar levels of cGAS across the different tumour passages (Figure 6.1a). Next, I investigated whether the inhibition of cGAS by RU.521 could decrease the expression of MHC-I, PD-L1, and Qa-1. RU.521 is a potent and selective inhibitor of murine cGAS and interferes with cGAS's capacity to produce cGAMP upon DNA binding by occupying its catalytic pocket. This then leads to inhibition of IFN upregulation without affecting other inflammatory pathways (Vincent et al., 2017; W. Zhou et al., 2018). To validate the activity of RU.521, BALB/c splenocytes were treated with RU.521 for 3 hours and then transfected with DNA fragments generated by sonication. After 24 hours, splenocytes were stained with the panel used in Figure 4.1 to identify DCs. Then, I gated on DCs which uptake the foreign DNA leading to cGAS activation and IFN signalling (G. Li et al., 2024), and assessed the expression of ISGs, MHC-I and PD-L1. DNA transfection significantly upregulated the expression of MHC-I in DCs, and the treatment with 3 different concentrations (10 μM, 20 μM, and 30 μM) of RU.521 significantly inhibited that upregulation but

apparently not in a dose-dependent manner (Figure 6.1b,c). DNA stimulation did not upregulate, and appeared to downregulate, PD-L1 expression in transfected relative to untransfected DCs and no effect was seen with RU.521 (Figure 6.1d,e), suggesting a high degree of endogenous upregulation of PD-L1. The non-classical MHC Qa-1 was not expressed on DCs.

Next, we evaluated the effect of RU.521 treatment on the expression of MHC-I, PD-L1, and Qa-1 in Balb/c-2 tumours. Tumour cells were incubated with the same concentrations of RU.521 for 24 hours and then stained for MHC-I, PD-L1, and Qa-1. RU.521 did not downregulate the expression of MHC-I, PD-L1, and Qa-1 in these cells (Figure 6.1f-i). The data indicated that cGAS is not involved in the upregulation of the immunomodulatory markers that allow tumour growth in allogeneic hosts.

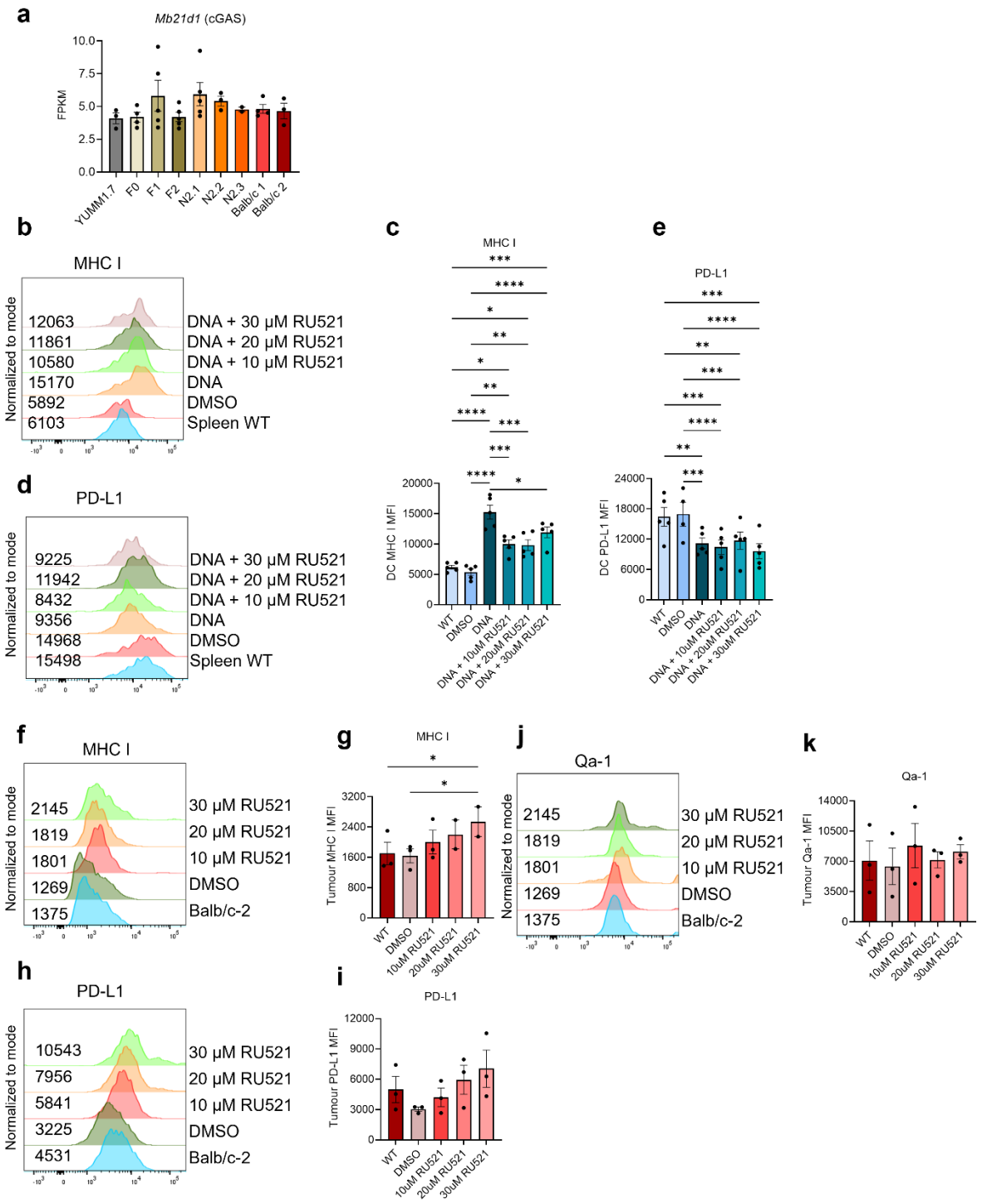

Figure 6.1. cGAS inhibition in Balb/c-2 tumour cells. a) After dissociation, tumour cells were grown *in vitro* for 2-4 passages to eliminate host immune cells then total RNA extracted and RNA libraries sequenced. Gene expression values in FPKM for *Mb2d1* (cGAS) gene. b) 1 million splenocytes from BALB/c mice were treated with

the cGAS inhibitor RU.521 or DMSO for 3 hours, then transfected with DNA fragments. After 24 hours splenocytes were stained and gated on DCs. Flow cytometry histograms are shown for MHC-I. c) MHC-I intensity in DCs (n=5). d) Flow cytometry histograms are shown for PD-L1. e) PD-L1 intensity in DCs (n=5). f) 1 million Balb/c-2 tumour cells were added to 1 ml of media containing the indicated concentration of RU.521 or DMSO and incubated for 24 hours. Flow cytometry histograms are shown for MHC-I. g) MHC-I intensity in Balb/c-2 tumours (n=3). h) Flow cytometry histograms are shown for PD-L1. i) PD-L1 intensity in Balb/c-2 tumours (n=3). j) Flow cytometry histograms are shown for Qa-1. k) Qa-1 intensity in Balb/c-2 tumours (n=3). Each dot represents a different tumour sample. Statistical analysis was carried out using one-way ANOVA (a), and two-way ANOVA with Tukey's multiple comparison correction (c,e,g,k,i). * Denotes (P= < 0.05). ** Denotes (P= <0.01). *** Denotes (P=0.001) **** Denotes (P<0.0001).

6.2.2 RIG-I KO in Tumours

Inhibition of cGAS in tumour cells did not abrogate the upregulation of MHC-I and the inhibitory molecules PD-L1 and Qa-1. I therefore investigated the other arm of nucleic acid sensing RIG-I. Our RNA-seq results showed significant upregulation of the RIG-I gene (*Ddx58*) as well as the other RNA sensing molecules MDA5 (*Ifih1*) and LGP2 (*Dhx58*) starting at the N2.1 tumour passage and reaching the highest levels in Balb/c-1 and Balb/c-2 tumours (Figure 6.2a). Due to the lack of selective inhibitors of RIG-I, I knocked out RIG-I using a CRISPR-Cas9 expressing lentivirus with two guide RNAs (gRNAs) targeting exon 3 and exon 4 of the *Ddx58* gene (Figure

6.2b). Balb/c-2 cells were transduced with the lentivector, selected in media containing puromycin for 7 days and individual clones were isolated by limiting dilution. Clones were screened by PCR using primer sets specifically designed to flank the targeted exons hence lack of PCR amplification signalled the excision of the exons. Four clones showed successful KO results of *Ddx58*. Clone 6 showed KO of both exons but the selected cells had poor viability and slow growth which led to the exclusion of this clone. Clone 9 (exon 3 KO) and clone 23 (exon 4 KO) (Figure 6.2c) showed better viability *in vitro* and therefore were selected for further analysis.

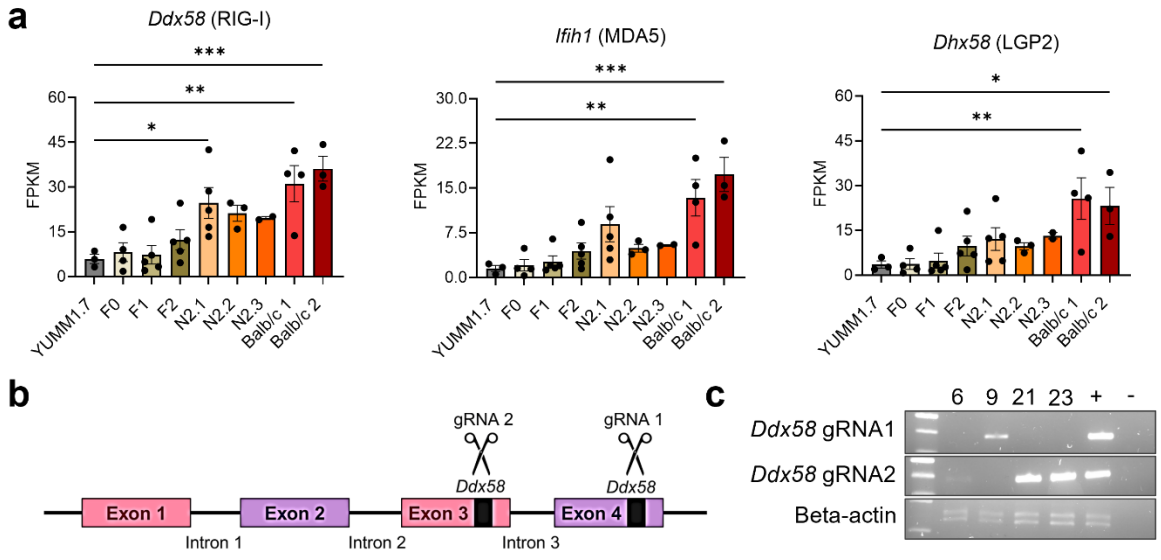

Figure 6.2. RIG-I KO in Balb/c-2 tumour cells. a) Gene expression values in FPKM for *Ddx58* (left panel), *Ifih1* (middle panel), *Dhx58* (right panel). YUMM1.7 (n=3), F0 (n=4), F1 (n=5), F2 (n=5), N2.1 (n=5), N2.2 (n=3), N2.3 (n=2), Balb/c-1 (n=4), Balb/c-2 (n=3). Each dot represents a different tumour. Statistical analysis was carried out using one-way ANOVA. * Denotes (*P*= < 0.05). ** Denotes (*P*= <0.01). *** Denotes

(*P*=0.001) **** Denotes (*P*<0.0001). b) schematic depiction of the *Ddx58* (RIG-I) exons targeted by the gRNAs in the CRISPR/Cas9 lentiviral vector. c) gel electrophoresis of PCR products specific for *Ddx58* exon 3 or exon 4 and Beta-actin after amplification of DNA from four KO clones and original Balb/c-2 (+) or no DNA control (-).

Next, I evaluated the effect of RIG-I KO in clone 9 and clone 23 and compared them to tumour cells transduced with an empty lentivector (EV) expressing the puromycin-resistance gene, and to the parental Balb/c-2 cells. RIG-I KO clones expressed lower levels of MHC-I relative to both parental Balb/c-2 cells and EV-transduced cells, although EV-transduced cells expressed less MHC-I than parental cells, which may be caused by selection with puromycin (Figure 6.3a-c). The percentage of cells expressing PD-L1 was also lower in RIG-I KO clones relative to the controls (Figure 6.4 a,c), and the MFI was lower too. EV-transduced cells had a low PD-L1 MFI, in between parental Balb/c-2 and RIG-I KO cells (Figure 6.4c).

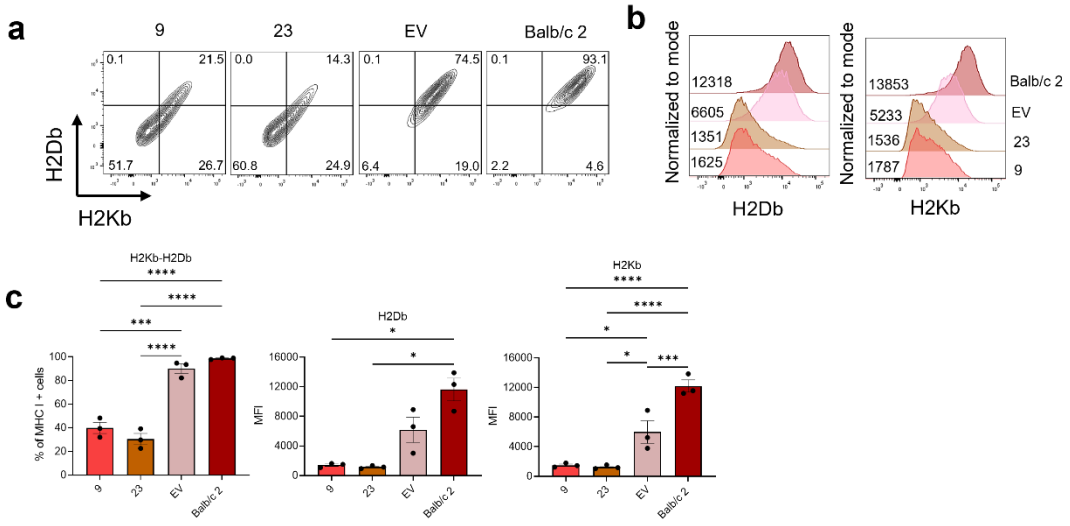

Figure 6.3. MHC-I expression in Balb/c-2 RIG-I KO tumour cells. a) Tumour cells were grown *in vitro* and then stained with anti-H2-Kb and anti-H2-Db antibodies. a) Flow cytometry plots for surface expression levels of H2-Db and H2-Kb by flow cytometry in clones 9, 23, EV and parental Balb/c-2 cells. b) Histogram plots showing the MFI distributions of H2-Db and H2-Kb, c) Left panel, percentage of H2-Db+ H2-Kb+ cells in clone 9, 23, EV and Balb/c-2 cells, middle and right panels, MFI of H2-Db and H2-Kb (n=3). Each dot represents a different tumour sample. Statistical analysis was carried out using two-way ANOVA with Tukey's. Each dot represents a different tumour. * Denotes (P= < 0.05). ** Denotes (P= <0.01). *** Denotes (P=0.001) **** Denotes (P<0.0001).

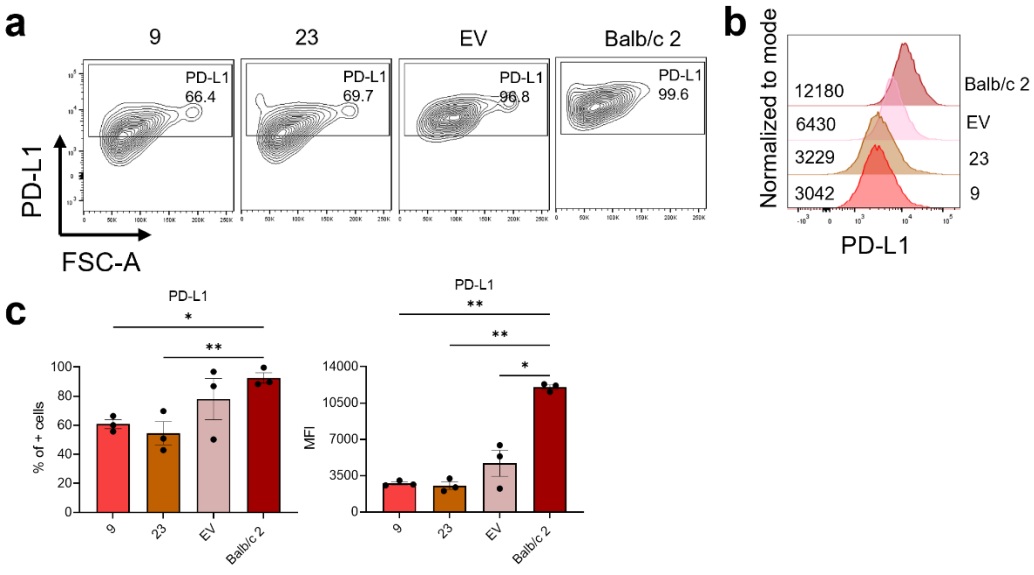

Figure 6.4. PD-L1 expression in Balb/c-2 RIG-I KO tumour cells. a) Tumour cells were grown *in vitro* and then stained with anti-PD-L1 antibodies. a) Flow cytometry plots for surface expression levels of PD-L1 by flow cytometry in clones 9, 23, EV and parental Balb/c-2 cells. b) Histogram plots showing the MFI distributions of PD-

L1, c) Left panel, percentage of PD-L1+ cells in clones 9, 23, EV and Balb/c-2 cells, right panel, MFI of PD-L1 (n=3). Each dot represents a different tumour sample. Statistical analysis was carried out using two-way ANOVA with Tukey's. Each dot represents a different tumour. * Denotes (P= < 0.05). ** Denotes (P= <0.01). *** Denotes (P=0.001) **** Denotes (P<0.0001).

RIG-I KO clones 9 and 23 and EV transduced cells showed lower percentages of cells expressing the non-classical MHC molecule Qa-1 compared to parental Balb/c-2 cells (Figure 6.5 a,c). Clones 9 and 23 also showed significantly lower intensity of expression of Qa-1 compared to parental Balb/c-2 cells while EV cells downregulation did not reach statistical significance (Figure 6.5 b,c).

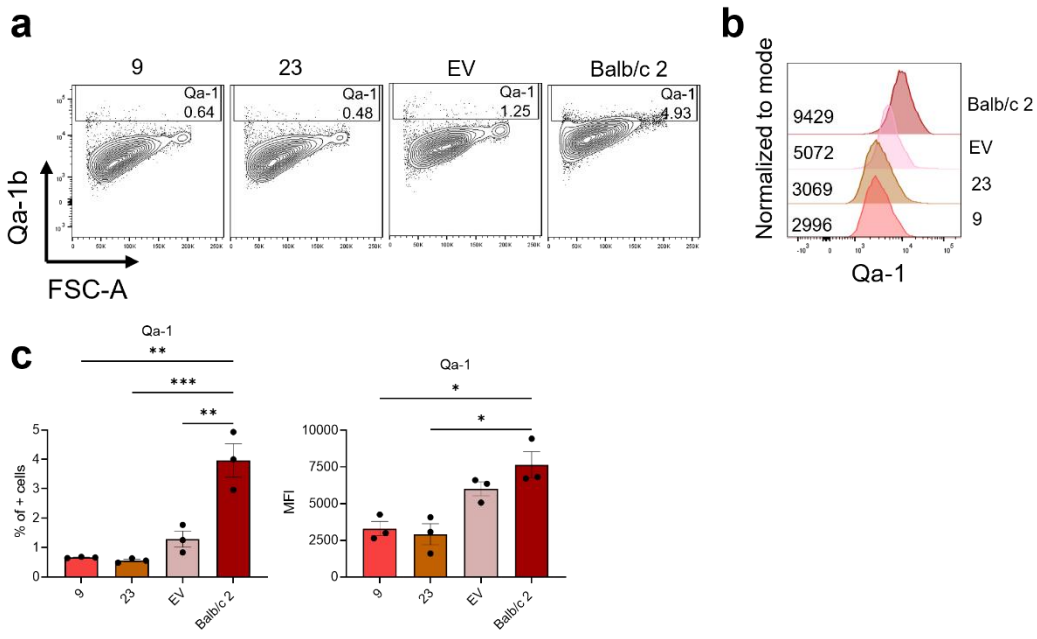

Figure 6.5. Qa-1 expression in Balb/c-2 RIG-I KO tumour cells. a) Tumour cells were grown *in vitro* and then stained with anti-Qa-1 antibodies. a) Flow cytometry plots for surface expression levels of PD-L1 by flow cytometry in clones 9, 23, EV

and parental Balb/c-2 cells. b) Histogram plots showing the MFI distributions of Qa-1, c) Left panel, percentage of Qa-1+ cells in clones 9, 23, EV and Balb/c-2 cells, right panel, MFI of Qa-1 (n=3). Each dot represents a different tumour sample. Statistical analysis was carried out using two-way ANOVA with Tukey's. Each dot represents a different tumour. * Denotes (P= < 0.05). ** Denotes (P= <0.01). *** Denotes (P=0.001) **** Denotes (P<0.0001).

Taken together, the KO of RIG-I produced phenotypic changes in these cells characterised by the downregulation of MHC-I, PD-L1, and Qa-1 relative to parental Balb/c-2 cells, suggesting that RIG-I is involved in the upregulation of these molecules. EV transduced cells also showed some reduction in the expression of these markers but to a lesser degree than RIG-I Ko cells. This could be due to the exposure to puromycin in the selection step or to changes associated with the introduction of the CRISPR-Cas9 lentiviral vector.

6.2.3 RIG-I KO Tumours Transplantation

Following the KO of RIG-I in Balb/c-2 tumour cells I sought to evaluate whether the lack of RIG-I and subsequent downregulation of MHC, PD-L1, and Qa-1 could lead to tumour regression in BALB/c mice. Therefore, I performed a tumour cell injection experiment in BALB/c mice consisting of 4 groups with 12 mice each. The first group received Balb/c-2 tumour cells injection. The second group was injected with Balb/c-2 EV transduced cells. The third group was injected with Balb/c-2 RIG-I KO clone 9. The fourth group received Balb/c-2 RIG-I KO clone 23 tumour cells. The Balb/c-2

tumours take was over 90% (11/12). BALB/c mice injected with EV tumour cells showed a high rejection rate (Table 6.1) and only 1 out of 12 mice injected showed tumour growth (Table 6.1). Similarly, Balb/c-2 RIG-I KO clone 9 showed lower levels of tumour take with only 3 out of 12 injected tumours growing (Table 6.1). Finally, Balb/c-2 RIG-I KO clone 23 showed no tumour growth at all in BALB/c mice (Table 6.1).

Table 6.1. Tumour Takes in Balb/c-2, EV, RIG-I KO 9, and Rig-I KO 23 tumour cells.

Mouse strain	Tumour Injected	No of injected mice	No of takes
BALB/c	Balb/c-2	12	11
BALB/c	EV	12	1
BALB/c	RIG-I KO 9	12	3
BALB/c	RIG-I KO 23	12	0

In summary, the tumour transplantation of the RIG-I KO cells showed that they lost their ability to grow in allogeneic BALB/c mice, but we also observed a reduced ability of the control group EV cells to grow in these hosts. Rejection of EV cells may be due to the de-novo expression of Cas9 or puromycin N-acetyl transferase, which might have triggered an immune response, or to other changes caused by transduction with the lentiviral vector. Therefore, regrettably, no clear conclusions could be drawn from this experiment.

6.2.4 Blocking PD-1 and Qa-1 by Monoclonal Antibody Treatment

The tumour transplantation of the RIG-I KO and EV transduced Balb/c-2 showed that both groups lost their ability to grow in BALB/c mice and both groups showed downregulation of PD-L1 and Qa-1 expression, albeit to a different degree. Therefore, we hypothesized that successful tumour growth is dependent on the high expression levels of these inhibitory molecules and that blocking the interaction of these molecules with their receptors on immune cells could control tumour growth or lead to tumour clearance. To assess the effect of PD-L1 and Qa-1 on tumour growth, mice were injected with 1 million Balb/c-2 tumour cells and when tumours became palpable, mice were injected with (5mg/Kg) of anti-PD-1, anti-Qa-1 or the combination of anti-PD-1 + anti-Qa-1 neutralizing antibodies or with isotype control antibodies on days 4, 7, 10, and 13 post tumour injection (Figure 6.6a). Tumours in mice treated with the isotype control antibodies reached an average of 262 mm^3 on day 14 post-tumour cell injection (Figure 6.6b). Treatment with neutralizing anti-PD-1 (89 mm^3) and anti-Qa-1 (59 mm^3) significantly controlled the tumour growth compared to the isotype control group (Figure 6.6b). The combination of anti-PD-1 + anti-Qa-1 led to tumour regression (39 mm^3) (Figure 6.5b).

Taken together, the data showed that blocking the interaction between PD-L1 and Qa-1 with their receptors successfully controlled tumour growth, or induced regression of established tumours. These results supported our hypothesis that upregulation of PD-L1 and non-classical MHC was critical for tumour escape from allogeneic rejection.

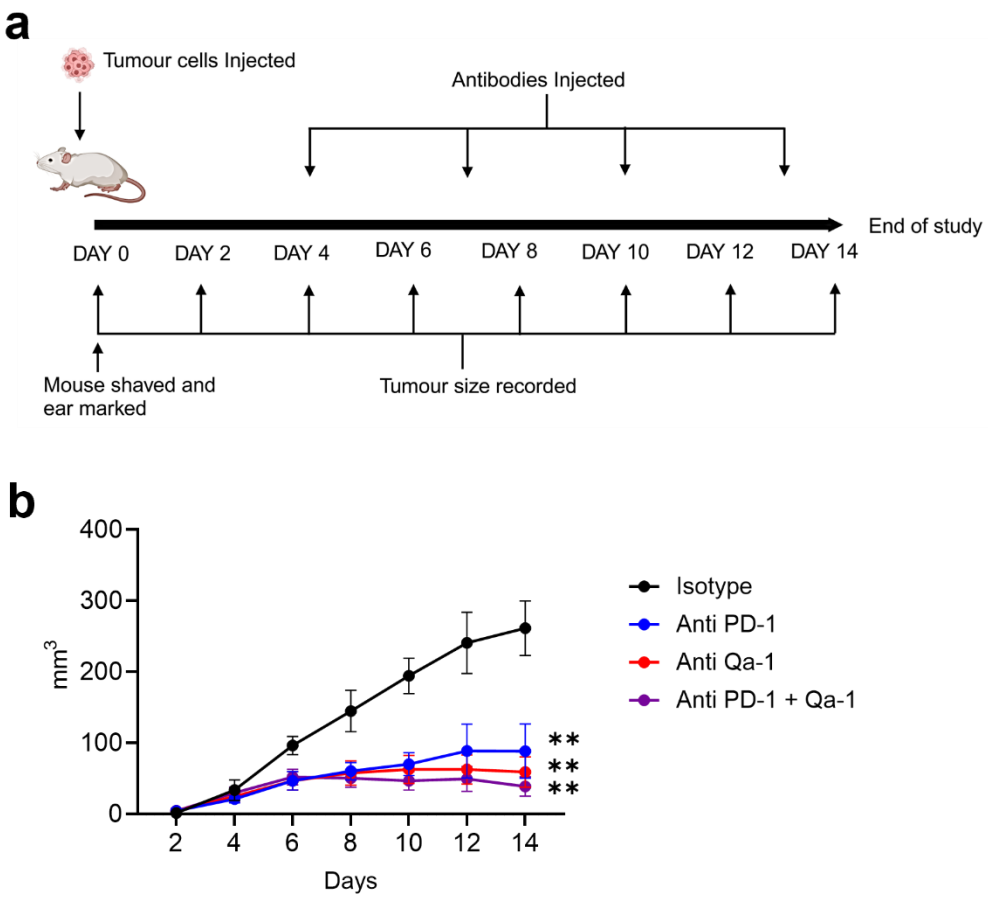

Figure 6.6. Treatment with neutralizing anti-PD-1 and anti-Qa-1 antibodies. a) BALB/c mice were injected with 1 million cells of Balb/c-2 tumours. Once tumours were palpable treatment with neutralizing antibodies started. Mice were injected with (5mg/Kg) anti-PD-1, anti-Qa-1, anti-PD-1 + anti-Qa-1, and isotype control on days 4, 7, 10, and 13 post tumour injection. a) Schematic depiction of study design and treatment schedule. b) Tumour growth curves in mm^3. Isotype, Anti PD-1, Anti Qa-1, Anti PD-1 + Qa-1 (n=6). Statistical analysis was carried out using an unpaired t-test to compare tumour volumes on day 14 post tumour injection. Each dot represents a different tumour. * Denotes (P= < 0.05). ** Denotes (P= <0.01). *** Denotes (P=0.001) **** Denotes (P<0.0001).

6.3 Discussion

The previous chapter showed that the upregulation of RTEs in later tumour passages was associated with activation of RIG-I sensing and upregulation of ISGs. By inducing the upregulation of several immunosuppressive ligands and molecules, this anti-viral transcriptional response likely plays a role in the tumours' escape from allogeneic rejection. To examine this link further, we have tested if inhibition of nucleic acid sensing reduced the expression of immune protective molecules and triggered tumour rejection.

cGAS can sense ERV in general or retroelements due to the process of reverse transcription of RNA to DNA in retroviruses (Dhillon et al., 2023). Therefore, I first tested cGAS but its chemical inhibition with RU.521 did not abrogate the tumour signature. In contrast, CRISPR/Cas9 KO of the RIG-I gene *Ddx58* in Balb/c-2 tumour cells reduced expression of MHC-I, PD-L1, and Qa-1, suggesting a critical role of RIG-I in establishing the anti-viral signature linked to escape from allogeneic rejection. Surprisingly, the transduction of parental Balb/c-2 cells with an empty vector expressing CRISPR/Cas9 and the puromycin-resistance gene also lowered the expression of MHC-I, PD-L1, and Qa-1 but to a lesser extent than the RIG-I KO clones. We speculate that this phenotype may be due to the selection of the cells in puromycin, an antibiotic known to perturb protein synthesis, or to the transduction with the lentivector, which might affect nucleic acid sensing.

Tumour transplantation experiments with two RIG-I KO clones and EV Balb/c-2 tumour cells resulted in lower tumour takes in BALB/c mice, which may be due to de-novo expression of Cas9 and puromycin N-acetyl transferase, or to the observed

lower levels of PD-L1 and Qa-1 in the EV cells relative to the parental cells. However, treatment of injected mice with either anti-PD-1 or anti-Qa-1 mAbs resulted in tumour growth control, and treatment with a combination of anti-PD-1 and Qa-1 antibodies resulted in regression of established tumours. Taken together, these results confirmed the critical role of PD-L1 and Qa-1 in the tumours' escape from allogeneic rejection and supported the overall hypothesis that upregulation of RTEs triggered sensing, which then induced an antiviral signature that contributed to tumour immune evasion.

The results emphasize the importance of PD-L1 and Qa-1 in inducing immune tolerance in the allogeneic tumour passages, which could be leveraged in organ transplantation to reduce or delay organ rejections. This agrees with clinical data showing that HLA-G expression on grafted organs is associated with a lower incidence of acute rejection (Crispim et al., 2008). The analysis of biopsies from renal transplant patients with HLA-G expression showed that only 5% exhibited acute rejection and 5% exhibited chronic rejection, while 90% exhibited no signs of rejection (Crispim et al., 2008). The recent advances in xenotransplantation, whereby genetically edited pig kidneys were transplanted to Non-Human Primates (NHP) elucidated the important roles of PD-L1 and non-classical MHC-I in establishing tolerance (Sykes & Sachs, 2022) (Ma et al., 2022). Kidney transplants from triple KO (TKO) for the three major carbohydrate xenoantigens and expressing additional human Transgenes (hTG) including PD-L1 and HLA-E survived for longer in NHPs than the TKO group alone, lasting up to 316 days (Ma et al., 2022).

Our results also have some limitations. First, even though the KO of RIG-I showed phenotypic changes consistent with an abrogation of the anti-viral and inflammatory

signature, the results *in vivo* were still inconclusive because similar, albeit weaker, changes were also detected in the control EV group. Furthermore, both RIG-I and EV cells were rejected in BALB/c mice whereas parental Balb/c-2 cells were not. Therefore, at this stage, it is not possible to conclude that rejection is solely due to RIG-I KO. Indeed, de-novo expression of Cas9 or puromycin N-acetyl transferase from the lentiviral vector might have induced an immune response against injected cells. Second, the neutralizing antibodies showed an ability to control tumour growth in the short term, but we do not know whether this effect is long-lasting or whether tumours can circumvent that effect and develop therapy resistance with time. Third, the effect of the other RNA sensing molecules MDA5 and LGP2 was not investigated in depth due to the limited time remaining. Lastly, the effect of the neutralizing antibodies on the infiltrating immune cells was not analysed due to the smaller tumour sizes of the treated group.

7

Discussion

Chapter 7: Discussion

Here, we demonstrated that, consistent with Barret and Deringer's findings from the 1950s (Barrett & Deringer, 1952), through serial tumour passaging into more mismatched mouse hybrids, tumours were able to evade the histocompatibility barrier and grow in completely mismatched mouse strains. We used fully immunocompetent mice to develop the allo-transplantable tumour, which has benefits over immunocompromised mice. Immunocompromised mice, including Nude, SCID, and NOD SCID, are deficient in critical immune cells that are necessary for the immune responses to tumours and transplants. Consequently, the absence of immune system-induced selection pressure on tumour cells may prevent tumour adaptation. The data showed that repeated passaging of the tumours in the same mouse cross or strain led to better adaptation in this host. This is demonstrated by increased numbers of tumours that survive, and better growth kinetics as seen in N2 and Balb/c tumours. Genotypically, tumours maintained their origin, but phenotypic changes occurred as shown by MHC-I expression changes and the tumour signature analysis.

Our findings suggest that tumour adaptation to growing in allo-mismatched mice altered the immune infiltration of tumours. The F0 passage showed a moderate level of immunogenicity, but the N2.1 passage which had the highest rejection rate-showed a higher level of immunogenicity and tumours subsequently decreased their immunogenicity in the Balb/c-2, CBA/Ca, and FVB/N passages, even though the host and transplanted tumour had completely mismatched MHC-I haplotypes. Higher T cell infiltration levels were found in N2.1 tumours which showed increased immunogenicity. Lower T and NK cell immune infiltration was observed in the Balb/c-

2, CBA/Ca, and FVB/N tumours, indicating a less immunogenic tumour profile and a highly suppressive TME. Interestingly, DC infiltration was higher in serially passaged Balb/c-2 tumours in terms of both relative percentage and counts, and macrophage infiltration was higher in terms of relative percentage and, to a lesser extent, counts.

Our results reaffirmed the importance of CD8+ T cells in the antitumour response and allograft rejection. This is highlighted by the very low frequency and counts of CTLs in later tumour passages in completely mismatched hosts. Surprisingly, this low CTL infiltration was accompanied by high MHC-I expression in tumour cells indicating that tumours are adopting a different strategy to MHC-I downregulation to inhibit CTLs functions. One strategy detected in tumour cells is the upregulation of immune inhibitory ligands such as PD-L1 and B7-H3 that can prevent CTLs effector function and prevent their proliferation. CD4+ T cells frequency followed a different trajectory to CD8+ T cells as they tended to increase with passaging. This might suggest that they are the immunosuppressive Tregs that are enriched in tumours where they are involved in suppressing CTLs effector functions by secreting TGF-β (Facciabene et al., 2012) and have a role in the prevention of acute and chronic skin and cardiac allograft rejection (Joffre et al., 2008). Unfortunately, no in-depth analysis of CD4+ T cells to check if they are Tregs was done in this project.

Using a panel of activation markers to examine tumour-infiltrating T cells at different passages revealed that a significant percentage of CD4+ T cells were highly activated in the F0 tumour; later tumour passages, however, revealed a more inhibited and less activated state. Compared to F0 tumours, CD4+ T cells in the TME of subsequent passages were characterised by greater PD-1 expression and lower

levels of the activation markers CD44 and CD69, suggesting that CD4+ T cells may be dysfunctional.

Our double injection experiments showed that in mice that received YUMM1.7 cells after an injection of Balb/c tumour cells, tolerance was not due to systemic immunosuppression, rather it was achieved locally. Similar to what is seen in CTVT, the rejection of both YUMM1.7 and Balb/c-2 cells in doubly injected mice indicates that tolerance is metastable and can be disrupted under the correct conditions (Frampton et al., 2018). Moreover, the data suggest that a population of cells that are CD3+ and NKp46+ play an important role in tumour regression as it is only seen in regressing tumours, where this was the predominant population, but not seen in progressing tumours. The double expression of lymphocyte and NK cells markers suggest that they are NKT cells but that could not be determined conclusively due to the lack of analysis of important NKT cells markers such as NK1.1, CD44, and CD24 (Soboloff & Kappes, 2018). The double injection revealed that the immune tolerance in Balb/c-2 is reversible and the immune system of BALB/c mice was able to attack and kill the tumour cells after the introduction of the immunogenic YUMM1.7 cells.

Analysis of MHC-I expression in YUMM1.7 and the subsequent tumour passages showed an unexpected pattern: tumours progressively reduced MHC-I levels, with the N2.1 passage, which had the highest tumour rejection rates, having the lowest levels of MHC-I expression. Tumours frequently use MHC-I downregulation as a strategy to avoid immunological rejection (Cornel et al., 2020; Dhatchinamoorthy et al., 2021; Wu et al., 2023). In the next tumour passages, such as in allogeneic BALB/c, CBA/Ca, and FVB/N mice, this pattern was reversed, suggesting the use of an alternative immune escape or immune suppressive approaches. In contrast to

what is seen in our late mouse tumour passages, transmissible cancers such as CTVT and DFT1 downregulate MHC-I, whereas DFT2 expresses MHC-I alleles that are common in its environment hosts (Kosack et al., 2019; Siddle et al., 2013). A possible explanation of this difference is the constitutive upregulation of PD-L1 in our tumours without stimulation. DFTD tumours do not express PD-L1 normally but can express it after immune challenge by IFN- γ (Flies et al., 2016). Moreover, our tumour passages expression of the inhibitory non-classical MHC could inhibit CD8+ T cells ability to destroy tumour cells with detectable MHC-I expression (Lohwasser et al., 2001).

The defect in antigen presentation in N2.1 and N2.2 tumour passages was not due to transcriptional regulation of MHC-I but potentially it might be due to transcriptional downregulation of chaperones involved in the folding of MHC-I for cell surface presentation. Other mechanisms could be in play as the gene expression differences of these chaperones between tumours with downregulated and other tumours were modest. Gene expression analysis of the MHC-I heavy chain and APM showed upregulation in the later tumour passages. This is likely because of activation of RIG-I and MDA5 by RTEs either directly, or indirectly by the upregulation of IFN signalling. The upregulation of the APM could be beneficial for the tumour in inhibiting NK cells functions due to MHC-I upregulation and non-classical MHC upregulation, which uses the same genes for its surface expression (Pishesha et al., 2022). The high expression of MHC-I is not usually linked to immune escape and tolerance in human tumours. However, a study where mouse melanoma that invades lymph nodes and were serially passages in syngeneic mice exhibited similar upregulation of MHC-I

and PD-L1 (Reticker-Flynn et al., 2022b) suggesting a common evolutionary pathway to immune evasion.

Interestingly, the late passage tumours acquired an inflammatory and antiviral signature that may cause the exhaustion of effector cells and recruitment of suppressor cells (Fang et al., 2022; Zhao et al., 2021). Additionally, these tumours displayed markers that can selectively suppress T and NK cells (Cha et al., 2019; J. Gao et al., 2017; Kochan et al., 2013; Leitner et al., 2009; Vaitaitis & Wagner, 2012). The data suggest that when RIG-I detects RTEs, it upregulates interferon-stimulated genes such as MHC-I, PD-L1 and non-classical MHC molecules. The upregulation of non-classical MHC-I is a mechanism utilized by Choriocarcinoma to induce immune tolerance (Gobin et al., 1997b) and some reports suggests that non-classical MHC molecules also play a role in DFTD (Cheng & Belov, 2014; Hussey et al., 2022).

Our RNA-seq data showed that tumours developed an inflammatory anti-viral signature. This was likely triggered by the sensing of RTE by RIG-I. Concurrently, tumours upregulated the expression of ISGs that are immune inhibitory most likely as a result of this inflammatory tumour signature. The activation of RTEs can lead to immune clearance of tumours if it induces acute inflammation, as is seen upon treatment of mouse melanoma with DNA Methyltransferase Inhibitors (DNMTis) that release RTEs silencing (Chiappinelli et al., 2015b). However, RTEs activation is also linked to tumour immune resistance and progression through the activation of immune inhibitory molecules such as HLA-G (Senft & Macfarlan, 2021).

To investigate the role of nucleic acid sensing and its effect on the upregulation of the immunomodulatory molecules on tumour cells, I initially examined cGAS, however its chemical suppression with RU.521 did not abrogate the immunological tumour signature. Conversely, CRISPR/Cas9 knockout of the RIG-I gene *Ddx58* in Balb/c-2 tumour cells reduced the expression of MHC-I, PD-L1, and Qa-1, indicating a critical role of RIG-I in the formation of the anti-viral signature associated with evasion from allogeneic rejection. Unexpectedly, the transduction of parental Balb/c-2 cells with an empty vector encoding CRISPR/Cas9 and the puromycin-resistance gene also reduced the expression of MHC-I, PD-L1, and Qa-1, albeit to a lesser degree than the RIG-I knockout clones. Tumour transplantation experiments including two RIG-I knockout clones and EV Balb/c-2 tumour cells showed reduced tumour takes in BALB/c mice, and this could be either due to de-novo expression of Cas9 and puromycin N-acetyltransferase, or the decreased levels of PD-L1 and Qa-1 in the EV cells compared to the parental cells. However, administering anti-PD-1 or anti-Qa-1 monoclonal antibodies to tumour injected mice led to tumour growth control, while the combination of anti-PD-1 and Qa-1 antibodies induced regression of established

The upregulation of MHC-I, PD-L1, and Qa-1 correlated with the upregulation of RTEs and RIG-I. However, it is not clear whether this is due to activation of IFN signalling or directly, bypassing the IFN step as both mechanisms have been reported. More work to determine which mechanism is critical might help with designing and administering therapeutics for tumours with the same signature. Treatment with anti PD-1 and Qa-1 also is effective against this tumour signature as it showed that it can significantly control tumour growth in the short term.

Our results suggest that genetically modified grafts may potentially be transplanted where the organ is tolerated locally without the need of potent systemic immune suppression that come with many deleterious side effects. This notion is supported by transmissible cancers, which can grow in immunocompetent dogs, and the limited experiments of humanized pig kidney xenotransplants in humans and NHP. In these experiments, genetically modified humanized pig kidneys and hearts to delete pig xenoantigens and expressing additional human transgenes were used. In NHP, functioning humanized pig kidneys showed that they can survive for years. In humans, a humanized pig heart transplanted into a human patient lasted for 7 weeks (Sykes & Sachs, 2022).

Our mouse model provided insights into how tumours adapt to escape allogeneic rejection, but there are still limitations and challenges. These include: first, the long time it takes to do the experiments due to the need for breeding different types of mice hybrids and backcrosses. Second, the study focuses on acute rejection, therefore no information on whether these tumours can grow for the long term and whether the same mechanisms are employed to avoid chronic rejection. In addition, the reasons for Balb/c-2 tumours regression after YUMM1.7 introduction in the double injection experiment are not known and more work is needed to identify the CD3+ and NKp46+ population enriched in regressing tumours. Fourth, the mechanism of RTEs upregulation is not known and whether that upregulation is due epigenetic derepression of RTEs or another mechanism.

This model has numerous benefits and can be utilized to study different topics including tumour evolution, tumour-immune interactions, allogeneic rejection, and immune escape mechanisms. The implications of this work in organ transplantation

could be through the over expression of the immune modulatory molecules PD-L1 and the human ortholog of Qa-1 (HLA-E) in transplanted organs to induce tolerance. In cancer therapy, the human orthologues of non-classical MHC are upregulated in different cancers and although there is a monoclonal antibody against NKG2A, which is the receptor for HLA-E, this has not yet been employed therapeutically.

In the future, it will be interesting to investigate the TCR repertoire of tumour infiltrating lymphocyte in the different tumour passages to study their diversity and clonal expansion and whether certain TCRs are enriched in late tumours that are defective in responding to the mismatched MHC-I. It will also be important to examine if the Balb/c-2 tumour signature is detected in human cancers and if it influences progression and response to therapy.

Our model could provide important information about tumour evolution and immune evasion. It could shed light on the process regulating cancer-immune system interactions and how the process of immune escape happens in tumour through immunoediting . In addition, the model is useful in cancer immunology studies and to study how tumours modulate the immune infiltrate to enhance their growth or induce an immune suppressive environment.

References:

affymetrix. (2024). *Mouse Haplotype Table*. https://assets.thermofisher.com/TFS-Assets/LSG/brochures/Mouse_Haplotype_Table.pdf

Al-Attar, M. M., Zou, T., Fischer, A. H., & Cosar, E. F. (2021). Choriocarcinoma Presenting as a Metastatic Pancreatic Mass: a Cytopathologic Diagnostic Challenge. *American Journal of Clinical Pathology*, *156*(Supplement_1), S42–S43. https://doi.org/10.1093/ajcp/aqab191.085

Alfaro, G., Lomeli, C., Ocadiz, R., Ortega, V., Barrera, R., Ramirez, M., & Nava, G. (1992). Immunologic and genetic characterization of S 180, a cell line of murine origin capable of growing in different inbred strains of mice. In *Veterinary Immunology and Immunopathology* (Vol. 30).

Amariglio, E. N., Hakim, I., Brok-Simoni, F., Grossman, Z., Katzir, N., Harmelint, A., Ramot, B., & Rechavi, G. (1991). Identity of rearranged LINE/c-MYC junction sequences specific for the canine transmissible venereal tumor (transposable elements/oncogene/polymerase chain reaction). In *Proc. Nati. Acad. Sci. USA* (Vol. 88). https://www.pnas.org

Andersen, M. H., Schrama, D., & Becker, J. C. (2006). Cytotoxic T Cells. *PERSPECTIVE 32 Journal of Investigative Dermatology*, *126*, 32–41. https://doi.org/10.1038/sj.jid5700001

André, P., Denis, C., Soulas, C., Bourbon-Caillet, C., Lopez, J., Arnoux, T., Bléry, M., Bonnafous, C., Gauthier, L., Morel, A., Rossi, B., Remark, R., Breso, V., Bonnet, E., Habif, G., Guia, S., Lalanne, A. I., Hoffmann, C., Lantz, O., … Vivier, E. (2018). Anti-NKG2A mAb Is a Checkpoint Inhibitor that Promotes Anti-tumor Immunity by Unleashing Both T and NK Cells. *Cell*, *175*(7), 1731-1743.e13. https://doi.org/10.1016/j.cell.2018.10.014

Appleman, L. J., & Boussiotis, V. A. (2003). T cell anergy and costimulation. *Immunological Reviews*, *192*(1), 161–180. https://doi.org/10.1034/J.1600-065X.2003.00009.X

Apps, R., Murphy, S. P., Fernando, R., Gardner, L., Ahad, T., & Moffett, A. (2009). Human leucocyte antigen (HLA) expression of primary trophoblast cells and placental cell lines, determined using single antigen beads to characterize allotype specificities of anti-HLA antibodies. *Immunology*, *127*(1), 26–39. https://doi.org/10.1111/j.1365-2567.2008.03019.x

Arakawa, A., Ichikawa, H., Kubo, T., Motoi, N., Kumamoto, T., Nakajima, M., Yonemori, K., Noguchi, E., Sunami, K., Shiraishi, K., Kakishima, H., Yoshida, H., Hishiki, T., Kawakubo, N., Kuroda, T., Kiyokawa, T., Yamada, K., Yanaihara, N., Takahashi, K., … Ogawa, C. (2021). Vaginal Transmission of Cancer from Mothers with Cervical Cancer to Infants. *New England Journal of Medicine*, *384*(1), 42–50. https://doi.org/10.1056/nejmoa2030391

Arakawa, A., Tao, K., Kohno, T., & Ogawa, C. (2024). Cross-individual cancer transmission to children during the gestational and perinatal periods. In *Cancer Science* (Vol. 115, Issue 4, pp. 1039–1047). John Wiley and Sons Inc. https://doi.org/10.1111/cas.16102

Attig, J., Young, G. R., Stoye, J. P., & Kassiotis, G. (2017). Physiological and pathological transcriptional activation of endogenous retroelements assessed by RNA-sequencing of B lymphocytes. *Frontiers in Microbiology*, *8*(DEC). https://doi.org/10.3389/fmicb.2017.02489

Avril, T., Jarousseau, A.-C., Watier, H., Boucraut, J., Le Bouteiller, P., Bardos, P., & Thibault, G. (1999). Trophoblast Cell Line Resistance to NK Lysis Mainly Involves an HLA Class I-Independent Mechanism 1. In *The Journal of Immunology* (Vol. 162). http://journals.aai.org/jimmunol/article-pdf/162/10/5902/1099543/5902.pdf

Baez-Ortega, A., Gori, K., Strakova, A., Allen, J. L., Allum, K. M., Bansse-Issa, L., Bhutia, T. N., Bisson, J. L., Briceño, C., Domracheva, A. C., Corrigan, A. M., Cran, H. R., Crawford, J. T., Davis, E., De Castro, K. F., De Nardi, A. B., De Vos, A. P., Keenan, L. D., Donelan, E. M., … Murchison, E. P. (2019). Somatic evolution and global expansion of an ancient transmissible cancer lineage. *Science*, *365*(6452). https://doi.org/10.1126/science.aau9923

Bald, T., Krummel, M. F., Smyth, M. J., & Barry, K. C. (2020). The NK cell-cancer cycle: advances and new challenges in NK cell-based immunotherapies. *Nature Immunology*, *21*(8), 835–847. https://doi.org/10.1038/S41590-020-0728-Z

Ballestero Fêo, H., Montoya Flórez, L., Yamatogi, R. S., Prado Duzanski, A., Araújo, J. P., Oliveira, R. A., & Rocha, N. S. (2018). Does the tumour microenvironment alter tumorigenesis and clinical response in transmissible venereal tumour in dogs? *Veterinary and Comparative Oncology*, *16*(3), 370–378. https://doi.org/10.1111/vco.12388

Baltazar, J. C. (1976). Epidemiological features of choriocarcinoma. *Bulletin of the World Health Organization*, *54*(5), 523–532. http://www.ncbi.nlm.nih.gov/pubmed/1088402

Barnes, A. D., & Krohn, P. L. (1957). The Estimation of the Number of Histocompatibility Genes Controlling the Successful Transplantation of Normal Skin in Mice. In *Biological Sciences* (Vol. 146, Issue 925).

BARRETT, M. K., & DERINGER, M. K. (1950). An induced adaptation in a transplantable tumor of mice. *Journal of the National Cancer Institute*, *11*(1), 51–59. http://www.ncbi.nlm.nih.gov/pubmed/14784841

Barrett, M. K., & Deringer, M. K. (1952). Induced Adaptation in a Tumor: Permanence of the Change. *JNCI: Journal of the National Cancer Institute*, *12*(5), 1011–1017. https://doi.org/10.1093/JNCI/12.5.1011

Benichou, G., & Thomson, A. W. (2009). Direct versus indirect allorecognition pathways: On the right track. In *American Journal of Transplantation* (Vol. 9, Issue 4, pp. 655–656). https://doi.org/10.1111/j.1600-6143.2009.02572.x

Benichou, G., Yamada, Y., Yun, S. H., Lin, C., Fray, M., & Tocco, G. (2011). Immune recognition and rejection of allogeneic skin grafts. *Immunotherapy*, *3*(6), 757–770. https://doi.org/10.2217/IMT.11.2/ASSET/IMAGES/LARGE/FIGURE3.JPEG

Bio-Rad. (2017). Cell Frequency. *Reference*, *488*, 1–2. https://www.bio-rad-antibodies.com/static/2017/flow/flow-cytometry-cell-frequency.pdf

Boardman, D. A., Jacob, J., Smyth, L. A., Lombardi, G., & Lechler, R. I. (2016). What Is Direct Allorecognition? *Current Transplantation Reports*, *3*(4), 275–283. https://doi.org/10.1007/s40472-016-0115-8

Bogani, G., Ray-Coquard, I., Mutch, D., Vergote, I., Ramirez, P. T., Prat, J., Concin, N., Li Ngoi, N. Y., Coleman, R. L., Enomoto, T., Takehara, K., Denys, H., Lorusso, D., Takano, M., Sagae, S., Wimberger, P., Segev, Y., Kim, S. I., Kim, J. W., … Monk, B. J. (2023). Gestational choriocarcinoma. *International Journal of Gynecological Cancer*, *33*(10), 1504–1514. https://doi.org/10.1136/ijgc-2023-004704

Böttcher, J. P., Bonavita, E., Chakravarty, P., Blees, H., Cabeza-Cabrerizo, M., Sammicheli, S., Rogers, N. C., Sahai, E., Zelenay, S., & Reis e Sousa, C. (2018). NK Cells Stimulate Recruitment of cDC1 into the Tumor Microenvironment Promoting Cancer Immune Control. *Cell*, *172*(5), 1022-1037.e14. https://doi.org/10.1016/J.CELL.2018.01.004

Bouallegui, Y. (2019). Immunity in mussels: An overview of molecular components and mechanisms with a focus on the functional defenses. In *Fish and Shellfish Immunology* (Vol. 89, pp. 158–169). Academic Press. https://doi.org/10.1016/j.fsi.2019.03.057

Brewer, J. I., Torok, E. E., Kahan2, B. D., Stanhope, C. R., & Halpern, B. (1978). GESTATIONAL TROPHOBLASTIC DISEASE: ORIGIN OF CHORIOCARCINOMA, INVASIVE MOLE AND CHORIOCARCINOMA ASSOCIATED WITH HYDXTIDIFORM MOLE, AND SOME IMMUNOLOGIC ASPECTS'. In *ADVANCES IN CAhCER RESEARCH* (Vol. 27).

Brinton, L. A., Bracken, M. B., Connelly, R. R., Nci, L. A., Bracken, M. B., & Connelly, R. R. (1986). Printed m U.SA. Choriocarcinoma incidence in the United States. In *Am J Epidemiol* (Vol. 123, Issue 6). https://academic.oup.com/aje/article/123/6/1094/134375

Broit, N., Johansson, P. A., Rodgers, C. B., Walpole, S. T., Newell, F., Hayward, N. K., & Pritchard, A. L. (2021). Meta-Analysis and Systematic Review of the Genomics of Mucosal Melanoma. *Molecular Cancer Research*, *19*(6), 991–1004. https://doi.org/10.1158/1541-7786.MCR-20-0839

Bronte, V., Brandau, S., Chen, S. H., Colombo, M. P., Frey, A. B., Greten, T. F., Mandruzzato, S., Murray, P. J., Ochoa, A., Ostrand-Rosenberg, S., Rodriguez, P. C., Sica, A., Umansky, V., Vonderheide, R. H., & Gabrilovich, D. I. (2016). Recommendations for myeloid-derived suppressor cell nomenclature and characterization standards. In *Nature Communications* (Vol. 7). Nature Publishing Group. https://doi.org/10.1038/ncomms12150

Brownell, J., Bruckner, J., Wagoner, J., Thomas, E., Loo, Y.-M., Gale, M., Liang, T. J., & Polyak, S. J. (2014). Direct, Interferon-Independent Activation of the CXCL10 Promoter by NF-κB and Interferon Regulatory Factor 3 during Hepatitis C Virus Infection. *Journal of Virology*, *88*(3), 1582–1590. https://doi.org/10.1128/jvi.02007-13

Bruzos, A. L., Santamarina, M., García-Souto, D., Díaz, S., Rocha, S., Zamora, J., Lee, Y., Viña-Feás, A., Quail, M. A., Otero, I., Pequeño-Valtierra, A., Temes, J., Rodriguez-Castro, J., Aramburu, L., Vidal-Capón, A., Villanueva, A., Costas, D., Rodríguez, R., Prieto, T., … Tubio, J. M. C. (2023). Somatic evolution of marine transmissible leukemias in the common cockle, Cerastoderma edule. *Nature Cancer*, *4*(11), 1575–1591. https://doi.org/10.1038/s43018-023-00641-9

Burioli, E. A. V., Hammel, M., Vignal, E., Vidal-Dupiol, J., Mitta, G., Thomas, F., Bierne, N., Destoumieux-Garzón, D., & Charrière, G. M. (2023). Transcriptomics of mussel transmissible cancer MtrBTN2 suggests accumulation of multiple cancer traits and oncogenic pathways shared among bilaterians. *Open Biology*, *13*(10). https://doi.org/10.1098/rsob.230259

Caldwell, A., Coleby, R., Tovar, C., Stammnitz, M. R., Kwon, Y. M., Owen, R. S., Tringides, M., Murchison, E. P., Skjødt, K., Thomas, G. J., Kaufman, J., Elliott, T., Woods, G. M., & Siddle, H. V. (2018). The newly-arisen Devil facial tumour disease 2 (DFT2) reveals a mechanism for the emergence of a contagious cancer. *ELife*, *7*. https://doi.org/10.7554/eLife.35314

Cankovic, M., Gaba, A. R., Meier, F., Kim, W. S., & Zarbo, R. J. (2006). Detection of non-maternal components of gestational choriocarcinoma by PCR-based microsatellite DNA assay. *Gynecologic Oncology*, *103*(2), 614–617. https://doi.org/10.1016/j.ygyno.2006.04.008

Carreras, E., Dufour, C., Mohty, M., & Kröger, N. (2019). *Hematopoietic Stem Cell Transplantation and Cellular Therapies The EBMT Handbook*.

Castellani, G., Buccarelli, M., Arasi, M. B., Rossi, S., Pisanu, M. E., Bellenghi, M., Lintas, C., & Tabolacci, C. (2023). BRAF Mutations in Melanoma: Biological Aspects, Therapeutic Implications, and Circulating Biomarkers. In *Cancers* (Vol. 15, Issue 16). Multidisciplinary Digital Publishing Institute (MDPI). https://doi.org/10.3390/cancers15164026

Celada, F., & Welshons, W. J. (1962). DEMONSTRATION OF F 1 HYBRID ANTI-PARENT IMMUNOLOGICAL REACTION. *Proceedings of the National Academy of Sciences*, *48*(3), 326–331. https://doi.org/10.1073/pnas.48.3.326

Cha, J. H., Chan, L. C., Li, C. W., Hsu, J. L., & Hung, M. C. (2019). Mechanisms Controlling PD-L1 Expression in Cancer. *Molecular Cell*, *76*(3), 359–370. https://doi.org/10.1016/J.MOLCEL.2019.09.030

Cheng, Y., & Belov, K. (2014). Characterisation of non-classical MHC class I genes in the Tasmanian devil (Sarcophilus harrisii). *Immunogenetics*, *66*(12), 727–735. https://doi.org/10.1007/s00251-014-0804-3

Chiappinelli, K. B., Strissel, P. L., Desrichard, A., Li, H., Henke, C., Akman, B., Hein, A., Rote, N. S., Cope, L. M., Snyder, A., Makarov, V., Buhu, S., Slamon, D. J., Wolchok, J. D., Pardoll, D. M., Beckmann, M. W., Zahnow, C. A., Mergoub, T., Chan, T. A., … Strick, R. (2015a). Inhibiting DNA Methylation Causes an Interferon Response in Cancer via dsRNA Including Endogenous Retroviruses. *Cell*, *162*(5), 974–986. https://doi.org/10.1016/J.CELL.2015.07.011

Chiappinelli, K. B., Strissel, P. L., Desrichard, A., Li, H., Henke, C., Akman, B., Hein, A., Rote, N. S., Cope, L. M., Snyder, A., Makarov, V., Buhu, S., Slamon, D. J., Wolchok, J. D., Pardoll, D. M., Beckmann, M. W., Zahnow, C. A., Mergoub, T., Chan, T. A., … Strick, R. (2015b). Inhibiting DNA Methylation Causes an Interferon Response in Cancer via dsRNA Including Endogenous Retroviruses. *Cell*, *162*(5), 974–986. https://doi.org/10.1016/j.cell.2015.07.011

Chiu, D. K. C., Tse, A. P. W., Xu, I. M. J., Di Cui, J., Lai, R. K. H., Li, L. L., Koh, H. Y., Tsang, F. H. C., Wei, L. L., Wong, C. M., Ng, I. O. L., & Wong, C. C. L. (2017). Hypoxia inducible factor HIF-1 promotes myeloid-derived suppressor cells accumulation through ENTPD2/CD39L1 in hepatocellular carcinoma. *Nature Communications*, *8*(1). https://doi.org/10.1038/S41467-017-00530-7

Churchill, G. A., & Doerge, R. W. (1994). Empirical Threshold Values for Quantitative Trait Mapping. In *Genetics* (Vol. 138). https://academic.oup.com/genetics/article/138/3/963/6012760

Cohen, D. (1985). The Canine Transmissible Venereal Tumor: a Unique Result of Tumor Progression. *Advances in Cancer Research*, *43*(C), 75–112. https://doi.org/10.1016/S0065-230X(08)60943-4

Cohen, D., Shalev, A., & Krup4, M. (1984). Lack of β₂-Microglobulin on the Surface of Canine Transmissible Venereal Tumor Cells<xref ref-type="fn" rid="FN2">2</xref><xref ref-type="fn" rid="FN3">3</xref> *JNCI: Journal of the National Cancer Institute*. https://doi.org/10.1093/jnci/72.2.395

Connelley, T. K., Longhi, C., Burrells, A., Degnan, K., Hope, J., Allan, A. J., Hammond, J. A., Storset, A. K., & Morrison, W. I. (2014). NKp46+ CD3+ cells:

a novel nonconventional T cell subset in cattle exhibiting both NK cell and T cell features. *Journal of Immunology (Baltimore, Md. : 1950)*, *192*(8), 3868–3880. https://doi.org/10.4049/JIMMUNOL.1302464

Cornel, A. M., Mimpen, I. L., & Nierkens, S. (2020). MHC class I downregulation in cancer: Underlying mechanisms and potential targets for cancer immunotherapy. In *Cancers* (Vol. 12, Issue 7, pp. 1–33). MDPI AG. https://doi.org/10.3390/cancers12071760

Crispim, J. C. O., Duarte, R. A., Soares, C. P., Costa, R., Silva, J. S., Mendes-Júnior, C. T., Wastowski, I. J., Faggioni, L. P., Saber, L. T., & Donadi, E. A. (2008). Human leukocyte antigen-G expression after kidney transplantation is associated with a reduced incidence of rejection. *Transplant Immunology*, *18*(4), 361–367. https://doi.org/10.1016/j.trim.2007.10.010

Cui, Z., Willingham, M. C., Hicks, A. M., Alexander-Miller, M. A., Howard, T. D., Hawkins, G. A., Miller, M. S., Weir, H. M., Du, W., & DeLong, C. J. (2003). Spontaneous regression of advanced cancer: identification of a unique genetically determined, age-dependent trait in mice. *Proceedings of the National Academy of Sciences of the United States of America*, *100*(11), 6682–6687. https://doi.org/10.1073/pnas.1031601100

de Angelis, M. H., Adler, A., Beckers, J., Soewarto, D., Wagner, S., Gailus-Durner, V., & Imai, K. (2004). Mouse Genomics. In *The Laboratory Mouse* (pp. 47–84). Elsevier. https://doi.org/10.1016/B978-012336425-8/50057-1

Dean, I., Lee, C. Y. C., Tuong, Z. K., Li, Z., Tibbitt, C. A., Willis, C., Gaspal, F., Kennedy, B. C., Matei-Rascu, V., Fiancette, R., Nordenvall, C., Lindforss, U., Baker, S. M., Stockmann, C., Sexl, V., Hammond, S. A., Dovedi, S. J., Mjösberg, J., Hepworth, M. R., … Withers, D. R. (2024). Rapid functional impairment of natural killer cells following tumor entry limits anti-tumor immunity. *Nature Communications*, *15*(1). https://doi.org/10.1038/s41467-024-44789-z

Del Prete, A., Salvi, V., Soriani, A., Laffranchi, M., Sozio, F., Bosisio, D., & Sozzani, S. (2023). Dendritic cell subsets in cancer immunity and tumor antigen sensing. In *Cellular and Molecular Immunology* (Vol. 20, Issue 5, pp. 432–447). Springer Nature. https://doi.org/10.1038/s41423-023-00990-6

Dhatchinamoorthy, K., Colbert, J. D., & Rock, K. L. (2021). Cancer Immune Evasion Through Loss of MHC Class I Antigen Presentation. In *Frontiers in Immunology* (Vol. 12). Frontiers Media S.A. https://doi.org/10.3389/fimmu.2021.636568

Dhillon, P., Mulholland, K. A., Hu, H., Park, J., Sheng, X., Abedini, A., Liu, H., Vassalotti, A., Wu, J., & Susztak, K. (2023). Increased levels of endogenous retroviruses trigger fibroinflammation and play a role in kidney disease

development. *Nature Communications*, *14*(1). https://doi.org/10.1038/s41467-023-36212-w

Diao, J., Gu, H., Tang, M., Zhao, J., & Cattral, M. S. (2018). Tumor Dendritic Cells (DCs) Derived from Precursors of Conventional DCs Are Dispensable for Intratumor CTL Responses. *The Journal of Immunology*, *201*(4), 1306–1314. https://doi.org/10.4049/jimmunol.1701514

Doi, T., Ishikawa, T., Okayama, T., Oka, K., Mizushima, K., Yasuda, T., Sakamoto, N., Katada, K., Kamada, K., Uchiyama, K., Handa, O., Takagi, T., Naito, Y., & Itoh, Y. (2017). The JAK/STAT pathway is involved in the upregulation of PD-L1 expression in pancreatic cancer cell lines. *Oncology Reports*, *37*(3), 1545–1554. https://doi.org/10.3892/or.2017.5399

Dolina, J. S., Van Braeckel-Budimir, N., Thomas, G. D., & Salek-Ardakani, S. (2021). $CD8^+$ T Cell Exhaustion in Cancer. *Frontiers in Immunology*, *12*, 715234–715234. https://doi.org/10.3389/FIMMU.2021.715234

Dunay, I. R., DaMatta, R. A., Fux, B., Presti, R., Greco, S., Colonna, M., & Sibley, L. D. (2008). Gr1+ Inflammatory Monocytes Are Required for Mucosal Resistance to the Pathogen Toxoplasma gondii. *Immunity*, *29*(2), 306–317. https://doi.org/10.1016/J.IMMUNI.2008.05.019

Dunham, L. J., & Stewart, H. L. (1953). A Survey of Transplantable and Transmissible Animal Tumors. *JNCI: Journal of the National Cancer Institute*, *13*(5), 1299–1377. https://doi.org/10.1093/JNCI/13.5.1299

Dunn, G. P., Old, L. J., & Schreiber, R. D. (2004). The three Es of cancer immunoediting. In *Annual Review of Immunology* (Vol. 22, pp. 329–360). https://doi.org/10.1146/annurev.immunol.22.012703.104803

Efimova, E. V., Liang, H., Pitroda, S. P., Labay, E., Darga, T. E., Levina, V., Lokshin, A., Roizman, B., Weichselbaum, R. R., & Khodarev, N. N. (2009). Radioresistance of Stat1 over-expressing tumour cells is associated with suppressed apoptotic response to cytotoxic agents and increased IL6-IL8 signalling. *International Journal of Radiation Biology*, *85*(5), 421–431. https://doi.org/10.1080/09553000902838566

Erkes, D. A., Cai, W., Sanchez, I. M., Purwin, T. J., Rogers, C., Field, C. O., Berger, A. C., Hartsough, E. J., Rodeck, U., Alnemri, E. S., & Aplin, A. E. (2020). Mutant BRAF and MEK inhibitors regulate the tumor immune microenvironment via pyroptosis. *Cancer Discovery*, *10*(2), 255–269. https://doi.org/10.1158/2159-8290.CD-19-0672/333422/AM/MUTANT-BRAF-AND-MEK-INHIBITORS-REGULATE-THE-TUMOR

Facciabene, A., Motz, G. T., & Coukos, G. (2012). T-Regulatory cells: Key players in tumor immune escape and angiogenesis. In *Cancer Research* (Vol. 72, Issue 9, pp. 2162–2171). https://doi.org/10.1158/0008-5472.CAN-11-3687

Falconer, D. S., & Mackay, T. F. C. (1996). Introduction to Quantitative Genetics (Fourth Edition). In *Trends in Genetics* (Vol. 12).

Fang, L., Liu, K., Liu, C., Wang, X., Ma, W., Xu, W., Wu, J., & Sun, C. (2022). Tumor accomplice: T cell exhaustion induced by chronic inflammation. *Frontiers in Immunology*, *13*, 5219. https://doi.org/10.3389/FIMMU.2022.979116/BIBTEX

Fassati, A. (2018). What a dog transmissible tumor can teach us about cancer regression. *Molecular and Cellular Oncology*, *5*(4). https://doi.org/10.1080/23723556.2018.1472059

Favier, B., LeMaoult, J., Lesport, E., & Carosella, E. D. (2010). ILT2/HLA-G interaction impairs NK-cell functions through the inhibition of the late but not the early events of the NK-cell activating synapse. *The FASEB Journal*, *24*(3), 689–699. https://doi.org/10.1096/fj.09-135194

Fêo, H. B., Flórez, L. M. M., Yamatogi, R. S., Duzanski, A. P., Junior, J. P. A., Oliveira, R. A., & Rocha, N. S. (2022). Could dysregulation of RASSF1 expression be a mechanism of tumorigenesis in CTVT? *China Journal of Leprosy and Skin Diseases*, *42*. https://doi.org/10.1590/1678-5150-PVB-7082

Fishman, J. A. (2017). Infection in Organ Transplantation. In *American Journal of Transplantation* (Vol. 17, Issue 4, pp. 856–879). Blackwell Publishing Ltd. https://doi.org/10.1111/ajt.14208

Flies, A. S., Bruce Lyons, A., Corcoran, L. M., Papenfuss, A. T., Murphy, J. M., Knowles, G. W., Woods, G. M., & Hayball, J. D. (2016). PD-L1 is not constitutively expressed on tasmanian devil facial tumor cells but is strongly upregulated in response to IFN-γ and can be expressed in the tumor microenvironment. *Frontiers in Immunology*, *7*(DEC). https://doi.org/10.3389/fimmu.2016.00581

Flurkey, K., Currer, J. M., & Harrison, D. E. (2007). *Mouse Models in Aging Research*.

Frampton, D., Schwenzer, H., Marino, G., Butcher, L. M., Pollara, G., Kriston-Vizi, J., Venturini, C., Austin, R., de Castro, K. F., Ketteler, R., Chain, B., Goldstein, R. A., Weiss, R. A., Beck, S., & Fassati, A. (2018). Molecular Signatures of Regression of the Canine Transmissible Venereal Tumor. *Cancer Cell*, *33*(4), 620-633.e6. https://doi.org/10.1016/J.CCELL.2018.03.003

Gabrilovich, D. I. (2017). Myeloid-derived suppressor cells. *Cancer Immunology Research*, *5*(1), 3–8. https://doi.org/10.1158/2326-6066.CIR-16-0297

Ganguly, B., Das, U., & Das, A. K. (2016). Canine transmissible venereal tumour: A review. In *Veterinary and Comparative Oncology* (Vol. 14, Issue 1, pp. 1–12). Blackwell Publishing Ltd. https://doi.org/10.1111/vco.12060

Gao, D., Wu, J., Wu, Y. T., Du, F., Aroh, C., Yan, N., Sun, L., & Chen, Z. J. (2013). Cyclic GMP-AMP synthase is an innate immune sensor of HIV and other retroviruses. *Science*, *341*(6148), 903–906. https://doi.org/10.1126/science.1240933

Gao, J., Zheng, Q., Xin, N., Wang, W., & Zhao, C. (2017). CD155, an onco-immunologic molecule in human tumors. *Cancer Science*, *108*(10), 1934–1938. https://doi.org/10.1111/CAS.13324

Garg, N., Farhat, J., Dhankhar, S., Chauhan, S., Bala, R., Madaan, R., Sharma, H., Saini, M., Singh, T. G., Aldahish, A. A., Almarhoon, Z., Al-Omari, B., & Sharifi-Rad, J. (2024). Vincristine in Cancer Therapy: Mechanisms, Efficacy, and Future Perspectives. *Current Medicinal Chemistry*, *31*. https://doi.org/10.2174/0109298673319496240911060138

Garrido, F., & Aptsiauri, N. (2019). Cancer immune escape: MHC expression in primary tumours versus metastases. *Immunology*, *158*(4), 255–266. https://doi.org/10.1111/IMM.13114

Gärtner, H.-V., Seidl, C., Luckenbach, C., Schumm, G., Seifried, E., Ritter, H., & Bültmann, B. (1996). Genetic Analysis of a Sarcoma Accidentally Transplanted from a Patient to a Surgeon. *New England Journal of Medicine*, *335*(20), 1494–1497. https://doi.org/10.1056/NEJM199611143352004

Gessani, S., Conti, L., Del Cornò, M., & Belardelli, F. (2014). Type I interferons as regulators of human antigen presenting cell functions. In *Toxins* (Vol. 6, Issue 6, pp. 1696–1723). MDPI AG. https://doi.org/10.3390/toxins6061696

Gibson, T., & Medawar, P. B. (1943). The fate of skin homografts in man. *Journal of Anatomy*, *77*(Pt 4), 299-310.4. http://www.ncbi.nlm.nih.gov/pubmed/17104936

Gobin, S. J. P., Wilson, L., Keijsers, V., & Van Den Elsen, P. J. (1997a). Antigen Processing and Presentation by Human Trophoblast-Derived Cell lines'. In *The Journal of Immunology* (Vol. 158). http://journals.aai.org/jimmunol/article-pdf/158/8/3587/1076106/3587.pdf

Gobin, S. J. P., Wilson, L., Keijsers, V., & Van Den Elsen, P. J. (1997b). Antigen Processing and Presentation by Human Trophoblast-Derived Cell lines'. In *The Journal of Immunology* (Vol. 158). http://journals.aai.org/jimmunol/article-pdf/158/8/3587/1076106/3587.pdf

Gonzalez, C. M., Griffey, S. M., Naydan, D. K., Flores, E., Cepeda, R., Cattaneo, G., & Madewell, B. R. (2000). Canine transmissible venereal tumour: A morphological and immunohistochemical study of 11 tumours in growth phase and during regression after chemotherapy. *Journal of Comparative Pathology*, *122*(4), 241–248. https://doi.org/10.1053/jcpa.1999.0366

Goodall, K. J., Nguyen, A., Sullivan, L. C., & Andrews, D. M. (2019). The expanding role of murine class Ib MHC in the development and activation of Natural Killer cells. In *Molecular Immunology* (Vol. 115, pp. 31–38). Elsevier Ltd. https://doi.org/10.1016/j.molimm.2018.05.001

Griffin, G. K., Wu, J., Iracheta-Vellve, A., Patti, J. C., Hsu, J., Davis, T., Dele-Oni, D., Du, P. P., Halawi, A. G., Ishizuka, J. J., Kim, S. Y., Klaeger, S., Knudsen, N. H., Miller, B. C., Nguyen, T. H., Olander, K. E., Papanastasiou, M., Rachimi, S., Robitschek, E. J., … Bernstein, B. E. (2021). Epigenetic silencing by SETDB1 suppresses tumour intrinsic immunogenicity. *Nature*, *595*(7866), 309–314. https://doi.org/10.1038/S41586-021-03520-4

Guijarro, L. G., Sanmartin-Salinas, P., Pérez-Cuevas, E., Toledo-Lobo, M. V., Monserrat, J., Zoullas, S., Sáez, M. A., Álvarez-Mon, M. A., Bujan, J., Noguerales-Fraguas, F., Arilla-Ferreiro, E., Álvarez-Mon, M., & Ortega, M. A. (2021). Actinomycin d arrests cell cycle of hepatocellular carcinoma cell lines and induces p53-dependent cell death: A study of the molecular mechanism involved in the protective effect of irs-4. *Pharmaceuticals*, *14*(9). https://doi.org/10.3390/ph14090845

Hammel, M., Simon, A., Arbiol, C., Villalba, A., Burioli, E. A. V., Pépin, J. F., Lamy, J. B., Benabdelmouna, A., Bernard, I., Houssin, M., Charrière, G. M., Destoumieux-Garzon, D., Welch, J. J., Metzger, M. J., & Bierne, N. (2022). Prevalence and polymorphism of a mussel transmissible cancer in Europe. *Molecular Ecology*, *31*(3), 736–751. https://doi.org/10.1111/mec.16052

Hammel, M., Touchard, F., Burioli, E. A. V., Paradis, L., Cerqueira, F., Chailler, E., Bernard, I., Cochet, H., Simon, A., Thomas, F., Destoumieux-Garzón, D., Charrière, G. M., & Bierne, N. (2024). Marine transmissible cancer navigates urbanized waters, threatening spillover. *Proceedings of the Royal Society B: Biological Sciences*, *291*(2017). https://doi.org/10.1098/rspb.2023.2541

Hanahan, D., & Weinberg, R. A. (2011). Hallmarks of cancer: the next generation. *Cell*, *144*(5), 646–674. https://doi.org/10.1016/J.CELL.2011.02.013

Hart, S. F. M., Giersch, R. M., Yonemitsu, M. A., Beal, B., Goff, S. P., & Metzger, M. J. (2022). Abstract A003: Genome evolution of a transmissible cancer in the soft-shell clam (*Mya arenaria*). *Cancer Research*, *82*(10_Supplement), A003–A003. https://doi.org/10.1158/1538-7445.EVODYN22-A003

Hartmann, G. (2017). Nucleic Acid Immunity. *Advances in Immunology*, *133*, 121–169. https://doi.org/10.1016/BS.AI.2016.11.001

Hayes, A. M., Schiavo, L., Constantino-Casas, F., Desmas, I., Dobson, J., Draper, A., Elliot, J., Genain, M. A., Wang, J., & Murchison, E. P. (2023). Transmission of canine transmissible venereal tumour between two dogs in the UK. *Journal of Small Animal Practice*, *64*(9), 590–594. https://doi.org/10.1111/jsap.13607

Henry, K. R., & Chole, R. A. (1980). Genotypic Differences in Behavioral, Physiological and Anatomical Expressions of Age-Related Hearing Loss in the Laboratory Mouse: Original Papers Travaux originaux. *International Journal of Audiology*, *19*(5), 369–383. https://doi.org/10.3109/00206098009070071

Hsiao, Y. W., Liao, K. W., Chung, T. F., Liu, C. H., Hsu, C. Da, & Chu, R. M. (2008). Interactions of host IL-6 and IFN-γ and cancer-derived TGF-β1 on MHC molecule expression during tumor spontaneous regression. *Cancer Immunology, Immunotherapy*, *57*(7), 1091–1104. https://doi.org/10.1007/s00262-007-0446-5

Hsiao, Y.-W., Liao, K.-W., Hung, S.-W., & Chu, R.-M. (2002). Effect of tumor infiltrating lymphocytes on the expression of MHC molecules in canine transmissible venereal tumor cells. *Veterinary Immunology and Immunopathology*, *87*(1–2), 19–27. https://doi.org/10.1016/s0165-2427(02)00026-0

Huang, H., Langenkamp, E., Georganaki, M., Loskog, A., Fuchs, P. F., Dieterich, L. C., Kreuger, J., & Dimberg, A. (2015). VEGF suppresses T-lymphocyte infiltration in the tumor microenvironment through inhibition of NF-κB-induced endothelial activation. *FASEB Journal*, *29*(1), 227–238. https://doi.org/10.1096/fj.14-250985

Huang, L., Yang, J., Zhu, J., Wang, H., Dong, L., Guo, Y., Chen, Y., Zhang, F., Xu, D. J., Ou, L., Xu, J. R., Guan, L., Doan, Q. D., Fan, A. Y., Zhong, W., Ko, J., Liang, C., Herlyn, M., Guo, W., … Liu, S. (2024). PD-L1 in Melanoma and Extracellular Vesicles Promotes Local and Regional Immune Suppression through M2-like Macrophage Polarization. *The American Journal of Pathology*. https://doi.org/10.1016/j.ajpath.2024.09.011

Huennekens, F. M. (1994). 0065-2571(93)E0012-D THE METHOTREXATE STORY: A PARADIGM FOR DEVELOPMENT OF CANCER CHEMOTHERAPEUTIC AGENTS. In *Enzyme Regul* (Vol. 34).

Hussey, K., Caldwell, A., Kreiss, A., Skjødt, K., Gastaldello, A., Pye, R., Hamede, R., Woods, G. M., & Siddle, H. V. (2022). Expression of the Nonclassical MHC Class I, Saha-UD in the Transmissible Cancer Devil Facial Tumour Disease (DFTD). *Pathogens*, *11*(3). https://doi.org/10.3390/pathogens11030351

Initial sequencing and comparative analysis of the mouse genome. (2002). *Nature*, *420*(6915), 520–562. https://doi.org/10.1038/nature01262

Jacobs, P. A., Wilson, C. M., Sprenkle, J. A., Rosenshein, N. B., & Migeon, B. R. (1980). Mechanism of origin of complete hydatidiform moles. *Nature*, *286*(5774), 714–716. https://doi.org/10.1038/286714a0

Jacquelot, N., Yamazaki, T., Roberti, M. P., Duong, C. P. M., Andrews, M. C., Verlingue, L., Ferrere, G., Becharef, S., Vétizou, M., Daillère, R., Messaoudene, M., Enot, D. P., Stoll, G., Ugel, S., Marigo, I., Foong Ngiow, S.,

Marabelle, A., Prevost-Blondel, A., Gaudreau, P. O., … Zitvogel, L. (2019). Sustained Type I interferon signaling as a mechanism of resistance to PD-1 blockade. *Cell Research*, *29*(10), 846–861. https://doi.org/10.1038/s41422-019-0224-x

Jang, H. S., Shah, N. M., Du, A. Y., Dailey, Z. Z., Pehrsson, E. C., Godoy, P. M., Zhang, D., Li, D., Xing, X., Kim, S., O'Donnell, D., Gordon, J. I., & Wang, T. (2019). Transposable elements drive widespread expression of oncogenes in human cancers. In *Nature Genetics* (Vol. 51, Issue 4, pp. 611–617). Nature Publishing Group. https://doi.org/10.1038/s41588-019-0373-3

Joffre, O., Santolaria, T., Calise, D., Saati, T. Al, Hudrisier, D., Romagnoli, P., & Van Meerwijk, J. P. M. (2008). Prevention of acute and chronic allograft rejection with CD4 +CD25+Foxp3+ regulatory T lymphocytes. *Nature Medicine*, *14*(1), 88–92. https://doi.org/10.1038/nm1688

Jung, S. H., Choi, Y. J., Kim, M. S., Park, H. C., Han, M. R., Hur, S. Y., Lee, A. W., Shin, O. R., Kim, J., Lee, S. H., Hong, D., Song, S. Y., Chung, Y. J., & Lee, S. H. (2020). Distinct genomic profiles of gestational choriocarcinoma, a unique cancer of pregnant tissues. *Experimental and Molecular Medicine*, *52*(12), 2046–2054. https://doi.org/10.1038/s12276-020-00544-0

Kassiotis, G., & Stoye, J. P. (2016). Immune responses to endogenous retroelements: Taking the bad with the good. In *Nature Reviews Immunology* (Vol. 16, Issue 4, pp. 207–219). Nature Publishing Group. https://doi.org/10.1038/nri.2016.27

Kato, H., Takeuchi, O., Sato, S., Yoneyama, M., Yamamoto, M., Matsui, K., Uematsu, S., Jung, A., Kawai, T., Ishii, K. J., Yamaguchi, O., Otsu, K., Tsujimura, T., Koh, C. S., Reis E Sousa, C., Matsuura, Y., Fujita, T., & Akira, S. (2006). Differential roles of MDA5 and RIG-I helicases in the recognition of RNA viruses. *Nature*, *441*(1), 101–105. https://doi.org/10.1038/nature04734

Kaulfuss, M., Mietz, J., Fabri, A., vom Berg, J., Münz, C., & Chijioke, O. (2023). The NK cell checkpoint NKG2A maintains expansion capacity of human NK cells. *Scientific Reports*, *13*(1). https://doi.org/10.1038/s41598-023-37779-6

Kim, D., Langmead, B., & Salzberg, S. L. (2015). HISAT: a fast spliced aligner with low memory requirements. *Nature Methods*, *12*(4), 357–360. https://doi.org/10.1038/nmeth.3317

Kim, H., & Suyama, M. (2023). Genome-wide identification of copy neutral loss of heterozygosity reveals its possible association with spatial positioning of chromosomes. *Human Molecular Genetics*, *32*(7), 1175–1183. https://doi.org/10.1093/hmg/ddac278

Klement, J. D., Paschall, A. V., Redd, P. S., Ibrahim, M. L., Lu, C., Yang, D., Celis, E., Abrams, S. I., Ozato, K., & Liu, K. (2018). An osteopontin/CD44 immune checkpoint controls CD8+ T cell activation and tumor immune evasion. *Journal*

of Clinical Investigation, *128*(12), 5549–5560. https://doi.org/10.1172/JCI123360

Kochan, G., Escors, D., Breckpot, K., & Guerrero-Setas, D. (2013). Role of non-classical MHC class I molecules in cancer immunosuppression. *Oncoimmunology*, *2*(11). https://doi.org/10.4161/ONCI.26491

Köhler, G., & Milstein, C. (1975). Continuous cultures of fused cells secreting antibody of predefined specificity. *Nature*, *256*(5517), 495–497. https://doi.org/10.1038/256495a0

Kohli, K., Pillarisetty, V. G., & Kim, T. S. (2022). Key chemokines direct migration of immune cells in solid tumors. In *Cancer Gene Therapy* (Vol. 29, Issue 1, pp. 10–21). Springer Nature. https://doi.org/10.1038/s41417-021-00303-x

Kosack, L., Wingelhofer, B., Popa, A., Orlova, A., Agerer, B., Vilagos, B., Majek, P., Parapatics, K., Lercher, A., Ringler, A., Klughammer, J., Smyth, M., Khamina, K., Baazim, H., de Araujo, E. D., Rosa, D. A., Park, J., Tin, G., Ahmar, S., … Bergthaler, A. (2019). The ERBB-STAT3 Axis Drives Tasmanian Devil Facial Tumor Disease. *Cancer Cell*, *35*(1), 125-139.e9. https://doi.org/10.1016/j.ccell.2018.11.018

Kovats, S., Main, E. K., Librach, C., Stubblebine, M., Fisher, S. J., & DeMars, R. (1990). A class I antigen, HLA-G, expressed in human trophoblasts. *Science (New York, N.Y.)*, *248*(4952), 220–223. https://doi.org/10.1126/science.2326636

Kupiec-Weglinski, J. W. (2022). Grand Challenges in Organ Transplantation. *Frontiers in Transplantation*, *1*. https://doi.org/10.3389/frtra.2022.897679

Kwon, Y. M., Stammnitz, M. R., Wang, J., Swift, K., Knowles, G. W., Pye, R. J., Kreiss, A., Peck, S., Fox, S., Pemberton, D., Jones, M. E., Hamede, R., & Murchison, E. P. (2018). Tasman-PCR: A genetic diagnostic assay for Tasmanian devil facial tumour diseases. *Royal Society Open Science*, *5*(10). https://doi.org/10.1098/rsos.180870

Landers, J. E., Cassel, S. L., & George, D. L. (1997). Translational enhancement of mdm2 oncogene expression in human tumor cells containing a stabilized wild-type p53 protein. *Cancer Research*, *57*(16), 3562–3568. http://www.ncbi.nlm.nih.gov/pubmed/9270029

Lawson, K. A., Sousa, C. M., Zhang, X., Kim, E., Akthar, R., Caumanns, J. J., Yao, Y., Mikolajewicz, N., Ross, C., Brown, K. R., Zid, A. A., Fan, Z. P., Hui, S., Krall, J. A., Simons, D. M., Slater, C. J., De Jesus, V., Tang, L., Singh, R., … Moffat, J. (2020). Functional genomic landscape of cancer-intrinsic evasion of killing by T cells. *Nature*, *586*(7827), 120–126. https://doi.org/10.1038/s41586-020-2746-2

Lefebvre, S., Moreau, P., Dausset, J., Carosella, E. D., & Paul, P. (1999). Downregulation of HLA Class I Gene Transcription in Choriocarcinoma Cells is Controlled by the Proximal Promoter Element and Can be Reversed by CIITA. In *Placenta* (Vol. 20).

Leisching, G., Cole, V., Ali, A. T., & Baker, B. (2019). OAS1, OAS2 and OAS3 restrict intracellular M. tb replication and enhance cytokine secretion. *International Journal of Infectious Diseases : IJID : Official Publication of the International Society for Infectious Diseases*, *80S*, S77–S84. https://doi.org/10.1016/J.IJID.2019.02.029

Leitner, J., Klauser, C., Pickl, W. F., Stökl, J., Majdic, O., Bardet, A. F., Kreil, D. P., Dong, C., Yamazaki, T., Zlabinger, G., Pfistershammer, K., & Steinberger, P. (2009). B7-H3 is a potent inhibitor of human T-cell activation: No evidence for B7-H3 and TREML2 interaction. *European Journal of Immunology*, *39*(7), 1754–1764. https://doi.org/10.1002/EJI.200839028

Li, G., Zhao, X., Zheng, Z., Zhang, H., Wu, Y., Shen, Y., & Chen, Q. (2024). cGAS-STING pathway mediates activation of dendritic cell sensing of immunogenic tumors. In *Cellular and Molecular Life Sciences* (Vol. 81, Issue 1). Springer Science and Business Media Deutschland GmbH. https://doi.org/10.1007/s00018-024-05191-6

Li, M., He, L., Zhu, J., Zhang, P., & Liang, S. (2022a). Targeting tumor-associated macrophages for cancer treatment. In *Cell and Bioscience* (Vol. 12, Issue 1). BioMed Central Ltd. https://doi.org/10.1186/s13578-022-00823-5

Li, M., He, L., Zhu, J., Zhang, P., & Liang, S. (2022b). Targeting tumor-associated macrophages for cancer treatment. *Cell & Bioscience 2022 12:1*, *12*(1), 1–13. https://doi.org/10.1186/S13578-022-00823-5

Lin, Y. C., Wu, C. H., Chen, P. J., Huang, C. H., Yang, C. K., Dutta, A., Huang, C. T., & Lin, C. Y. (2023). Murine cytotoxic CD4+T cells in the tumor microenvironment are at a hyper-maturation stage of Th1 CD4+T cells sustained by IL-12. *International Immunology*, *35*(8), 387–400. https://doi.org/10.1093/intimm/dxad015

Little, C. C., & Johnson, B. W. (1922). The inheritance of susceptibility to implants of splenic tissue in mice. 1. Japanese waltzing mice, albinos, and their F1 generation hybrids. *Experimental Biology and Medicine*, *19*(4), 163–167. https://doi.org/10.3181/00379727-19-76

Little, C. C., & Tyzzer, E. E. (1916). Further experimental studies on the inheritance of susceptibility to a Transplantable tumor, Carcinoma (J. W. A.) of the Japanese waltzing Mouse. *The Journal of Medical Research*, *33*(3), 393–453. http://www.ncbi.nlm.nih.gov/pubmed/19972275

Liu, C. C., Wang, Y. S., Lin, C. Y., Chuang, T. F., Liao, K. W., Chi, K. H., Chen, M. F., Chiang, H. C., & Chu, R. M. (2008). Transient downregulation of monocyte-

derived dendritic-cell differentiation, function, and survival during tumoral progression and regression in an in vivo canine model of transmissible venereal tumor. *Cancer Immunology, Immunotherapy*, *57*(4), 479–491. https://doi.org/10.1007/s00262-007-0386-0

Lohwasser, S., Kubota, A., Salcedo, M., Lian, R. H., & Takei1, F. (2001). The non-classical MHC class I molecule Qa-1 b inhibits classical MHC class I-restricted cytotoxicity of cytotoxic T lymphocytes. In *International Immunology* (Vol. 13, Issue 3).

Love, M. I., Huber, W., & Anders, S. (2014a). Moderated estimation of fold change and dispersion for RNA-seq data with DESeq2. *Genome Biology*, *15*(12), 550. https://doi.org/10.1186/s13059-014-0550-8

Love, M. I., Huber, W., & Anders, S. (2014b). Moderated estimation of fold change and dispersion for RNA-seq data with DESeq2. *Genome Biology*, *15*(12), 550. https://doi.org/10.1186/s13059-014-0550-8

Luangrath, M. A., Schmidt, M. E., Hartwig, S. M., & Varga, S. M. (2021). Tissue-Resident Memory T Cells in the Lungs Protect against Acute Respiratory Syncytial Virus Infection. *ImmunoHorizons*, *5*(2), 59–69. https://doi.org/10.4049/immunohorizons.2000067

Ma, D., Hirose, T., Lassiter, G., Sasaki, H., Rosales, I., Coe, T. M., Rickert, C. G., Matheson, R., Colvin, R. B., Qin, W., Kan, Y., Layer, J. V., Paragas, V. B., Stiede, K., Hall, K. C., Youd, M. E., Queiroz, L. M., Westlin, W. F., Curtis, M., … Kawai, T. (2022). Kidney transplantation from triple-knockout pigs expressing multiple human proteins in cynomolgus macaques. *American Journal of Transplantation*, *22*(1), 46–57. https://doi.org/10.1111/ajt.16780

Mangla, M., Palo, S., Kanikaram, P., & Kaur, H. (2024). Non-gestational choriocarcinoma: Unraveling the similarities and distinctions from its gestational counterpart. In *International Journal of Gynecological Cancer* (Vol. 34, Issue 6, pp. 926–934). BMJ Publishing Group. https://doi.org/10.1136/ijgc-2023-004906

Mangla, M., Singla, D., Kaur, H., & Sharma, S. (2017). Unusual clinical presentations of choriocarcinoma: A systematic review of case reports. In *Taiwanese Journal of Obstetrics and Gynecology* (Vol. 56, Issue 1, pp. 1–8). Elsevier Ltd. https://doi.org/10.1016/j.tjog.2015.05.011

Martín-Gómez, L., Villalba, A., Carballal, M. J., & Abollo, E. (2013). Identification of Relevant Cancer Related-Genes in the Flat Oyster Ostrea edulis Affected by Disseminated Neoplasia. *Marine Biotechnology*, *15*(2), 159–174. https://doi.org/10.1007/s10126-012-9472-1

Meeth, K., Wang, J. X., Micevic, G., Damsky, W., & Bosenberg, M. W. (2016). The YUMM lines: a series of congenic mouse melanoma cell lines with defined

genetic alterations. *Pigment Cell & Melanoma Research*, *29*(5), 590–597. https://doi.org/10.1111/PCMR.12498

Metzger, M. J., Reinisch, C., Sherry, J., & Goff, S. P. (2015a). Horizontal transmission of clonal cancer cells causes leukemia in soft-shell clams. *Cell*, *161*(2), 255–263. https://doi.org/10.1016/j.cell.2015.02.042

Metzger, M. J., Reinisch, C., Sherry, J., & Goff, S. P. (2015b). Horizontal transmission of clonal cancer cells causes leukemia in soft-shell clams. *Cell*, *161*(2), 255–263. https://doi.org/10.1016/j.cell.2015.02.042

Metzger, M. J., Villalba, A., Carballal, M. J., Iglesias, D., Sherry, J., Reinisch, C., Muttray, A. F., Baldwin, S. A., & Goff, S. P. (2016). Widespread transmission of independent cancer lineages within multiple bivalve species. *Nature*, *534*(7609), 705–709. https://doi.org/10.1038/nature18599

Michnowska, A., Hart, S. F. M., Smolarz, K., Hallmann, A., & Metzger, M. J. (2022). Horizontal transmission of disseminated neoplasia in the widespread clam Macoma balthica from the Southern Baltic Sea. *Molecular Ecology*, *31*(11), 3128–3136. https://doi.org/10.1111/mec.16464

Mita, Y., Kimura, M. Y., Hayashizaki, K., Koyama-Nasu, R., Ito, T., Motohashi, S., Okamoto, Y., & Nakayama, T. (2018). Crucial role of CD69 in anti-tumor immunity through regulating the exhaustion of tumor-infiltrating T cells. *International Immunology*, *30*(12), 559–567. https://doi.org/10.1093/intimm/dxy050

Mitchell, D., Chintala, S., & Dey, M. (2018). Plasmacytoid dendritic cell in immunity and cancer. *Journal of Neuroimmunology*, *322*, 63–73. https://doi.org/10.1016/J.JNEUROIM.2018.06.012

Mitsdoerffer, M., Schreiner, B., Kieseier, B. C., Neuhaus, O., Dichgans, J., Hartung, H. P., Weller, M., & Wiendl, H. (2005). Monocyte-derived HLA-G acts as a strong inhibitor of autologous CD4 T cell activation and is upregulated by interferon-β in vitro and in vivo: Rationale for the therapy of multiple sclerosis. *Journal of Neuroimmunology*, *159*(1–2), 155–164. https://doi.org/10.1016/j.jneuroim.2004.09.016

Miyamae, J., Okano, M., Katakura, F., Kulski, J. K., Moritomo, T., & Shiina, T. (2023). Large-Scale Polymorphism Analysis of Dog Leukocyte Antigen Class I and Class II Genes (DLA-88, DLA-12/88L and DLA-DRB1) and Comparison of the Haplotype Diversity between Breeds in Japan. *Cells*, *12*(5). https://doi.org/10.3390/cells12050809

Montecucco, A., Zanetta, F., & Biamonti, G. (2015). Molecular mechanisms of etoposide. In *EXCLI Journal* (Vol. 14, pp. 95–108). Leibniz Research Centre for Working Environment and Human Factors. https://doi.org/10.17179/excli2014-561

Moreno, B. H., Zaretsky, J. M., Garcia-Diaz, A., Tsoi, J., Parisi, G., Robert, L., Meeth, K., Ndoye, A., Bosenberg, M., Weeraratna, A. T., Graeber, T. G., Comin-Anduix, B., Hu-Lieskovan, S., & Ribas, A. (2016). Response to programmed cell death-1 blockade in a murine melanoma syngeneic model requires costimulation, CD4, and CD8 T cells. *Cancer Immunology Research*, *4*(10), 845–857. https://doi.org/10.1158/2326-6066.CIR-16-0060

Murchison, E. P. (2008). Clonally transmissible cancers in dogs and Tasmanian devils. In *Oncogene* (Vol. 27, pp. S19–S30). https://doi.org/10.1038/onc.2009.350

Murchison, E. P., Schulz-Trieglaff, O. B., Ning, Z., Alexandrov, L. B., Bauer, M. J., Fu, B., Hims, M., Ding, Z., Ivakhno, S., Stewart, C., Ng, B. L., Wong, W., Aken, B., White, S., Alsop, A., Becq, J., Bignell, G. R., Cheetham, R. K., Cheng, W., … Stratton, M. R. (2012). Genome sequencing and analysis of the Tasmanian devil and its transmissible cancer. *Cell*, *148*(4), 780–791. https://doi.org/10.1016/j.cell.2011.11.065

Murchison, E. P., Wedge, D. C., Alexandrov, L. B., Fu, B., Martincorena, I., Ning, Z., Tubio, J. M. C., Werner, E. I., Allen, J., De Nardi, A. B., Donelan, E. M., Marino, G., Fassati, A., Campbell, P. J., Yang, F., Burt, A., Weiss, R. A., & Stratton, M. R. (2014). Transmissible dog cancer genome reveals the origin and history of an ancient cell lineage. *Science*, *343*(6169), 437–440. https://doi.org/10.1126/science.1247167

Murgia, C., Pritchard, J. K., Kim, S. Y., Fassati, A., & Weiss, R. A. (2006). Clonal origin and evolution of a transmissible cancer. *Cell*, *126*(3), 477–487. https://doi.org/10.1016/J.CELL.2006.05.051

Nasr, A. M. A., Ahmed, Y. A. M., Gafar, A. A. M., Ahmed, S. A., Barri, B. khalid A., TalibMeshref, E., Ahamed, E. A. M., & Alanazi, W. A. (2022). Prevalence and Risk Factors of Choriocarcinoma in Saudi Arabia: A Systematic Review. *Clinical Cancer Investigation Journal*, *11*(6), 4–8. https://doi.org/10.51847/nczqkf18st

Ness, S., Lin, S., & Gordon, J. R. (2021a). Regulatory Dendritic Cells, T Cell Tolerance, and Dendritic Cell Therapy for Immunologic Disease. *Frontiers in Immunology*, *12*. https://doi.org/10.3389/FIMMU.2021.633436

Ness, S., Lin, S., & Gordon, J. R. (2021b). Regulatory Dendritic Cells, T Cell Tolerance, and Dendritic Cell Therapy for Immunologic Disease. In *Frontiers in Immunology* (Vol. 12). Frontiers Media S.A. https://doi.org/10.3389/fimmu.2021.633436

Nunès, J. A., & Olive, D. (2021). CD28 costimulation promotes an antitumor CD8+ T cell response in myeloid antigen-presenting cell niches. *Cellular & Molecular Immunology 2021 19:2*, *19*(2), 147–149. https://doi.org/10.1038/s41423-021-00818-1

Okada, S., Vaeteewoottacharn, K., & Kariya, R. (2019). Application of highly immunocompromised mice for the establishment of patient-derived xenograft (PDX) models. In *Cells* (Vol. 8, Issue 8). MDPI. https://doi.org/10.3390/cells8080889

Ottina, E., Levy, P., Eksmond, U., Merkenschlager, J., Young, G. R., Roels, J., Stoye, J. P., Tüting, T., Calado, D. P., & Kassiotis, G. (2018). Restoration of endogenous retrovirus infectivity impacts mouse cancer models. *Cancer Immunology Research*, *6*(11), 1292–1300. https://doi.org/10.1158/2326-6066.CIR-18-0038

Ozturk, M., Berkowitz, R., Goldstein, D., Bellet, D., & Wands, J. R. (1988). Differential production of human chorionic gonadotropin and free subunits in gestational trophoblastic disease. *American Journal of Obstetrics and Gynecology*, *158*(1), 193–198. https://doi.org/10.1016/0002-9378(88)90809-5

Padariya, M., Sznarkowska, A., Kote, S., Gómez-Herranz, M., Mikac, S., Pilch, M., Alfaro, J., Fahraeus, R., Hupp, T., & Kalathiya, U. (2021). Functional interfaces, biological pathways, and regulations of interferon-related dna damage resistance signature (Irds) genes. In *Biomolecules* (Vol. 11, Issue 5). MDPI AG. https://doi.org/10.3390/biom11050622

Pai, C. C., Kuo, T. F., Mao, S. J. T., Chuang, T. F., Lin, C. S., & Chu, R. M. (2011). Immunopathogenic behaviors of canine transmissible venereal tumor in dogs following an immunotherapy using dendritic/tumor cell hybrid. *Veterinary Immunology and Immunopathology*, *139*(2–4), 187–199. https://doi.org/10.1016/j.vetimm.2010.10.013

Park, M. Y., Kim, H. S., Lee, H. Y., Zabel, B. A., & Bae, Y. S. (2020). Novel CD11b+Gr-1+Sca-1+ myeloid cells drive mortality in bacterial infection. *Science Advances*, *6*(4). https://doi.org/10.1126/SCIADV.AAX8820/SUPPL_FILE/AAX8820_SM.PDF

Park, S. L., Gebhardt, T., & Mackay, L. K. (2019). Tissue-Resident Memory T Cells in Cancer Immunosurveillance. In *Trends in Immunology* (Vol. 40, Issue 8, pp. 735–747). Elsevier Ltd. https://doi.org/10.1016/j.it.2019.06.002

Patchett, A. L., Darby, J. M., Tovar, C., Lyons, A. B., & Woods, G. M. (2016). The Immunomodulatory Small Molecule Imiquimod Induces Apoptosis in Devil Facial Tumour Cell Lines. *PLoS ONE*, *11*(12). https://doi.org/10.1371/journal.pone.0168068

Patchett, A. L., Tovar, C., Blackburn, N. B., Woods, G. M., & Lyons, A. B. (2021). Mesenchymal plasticity of devil facial tumour cells during in vivo vaccine and immunotherapy trials. *Immunology and Cell Biology*, *99*(7), 711–723. https://doi.org/10.1111/imcb.12451

Patchett, A. L., Wilson, R., Charlesworth, J. C., Corcoran, L. M., Papenfuss, A. T., Lyons, B. A., Woods, G. M., & Tovar, C. (2018). *Transcriptome and proteome*

profiling reveals stress-induced expression signatures of imiquimod-treated Tasmanian devil facial tumor disease (DFTD) cells. www.oncotarget.com

Pauken, K. E., & Wherry, E. J. (2015). Overcoming T cell exhaustion in infection and cancer. In *Trends in Immunology* (Vol. 36, Issue 4, pp. 265–276). Elsevier Ltd. https://doi.org/10.1016/j.it.2015.02.008

Perez-Lanzon, M., Maiuri, M. C., Lopez-Otin, C., & Kroemer, G. (2024). Preclinical models of breast cancer: B6BC, a transplantable hormone receptor-positive C57BL/6 mouse cell line. *Genes and Immunity*. https://doi.org/10.1038/s41435-023-00241-8

Pishesha, N., Harmand, T. J., & Ploegh, H. L. (2022). A guide to antigen processing and presentation. In *Nature Reviews Immunology* (Vol. 22, Issue 12, pp. 751–764). Nature Research. https://doi.org/10.1038/s41577-022-00707-2

Podestà, M. A., Cucchiari, D., & Ponticelli, C. (2015a). The diverging roles of dendritic cells in kidney allotransplantation. In *Transplantation Reviews* (Vol. 29, Issue 3, pp. 114–120). W.B. Saunders. https://doi.org/10.1016/j.trre.2015.04.001

Podestà, M. A., Cucchiari, D., & Ponticelli, C. (2015b). The diverging roles of dendritic cells in kidney allotransplantation. *Transplantation Reviews*, *29*(3), 114–120. https://doi.org/10.1016/J.TRRE.2015.04.001

Podestà, M. A., Cucchiari, D., & Ponticelli, C. (2015c). The diverging roles of dendritic cells in kidney allotransplantation. In *Transplantation Reviews* (Vol. 29, Issue 3, pp. 114–120). W.B. Saunders. https://doi.org/10.1016/j.trre.2015.04.001

Pye, R. J., Pemberton, D., Tovar, C., Tubio, J. M. C., Dun, K. A., Fox, S., Darby, J., Hayes, D., Knowles, G. W., Kreiss, A., Siddle, H. V. T., Swift, K., Lyons, A. B., Murchison, E. P., & Woods, G. M. (2016). A second transmissible cancer in Tasmanian devils. *Proceedings of the National Academy of Sciences of the United States of America*, *113*(2), 374–379. https://doi.org/10.1073/pnas.1519691113

Pyecroft, S. B., Pearse, A. M., Loh, R., Swift, K., Belov, K., Fox, N., Noonan, E., Hayes, D., Hyatt, A., Wang, L., Boyle, D., Church, J., Middleton, D., & Moore, R. (2007). Towards a case definition for devil facial tumour disease: What is it? *EcoHealth*, *4*(3), 346–351. https://doi.org/10.1007/s10393-007-0126-0

Qiao, T., Yang, W., He, X., Song, P., Chen, X., Liu, R., Xiao, J., Yang, X., Li, M., Gao, Y., Chen, G., Lu, Y., Zhang, J., Leng, J., & Ren, H. (2023). Dynamic differentiation of F4/80+ tumor-associated macrophage and its role in tumor vascularization in a syngeneic mouse model of colorectal liver metastasis. *Cell Death and Disease*, *14*(2). https://doi.org/10.1038/s41419-023-05626-1

Quinlan, A. R., & Hall, I. M. (2010). BEDTools: a flexible suite of utilities for comparing genomic features. *Bioinformatics*, *26*(6), 841–842. https://doi.org/10.1093/bioinformatics/btq033

Quintana, E., Shackleton, M., Sabel, M. S., Fullen, D. R., Johnson, T. M., & Morrison, S. J. (2008). Efficient tumour formation by single human melanoma cells. *Nature 2008 456:7222*, *456*(7222), 593–598. https://doi.org/10.1038/nature07567

Raso, A., Mascelli, S., Nozza, P., Biassoni, R., Negri, F., Garaventa, A., Tarantino, V., Garrè, M. L., Cama, A., & Capra, V. (2010). *Detection of Transplacental Melanoma Metastasis Using Quantitative PCR*. www.moleculardpathology.com

Redman, C. W. G. (1990). The fetal allograft. *Fetal and Maternal Medicine Review*, *2*(1), 21–43. https://doi.org/10.1017/S0965539500000243

Reeves, E., & James, E. (2017a). Antigen processing and immune regulation in the response to tumours. *Immunology*, *150*(1), 16–24. https://doi.org/10.1111/IMM.12675

Reeves, E., & James, E. (2017b). Antigen processing and immune regulation in the response to tumours. *Immunology*, *150*(1), 16–24. https://doi.org/10.1111/IMM.12675

Rehwinkel, J., & Gack, M. U. (2020a). RIG-I-like receptors: their regulation and roles in RNA sensing. In *Nature Reviews Immunology* (Vol. 20, Issue 9, pp. 537–551). Nature Research. https://doi.org/10.1038/s41577-020-0288-3

Rehwinkel, J., & Gack, M. U. (2020b). RIG-I-like receptors: their regulation and roles in RNA sensing. In *Nature Reviews Immunology* (Vol. 20, Issue 9, pp. 537–551). Nature Research. https://doi.org/10.1038/s41577-020-0288-3

Reticker-Flynn, N. E., Zhang, W., Belk, J. A., Basto, P. A., Escalante, N. K., Pilarowski, G. O. W., Bejnood, A., Martins, M. M., Kenkel, J. A., Linde, I. L., Bagchi, S., Yuan, R., Chang, S., Spitzer, M. H., Carmi, Y., Cheng, J., Tolentino, L. L., Choi, O., Wu, N., … Engleman, E. G. (2022a). Lymph node colonization induces tumor-immune tolerance to promote distant metastasis. *Cell*, *185*(11), 1924-1942.e23. https://doi.org/10.1016/J.CELL.2022.04.019

Reticker-Flynn, N. E., Zhang, W., Belk, J. A., Basto, P. A., Escalante, N. K., Pilarowski, G. O. W., Bejnood, A., Martins, M. M., Kenkel, J. A., Linde, I. L., Bagchi, S., Yuan, R., Chang, S., Spitzer, M. H., Carmi, Y., Cheng, J., Tolentino, L. L., Choi, O., Wu, N., … Engleman, E. G. (2022b). Lymph node colonization induces tumor-immune tolerance to promote distant metastasis. *Cell*, *185*(11), 1924-1942.e23. https://doi.org/10.1016/j.cell.2022.04.019

Robinson, J., Malik, A., Parham, P., Bodmer, J. G., & Marsh, S. G. E. (2000). IMGT/HLA Database - A sequence database for the human major

histocompatibility complex. In *Tissue Antigens* (Vol. 55, Issue 3, pp. 280–287). https://doi.org/10.1034/j.1399-0039.2000.550314.x

Roitt, I., Roth, D., Brostoff, J., & Male, D. (2006). *IMMUNOLOGY*.

Savage, J., Adams, E., Veras, E., Murphy, K. M., & Ronnett, B. M. (2017). *Choriocarcinoma in Women Analysis of a Case Series With Genotyping*. www.ajsp.com

Schoggins, J. W., & Rice, C. M. (2011). Interferon-stimulated genes and their antiviral effector functions. In *Current Opinion in Virology* (Vol. 1, Issue 6, pp. 519–525). Elsevier B.V. https://doi.org/10.1016/j.coviro.2011.10.008

Schreiber, R. D., Old, L. J., & Smyth, M. J. (2011). Cancer immunoediting: integrating immunity's roles in cancer suppression and promotion. *Science (New York, N.Y.)*, *331*(6024), 1565–1570. https://doi.org/10.1126/SCIENCE.1203486

Schumann, J., Stanko, K., Schliesser, U., Appelt, C., & Sawitzki, B. (2015). Differences in CD44 surface expression levels and function discriminates IL-17 and IFN-γ producing helper T cells. *PLoS ONE*, *10*(7). https://doi.org/10.1371/journal.pone.0132479

Seliger, B., Ruiz-Cabello, F., & Garrido, F. (2008). Chapter 7 IFN Inducibility of Major Histocompatibility Antigens in Tumors. In *Advances in Cancer Research* (Vol. 101, pp. 249–276). https://doi.org/10.1016/S0065-230X(08)00407-7

Senft, A. D., & Macfarlan, T. S. (2021). Transposable elements shape the evolution of mammalian development. In *Nature Reviews Genetics* (Vol. 22, Issue 11, pp. 691–711). Nature Research. https://doi.org/10.1038/s41576-021-00385-1

Sharma, P., & Allison, J. P. (2015). The future of immune checkpoint therapy. *Science (New York, N.Y.)*, *348*(6230), 56–61. https://doi.org/10.1126/SCIENCE.AAA8172

Shekhar Gogna; Karan Ramakrishna; Savio John. (2024). *Posttransplantation Cancer*. StatPearls. https://www.ncbi.nlm.nih.gov/books/NBK537256/

Sheng, W., LaFleur, M. W., Nguyen, T. H., Chen, S., Chakravarthy, A., Conway, J. R., Li, Y., Chen, H., Yang, H., Hsu, P. H., Van Allen, E. M., Freeman, G. J., De Carvalho, D. D., He, H. H., Sharpe, A. H., & Shi, Y. (2018). LSD1 Ablation Stimulates Anti-tumor Immunity and Enables Checkpoint Blockade. *Cell*, *174*(3), 549-563.e19. https://doi.org/10.1016/J.CELL.2018.05.052

Shklovskaya, E., & Rizos, H. (2021). MHC Class I Deficiency in Solid Tumors and Therapeutic Strategies to Overcome It. *International Journal of Molecular Sciences 2021, Vol. 22, Page 6741*, *22*(13), 6741. https://doi.org/10.3390/IJMS22136741

Siddle, H. V., & Kaufman, J. (2013). A tale of two tumours: Comparison of the immune escape strategies of contagious cancers. In *Molecular Immunology* (Vol. 55, Issue 2, pp. 190–193). https://doi.org/10.1016/j.molimm.2012.10.017

Siddle, H. V., & Kaufman, J. (2015). Immunology of naturally transmissible tumours. *Immunology*, *144*(1), 11–20. https://doi.org/10.1111/IMM.12377

Siddle, H. V., Kreiss, A., Tovar, C., Yuen, C. K., Cheng, Y., Belov, K., Swift, K., Pearse, A. M., Hamede, R., Jones, M. E., Skjødt, K., Woods, G. M., & Kaufman, J. (2013). Reversible epigenetic down-regulation of MHC molecules by devil facial tumour disease illustrates immune escape by a contagious cancer. *Proceedings of the National Academy of Sciences of the United States of America*, *110*(13), 5103–5108. https://doi.org/10.1073/pnas.1219920110

Sigmon, J. S., Blanchard, M. W., Baric, R. S., Bell, T. A., Brennan, J., Brockmann, G. A., Wesley Burks, A., Mauro Calabrese, J., Caron, K. M., Cheney, R. E., Ciavatta, D., Conlon, F., Darr, D. B., Faber, J., Franklin, C., Gershon, T. R., Gralinski, L., Gu, B., Gaines, C. H., … Manuel de Villena, F. P. (2020). Content and performance of the MiniMUGA genotyping array: A new tool to improve rigor and reproducibility in mouse research. *Genetics*, *216*(4), 905–930. https://doi.org/10.1534/genetics.120.303596

Silver, L. M. (1995). *Mouse Genetics* Concepts and Applications. Oxford University PressNew York, NY. https://doi.org/10.1093/oso/9780195075540.001.0001

Skazina, M., Odintsova, N., Maiorova, M., Frolova, L., Dolganova, I., Regel, K., & Strelkov, P. (2023). Two lineages of bivalve transmissible neoplasia affect the blue mussel Mytilus trossulus Gould in the subarctic Sea of Okhotsk. *Current Zoology*, *69*(1), 91–102. https://doi.org/10.1093/cz/zoac012

Skazina, M., Odintsova, N., Maiorova, M., Ivanova, A., Väinölä, R., & Strelkov, P. (2021a). First description of a widespread Mytilus trossulus-derived bivalve transmissible cancer lineage in M. trossulus itself. *Scientific Reports*, *11*(1). https://doi.org/10.1038/s41598-021-85098-5

Skazina, M., Odintsova, N., Maiorova, M., Ivanova, A., Väinölä, R., & Strelkov, P. (2021b). First description of a widespread Mytilus trossulus-derived bivalve transmissible cancer lineage in M. trossulus itself. *Scientific Reports*, *11*(1). https://doi.org/10.1038/s41598-021-85098-5

Skazina, M., Ponomartsev, N., Maiorova, M., Khaitov, V., Marchenko, J., Lentsman, N., Odintsova, N., & Strelkov, P. (2023a). Genetic features of bivalve transmissible neoplasia in blue mussels from the Kola Bay (Barents Sea) suggest a recent trans-Arctic migration of the cancer lineages. *Molecular Ecology*, *32*(21), 5724–5741. https://doi.org/10.1111/mec.17157

Skazina, M., Ponomartsev, N., Maiorova, M., Khaitov, V., Marchenko, J., Lentsman, N., Odintsova, N., & Strelkov, P. (2023b). Genetic features of bivalve transmissible neoplasia in blue mussels from the Kola Bay (Barents

Sea) suggest a recent trans-Arctic migration of the cancer lineages. *Molecular Ecology*, *32*(21), 5724–5741. https://doi.org/10.1111/mec.17157

Smith, H. O., Qualls, C. R., Prairie, B. A., Padilla, L. A., Rayburn, W. F., & Key, C. R. (2003). Trends in gestational choriocarcinoma: A 27-year perspective. *Obstetrics and Gynecology*, *102*(5), 978–987. https://doi.org/10.1016/s0029-7844(03)00669-0

Soboloff, J., & Kappes, D. J. (2018). *Signaling Mechanisms Regulating T Cell Diversity and Function*. https://doi.org/10.1201/9781315371689

Stammnitz, M. R., Coorens, T. H. H., Gori, K. C., Hayes, D., Fu, B., Wang, J., Martin-Herranz, D. E., Alexandrov, L. B., Baez-Ortega, A., Barthorpe, S., Beck, A., Giordano, F., Knowles, G. W., Kwon, Y. M., Hall, G., Price, S., Pye, R. J., Tubio, J. M. C., Siddle, H. V. T., … Murchison, E. P. (2018). The Origins and Vulnerabilities of Two Transmissible Cancers in Tasmanian Devils. *Cancer Cell*, *33*(4), 607-619.e15. https://doi.org/10.1016/j.ccell.2018.03.013

Stammnitz, M. R., Gori, K., Kwon, Y. M., Harry, E., Martin, F. J., Billis, K., Cheng, Y., Baez-Ortega, A., Chow, W., Comte, S., Eggertsson, H., Fox, S., Hamede, R., Jones, M., Lazenby, B., Peck, S., Pye, R., Quail, M. A., Swift, K., … Murchison, E. P. (2023). The evolution of two transmissible cancers in Tasmanian devils. *Science*, *380*(6642), 283–293. https://doi.org/10.1126/science.abq6453

Stemcell Technologies. (2013). マウス脾臓のリンパ球分画. *Stemcell Technologies*, *5*, 13485. http://www.stemcell.com/~/media/Technical Resources/1/D/F/8/4/WA010CSMouseFreqWEB.pdf?la=en

Stiewe, T., & Pu, B. M. (2002). Role of p73 in malignancy: tumor suppressor or oncogene? *Cell Death and Differentiation*, *9*, 237–245. https://doi.org/10.1038/sj/cdd/4400995

Strakova, A., & Murchison, E. P. (2014). The changing global distribution and prevalence of canine transmissible venereal tumour. *BMC Veterinary Research*, *10*(1). https://doi.org/10.1186/s12917-014-0168-9

Strong, L. C. (1926a). A genetic study of the growth of a transplantable tumor (adenocarcinoma, dBrB). *Journal of Experimental Zoology*, *45*(1), 231–253. https://doi.org/10.1002/jez.1400450107

Strong, L. C. (1926b). ON THE OCCURRENCE OF MUTATIONS WITHIN TRANSPLANTABLE NEOPLASMS. *Genetics*, *11*(3), 294–303. https://doi.org/10.1093/GENETICS/11.3.294

Subramanian, A., Tamayo, P., Mootha, V. K., Mukherjee, S., Ebert, B. L., Gillette, M. A., Paulovich, A., Pomeroy, S. L., Golub, T. R., Lander, E. S., & Mesirov, J. P. (2005). Gene set enrichment analysis: A knowledge-based approach for interpreting genome-wide expression profiles. *Proceedings of the National*

Academy of Sciences of the United States of America, *102*(43), 15545–15550. https://doi.org/10.1073/PNAS.0506580102/SUPPL_FILE/06580FIG7.JPG

Swaraj, S., & Tripathi, S. (2024a). Interference without interferon: interferon-independent induction of interferon-stimulated genes and its role in cellular innate immunity. In *mBio* (Vol. 15, Issue 10, p. e0258224). https://doi.org/10.1128/mbio.02582-24

Swaraj, S., & Tripathi, S. (2024b). Interference without interferon: interferon-independent induction of interferon-stimulated genes and its role in cellular innate immunity. In *mBio* (Vol. 15, Issue 10, p. e0258224). https://doi.org/10.1128/mbio.02582-24

Swets, M., König, M. H., Zaalberg, A., Dekker-Ensink, N. G., Gelderblom, H., van de Velde, C. J. H., van den Elsen, P. J., & Kuppen, P. J. K. (2016). HLA-G and classical HLA class I expression in primary colorectal cancer and associated liver metastases. *Human Immunology*, *77*(9), 773–779. https://doi.org/10.1016/j.humimm.2016.03.001

Sykes, M., & Sachs, D. H. (2022). Progress in xenotransplantation: overcoming immune barriers. In *Nature Reviews Nephrology* (Vol. 18, Issue 12, pp. 745–761). Nature Research. https://doi.org/10.1038/s41581-022-00624-6

Taketo, M., Schroeder, A. C., Mobraaten, L. E., Gunning, K. B., Hanten, G., Fox, R. R., Roderick, T. H., Stewart$, C. L., Ii, F. L., Hansen, C. T., & Overbeek, P. A. (1991). FVB/N: An inbred mouse strain preferable for transgenic analyses (ES ceils/blastocyst chimera/germ-line tanission). In *Proc. Natl. Acad. Sci. USA* (Vol. 88). https://www.pnas.org

Tay, R. E., Richardson, E. K., & Toh, H. C. (2021). Revisiting the role of CD4+ T cells in cancer immunotherapy—new insights into old paradigms. *Cancer Gene Therapy*, *28*(1–2), 5–17. https://doi.org/10.1038/s41417-020-0183-x

Thommen, D. S., & Schumacher, T. N. (2018). T Cell Dysfunction in Cancer. *Cancer Cell*, *33*(4), 547–562. https://doi.org/10.1016/J.CCELL.2018.03.012

Thoresen, D., Wang, W., Galls, D., Guo, R., Xu, L., & Pyle, A. M. (2021). The molecular mechanism of RIG-I activation and signaling. In *Immunological Reviews* (Vol. 304, Issue 1, pp. 154–168). John Wiley and Sons Inc. https://doi.org/10.1111/imr.13022

Tian, Q., Zhang, Z., Tan, L., Yang, F., Xu, Y., Guo, Y., Wei, D., Wu, C., Cao, P., Ji, J., Wang, W., Xie, X., & Zhao, Y. (2022). Skin and heart allograft rejection solely by long-lived alloreactive T RM cells in skin of severe combined immunodeficient mice. In *Sci. Adv* (Vol. 8). https://www.science.org

Tietscher, S., Wagner, J., Anzeneder, T., Langwieder, C., Rees, M., Sobottka, B., de Souza, N., & Bodenmiller, B. (2023). A comprehensive single-cell map of T

cell exhaustion-associated immune environments in human breast cancer. *Nature Communications*, *14*(1). https://doi.org/10.1038/s41467-022-35238-w

Tomasello, E., Yessaad, N., Gregoire, E., Hudspeth, K., Luci, C., Mavilio, D., Hardwigsen, J., & Vivier, E. (2012). Mapping of NKp46+ cells in healthy human lymphoid and non-lymphoid tissues. *Frontiers in Immunology*, *3*(NOV), 344. https://doi.org/10.3389/FIMMU.2012.00344/ABSTRACT

Topham, D. J., & Reilly, E. C. (2018). Tissue-resident memory CD8+ T cells: From phenotype to function. In *Frontiers in Immunology* (Vol. 9, Issue MAR). Frontiers Media S.A. https://doi.org/10.3389/fimmu.2018.00515

Torrey, C. E., Wall, H. G., Campbell, J. A., Kwanyuen, P., Hoivik, D. J., Miller, R. T., Allen, J. S., Jayo, M. J., Selinger, K., & Santostefano, M. J. (2005). Evaluation of the carcinogenic potential of clofibrate in the FVB/Tg.AC mouse after dermal application - Part II. *International Journal of Toxicology*, *24*(SUPPL. 5), 327–339. https://doi.org/10.1080/10915810500208199

Tovar, C., Obendorf, D., Murchison, E. P., Papenfuss, A. T., Kreiss, A., & Woods, G. M. (2011). Tumor-specific diagnostic marker for transmissible facial tumors of tasmanian devils: Immunohistochemistry studies. *Veterinary Pathology*, *48*(6), 1195–1203. https://doi.org/10.1177/0300985811400447

Tovar, C., Pye, R. J., Kreiss, A., Cheng, Y., Brown, G. K., Darby, J., Malley, R. C., Siddle, H. V. T., Skjødt, K., Kaufman, J., Silva, A., Baz Morelli, A., Papenfuss, A. T., Corcoran, L. M., Murphy, J. M., Pearse, M. J., Belov, K., Lyons, A. B., & Woods, G. M. (2017). Regression of devil facial tumour disease following immunotherapy in immunised Tasmanian devils. *Scientific Reports*, *7*. https://doi.org/10.1038/srep43827

Tsuji, K., Ojima, M., Otabe, K., Horie, M., Koga, H., Sekiya, I., & Muneta, T. (2017). Effects of different cell-detaching methods on the viability and cell surface antigen expression of synovial mesenchymal stem cells. *Cell Transplantation*, *26*(6), 1089–1102. https://doi.org/10.3727/096368917X694831/ASSET/IMAGES/LARGE/10.3727_096368917X694831-FIG2.JPEG

Turkowski, K., Brandenburg, S., Mueller, A., Kremenetskaia, I., Bungert, A. D., Blank, A., Felsenstein, M., & Vajkoczy, P. (2018). VEGF as a modulator of the innate immune response in glioblastoma. *GLIA*, *66*(1), 161–174. https://doi.org/10.1002/glia.23234

UNOS. (2025, January 6). *UNOS*. Https://Unos.Org/Data/.

Uzman, A., Lodish, H., Berk, A., Zipursky, L., & Baltimore, D. (2000). Molecular Cell Biology (4th edition) New York, NY, 2000, ISBN 0-7167-3136-3. *Biochemistry and Molecular Biology Education*, *29*(3), Section 1.2The Molecules of Life. https://doi.org/10.1016/S1470-8175(01)00023-6

Vaitaitis, G. M., & Wagner, D. H. (2012). Galectin-9 Controls CD40 Signaling through a Tim-3 Independent Mechanism and Redirects the Cytokine Profile of Pathogenic T Cells in Autoimmunity. *PLoS ONE*, *7*(6), e38708. https://doi.org/10.1371/journal.pone.0038708

Valiente, M., Andrés-Pons, A., Gomar, B., Torres, J., Gil, A., Tapparel, C., Antonarakis, S. E., & Pulido, R. (2005). Binding of PTEN to specific PDZ domains contributes to PTEN protein stability and phosphorylation by microtubule-associated serine/threonine kinases. *Journal of Biological Chemistry*, *280*(32), 28936–28943. https://doi.org/10.1074/jbc.M504761200

Valujskikh, A., Fedoseyeva, E., Benichou, G., & Heeger, P. S. (2002). Development of autoimmunity after skin graft rejection via an indirect alloresponse1. *Transplantation*, *73*(7), 1130–1137. https://doi.org/10.1097/00007890-200204150-00021

van Breeschoten, J., Wouters, M. W. J. M., Hilarius, D. L., Haanen, J. B., Blank, C. U., Aarts, M. J. B., van den Berkmortel, F. W. P. J., de Groot, J. W. B., Hospers, G. A. P., Kapiteijn, E., Piersma, D., van Rijn, R. S., Suijkerbuijk, K. P. M., Blokx, W. A. M., Tije, B. J. J. ten, Veldt, A. A. M. van der, Vreugdenhil, A., Boers-Sonderen, M. J., & van den Eertwegh, A. J. M. (2021). First-line BRAF/MEK inhibitors versus anti-PD-1 monotherapy in BRAFV600-mutant advanced melanoma patients: a propensity-matched survival analysis. *British Journal of Cancer*, *124*(7), 1222–1230. https://doi.org/10.1038/s41416-020-01229-1

Vance, R. E., Kraft, J. R., Altman, J. D., Jensen, P. E., & Raulet, D. H. (1998). Mouse CD94/NKG2A Is a Natural Killer Cell Receptor for the Nonclassical Major Histocompatibility Complex (MHC) Class I Molecule Qa-1 b. In *J. Exp. Med* (Vol. 188, Issue 10). http://www.jem.org

Veras, E., Kurman, R. J., Wang, T. L., & Shih, I. M. (2017). PD-L1 expression in human placentas and gestational trophoblastic diseases. *International Journal of Gynecological Pathology*, *36*(2), 146–153. https://doi.org/10.1097/PGP.0000000000000305

Vesely, M. D., Kershaw, M. H., Schreiber, R. D., & Smyth, M. J. (2011). Natural innate and adaptive immunity to cancer. *Annual Review of Immunology*, *29*, 235–271. https://doi.org/10.1146/ANNUREV-IMMUNOL-031210-101324

Vinay, D. S., Ryan, E. P., Pawelec, G., Talib, W. H., Stagg, J., Elkord, E., Lichtor, T., Decker, W. K., Whelan, R. L., Kumara, H. M. C. S., Signori, E., Honoki, K., Georgakilas, A. G., Amin, A., Helferich, W. G., Boosani, C. S., Guha, G., Ciriolo, M. R., Chen, S., … Kwon, B. S. (2015). Immune evasion in cancer: Mechanistic basis and therapeutic strategies. In *Seminars in Cancer Biology* (Vol. 35, pp. S185–S198). Academic Press. https://doi.org/10.1016/j.semcancer.2015.03.004

Vincent, J., Adura, C., Gao, P., Luz, A., Lama, L., Asano, Y., Okamoto, R., Imaeda, T., Aida, J., Rothamel, K., Gogakos, T., Steinberg, J., Reasoner, S., Aso, K., Tuschl, T., Patel, D. J., Glickman, J. F., & Ascano, M. (2017). Small molecule inhibition of cGAS reduces interferon expression in primary macrophages from autoimmune mice. *Nature Communications*, *8*(1). https://doi.org/10.1038/s41467-017-00833-9

Voelcker, G. (2020). The mechanism of action of cyclophosphamide and its consequences for the development of a new generation of oxazaphosphorine cytostatics. In *Scientia Pharmaceutica* (Vol. 88, Issue 4, pp. 1–13). MDPI AG. https://doi.org/10.3390/scipharm88040042

Wahaibi, F. Al, Gowri, V., Kharusi, S. Al, & Rawahi, T. Al. (2020). Prevalence of gestational choriocarcinoma in a parous population in ten years. *International Journal of Reproduction, Contraception, Obstetrics and Gynecology*, *9*(9), 3537. https://doi.org/10.18203/2320-1770.ijrcog20203824

Walsh, P. T., Taylor, D. K., & Turka, L. A. (2004). Tregs and transplantation tolerance. *Journal of Clinical Investigation*, *114*(10), 1398–1403. https://doi.org/10.1172/JCI23238

Walzer, T., Bléry, M., Chaix, J., Fuseri, N., Chasson, L., Robbins, S. H., Jaeger, S., André, P., Gauthier, L., Daniel, L., Chemin, K., Morel, Y., Dalod, M., Imbert, J., Pierres, M., Moretta, A., Romagné, F., & Vivier, E. (2007). Identification, activation, and selective in vivo ablation of mouse NK cells via NKp46. *Proceedings of the National Academy of Sciences of the United States of America*, *104*(9), 3384–3389. https://doi.org/10.1073/PNAS.0609692104

Wang, J., Perry, C. J., Meeth, K., Thakral, D., Damsky, W., Micevic, G., Kaech, S., Blenman, K., & Bosenberg, M. (2017a). UV-induced somatic mutations elicit a functional T cell response in the YUMMER1.7 mouse melanoma model. *Pigment Cell & Melanoma Research*, *30*(4), 428–435. https://doi.org/10.1111/PCMR.12591

Wang, J., Perry, C. J., Meeth, K., Thakral, D., Damsky, W., Micevic, G., Kaech, S., Blenman, K., & Bosenberg, M. (2017b). UV-induced somatic mutations elicit a functional T cell response in the YUMMER1.7 mouse melanoma model. *Pigment Cell and Melanoma Research*, *30*(4), 428–435. https://doi.org/10.1111/pcmr.12591

Weichselbaum, R. R., Ishwaran, H., Yoon, T., Nuyten, D. S. A., Baker, S. W., Khodarev, N., Su, A. W., Shaikh, A. Y., Roach, P., Kreike, B., Roizman, B., Bergh, J., Pawitan, Y., Van De Vijver, M. J., & Minn, A. J. (2008). *An interferon-related gene signature for DNA damage resistance is a predictive marker for chemotherapy and radiation for breast cancer*. www.pnas.org/cgi/content/full/

Weinandt, S. A., Child, Z. J., Lartey, D., Santos, A., Maxfield, H., Sevigny, J. K., Garrett, F. E. S., Smith, P. D., Giersch, R. M., Hart, S. F. M., Perez, F., Rabins, L., Kaiser, S., Boyar, A., Newton, J., Kerr, J., Dimond, J. L., & Metzger, M. J. (2024). *Identification of an Outbreak of Bivalve Transmissible Neoplasia in Soft-Shell Clams (* Mya arenaria *) in the Puget Sound Using Hemolymph and eDNA Surveys*. https://doi.org/10.1101/2024.12.03.626659

Wen, Y., Zhu, Y., Zhang, C., Yang, X., Gao, Y., Li, M., Yang, H., Liu, T., & Tang, H. (2022). Chronic inflammation, cancer development and immunotherapy. *Frontiers in Pharmacology*, *13*. https://doi.org/10.3389/FPHAR.2022.1040163

Whaley, R. D., Dougherty, R. E., Cheng, L., & Ulbright, T. M. (2020). Fluorescence in Situ Hybridization for the X and Y Chromosome Centromeres Helps Differentiate between Gestational and Nongestational Choriocarcinoma in Clinically Ambiguous Cases. *Archives of Pathology and Laboratory Medicine*, *144*(7), 863–868. https://doi.org/10.5858/arpa.2019-0207-OA

Willott, J. F. (1986). Effects of aging, hearing loss, and anatomical location on thresholds of inferior colliculus neurons in C57BL/6 and CBA mice. *Journal of Neurophysiology*, *56*(2), 391–408. https://doi.org/10.1152/jn.1986.56.2.391

Woods, G. M., Bruce Lyons, A., & Bettiol, S. S. (2020). A devil of a transmissible cancer. In *Tropical Medicine and Infectious Disease* (Vol. 5, Issue 2). MDPI AG. https://doi.org/10.3390/tropicalmed5020050

Woods, G. M., Fox, S., Flies, A. S., Tovar, C. D., Jones, M., Hamede, R., Pemberton, D., Lyons, A. B., & Bettiol, S. S. (2018). Two Decades of the Impact of Tasmanian Devil Facial Tumor Disease. *Integrative and Comparative Biology*, *58*(6), 1043–1054. https://doi.org/10.1093/icb/icy118

Wu, X., Li, T., Jiang, R., Yang, X., Guo, H., & Yang, R. (2023). Targeting MHC-I molecules for cancer: function, mechanism, and therapeutic prospects. In *Molecular Cancer* (Vol. 22, Issue 1). BioMed Central Ltd. https://doi.org/10.1186/s12943-023-01899-4

Xiang, X., Wang, J., Lu, D., & Xu, X. (2021). Targeting tumor-associated macrophages to synergize tumor immunotherapy. *Signal Transduction and Targeted Therapy 2021 6:1*, *6*(1), 1–12. https://doi.org/10.1038/s41392-021-00484-9

Yamamoto, H., & Yamamoto, I. (1996). Establishment and characterization of transplantable tumor derived from a spontaneous malignant fibrous histiocytoma in the mouse. *Experimental Animals*, *45*(1), 45–54. https://doi.org/10.1538/expanim.45.45

Yoneyama, M., & Fujita, T. (2010). Recognition of viral nucleic acids in innate immunity. In *Reviews in Medical Virology* (Vol. 20, Issue 1, pp. 4–22). https://doi.org/10.1002/rmv.633

Yun, W. Bin, Kim, J. E., Lee, M. L., Choi, J. Y., Park, J. J., Song, B. R., Kang, B. C., Nam, K. T., Lee, H. W., & Hwang, D. Y. (2021). Sensitivity to tumor development by TALEN-mediated Trp53 mutant genes in the susceptible FVB/N mice and the resistance C57BL/6 mice. *Laboratory Animal Research*, *37*(1). https://doi.org/10.1186/s42826-021-00107-y

Zalfa, C., & Paust, S. (2021). Natural Killer Cell Interactions With Myeloid Derived Suppressor Cells in the Tumor Microenvironment and Implications for Cancer Immunotherapy. *Frontiers in Immunology*, *12*. https://doi.org/10.3389/FIMMU.2021.633205

Zhao, H., Wu, L., Yan, G., Chen, Y., Zhou, M., Wu, Y., & Li, Y. (2021). Inflammation and tumor progression: signaling pathways and targeted intervention. *Signal Transduction and Targeted Therapy*, *6*(1). https://doi.org/10.1038/S41392-021-00658-5

Zhao, H., Zhang, L., Du, D., Mai, L., Liu, Y., Morigen, M., & Fan, L. (2024). The RIG-I-like receptor signaling pathway triggered by Staphylococcus aureus promotes breast cancer metastasis. *International Immunopharmacology*, *142*. https://doi.org/10.1016/j.intimp.2024.113195

Zhou, J., He, W., Luo, G., & Wu, J. (2013a). Fundamental immunology of skin transplantation and key strategies for tolerance induction. *Archivum Immunologiae et Therapiae Experimentalis*, *61*(5), 397–405. https://doi.org/10.1007/S00005-013-0233-2/FIGURES/1

Zhou, J., He, W., Luo, G., & Wu, J. (2013b). Fundamental immunology of skin transplantation and key strategies for tolerance induction. In *Archivum Immunologiae et Therapiae Experimentalis* (Vol. 61, Issue 5, pp. 397–405). https://doi.org/10.1007/s00005-013-0233-2

Zhou, W., Whiteley, A. T., de Oliveira Mann, C. C., Morehouse, B. R., Nowak, R. P., Fischer, E. S., Gray, N. S., Mekalanos, J. J., & Kranzusch, P. J. (2018). Structure of the Human cGAS–DNA Complex Reveals Enhanced Control of Immune Surveillance. *Cell*, *174*(2), 300-311.e11. https://doi.org/10.1016/j.cell.2018.06.026

Zhyvoloup, A., Melamed, A., Anderson, I., Planas, D., Lee, C. H., Kriston-Vizi, J., Ketteler, R., Merritt, A., Routy, J. P., Ancuta, P., Bangham, C. R. M., & Fassati, A. (2017). Digoxin reveals a functional connection between HIV-1 integration preference and T-cell activation. *PLoS Pathogens*, *13*(7). https://doi.org/10.1371/journal.ppat.1006460